LATERAL SUPPORT OF AXIALLY LOADED COLUMNS IN PORTAL FRAME STRUCTURES PROVIDED BY SHEETING RAILS

by

Graeme Scott Louw

Thesis presented in partial fulfilment of the requirements for the degree of
Master of Science of Engineering
at
Stellenbosch University

Department of Civil Engineering
Faculty of Engineering

Supervisor:
Professor P.E. Dunaiski

Stellenbosch University December 2008

Declaration

By submitting this thesis electronically, I declare that the entirety of the work contained therein is my own, original work, that I am the owner of the copyright thereof (unless to the extent explicitly otherwise stated) and that I have not previously in its entirety or in part submitted it for obtaining any qualification.

Date: 28 November 2008

Copyright © 2008 Stellenbosch University

All rights reserved

Abstract

Doubly symmetric I-section columns are often utilised in portal frame construction. The sheeting (or cladding) is carried by sheeting rails connected to the outer flange of these columns. Although it is common practice to include the sheeting rails in the longitudinal bracing system, by connecting the sheeting rail to the cross-bracing, designers must be wary because the connection between column and sheeting rail will not prevent twisting of the columns cross-section. It has been shown ([11], [12], [17]), that by including this eccentric restraint into the bracing of the column, that a torsional-flexural buckling mode of failure can occur when the column is subjected to axial load only. It was seen that this phenomenon is provided for in BS 5950 [18], but is not present in many other design codes of practice, in spite of this phenomenon being relatively well known. In some cases the compression resistance of a column can be significantly reduced when compared to that of a flexural buckled configuration.

Previous work performed by Helwig and Yura [15] proposed specific column to sheeting rail connections which would allow for the sheeting rails to be used as elastic torsional braces and effectively rigid lateral braces. However, it is the objective of this investigation to determine if it is possible to include the eccentric sheeting rails into the bracing system, even when using a relatively simple cleat connection with only two bolts onto the sheeting rail.

The objective of the research was investigated by conducting experimental tests coupled with a series of detailed finite element analyses. The purpose of the experimental set-up was to investigate the behaviour of a column laterally supported on one flange by a continuous sheeting rail and to compare it to the behaviour of a column laterally supported on both flanges by means of fly-braces ("*knee-braces*").

The behaviour of the columns, as determined by the experimental tests, was validated by the finite element analyses. The evident conclusion that can be drawn is that, for the case of a continuous sheeting rail, connected to column simply by two bolts and a cleat, that sufficient torsional restraint is provided to the column to prevent torsional-flexural buckling from being critical.

This result is helpful, as it means that the buckling capacity of a column can be increased four-fold by enforcing the second flexural buckling mode instead of the first mode through utilising a continuous sheeting rail connected to a cross-bracing system as longitudinal bracing on the columns. This can be achieved without the need to provide any specific detailing to the column to sheeting rail connection. It is however, recommended that further experimental work be conducted on varying lengths of column in order to further validate the results of this work.

Opsomming

Dubbel simmetriese I-profiel kolomme word dikwels gebruik in die konstruksie van portaal-rame. Die bekleding word gedra deur gebruik te maak van bekledingslatte wat weer aan die buite-flens van die kolomme bevestig word. Dit is algemene praktyk om die bekledingslatte in te sluit in die verstywerstelsel in die langsrigting as die bekledingslatte aan die kruisverstywerstelsel geheg is. Maar, die ontwerper moet versigtig wees, aangesien die verbinding tussen die kolom en die bekledingslatte nie verwringing van die kolom sal verhoed nie. Dit is al bewys ([11], [12], [17]) dat ‘n torsie-buig knik mode van faling kan voorkom in die kolom onder aksiale las deur hierdie eksentriese ondersteuning in te sluit by die verspanning van die kolom. Daar word voorsiening gemaak vir hierdie verskynsel in BS 5950 [18] maar nie in baie ander ontwerpkodes nie, alhoewel hierdie verskynsel redelik wel bekend is. In sekere omstandighede kan die drukkapasiteit van ‘n kolom noemenswaardig verminder word, wanner dit vergelyk word met ‘n buigknik konfigurasie.

Vorige werk, wat deur Helwig en Yura [15] uitgevoer is, stel spesifieke verbindings tussen kolomme en bekledingslatte voor, wat voorsiening sal maak vir die bekledingslatte om gebruik te word as elastiese torsie-verstywers asook starre laterale verstywers. Dit is egter die doelwit van hierdie navorsing om vas te stel of dit moontlik is om die eksentriese bekledingslatte in te sluit by die verstywerstelsel wanneer ‘n relatief eenvoudige hegstukverbinding gebruik word met slegs twee boute in die bekledingslat.

Die doelwit van die navorsing is ondersoek deur eksperimentele toetse sowel as ‘n reeks deeglike eindige element analises uit te voer. Die eksperimentele opstelling was daarop gemik om die gedrag van ‘n kolom te ondersoek, wat lateraal ondersteun word aan een flens deur ‘n deurlopende bekledingslat, en dit te vergelyk met die gedrag van ‘n kolom wat lateraal ondersteun word aan beide flense deur gebruik te maak van skuinsverstywers (“*knee-braces*”).

Die gedrag soos bepaal met die eksperimentele toetse is bevestig met die resultate van die eindige element analises. ‘n Duidelike gevolgtrekking wat gemaak kan word, is dat voldoende torsie-weerstand voorsien word om te voorkom dat torsie-buig knik kritiek word vir die geval van ‘n deurlopende bekledingslat wat aan die kolom verbind word met twee boute en ‘n hegstuk.

Hierdie resultaat is nuttig aangesien dit beteken dat die knik-kapasiteit van ‘n kolom viervoudig verhoog kan word bloot deur die tweede buig-knik mode in plaas van die eerste mode af te dwing deur van ‘n deurlopende bekledingslat wat aan die kruisverstywerstelsel bevestig is, as ‘n langsverstywer aan die kolom te voorsien. Hierdie resultaat kan verkry word sonder om enige spesifieke detailering van die kolom te voorsien. Daar word egter voorgestel dat toekomstige eksperimentele werk uitgevoer word om die lengtes van kolomme te varieer ten einde die resultate van hierdie navorsing te bevestig.

Acknowledgements

The work and effort required to complete this thesis was an ordeal which, although primarily my own work and my own responsibility, I could not have managed without the valuable input of various people along the way. Although words cannot fully express my gratitude to these people, I will nonetheless spare a few for them, in acknowledgement of my gratitude for their help.

Prof. Dunaiski:

The oblique manner in which you answered all my uninformed questions at the start of the research forced me to dig deeper and ultimately made me realize the full scope and implications of the topic. Your patience with me, as I occasionally ran past a deadline, was almost as beneficial as your experience with experimental work which saved me a lot of trial and error. Above all, you constantly remind me that I still have a lot to learn…

Wendy Henwood:

For always encouraging my enthusiasm and never failing to believe in me (even when I myself had no faith) I am especially grateful. The quality of this thesis can be in a large way be laid at your feet, due to your painstaking, marathon proof-reading session. No man could ask for more than the unbending and always generous love you have shown to me. I hope that over the coming years I can repay you and show my love for you as clearly.

My fellow masters students:

We had a special group of individuals who worked really well together as a group. Thanks for all your help and understanding over our two years together and especially for all the laughter (even if it was mostly aimed at me!!). I wish you all the best and I sincerely hope we stay in contact!

Dion Viljoen:

Thanks for always having an open door and a helpful suggestion whenever I needed a hand, which was pretty often. My practical know-how is pretty shaky, but you really taught me a lot, thanks.

Arthur Layman:

Thank you for all your assistance around the lab, especially with placing the columns into position. We managed to get a good system going at the end, but the initial problems we had will always make me laugh when I think back!

Table of Contents

Chapter *Page*

List of Symbols

Roman Letters:

A	Cross-sectional area
A	Factor applied to ideal torsional brace stiffness to control deformations and brace moments
A_b	Area of a bolt
A_f	Area of the flange of a cross-section
A_g	Gross cross-sectional area
$A_{g,min}$	Minimum required cross-sectional area
a	Coordinate of the offset axis of restraint relative to the centroid of a cross-section in the y- direction
b	Width of a cross-section or element of a cross-section
C	Torsional rigidity (= $G \cdot J$)
C_1	Warping rigidity (= $E \cdot C_w$)
C_A	Flexural stiffness of the sheeting rail
C_f	Compressive force on one flange
C_{max}	Maximum compressive force
C_r	Factored compressive resistance of member of component
$C_{r,y2}$	Factored compressive resistance of a member for buckling about the weak axis, in the second mode
C_w	Warping torsional constant
C_y	Applied compressive force in member at yield stress
c	Spacing of sheeting rails/girts acting as lateral supports
D	Overall height of cross-section
d	Overall height of cross-section
d'	Depth of an element of a cross-section
E	Young's modulus
f_{cr}	Critical buckling stress
f_{ex}	Elastic critical buckling stress in compression (for strong axis flexural buckling)
f_{ey}	Elastic critical buckling stress in compression (for weak axis flexural buckling)
f_{eTF}	Elastic critical buckling stress in compression (for torsional-flexural buckling)
f_{ez}	Elastic critical buckling stress in compression (for torsional buckling)
F_c	Applied compressive force

F_x Component of a force in the *x*- direction

F_y Component of a force in the *y*- direction

f_u Specified minimum tensile strength

f_y Specified minimum yield stress

G Shear modulus

h Overall height of cross-section

h_s Distance between the centroids of two flanges

h_w Height of the web

h_x Coordinate of the offset axis of restraint relative to the centroid of a cross-section in the *x*- direction

h_y Coordinate of the offset axis of restraint relative to the centroid of a cross-section in the *y*- direction

I Second moment of inertia about a given axis (e.g. I_x or I_y)

I_b Second moment of inertia of the sheeting rail for bending about its weak axis

I_c Second moment of inertia of the column for bending about its weak axis

I_o Polar moment of inertia

I_{sr} Second moment of inertia of the sheeting rail for bending about its strong axis

i_s Polar radius of gyration about an offset axis of rotation

J St. Venant torsion constant of a cross-section

K Effective length factor (subscripts x- and y- denote the buckling direction considered)

K_c Stiffness of column section against distortion

K_f Flexural stiffness of sheeting rail

K_s Torsional stiffness of elastic rotational support $= \dfrac{1}{\left(\dfrac{1}{K_f} + \dfrac{1}{K_c}\right)}$

K_T Discrete torsional restraint stiffness

k Equivalent uniform torsional restraint (= K_s / s)

k_x Lateral stiffness of elastic supports in *x*- direction

k_y Lateral stiffness of elastic supports in *y*- direction

k_φ Torsional stiffness of elastic rotational support

$K{\cdot}L$ Effective length

L Length of the member being investigated (subscript x- and y- denote direction over which buckling is being considered)

L_{cr} Buckling length in plane considered

L_f	Length of unsupported flange (inside flange)
L_{sr}	Length of the sheeting rail between inflection points
L_T	Spacing of torsional restraints
L_x	Unbraced length for strong axis flexural buckling
L_y	Unbraced length for weak axis flexural buckling, or segment length.
L_z	Unbraced length for torsional or torsional-flexural buckling
M_b	Buckling resistance moment (Lateral-torsional buckling)
M_r	Restraining moment on a column due to flexure of a connected sheeting rail
M_r	Factored moment resistance of a member
M_x	Bending moment about the x- axis
M_z	Internal bending moment at a distance z along the column
m_1	Number of column lengths between supports
m_t	Equivalent uniform moment factor
$N_{b,Rd}$	Design buckling resistance
N_{cr}	Elastic critical force
$N_{cr,T}$	Elastic torsional buckling force
$N_{cr,TF}$	Elastic torsional-flexural buckling force
N_{ed}	Design value of compression force
n	Integer determining which buckling mode is being calculated
n_b	Number of torsional braces attached to the column
n_w	Number of half sine-waves in the buckled shape
P	Applied axial load
P_c	Compression resistance
P_E	Elastic critical Euler buckling load
P_{cr}	Critical buckling load
$P_{cr,TF}$	Critical buckling load for torsional-flexural buckling
$P_{cr,x}$	Critical buckling load for strong axis buckling
$P_{cr,y}$	Critical buckling load for weak axis buckling
$P_{cr,z}$	Critical buckling load for torsional buckling
P_o	Weak axis flexural buckling over the full columns length
P_n	Nominal compressive strength
p_c	Compressive strength
r	Radius of gyration about a given axis (e.g. r_x or r_y)

$\overline{r_o^2}$	Polar radius of gyration
r_s	Polar radius od gyration about the offset axis of support
s	Spacing of sheeting rails/girts acting as lateral supports
T	Thickness of a flange
T_r	Factored tensile resistance of a member
t	thickness
t_f	Thickness of the flange
t_w	Thickness of the web
u	Lateral deflections in the *x*- direction
V_r	Factored shear resistance of a member
v	Lateral deflections in the *y*- direction
W_n	Nominal wind load
x	Torsional index of a cross-section (= D / T)
x_o	Principle coordinates of the shear centre with respect to the centroid of the cross-section in the *x*- direction
y_o	Principle coordinates of the shear centre with respect to the centroid of the cross-section in the *y*- direction
Z	Elastic section modulus of steel section

Greek letters:

α	Imperfection factor
β_T	Torsional stiffness of elastic rotational support
Γ_o	Warping constant
γ_{m1}	Partial factor for resistance of members to instability assessed by member checks
Δ	Measured lateral deflection
θ	Joint rotation
κ	Ratio of torsional restraint provided by lateral restraints to a flexural characteristic of the column
λ	Half-wavelength in torsion
λ	Non-dimensional slenderness ratio
$\bar{\lambda}$	Non-dimensional slenderness
λ_1	Slenderness value to determine relative slenderness

σ_{max}	Compressive stress under maximum compressive force
σ_R	Residual stresses
σ_{y1}	Elastic buckling stress for the first mode of weak axis flexural buckling
σ_{y2}	Elastic buckling stress for the second mode of weak axis flexural buckling
σ_{y3}	Elastic buckling stress for the third mode of weak axis flexural buckling
σ_{yz1}	Elastic buckling stress for the first mode of torsional-flexural buckling
Φ	Value to determine reduction factor (χ)
φ	Twist angle of the cross-section
φ	Resistance factor for structural steel
χ	Reduction factor for relevant buckling curve
ω_n	Warping function
Ω	A factor which takes into account the position of the shear centre relative to the centroid of the cross-section as well as the radii of gyration

Abbreviations:

BC	Boundary conditions
BS	British standard
CFLC	Cold formed lipped channel
CHS	Circular hollow section
DOF	Degree of freedom
HBM	Hottinger Baldwin Messtechnik
GMNLA	Geometrically and materially non-linear analysis
LVDT	Linear variable displacement transducer
SANS	South African National Standard
TF	Torsional-flexural

List of Figures

Figure ***Page***

List of Tables

Table ***Page***

1. Introduction

The portal frame structure is a very versatile structural system which has found many varied uses throughout a wide range of industrial applications. The main reasons behind this popularity are the cost-effectiveness of the structure and the ease of design. The cost-effectiveness mainly arises due to the relatively small amount of material which is used to enclose a large volume. The out-of plane stability of these structures is always provided by a bracing system which means a two-dimensional analysis is sufficient for most of the design work.

The longitudinal bracing of these structures is normally provided by an eaves beam, transmitting the loads from the gable walls along the length of the building to panels of cross-bracing. These eaves beams are, by definition, at the top of the columns. Also, spanning along the length of the building are the sheeting rails. These members are primarily designed to support the sheeting and to transfer any loads, acting on the sheeting, directly onto the columns.

The strength requirement for lateral bracing members is very low - 0.02 times the axial load in the member being braced. As a result of this, a structural design can quite realistically include the sheeting rails into the bracing system. This would be most effective if there were two crosses of bracing over the height of the column, such that, the mid-height sheeting rail could be tied in directly to the bracing system.

If this approach is followed, a new failure mode can occur in the column, which is mainly caused by the fact that the sheeting rail will only be laterally supporting one of the columns flanges. This failure mode is torsional-flexural buckling, which can loosely be described as the torsional buckling of the column about an offset axis of rotation. This axis of rotation has been shown (Gelderblom, *et al* [17]) to be the sheeting rails centroid.

The benefits of providing a mid-height lateral restraint, is that a lighter column section can be used, which will result in material cost savings. However, relatively little is known about this type of buckling as most lateral bracing systems are designed to prevent any twisting of the cross section.

This investigation will aim at determining if it is feasible to laterally support only one flange of the column. If this lateral support is inefficient, it will be determined whether or not supporting both flanges (by providing fly-braces) will improve the behaviour of the lateral support afforded to the column.

The scope of this investigation will be limited solely to consider the behaviour of a column which is acted upon by axial loads; although this is seldom found in portal frame structures. For a detailed justification of this limitation of scope, the reader is referred to Section 3.2 of this report.

The investigation will begin with a literature study which aims to improve and expand the overall understanding of the torsional-flexural buckling of columns, which are supported by an eccentric lateral restraint. The literature study will include a study of current codes of practice, in an effort to determine how such situations are currently handled. Once this deeper understanding has been achieved, a parameter study on the full system of laterally restrained columns will have to be performed, in order to enable a relevant and representative experimental set-up to be devised.

The chosen experimental set-up will then be used to further investigate the effects of providing an eccentric lateral restraint onto the column, as well as what the behaviour of this restraint is for different connections between the column and sheeting rail. The results obtained by this series of experimental tests will be incorporated into the refining of an analytical model, which will hopefully be able to provide accurate and reliable results very similar to those observed during the experimental tests.

Once this analytical model has been correctly set-up, it will be possible to determine the behaviour of alternative connections between the column and sheeting rail, as well as to investigate the behaviour of various combinations of column and sheeting rail cross-sections.

Finally, conclusions will be drawn regarding the effectiveness of the lateral restraint that a sheeting rail can provide to a column. Recommendations for future research and development (related to this topic) will also be proposed.

2. Literature Study

This chapter of the investigation serves as the theoretical background and justification for the research being conducted herein. The opening few sections are aimed at introducing the reader to the stability phenomenon that is known as buckling. After a general overview of how columns buckle in three dimensions, the literature study focuses more on the topic of torsional-flexural buckling.

Substantial research has been performed, over a long period of time regarding the torsional-flexural buckling of a column about an offset, or eccentric, axis of restraint. In spite of this, little attention is paid to this phenomenon in any design standard around the world [1].

The behavioural advantages which can be obtained by including the flexibility of the sheeting rail into the lateral support are highlighted, and attempts at quantifying these are discussed.

Finally, a study of a few international codes of practice is carried out in order to determine if any attention is paid to the phenomenon of torsional-flexural buckling.

2.1. Buckling of columns

2.1.1. Euler buckling

The work carried out by Leonard Euler in the 18th Century is known as the starting point in terms of understanding the real, physical behaviour of columns. Euler made a number of assumptions which enabled to him to simplify the problem so that it could be solved in a relatively straightforward manner. These assumptions (as laid out by Bresler, Lin and Scalzi [2]) are listed below:

- *The material is linearly elastic and proportional limit stress is nowhere exceeded.*
- *The elastic moduli in tension and compression are equal.*
- *The material is perfectly homogenous and isotropic.*
- *The member is perfectly straight initially and the load is perfectly concentric with the centroid of the section.*
- *The ends of the member are perfect frictionless hinges which are so supported that axial shortening is not restrained.*
- *The section of the member does not twist and its elements do not undergo local buckling.*
- *The member is free from residual stresses.*
- *Small-deflection approximation may be used in defining geometric curvature of the deformed shape.*

The assumptions above result in what is now called the Ideal or Euler Column. To illustrate the method that Euler used to solve for the critical load, I will use the derivation as put forward by R. Bjorhovde in [3]. The first step in solving for the critical buckling load is to look at the deformed state of the body shown below in Figure 2.1. If one takes a section at an arbitrary height, for example *z*, then for equilibrium the internal and external forces must be equal.

External moment:

$$\sum M_o = 0 :$$
$$M_z + (P \times v) = 0;$$
$$M_z = Pv$$

Internal moment:

$$\frac{d^2y}{dz^2} = v'' = -\frac{M_z}{EI}$$
$$v'' + \frac{M_z}{EI} = 0$$

Where

M_z is the internal moment in the column at a point *z* along the column;

E Young's modulus of elasticity;

I the moment of inertia about the axis of buckling (in this case I_x).

It follows that:

$$v'' + \frac{Pv}{EI} = 0 \qquad (2.1)$$

Now, in order to facilitate the solution, substitute in the following expression:

$$k^2 = \frac{P}{EI};$$

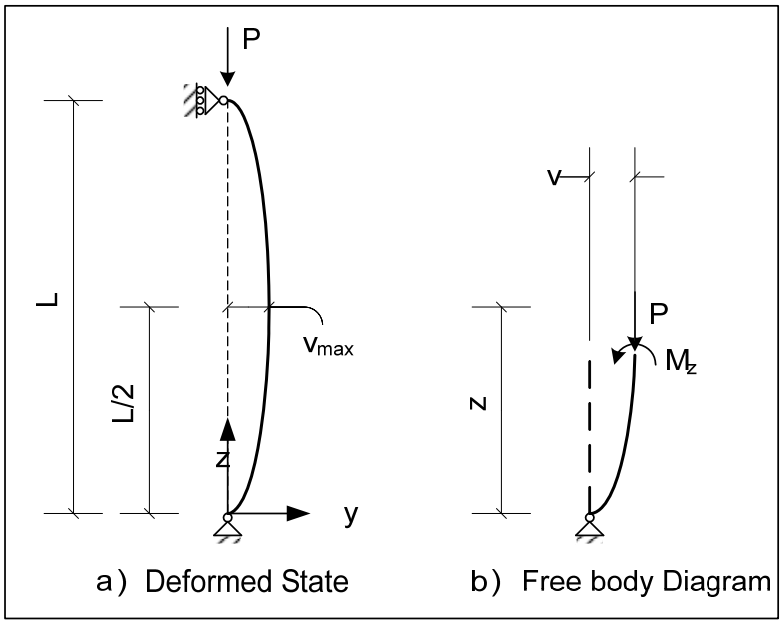

Figure 2.1 - Ideal Pin-ended column [3]

This yields the following differential equation:

$$v'' + k^2 v = 0 \qquad (2.2)$$

This equation (2.2) has the known solution of:

$$v = A \sin kz + B \cos k;$$

Where A and B are integration constants.

The boundary conditions for the system are the following:

$v = 0$ at $z = 0$ and $v = 0$ at $z = L$;

Upon substitution of the boundary conditions, it will be seen that $B = 0$, and thus the solution is:

$$A \sin kL = 0;$$

With the non-trivial solution only when:

$$\sin kL = 0,$$

Thus:

$$kL = n\pi; \ldots\ldots\ldots\ldots\ldots\ldots \text{ (n=1, 2, 3…)}$$

$$k = \frac{n\pi}{L}$$

$$\sqrt{\frac{P}{EI}} = \frac{n\pi}{L}$$

$$P_{cr} = P_E = \frac{(n\pi)^2 EI}{L^2}. \qquad (2.3)$$

It is common practice to only pay attention to the lowest mode (n = 1) as the structure will most likely fail in this mode. If one were to use a higher value of n in the calculations, which would still yield a correct answer and buckled configuration, one would determine the n^{th} mode of the structure. An illustration showing the different buckling modes can be seen in Figure 2.2. Also, in this figure, the relationship between the length of the member and the critical load that the member can carry is seen for the first time. It can be seen that, for a member with half the buckling length, the carrying capacity is increased by a factor of 4.

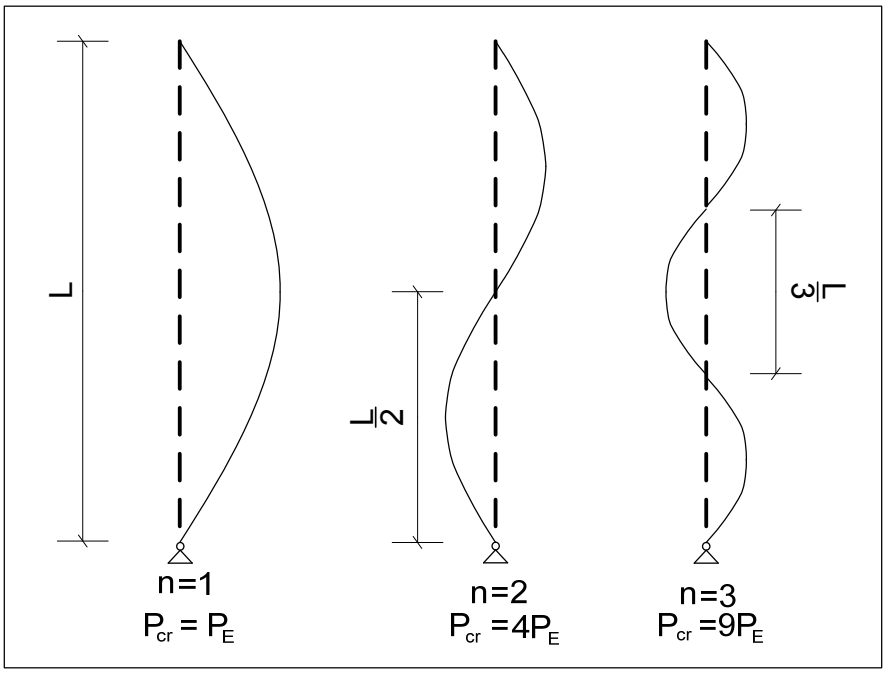

Figure 2.2 - Buckling modes [3]

This relationship follows from the fact that the Critical load is inversely proportional to the square of the member's length. That is:

$$P_{cr} \propto \frac{1}{L^2}$$

This means that the buckling load is sensitive to the length of the member under consideration. The other variable term in Euler's equation is the stiffness of the member, as expressed below:

$$P_{cr} \propto EI$$

2.1.2. Three dimensional and inelastic buckling

The assumptions used by Euler in deriving his buckling formulation are seldom found in practice. However, the Euler method still forms the basis of stability design in all structural design codes used today. A few modifications have been made on the original formula in order to account for the assumptions (which were made in order to simplify the calculations) not being justified by the material and layout of the columns. The Euler capacity of a column will be the upper limit of what any column can possibly carry (neglecting failure by yielding).

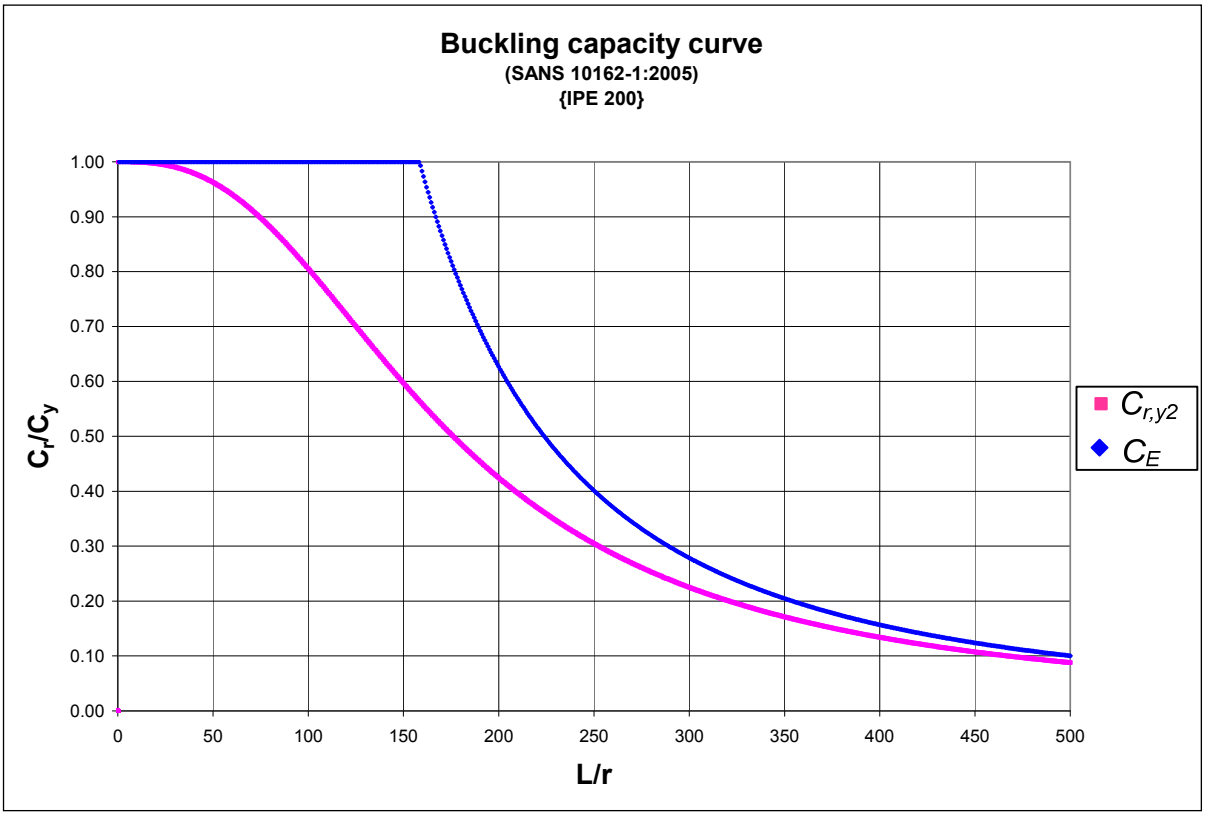

Figure 2.3 - Buckling capacity curve

The curve above illustrates that the actual column strength will always be lower than the Euler load, which forms the theoretical maximum value of the columns capacity. The upper (blue) curve is a piecewise function for the perfect columns capacity which shows the interaction between yielding and Euler buckling. The lower (pink) curve is the behaviour of a realistic column, which will always have some portions of the cross-section yielding even before buckling begins.

2.1.2.1. Effective length factor

If a given column does not have the pinned connection assumed by Euler, it is still possible to calculate the buckling load by using the Euler formulas. This is possible by using the effective length in place of the actual length of the member. The concept will be explained with the aid of the example below.

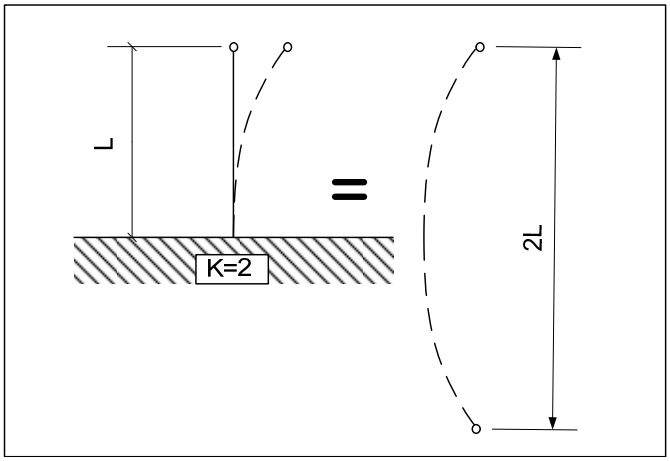

Figure 2.4 - Effective length principle

If the column, of length **L**, under investigation is fixed at the base whilst the top is free to move with no restrictions then it can be shown that the buckling load will be four times less than that of a pin-ended column of equivalent length. It can also be shown that the buckling load of our example column is the same as the buckling load of a pinned-end column with a length of **2L**. Thus:

$$P_{cr} = \frac{\pi^2 EI}{(2L)^2} = \frac{\pi^2 EI}{(KL)^2}. \qquad (2.4)$$

Based on the above example, it can therefore be said that the effective length of the column, for any combination of boundary conditions, is actually the equivalent length of a pin-ended column which would have the exact same buckling capacity as the column under investigation. Also, this effective length is easily obtainable as the distance between inflection points on the bent columns shape. Based on these statements, the effective length factor has been compiled into tables similar to the one shown below which can be found in most design codes:

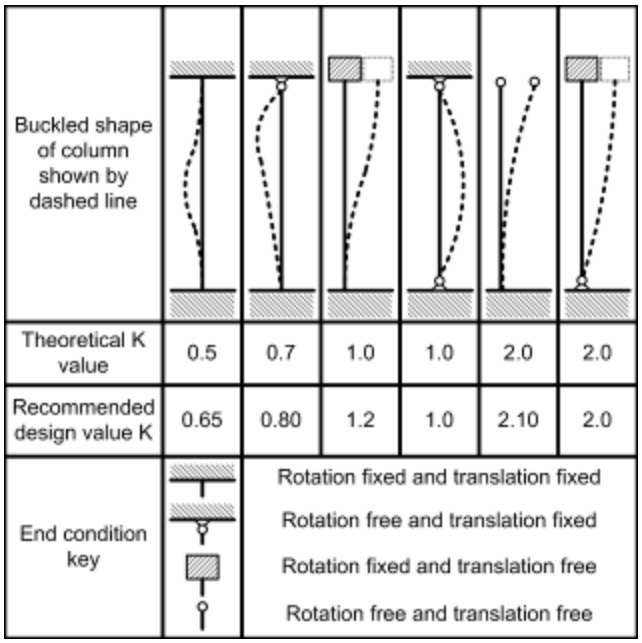

Figure 2.5 – Effective length factors [7]

2.1.2.2. Three dimensional buckling

In reality, a buckled body can have lateral displacements in either the *x*- or *y*- directions, or potentially a twist about the longitudinal (*z*-) axis. It was shown above in Section 2.1.1 that the solution, of the simple case, follows from the differential equation:

$$v'' + \frac{Pv}{EI} = 0\,;$$

Similarly, for the three dimensional case the solution follows from the following three differential equations, as reproduced from *Structural Members and Frames* by Galambos [4]:

$$\begin{aligned} EI_x v^{iv} + Pv'' - Px_o\varphi'' &= 0; \\ EI_y u^{iv} + Pu'' + Py_o\varphi'' &= 0; \\ C_w\varphi^{iv} - \left(GJ + \overline{K}\right)\cdot\varphi'' + Py_o u'' - Px_o v'' &= 0 \end{aligned} \qquad (2.5.a)$$

For cross-sections that are doubly symmetric, i.e. $x_o = y_o = 0$, the three equations (2.5) above separate into the three independent equations:

$$\begin{aligned} v^{iv} + \frac{Pv''}{EI_x} &= 0; \\ u^{iv} + \frac{Pu''}{EI_y} &= 0; \\ \varphi^{iv} + \left(\frac{P\bar{r}_o^{2} - GJ}{C_w}\right)\cdot\varphi'' &= 0 \end{aligned} \qquad (2.5.b)$$

Where

$$\bar{r}_o^{2} = \frac{I_x + I_y}{A}$$

Doubly symmetric sections include I- and H-sections, which are commonly used as columns in structural steel construction. Each of the above equations is independent, and thus there are three potential modes of failure. The critical load for each of these modes of buckling can then be solved in the manner shown above in Section 2.1.1, and the resulting loads are:

$$P_{cr,x} = \frac{\pi^2\cdot E\cdot I_x}{{L_x}^2}\,; \qquad (2.6.a)$$

$$P_{cr,y} = \frac{\pi^2\cdot E\cdot I_y}{{L_y}^2}\,; \qquad (2.6.b)$$

$$P_{cr,z} = \left(\frac{\pi^2 C_w}{{L_z}^2} + GJ\right)\frac{1}{\bar{r}_o^{2}}\,. \qquad (2.6.c)$$

For any given practical case the lowest value of the above equations will be the critical load of the column. The end connections must be taken into account when calculating the critical loads. The buckled configuration represented by each of the above equations is explained with the aid of the sketch below, which illustrates how a column will deform in each mode of buckling.

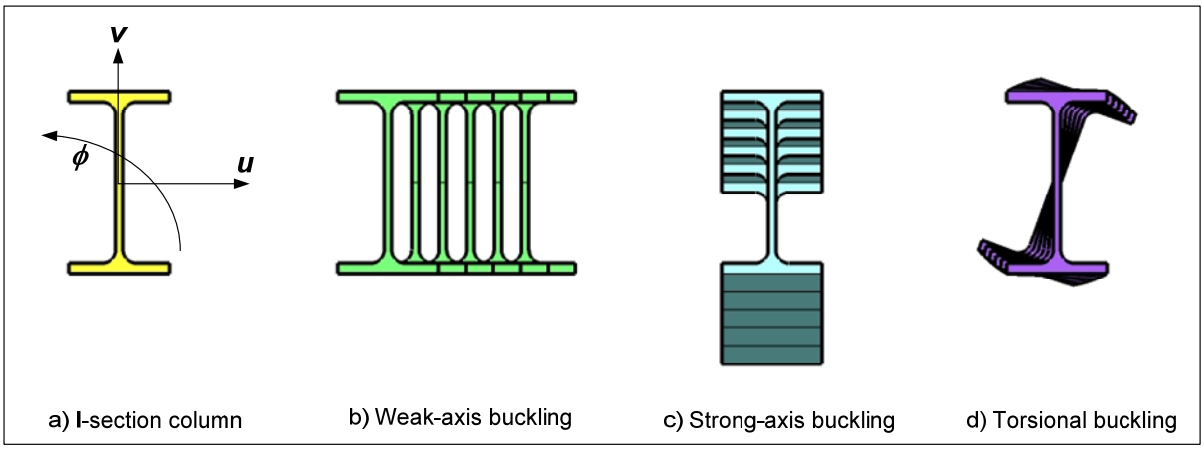

Figure 2.6 - Buckled configuration

2.1.2.3. Inelastic buckling

The main causes of inelastic behaviour in columns are residual stresses in the column cross-section, as well as initial imperfections (deformations or curvatures) in the column. These two factors will serve to reduce the columns capacity below its theoretically possible limit (the Euler load). As can be seen from the buckling capacity curve (Figure 2.3) long slender columns are not very sensitive to the presence of residual stresses and initial imperfections, however, large reductions in capacity can occur for columns of short or intermediate length. The behaviour of columns which buckle inelastically is neatly summed up by Bastiaanse [5] and the key points will be brought forward below.

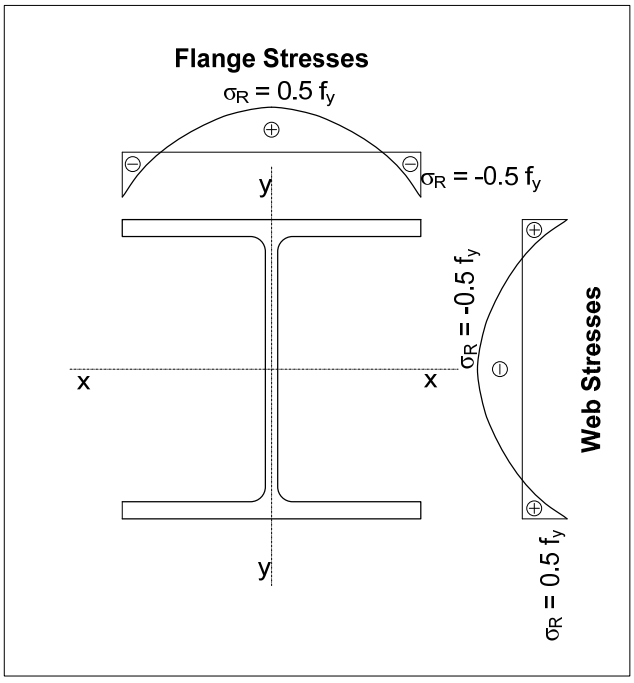

Figure 2.7 - Idealised residual stress distribution for an H-section

A typical residual stress distribution for H-sections is shown in Figure 2.7. These residual stresses arise in the member during the hot-rolling fabrication process. Different zones of the cross-section cool down at different rates. This non-uniform cooling process leaves the member with a set of self-equilibrating stresses locked into it. When the column is loaded (in axial compression) the regions of the cross-section with compressive residual stresses will yield first, before the remainder of the cross-section yields. This can often take place before the column reaches the buckling load. Once a fibre has yielded, it no longer provides any stiffness to the remainder of the column and this reduces the overall rigidity of the strut, which makes the behaviour inelastic.

Initial imperfections have the effect of inducing additional bending moments into the column. These bending moments can intensify the effect of residual stresses; these two parameters (residual stresses and initial imperfections) interact in many ways, the effects of which cannot easily be separated. Initial imperfections are often idealised as scaled down deflections of the critical buckling mode shape which is expected to cause failure; i.e. if the mode of failure is the first flexural mode about the weak axis, then the initial imperfections are taken as a half sine curve with the amplitude taken as $L/1000$ (an upper bound limited by the structural steel delivery specifications) in the x-direction. Modelling a column with these initial imperfections will always provide conservative results, because they are the worst case possible for a given buckling mode. The imperfections can be said to “kick-start” buckling, by making the column section pre-disposed to bend in a certain path.

There are numerous methods of designing columns to account for inelastic behaviour. One such method is the Perry-Robertson approach, which forms the basis of today’s Eurocode – (EN 1993-1-1:2005 [6]) which provides buckling curves for specified curvature parameters depending upon the columns cross-section. Another, more familiar, method is that used in SANS 10162-1:2005 [7] which is a method that can be called a single formula approach to inelastic buckling analyses. The SANS 10162-1:2005 [7] method is utilised in Chapter 4 in the design calculations for the experimental setup; the reader is referred to that chapter for an example of the procedure. The results of using these methods of accounting for inelastic column behaviour yield what is shown in Figure 2.3 above. The blue line shown is for the idealised elastic column, whilst the pink line will be a more realistic behaviour for an imperfect column.

2.2. Lateral supports

If one supplies a lateral support onto a column, it has the effect of reducing the effective length over which buckling occurs. Due to the relationship between the buckling load and the effective length of the column, seen above at the end of Section 2.1.1, this will have the effect of drastically increasing the buckling load of that same column. In order to illustrate this phenomenon Galambos [8] stated the following:

> "*It* [lateral restraint] *is most effective when it is attached at the location along the column where there is a point of contraflexure in one of the higher buckling modes of the column. For example, lateral bracing at the centre of a pinned-end column will increase the elastic buckling load by the factor of 4. In other words, the effective length of the column is reduced from the full length to one-half of the length."*

However, for a structural member to act as a lateral restraint it should have various properties that will enable it to fulfil its function adequately. These requirements will now be briefly discussed below in Section 2.2.1. The potential of using sheeting rails to act as lateral restraints in portal frame structures is also explored. This then poses the question of whether the support that a sheeting rail can supply is adequate. This question forms the main objective of this investigation, and the investigation is launched from this section onwards.

2.2.1. The requirements of bracing members

According to Galambos [8] the usual conservative practice is to take the design brace force to be 2% of the force in the column that is to be braced, indeed most modern design codes have a very similar stipulation. Several other requirements of bracing systems (also from Galambos [8]) are also listed below.

- Even though the bracing requirements are modest, braces are nevertheless vital parts of the structure and should not be relegated to a negligible role. If the braces are improperly attached, they will be ineffective.
- Braces must be properly attached to the member to be braced, and their ends must be anchored to rigid supports. Bracing two adjacent columns to each other is useless, since both columns may buckle in the same direction in a lower mode.
- Bracing must restrain twisting as well as lateral motion, to prevent a lower torsional buckling mode.
- Bracing systems that restrain multiple parallel columns must be stiff enough to take care of the sum of the axial forces in all the columns.

The third bulleted item above is of a central importance in the context of this thesis. It will be shown in the following paragraphs how sheeting rails can be incorporated into the bracing system of a portal frame structure but the issue of preventing twist, if indeed necessary, will be covered in full in this investigation.

2.2.2. Lateral supports in Portal frame structures

At this point it is deemed necessary to highlight a few differences in the building of portal frame structures from different regions, as the impact of these differences can drastically alter the assumptions made by designers, and thus the behaviour of the structure. In a more temperate climate the need for thermal insulation on an industrial structure is not present. This means that the sheeting used is most often of the simple corrugated iron variety (thin metal sheets). However, in climates with a harsher winter season, the need for thermal insulation is imperative. In this regard, a single layer of corrugated iron wall sheeting is inefficient and impractical. To provide the required level of thermal insulation it is general practice to use so-called “sandwich wall units”. These consist of metal sheeting on the two outer edges with various layers of insulation sandwiched in between them.

The shear resistance of such a sandwich unit is much greater than that which can be provided by a single layer of metal sheeting. This has led to a design philosophy in European countries which states that full lateral restraint is provided to the column at the level where each sheeting rail is connected to it. Furthermore, the need for insulation means that the wall units will be properly inspected and maintained during their service lifespan. Also, it is rather unlikely that a wall unit will be removed for any duration of time, so it makes good practical sense to take the stiffness of these units into account.

This is slightly different than when single layer wall sheeting is used. In structures with this wall type the shear stiffness is not effectively rigid, and thus columns are only said to be restrained elastically at the level of connection to the sheeting rails. This means that the connections between sheeting and sheeting rail are of critical importance. However, the method used to provide these connections often allows slip between the sheeting members [9], and thus can, in a large number of cases, be considered to be ineffective in providing lateral restraint. Furthermore, if rust or other structural damage occurs in the sheeting, the reliability of the structure as a whole can be jeopardised. Added to this is the fact that many building owners sometimes remove sheeting in parts of the building for various reasons. Thus, the lateral restraint that sheeting can provide is typically neglected in the design of portal frame structures in more temperate regions (as a general rule).

South Africa has a very temperate climate, and thus the single layer of sheeting is the predominant wall unit for industrial structures. Therefore, the sheeting members are neglected in design. However, the sheeting rails themselves can and often are relied upon, and this is justified if care is taken in the design process. The support that a properly connected sheeting rail can offer will be discussed below.

2.2.3. Sheeting rails as lateral support

The main function of a sheeting rail is to transfer the wind loading that acts on the surface of the structure (either external pressure or internal suction on the sheeting) as well as the dead load of the sheeting onto the columns. The wind load is often the main design action acting on these members. The sheeting rails can be incorporated into the bracing system without significantly increasing the demand on the cross-sections needed to carry the wind loads. This is true because of the small magnitude of the bracing forces as stated above in 2.2.1. However, the connections between the columns and the sheeting rails then need some attention.

Sheeting rails can be implemented on a structure in a variety of manners. A schematic view of these is shown below reproduced from the South African Steel Construction Handbook, hereinafter referred to as “The Red Book” [10].

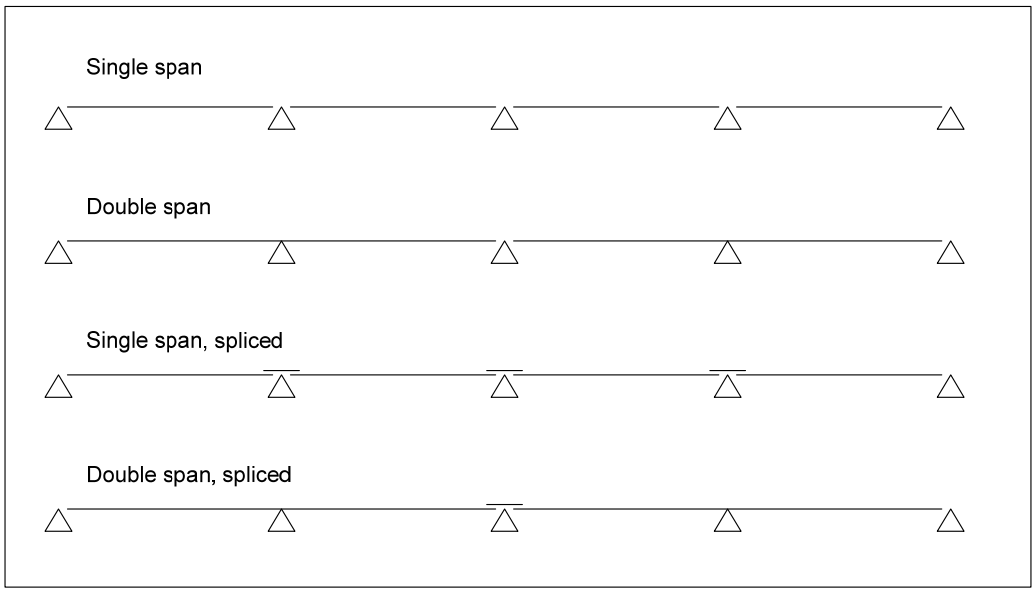

Figure 2.8 - Sheeting rail spanning systems [10]

As can be seen from the above figure, there are three main configurations for sheeting rail spanning systems. These are simply supported, two-span continuous and continuous (the location of the splicing makes no real impact on the structural behaviour of the configuration). If, for a certain structure, the design wind loading is a fixed value (say W_n) then by using continuous sheeting rails the magnitude of the bending moment in each sheeting rail will be much smaller than if a single span sheeting rail were to be used. This means that by choosing a continuous sheeting rail spanning system rather than a simply supported one, a smaller cross-section could be used with the same results. This does, however, have the consequence of increased material (splices and bolts/welds) and erection (more bolts per connection—takes longer) costs. The selection of which spanning system to use can thus be said to be an economic decision.

2.2.3.1. Lateral support on only one flange

We saw in 2.2.1 that one of the primary requirements for bracing members is that they restrain twisting of the section, to prevent a lower torsional mode of failure. If one looks at the manner in which sheeting rails are generally attached in practice (see Figure 2.9 below) it is doubtful whether such a connection can sufficiently restrain twisting of the columns cross-section, although this seems to be more likely for a continuous sheeting rail rather than for a discontinuous sheeting rail.

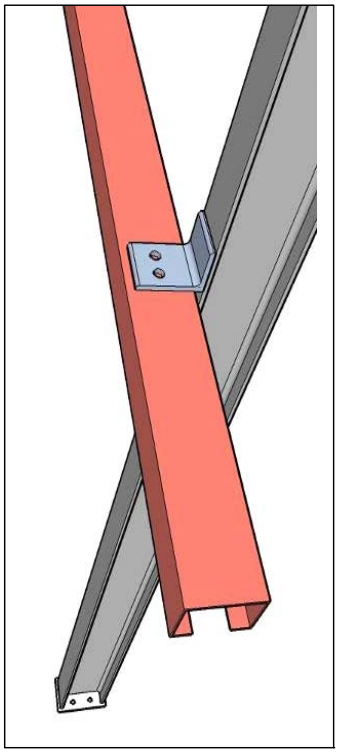

Figure 2.9 - Sheeting rail connection [ж]

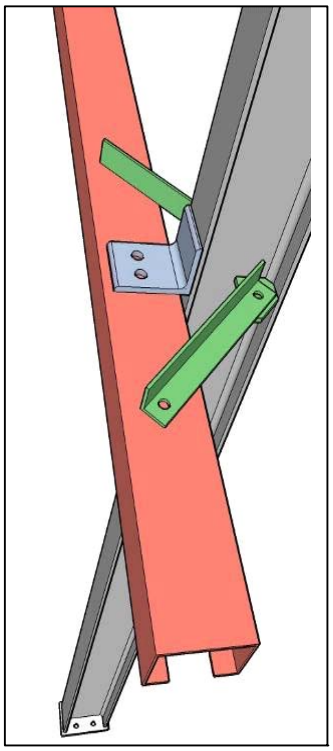

Figure 2.10 - Sheeting rail and Fly brace

This raises the question of whether or not the sheeting rail, supporting only one of the columns flanges, can restrain and/or prevent twisting of the cross section, or if it is necessary to provide a manner of restraining both flanges (for example by using fly braces) to eliminate a possible lower torsional mode of failure.

A thorough look at the collective research over the last sixty years that deals with torsional-flexural buckling and the influence of eccentric restraint will follow in the next section. This will be aimed at determining if and when support on only one flange will be sufficient to prevent a lower torsional-flexural buckling mode from occurring.

[ж] The above figures show two options for the sheeting rail connection (in both cases the sheeting rails are taken as Cold formed lipped channels, although the arrangement is valid for other sheeting rail types). It must be noted that the views shown above are seen from above looking down onto the top of the sheeting rail along the column.

2.3. Torsional-Flexural buckling in eccentrically restrained columns

The following section will introduce the phenomenon of torsional-flexural buckling by illustrating the physical behaviour of a member undergoing this buckling mode. It will also attempt to show that torsional-flexural buckling can be considered to be a feasible failure mode in some structural configurations. Also, this section will highlight some of the research that has previously been conducted into this type of buckling, as well as design methodologies on how to deal with it in practice.

2.3.1. Continuous elastic support

The problem was approached by Timoshenko and Gere [11] by looking at a column (with a general cross-section) which had continuous lateral and rotational restraints acting through some point of the body, which could be offset from the centroid. This can be seen in the diagram below.

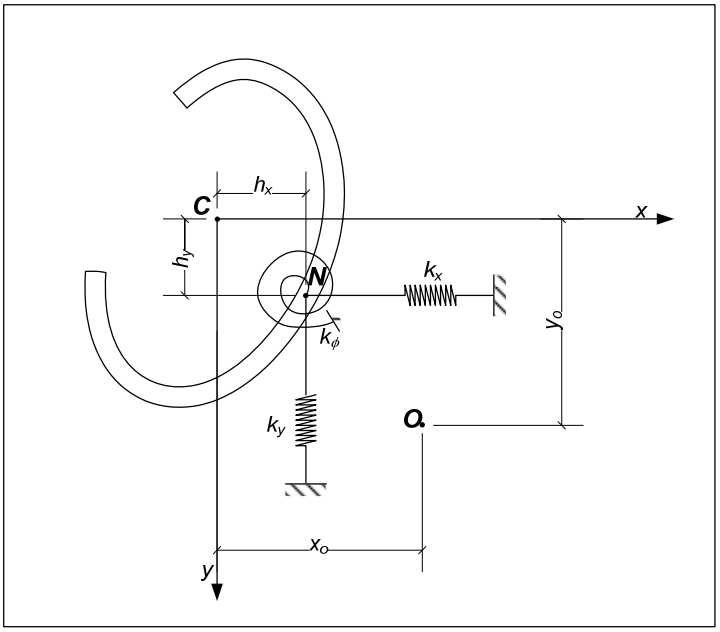

Figure 2.11 – Torsional-flexural buckling of a bar with continuous elastic supports [11]

The setting up of the equations and the method of solution are identical to those shown above in Section 2.1.2.2, however, due to the reactions acting through point *N* in the above figure the complexity of the differential equations is somewhat increased. For a detailed look at how the derivation is performed, the reader is referred to the text [11], as only the results will be presented here. The three simultaneous differential equations for the buckling of such a bar are presented below in the most general form:

$$EI_y u^{iv} + P(u'' + y_o\varphi'') + k_x\left[u + (y_o - h_y)\cdot\varphi\right] = 0$$
$$EI_x v^{iv} + P(v'' + x_o\varphi'') + k_y\left[v + (x_o - h_x)\cdot\varphi\right] = 0 \qquad (2.7)$$
$$C_1\varphi^{iv} - \left(C - \frac{I_o}{A}P\right)\cdot\varphi'' - P(x_o v'' - y_o u'') + k_x\left[u + (y_o - h_y)\cdot\varphi\right]\cdot(y_o - h_y) - k_y\left[v - (x_o - h_x)\cdot\varphi\right]\cdot(x_o - h_x) + k_\varphi\varphi = 0$$

These three equations can cater for any cross-sectional shape (shear centre removed from centroid – the ordinates x_o and y_o) and with the axis of support offset from, but parallel to, the longitudinal axis by any distance (the ordinates h_x and h_y). The authors look at a particular case of a bar with a prescribed axis of rotation in this case $k_x = k_y = \infty$. This agrees closely with a portal frame column (doubly symmetric) which is laterally supported by sheeting rails. In this case the column is forced to rotate about the axis through the sheeting rail attachment point. If this is the case, then the following terms will fall away from the above expressions:

$$x_o = y_o = h_x = 0;$$

Thus, the above simultaneous differential equations can be solved to determine the three respective solutions for the system. These solutions are shown below, with the top two equations being the well known flexural buckling equations for buckling about the strong and weak axis respectively, whilst the lower term is for the torsional-flexural buckling scenario.

$$P_{cr,x} = \frac{\pi^2\cdot E\cdot I_x}{L_x^{\,2}}; \qquad (2.6.a)$$
$$P_{cr,y} = \frac{\pi^2\cdot E\cdot I_y}{L_y^{\,2}}; \qquad (2.6.b)$$
$$P_{cr,z} = \frac{\left(C_1 + EI_y h_y^2\right)\cdot\left(n^2\pi^2/L_z^2\right) + C + k_\varphi\left(L_z^2/n^2\pi^2\right)}{h_y^2 + (I_o/A)}; \qquad (2.8)$$

Where:

$C_1 = E.C_w$;

C_w = Warping torsion constant (for I-sections) = $\int_0^E \omega_n^2 t\cdot ds = \frac{b^3 t(d')^2}{24}[m^6]$; (2.9)

$C = G.J$;

J = (for I-sections) = $\frac{2bt_f^2 + (h_w + t_f)\cdot t_w^2}{3}$; (2.10)

k_φ = rotational spring stiffness (will be dealt with in more detail later).

Thus, the torsional flexural buckling load can be expressed in a more general and well recognised form:

$$P_{cr,TF} = \frac{\left(C_w + I_y h_y^2\right)\cdot\left(n^2 E\pi^2/L_z^2\right) + GJ + k_\varphi\left(L_z^2/n^2\pi^2\right)}{h_y^2 + \overline{r_o^2}}; \qquad (2.8.a)$$

Where:

$$\overline{r_o^2} = r_x^2 + r_y^2 .$$

As stated previously, for a given situation, the lowest value of the critical load calculated from the above three expressions will govern. Thus, it is necessary to evaluate all three formulas' to ensure that the design load will be sufficient to prevent any type of buckling from occurring.

It must be noted that in calculating the torsional-flexural buckling load, $P_{cr,TF}$, several values of n need to be input and the lowest resulting load will be the critical one. This is done because the term n appears in both the numerator and the denominator, i.e. it is no longer a linear relationship between the critical load and the buckled configuration. This trial and error approach will vanish if the torsional spring stiffness is assumed to be zero.

The major drawback of these equations is the fact that the reaction forces (caused by k_x, k_y and k_φ) are assumed to be continuous over the full height of the column. In practice this is not so, as there are always discrete lateral and/or torsional restraints (the sheeting rails). For a case with only one lateral and torsional restraint at mid-height of the column, the validity of this equation becomes very questionable.

If k_φ = 0; (if we have no torsional restraint) then the critical load above reduces to the following equation:

$$P_{cr,TF} = \frac{\left(C_w + I_y h_y^2\right) \cdot \left(n^2 E\pi^2 / L_z^2\right) + GJ}{h_y^2 + \overline{r_o^2}}; \qquad (2.11)$$

This is a torsional-flexural buckling load about the enforced axis offset by a distance (h_y) from the centroid of the section, assuming that there is no torsional restraint acting at any point over the height of the column. The figure below is an explanatory figure, similar to Figure 2.6 which highlights the physical behaviour of the cross-section during torsional-flexural buckling about an offset axis:

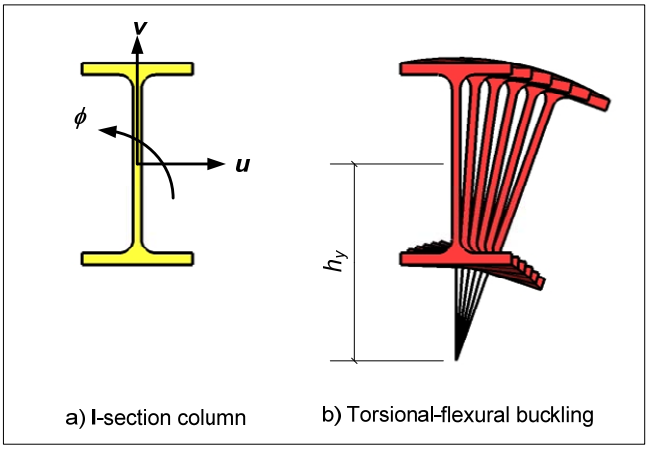

Figure 2.12 - Torsional-Flexural buckling configuration

2.3.2. Discrete lateral and torsional restraints

Dooley [12] published findings that are primarily focused on clarifying the major shortcoming, identified above, in the method proposed by Timoshenko and Gere [11]. To reiterate, this shortcoming is that the formulations are derived for the case of *continuous* rotational and lateral restraint. Dooley formulated expressions (using the energy principles) for the case of discrete lateral (rigid) and discrete rotational (elastic) restraints connected eccentrically onto a column. This can be seen below in Figure 2.13 and Figure 2.14 shown below, reproduced from the article.

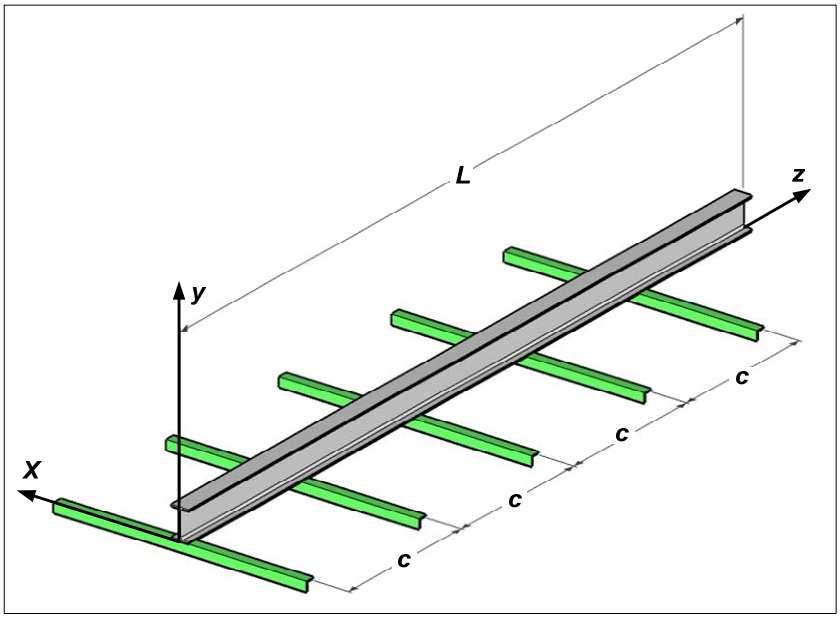

Figure 2.13 - Column with side rails [12]

Dooley showed that by calculating the energy stored by the column, for the case of discrete lateral restraints and for the case of continuous lateral restraints, that:

> "*The evident conclusion is that a column attached at discrete intervals to sheeting rails responds as if continuously attached to a foundation of uniform rotational stiffness*."

Dooley [12] proposed that the torsional-flexural buckling load could be calculated by the following formula; which takes into account the discreteness of the restraints. It can be seen that this equation is, for all practical purposes, identical to that proposed above by Timoshenko and Gere [11] (Equation 2.8.a).

$$P_{cr,TF} = \frac{1}{r_o^2}\left[\left(\frac{\pi}{\lambda}\right)^2 E \cdot \Gamma_o + GJ + \left(\frac{\lambda}{\pi}\right)^2 \frac{2K_s}{L} \sum_{p=1}^{m} \sin^2 \frac{p\pi c}{\lambda}\right] \qquad (2.12)$$

Where:

Γ_o = is the warping constant of the section about the axis of rotation;

$$\frac{2K_s}{L}\sum_{p=1}^{m}\sin^2\frac{p\pi c}{\lambda} = k_\varphi = \text{the torsional spring stiffness;} \qquad (2.13)$$

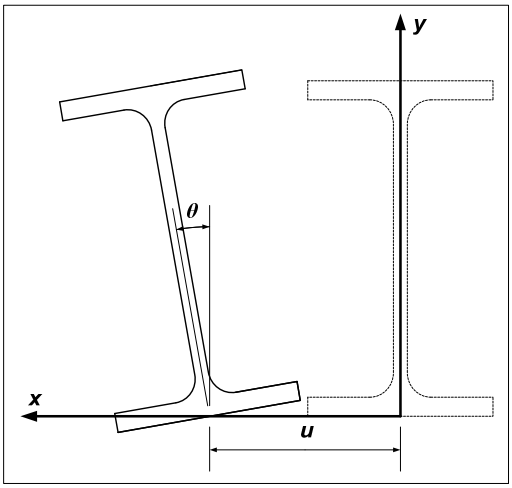

Figure 2.14 - Deflections of column [12]

This is a very useful conclusion, which allows one to use the formulation previously derived (Timoshenko and Gere [11]) even when a continuous restraint is not present.

Horne and Ajmani [13] extended the work done by Dooley [12] to include the effects of applying axial load in conjunction with bending moments about the strong axis of the column. These derivations are very applicable in practical situations, although for the goals of the current investigation purely axial loading on a column is to be studied.

The above equations that have been presented in this section have the potential to be very useful in design; however, all the above procedures require the designer to know the magnitude of the torsional restraint stiffness which is provided by the sheeting rails.

2.3.3. Stiffness of rotational restraints

In order to be able to exploit the advantages that arise from including torsional restraints in design of portal frame structures, it is imperative that designers have a method of quantifying the stiffness of the chosen torsional bracing system. The following sections will expound on how various people have approached the issue regarding how to calculate this stiffness. Furthermore, a moment resisting connection between the sheeting rail and the column, can lead to what can be described as a restoring rotational spring being present for rotation about the weak axis of the column. This too is explained and quantified below.

2.3.3.1. Stiffness of torsional restraints

As the column begins to twist, the sheeting rails will begin to bend about the strong axis (assuming a Cold Formed Lipped Channel cross-section). Thus, the torsional restraint that the sheeting rail can supply to the column is as a result of its flexural stiffness. Is that the only influence? Or are there more complicated measures that need to be addressed?

Dooley [12]

Dooley [12] states that the stiffness of the discrete torsional restraints, K_s, is made up of two component parts. Namely, the flexural stiffness of the sheeting rail, K_f, and the local stiffness of the column section against distortion under a concentrated torque at one flange, K_c.

As stated below, in Section 4.2.2, when a series of columns buckle, they will twist in alternate directions, so as to minimise the energy spent. This can be seen in Figure 4.9 further on in this report, which results in the sheeting rails bending in single curvature. The alternative would be for all the columns to twist in the same direction which is called double curvature. If the columns do twist in single curvature, the flexural stiffness of the sheeting rails can be given by:

$$K_{f,\sin gle} = \frac{2EI_{sr}}{L_{sr}} + \frac{2EI_{sr}}{L_{sr}} = \frac{4EI_{sr}}{L_{sr}} \qquad (2.14)$$

However, if the all the columns twist in the same direction, a situation of double curvature will develop in the sheeting rails, which changes the above to:

$$K_{f,double} = \frac{3EI_{sr}}{L_{sr}} + \frac{3EI_{sr}}{L_{sr}} = \frac{6EI_{sr}}{L_{sr}} \qquad (2.15)$$

The local stiffness of the column can be conservatively taken [12] to be:

$$K_c = \frac{GJ}{3D} \qquad (2.16)$$

Finally, Dooley [12] proposes that these two stiffness terms are combined in the following way to arrive at the effective stiffness of the elastic torsional restraint:

$$\frac{1}{K_s} = \frac{1}{K_f} + \frac{1}{K_c} \qquad (2.17)$$

Dooley further stated that there may be many other factors that could influence the effective stiffness against rotation and he suggested that experimental research was necessary to improve the accuracy of the expressions above.

Horne and Ajmani [13]

According to Horne and Ajmani [13] the torsional restraint that can be afforded by the sheeting rails depends on:

"(1) the flexibility of the side rails,
(2) the moment-rotation characteristic of the joint between side-rails and column and
(3) the local deformation of the column, since the restraint is transmitted through one flange only."

The first and third influencing item listed above are the same as those used by Dooley [12] in his method, however, the second item is unmentioned before. Unfortunately, no attention is spent on explaining how one would find out more information about the moment rotation characteristics of such a connection. This implies that an experimental study of typical connections is needed.

In a follow-up article, Horne and Ajmani [14] state the following:

> *"Standard connections between side-rails and the columns are not markedly moment-resistant. Moreover, as the connections are on one flange of the column only, these may lead to local deformation of the column flange and web. Unless the connections are moment-resistant and the local deformation of the column is prevented, it is safer to ignore the torsional restraint of the side-rails."*

Helwig and Yura [15]

More recently, the question of torsional bracing on a column was investigated by Helwig and Yura [15]. These authors state that a connection must be provided between the column and sheeting rail that will cause the sheeting rails to bend if the column twists. Furthermore, they state that the sheeting rail will thus bend in single curvature, similar to what Dooley [12] proposed. Helwig and Yura [15] consider this flexural stiffness to be the sole component of the stiffness of the torsional restraint, provided that a connection which can meet the strength requirements proposed in their article [15] is supplied to the column. Such typical connections that are proposed are shown below in Figure 2.15. These connections will transfer the bending moments to the column and will restrict cross-sectional

distortions, thus satisfying the other criterion which was proposed by Dooley [12] as well as Horne and Ajmani [13] for the torsional restraint stiffness.

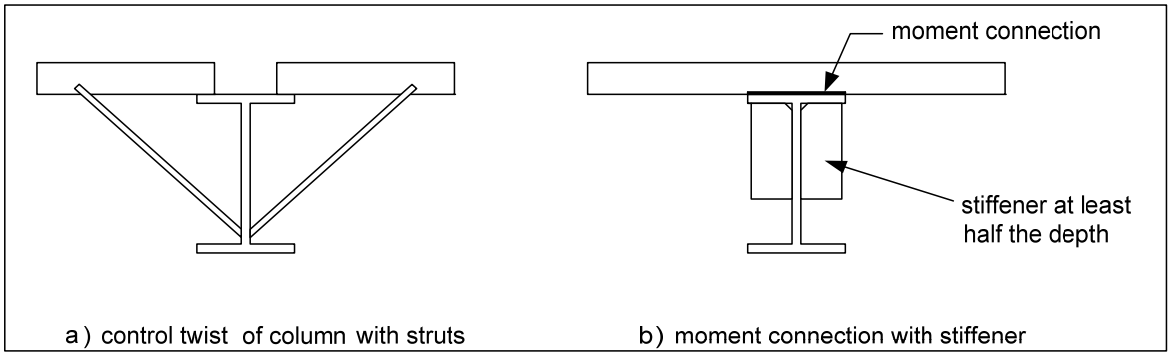

Figure 2.15 - Recommended torsional bracing details [15]

2.3.3.2. Stiffness of the rotational restraint

Up until this point the focus has been on the torsional rotation of the column, about some axis which has been offset by a distance (h_y) from the centroid of the cross-section. However, that is not the only rotation that the column undergoes. Due to the fact that we expect the buckled configuration of the column to have a largely flexural component (either coupled with torsional displacements or not), the sheeting rails are forced to bend about their weak axis as well. This is illustrated in Figure 2.16 below. The image below is reproduced from the dissertation of de Villiers Hugo [9]. The concept being explained can be called the restoring moment concept, which is almost identical to what happens with the torsional bracing of the column just in a different plane.

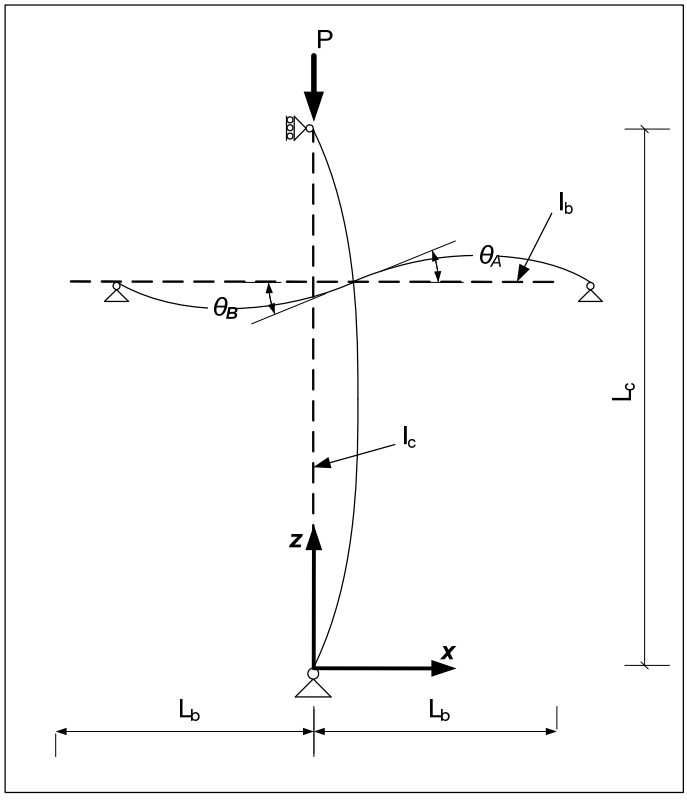

Figure 2.16 - Restoring moment concept [9]

As the column is loaded axially and deflects laterally the slope of the column changes accordingly. If a moment resisting connection is present, then the sheeting rail attached at a certain point along the column will be forced to rotate as well.

As the column buckles it exerts a moment (M_r) on the sheeting rail. The rotation of the joint will continue until it is balanced by the moments at either end of the sheeting rail. This develops a situation of double curvature in the sheeting rail. Thus, from the slope deflection method, de Villiers Hugo [9] summarised the above as:

$$M_r = \frac{3E_bI_b}{L_b}(\theta_A) + \frac{3E_bI_b}{L_b}(\theta_A)$$
$$\frac{M_r}{\theta_A} = C_A = \frac{6E_bI_b}{L_b} \qquad (2.18)$$
$$\therefore M_r = C_A \cdot \theta_A$$

Where:

M_r = restraining moment;

C_A = stiffness of thee sheeting rail;

θ_A = the angle of rotation at the height of the beam-column connection;

L_b = L_{sr} = Length of the sheeting rails;

This moment always acts to restrain the column. The connection is seldom very efficient, and thus de Villiers Hugo [9] proposes a method of calculating the effective rotational spring stiffness, which takes into account the characteristics of the cleat (most often taken as an angle cleat) to reduce the stiffness to a more realistic value.

Therefore, one can see that when a continuous sheeting rail is connected (via a moment transferring connection) to the column, that the sheeting rail will be forced to bend about both its weak axis (due to the flexural nature of the buckling) and its strong axis (due to the twisting of the cross-section), i.e. the sheeting rail will undergo biaxial bending.

2.3.4. Experimental verification of torsional-flexural buckling

Extensive experimental work investigating the failure of columns which are laterally supported on one flange was conducted by Horne and Ajmani [16] in the early 1970's. These investigations were aimed at verifying the design formulas proposed in the earlier articles ([13] and [14]) mentioned previously. Unfortunately, the method investigated by Horne and Ajmani dealt with the loading combination of both axial load and strong axis bending moments. As such, the results found could not be directly compared with the outcomes of the current investigation.

Torsional-flexural buckling of eccentrically restrained I-section columns which have been subjected to axial loads was experimentally studied more recently by Gelderblom, van Rensburg and Dekker [17]. In this investigation the authors neglected any torsional restraint that can be afforded to the column by the sheeting rails. The critical loads of these columns was thus determined using Equation 2.11. The experimental set-up is shown below in Figure 2.17, with both flanges of the column supported laterally at either end of the column and only one flange laterally supported at any intermediate point as determined by the member being tested.

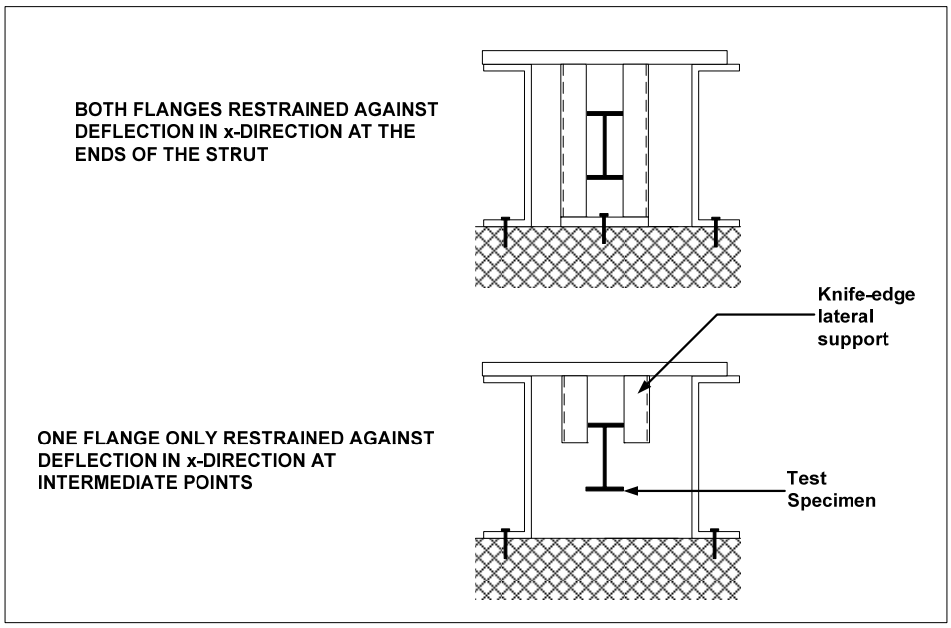

Figure 2.17 - Test set-up from Gelderblom, et al. [17]

The results from the experimental tests are also reproduced below in Figure 2.18. It can be seen that the Equation 2.11 used to calculate the torsional-flexural buckling capacity (Timoshenko and Gere [11]) does accurately predict the buckling capacity of eccentrically restrained columns. Remembering, of course, that the positive effects of any torsional restraint were been neglected in their study.

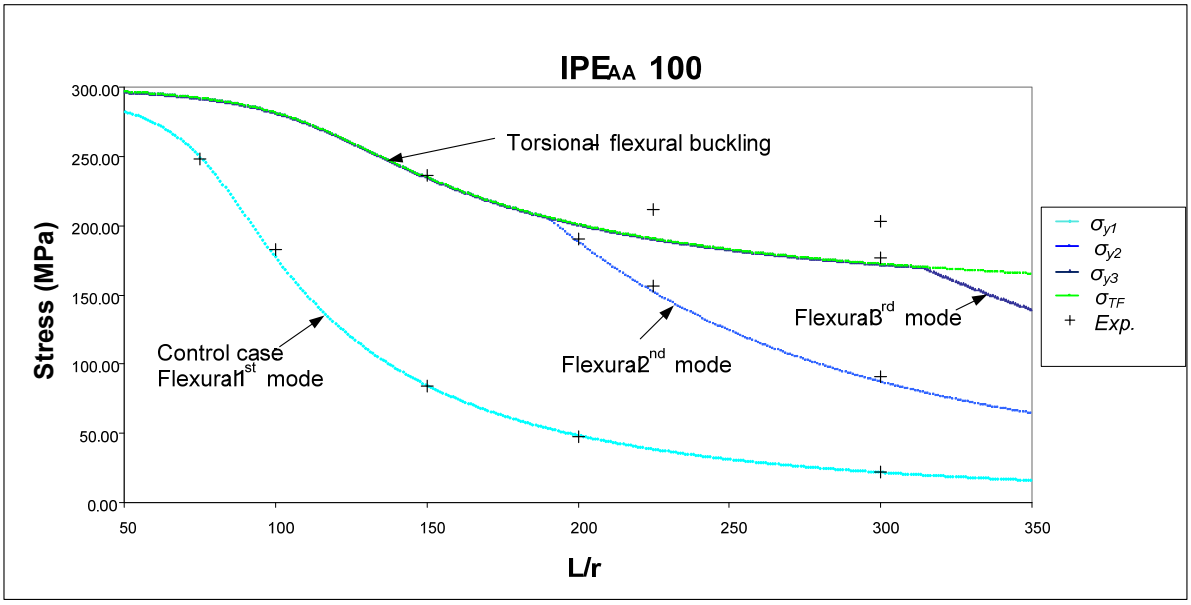

Figure 2.18 - Design curves and experimental data for IPE$_{AA}$ 100 [17]

The main conclusions drawn by Gelderblom et al [17] are that if a designer is unaware of the torsional-flexural buckling failure mode, and thus provides eccentric restraints (without torsional stiffness), that the possibility is very high that the column will not fail in a flexural mode, but will fail in a lower torsional-flexural mode. This could happen, for example, if discontinuous sheeting rails are used as a part of the lateral bracing system.

2.3.5. Strength and stiffness requirements for torsional braces

Helwig and Yura [15] performed research that was aimed at providing guidelines for the strength and stiffness criteria to be used in the design of torsional bracing members. It was noticed by the authors that inadequate attention is paid to the torsional bracing of eccentrically restrained columns in practice. Sensitivity studies were carried out on many parameters using a finite-element investigation. The finite-element model was set-up by using 8-node shell elements to model the column. The sheeting rail (torsional restraint) was taken as an angle section (also modelled by shells).

In order to design for the torsional-flexural buckling of columns it is necessary to have formula's which are accurate and conservative when calculating the buckling loads. The authors [15] begin with the theoretical solution (Equation 2.8.a), already encountered above in the work of Timoshenko and Gere [11], Dooley [12] and Horne and Ajmani [13], which is reproduced below. It must be noted that the slightly different form of the equation is simply an alternative method of displaying the term containing the warping torsional constant C_w, (**N.B**. slightly different notation than has been seen thus far is used for some of the terms in this equation).

$$P_{cr,TF} = \frac{1}{r_s^2}\left[GJ + \frac{P_o n_w^2\left(d^2 + 4a^2\right)}{4} + \frac{\beta_T}{s}\left(\frac{L}{n_w \pi}\right)^2\right] \leq P_{cr,y} \qquad (2.8.b)$$

Where:

$r_s^2 = r_x^2 + r_y^2 + a^2$

β_T = stiffness of one torsional brace;

n_w = number of half-waves in the buckled shape;

P_o = weak axis flexural buckling over full length of the column;

s = spacing of the sheeting rails;

d = depth of the cross sections;

a = offset to the point of lateral restraint (centroid of sheeting rail).

As stated previously, the buckled load must be calculated for several values of n_w and then the lowest of all these loads is taken as the critical load. In order to avoid this trial and error approach in the calculations of $P_{cr,TF}$ the following equation is proposed by the authors:

$$P_{cr,TF} = \frac{1}{r_s^2}\left[GJ + P_o\left(\frac{d^2}{4} + a^2\right) + \sqrt{\frac{4\beta_T E I_y}{s}\left(\frac{d^2}{4} + a^2\right)}\right] \qquad (2.19)$$

This formula is preferable to Equation 2.8.b) above, because the value obtained is a good indication of what the critical load will be, without any trial and error. However, the results of Equation 2.20 were seen to be slightly unconservative compared to the results of Equation 2.8.b between the changes in mode shape, although the results were exactly the same at the points of mode change (see Figure

2.19 below for clarity on this point). This is due to the fact that Equation 2.19 is a polynomial approximation to the step-wise linear curve produced from Equation 2.8.b.

The authors proceeded to obtain conservative estimates of the critical load by ignoring the *GJ* term in Equation 2.19. This then led to the authors proposing Equation 2.20, which was shown to always produce conservative values of the torsional-flexural buckling capacity.

$$P_{cr,TF} = \frac{1}{r_s^2}\left[P_o\left(\frac{d^2}{4}+a^2\right)+\sqrt{\frac{4n_b\beta_T EI_y}{l}\left(\frac{d^2}{4}+a^2\right)}\right] \qquad (2.20)$$

Another change between Equation 2.19 and Equation 2.20 is the method of converting the discrete torsional bracing to continuous bracing. This change was made because it was seen to improve the results when only a few torsional braces were present over the length of a column.

The three formulas which have been mentioned in this section can be visualised by considering the following example. A 2.4m high IPE 100 column, with torsional braces at 0.6m, 1.2m and 1.8m along the length of the column. In addition to this, one of the flanges is supported laterally at each of the torsional brace points. In Figure 2.19 below the Torsional-flexural critical load is plotted for varying values of the torsional bracing stiffness.

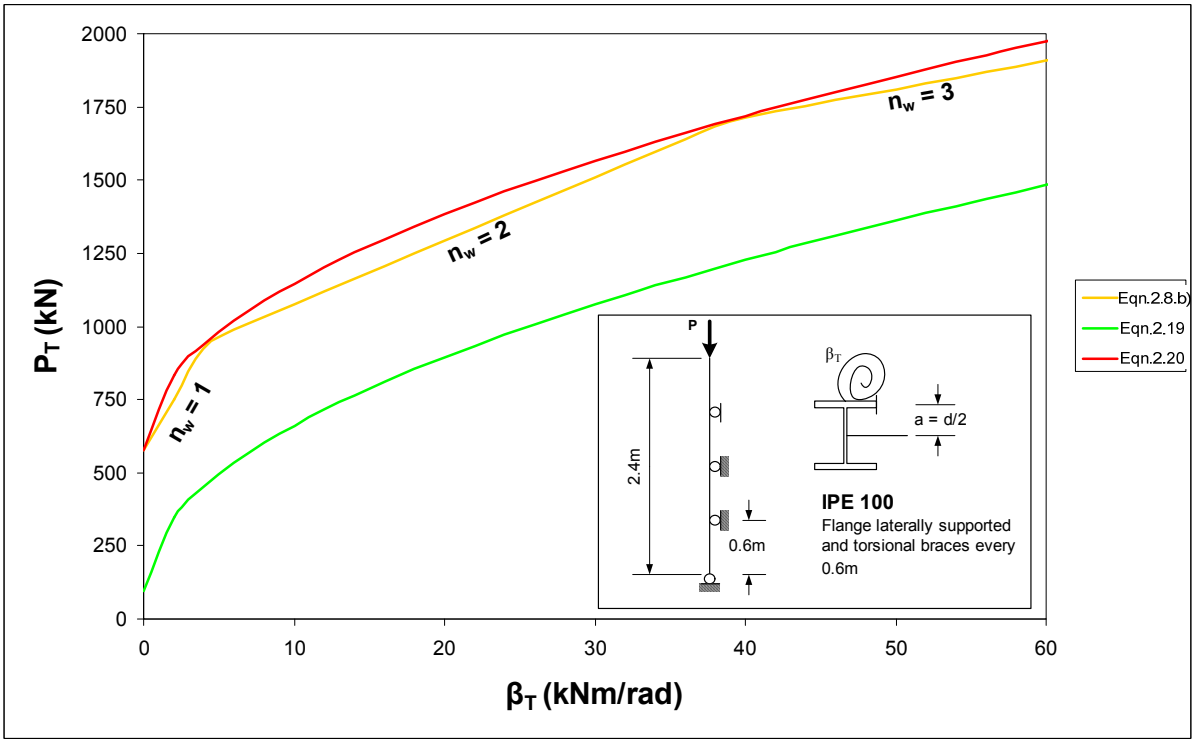

Figure 2.19 - Approximate solutions for discrete torsional braces [15]

If the applied load *P*, is substituted in for $P_{cr,TF}$ then the ideal torsional bracing stiffness, $\beta_{T,ideal}$, can be determined from Equation 2.20. However, the authors found from Eigenvalue analyses, that a value of

the torsional brace stiffness that is somewhat larger than the ideal stiffness is required to control brace forces and excessive deformations. They propose a magnification factor which must be applied to the ideal value to scale it up to the value, which is needed to limit the twist in the column to a value of twice the initial twist θ_o. This magnification factor is shown below:

$$A = 4 - \frac{a}{d} \geq 2 \qquad (2.21)$$

This factor is dependant on the distance of the offset of the torsional brace from the centroid of the column.

The formulas proposed are all based on the assumption that the connections between the sheeting rail and the column are capable of transferring the required bending moments. These connections must limit cross-sectional distortion at the point of connection. Typical connections that are proposed by the authors are shown above in Figure 2.15. The justification for these connections can be summed up by the following excerpt:

> *"The requirements for moment connections for stability bracing are different than moment connections in rigid frames. In rigid frames, the strength is usually based on developing inelastic bending capacity of members and therefore requires all elements of the cross section to be connected. The moments that are generated in bracing members are often small and can be developed by relatively simple connections."*

2.3.6. Summary

As previously stated, portal frame construction often utilises doubly-symmetric sections as columns. Secondary members, such as sheeting rails and cladding, are attached to only the outside flanges of these column sections. If a designer wishes to include these eccentric secondary members into the bracing system of the structure, they need to be aware of the consequences of such a decision. By providing eccentric lateral and/or torsional braces to the column, one enforces an offset axis of rotation to exist for the cross-section and this may have the consequence of causing the carrying capacity of the column to be significantly lower than that calculated by the flexural capacity. In cases where there is no torsional restraint afforded to the column but there is a lateral restraint, say, at mid-height of the column, then the possibility of the torsional-flexure buckling being critical is greatly increased.

Please note that in the following paragraphs the various notations and symbols used by the authors' above have been standardised into the notation system that will be used for the remainder of this investigation.

2.3.6.1. Calculation of the critical torsional-flexural capacity

Timoshenko and Gere [11] found solutions for the case when a continuous torsional brace was present over the full length of the column. This formula, limited to the specific case of when the offset axis of restraint lies a distance (h_y) from the centroid of the column, is presented below:

$$P_{cr,TF} = \frac{\left(C_w + I_y h_y^2\right) \cdot \left(n^2 E\pi^2 / L_z^2\right) + GJ + k_\varphi \left(L_z^2 / n^2 \pi^2\right)}{h_y^2 + \overline{r_o^2}}; \qquad (2.8.a)$$

The above design equation (2.8.a) is difficult to implement in practical situations due to the fact that a continuous torsional restraint is seldom present for most cases of portal frame structures. This was remedied by Dooley [12] when he determined, using the energy equations, that a column attached to discrete torsional braces over the length of the column behaves as if continuously attached to a foundation of uniform rotational stiffness. This means that the above equation can confidently be used in design. Dooley found that a continuous rotational restraint could be approximated from the discrete torsional restraint by using the following expression:

$$k_\varphi = \frac{K_T}{s} \qquad (2.22)$$

Where:

K_T = discrete torsional restraint stiffness;

s = distance between sheeting rails.

After conducting a Finite element analysis parameter study, Helwig and Yura [15] found the above equation to yield unconservative results (in relation to the model investigated). In order to rectify this, they proposed a design equation (which neglects the *GJ* term in the previous formulas) which will always yield conservative results. This equation is shown below. The first term in square parentheses

below is an alternate manner of representing the term containing the warping constant from the original equation, whilst the term that contains the torsional restraint term has been modified slightly to make the solutions more conservative for any number of discrete braces.

$$P_{cr,TF} = \frac{1}{\left(h_y^2 + \overline{r_o^2}\right)}\left[P_{cr,y1}\left(\frac{h^2}{4} + h_y^2\right) + \sqrt{\frac{4n_b K_T E I_y}{L}\left(\frac{h^2}{4} + h_y^2\right)}\right] \qquad (2.20)$$

2.3.6.2. Torsional bracing stiffness

Dooley [12] gives guidance about the method of calculating the torsional stiffness of a discrete brace. He states that the torsional brace stiffness is a combination of the flexural stiffness of the sheeting rail and the torsional stiffness of the cross-section itself.

$$\frac{1}{K_T} = \frac{1}{K_f} + \frac{1}{K_c}; \qquad (2.17)$$

With:

$$K_f = \frac{kEI_{sr}}{L_{sr}} \quad (2.14 \text{ or } 2.15) \quad \text{and} \quad K_c = \frac{GJ}{3h} \qquad (2.16)$$

The flexural stiffness of the sheeting rail will have a factor of $k = 6$, when the sheeting rail bends in double curvature; and $k = 4$, when the sheeting rail bends in single curvature.

Helwig and Yura [15] state that the torsional brace stiffness is dependant only upon the flexural stiffness of the sheeting rails, provided that suitable connections are used. These connections are designed to specifically limit the cross-sectional deformation thus eliminating it from the above expression. Furthermore, they state that the k factor to use should be taken as $k = 2$.

2.4. A study of Codes of Practice

As shown above, the phenomenon of an eccentrically restrained doubly symmetric column buckling in a torsional-flexural mode has been studied thoroughly over the past fifty years. This section of the report is a detailed look at several structural steel design codes from various countries. The aim of this section is twofold, firstly to determine if the design codes cater for such eccentric restraint, and secondly, if they do, how it is included in the design calculations.

The primary aim of this study of these codes of practice is to investigate the design of the individual compression members to resist buckling, but will also be expanded to include any relevant provisions made in the respective code dealing with stability and bracing systems.

2.4.1. SANS 10162-1: 2005 [7]

2.4.1.1. Stability and Bracing systems

Clause 9 of this code deals with the Stability of structures and members. This clause provides guidance about the functions and design of both structural systems (as a whole) and bracing systems (for individual members/elements) which ensure stability.

Structural stability is ensured, according to Clause 9.1, "*when the structural system is adequate to:*

a) resist the forces caused by factored loads,
b) transfer the factored loads to the foundations,
c) transfer forces from walls, floors or roofs, acting as shear-resisting elements or diaphragms to adjacent lateral-load resisting elements, and
d) resist torsional effects."

Bracing systems for columns must provide lateral support at the required positions, by being strong enough to resist the forces generated at those points and by limiting the deflections to acceptable levels (Clause 9.2.4). The bracing system must also prevent twisting and lateral displacements at points of support, **unless otherwise accounted for in design** (Clause 9.2.5).

When using a simplified analysis (Clause 9.2.6) the code specifies a strength requirement for the bracing system, such that it should be able to cope with a small design force. The magnitude of which is 0.02 times the factored compressive force, in the element or member being braced and that it must be taken to be perpendicular to the longitudinal axis of the member in the plane of buckling.

2.4.1.2. Axial compressive resistance

In order to limit the flexibility of compression members, the code provides a maximum slenderness ratio of 200. The slenderness ratio is the ratio of the effective length of the column, ***K·L,*** to the corresponding radius of gyration (Clause 10.4).

Structural elements used in construction need to be classified as either Class 1, 2, 3 or 4 sections (see Clause 11.1.1 for more information on the classification categories). The classification of a section is performed by looking at the width-thickness ratios of each element of the cross-section. For compression elements maximum width-thickness ratios are provided in Table 3 of the code. If a member of a given cross-section has a width-thickness ratio larger than the maximum stipulated value, then the cross-section is said to be Class 4. Class 4 cross-sections use a reduced cross-sectional area when computing factored axial compressive resistance.

The factored compressive resistance of a given member is determined (Clause 13.3) by the following expression:

$$C_r = \varphi \cdot A \cdot f_y \left(1 + \lambda^{2n}\right)^{-1/n} \qquad (2.23)$$

Where:

n = 1.34; for hot-rolled structural steel

(Because it is a single curvature parameter approach);

$\lambda = \sqrt{\frac{f_y}{f_e}}$ = non-dimensional slenderness ratio; (2.24)

Where f_e is given by the following expressions:

a) Doubly symmetric sections: the least of $\boldsymbol{f_{ex}}$ or $\boldsymbol{f_{ey}}$.

b) Doubly symmetric (sections which may be governed by torsional flexural buckling): the least of $\boldsymbol{f_{ex}}$, $\boldsymbol{f_{ey}}$ or $\boldsymbol{f_{ez}}$.

c) Singly symmetric sections (y-axis taken as the axis of symmetry): the lesser of $\boldsymbol{f_{ex}}$ and $\boldsymbol{f_{eyz}}$;

d) Asymmetric sections: $\boldsymbol{f_e}$ is the smallest root of:

$$\left(f_e - f_{ex}\right) \cdot \left(f_e - f_{ey}\right) \cdot \left(f_e - f_{ez}\right) - f_e^2 \cdot \left(f_e - f_{ey}\right) \cdot \left(\frac{x_o}{r_o}\right)^2 - f_e^2 \cdot \left(f_e - f_{ex}\right) \cdot \left(\frac{y_o}{r_o}\right)^2 = 0 \qquad (2.25)$$

Where:

$$f_{ex} = \frac{\pi^2 \cdot E}{\left(\frac{K_x \cdot L_x}{r_x}\right)^2} \quad ; \qquad (2.26)$$

$$f_{ey} = \frac{\pi^2 \cdot E}{\left(\frac{K_y \cdot L_y}{r_y}\right)^2} \; ; \qquad (2.27)$$

$$f_{ez} = \left(\frac{\pi^2 \cdot E \cdot C_w}{K_z^2 \cdot L_z^2} + G \cdot J \right) \frac{1}{A \cdot \overline{r_o^2}} \quad ; \tag{2.28}$$

$$f_{eyz} = \frac{f_{ey} + f_{ez}}{2\Omega} \left(1 - \sqrt{1 - \frac{4 \cdot f_{ey} \cdot f_{ez} \cdot \Omega}{\left(f_{ey} + f_{ez} \right)^2}} \right); \tag{2.29}$$

With the terms:

$$\overline{r_o^2} = x_o^2 + y_o^2 + r_x^2 + r_y^2 ;$$

$$\Omega = 1 - \left(\frac{x_o^2 + y_o^2}{\overline{r_o^2}} \right).$$

2.4.2. BS EN 1993-1-1:2005 [6]

As a preamble to the study of the Eurocode method, it is necessary to note that the convention of naming the axes of a structural member is different than that commonly used in South Africa. The differences can be seen in Figure 2.20 below. In the South African context, the longitudinal axis is the *z*- axis, whilst in the Eurocode method, the longitudinal axis is the *x*- axis.

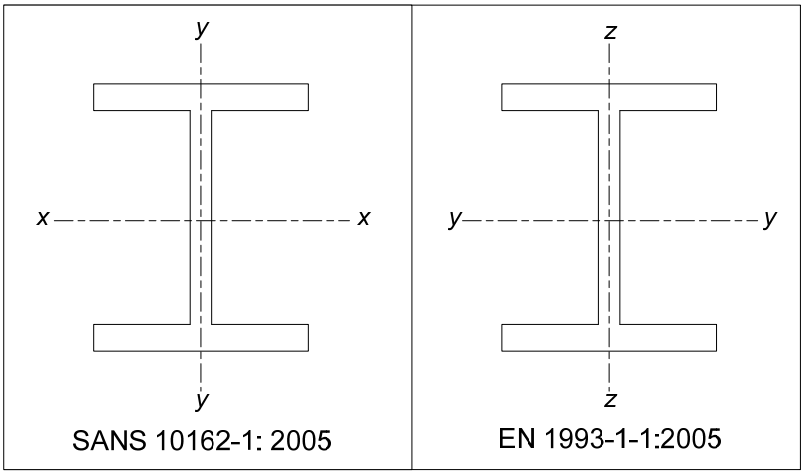

Figure 2.20 - Axes labelling system differences

2.4.2.1. Axial compressive resistance

The Eurocode enforces a check on the compressive resistance of the cross-section in terms of the yielding capacity strength, as well as checking the buckling resistance of the members under investigation. For the scope of this study, it was sufficient to consider the Buckling resistance of members (Clause 6.3) only.

The ultimate check used here is to check whether the factored applied load is less than or equal to the design buckling resistance, or:

$$\frac{N_{Ed}}{N_{b,Rd}} \leq 1.0 \qquad (2.30)$$

With:

N_{Ed} = design value of the compression force;

$N_{b,Rd}$ = design buckling resistance;

$$N_{b,Rd} = \frac{\chi \cdot A \cdot f_y}{\gamma_{m1}}; \qquad (2.31)$$

The term χ is determined for the given cross-section from the relevant buckling curve (depending upon section classification and buckling plane) and the non-dimensional slenderness ratio of the member, $\bar{\lambda}$.

$$\chi = \frac{1}{\Phi + \sqrt{\Phi^2 - \bar{\lambda}^2}}; \quad \text{but } \chi \leq 1.0 \qquad (2.32)$$

With:

$$\Phi = 0.5\left[1 + \alpha \cdot \left(\bar{\lambda}^2 - 0.2\right) + \bar{\lambda}^2\right] \quad ; \qquad (2.33)$$

$\bar{\lambda}$ = non-dimensional slenderness = $\sqrt{\frac{A \cdot f_y}{N_{cr}}}$; (2.34)

α = imperfection factor (determined from Table 6.1 and Table 6.2 in the code);

N_{cr} = elastic critical force;

The clause then highlights what the slenderness ratio should be taken as, firstly for flexural buckling, and secondly for torsional or torsional flexural buckling.

The slenderness ratio to be used for flexural buckling can alternatively be written as follows:

$$\bar{\lambda} = \sqrt{\frac{A \cdot f_y}{N_{cr}}} = \frac{L_{cr}}{i} \cdot \frac{1}{\lambda_1} \quad ; \qquad (2.35)$$

Where:

L_{cr} = the buckling length in the plane considered;

i = the radius of gyration in the plane being considered;

$$\lambda_1 = \pi\sqrt{\frac{E}{f_y}} \quad ; \qquad (2.36)$$

The slenderness ratio to be used in the case of torsional and/or torsional-flexural buckling should be:

$$\bar{\lambda} = \sqrt{\frac{A \cdot f_y}{N_{cr}}} \quad ; \qquad (2.37)$$

Where:

$N_{cr} = N_{cr,TF}$ but, $N_{cr} < N_{cr,T}$;

With:

$N_{cr,TF}$ = elastic torsional-flexural buckling force;

$N_{cr,T}$ = elastic torsional buckling force;

The code does not propose formulas or a method to determine either the torsional or the torsional-flexural buckling force. However, Bureau [18] proposes the same formulas that were put forward in Timoshenko and Gere [11] as the correct torsional critical load. Bureau [18] does state that for a designer to use the torsional critical load, both flanges of doubly symmetric I- and H- sections need to be supported laterally. The case of only a single flange being supported laterally is only specifically mentioned in Appendix BB.3 and this will be discussed below. The torsional-flexural critical load proposed [18] is to be utilised for cross-sections on which the shear centre and the centroid do not coincide. Sections that match this criterion do not fit into the scope of this study.

The work performed by Horne and Ajmani ([13], [14] and [16]) constitutes the theoretical background for **Appendix BB.3 - Stable lengths of segment containing plastic hinges for out-of-plane buckling.** This Appendix is very informative, but does not appear to be directly related to the topic at hand at first glance. However, at a closer inspection it was noticed that in the calculation of the term C_m (which is a modification factor for a linear moment gradient) the following formula is present:

$$N_{crT} = \frac{1}{i_s^2}\left(\frac{\pi^2 E I_z a^2}{L_t^2} + \frac{\pi^2 E I_w}{L_t^2} + G I_t\right) \qquad (2.38)$$

Where:

N_{crT} is the elastic critical torsional buckling force for an I-section between restraints to both flanges at a spacing of L_t with intermediate lateral restraints to the tension flange;

$i_s^2 = i_y^2 + i_z^2 + a^2$;

a is the distance between the centroid of the member and the centroid of the restraining members such as purlins restraining rafters.

This formula is identical to that proposed above named Equation 2.11, which was proposed by Timoshenko and Gere [11]. This formula is hidden away, and not easily accessible. It is only referred to when plastic design is to be performed, which could easily cause it to be overlooked.

2.4.3. ANSI AISC 360-05 [20]

2.4.3.1. Axial compression resistance

The limiting slenderness ratio stated by the code is the same as that in SANS 10162 [7] which is 200, however this code states that the slenderness ratio should preferably not exceed 200. This means that this limit is actually a guideline, and is not enforced.

The requirements of AISC 360 regarding buckling of members are laid out in Clause C3 and C4, for flexural and torsional buckling respectively.

The nominal compressive strength of a column P_n is determined based on the limit state of flexural buckling. It is determined by the following:

$$P_n = F_{cr} \cdot A_g \qquad (2.39)$$

Where the critical buckling stress F_{cr} is determined as follows:

(a) When $\frac{KL}{r} \leq 4.71\sqrt{\frac{E}{F_y}}$ (or $F_e \geq 0.44F_y$)

$$F_{cr} = \left[0.658^{\frac{F_y}{F_e}}\right]F_y \qquad (2.40)$$

(b) When $\frac{KL}{r} > 4.71\sqrt{\frac{E}{F_y}}$ (or $F_e < 0.44F_y$)

$$F_{cr} = 0.877F_e \qquad (2.41)$$

Where the elastic critical stress is given by the following:

For flexural buckling: $$F_e = \frac{\pi^2 E}{\left(\frac{KL}{r}\right)^2}; \qquad (2.42)$$

And for torsional buckling: $$F_e = \left[\frac{\pi^2 E C_w}{(K_z L)^2} + GJ\right]\frac{1}{I_x + I_y}. \qquad (2.43)$$

2.4.4. BS 5950-1:2000 [18]

In addition to the normal flexural buckling checks provided in Section 4.7, BS 5950 [18] provides a method for checking the out-of-plane stability of doubly-symmetric members which are laterally supported on only one flange in Annex G. In an effort to be concise, and remain focussed on the topic at hand, only the method in Annex G will be discussed.

For members with a uniform cross-section the relevant check for lateral buckling resistance is G.2.1. In this method the following criterion must be satisfied:

$$\frac{F_c}{P_c} + \frac{m_t M_x}{M_b} \leq 1.0 \qquad (2.44)$$

Where:

- F_c is the axial compression;
- M_b is the buckling resistance moment from **4.3.6** for an equivalent slenderness λ_{TB}, see **G.2.4**;
- M_x is the maximum moment about the major axis;
- m_t is the equivalent uniform moment factor for restrained buckling, see **G.4.2**;
- P_c is the compression resistance from **4.7.4** for a slenderness λ_{TC}, see**G.2.3** from the relevant design curve;

Since the scope of this investigation deals with the determination of the compression resistance only the term λ_{TC} will be discussed from **G.2.3.** This term is used to calculate P_c which is analogous to C_r from SANS 10162 [7].

$$\lambda_{TC} = y\lambda \qquad (2.45)$$

In which:

$$y = \left[\frac{1 + (2a/h_s)^2}{1 + (2a/h_s)^2 + 0.05(\lambda/x)^2} \right]^{0.5}; \qquad (2.46)$$

$$\lambda = L_y / r_y \qquad (2.47)$$

Where

- a is the distance between the reference axis and the axis of restraint;
- h_s is the distance between the shear centres of the flanges;
- L_y is the length of the segment;
- x = D / T;
- D is the depth of the cross-section;
- T is the thickness of the flanges.

The value of p_c is the determined from Table 24 by using λ_{TC} and the relevant steel grade and design strength. The value for P_c is thus:

$$P_c = A_g p_c \qquad (2.48)$$

Where

A_g is the gross cross-sectional area.

The values from Table 24 were calculated using the Perry-Robertson approach, the formulas for this method are provided in **Annex C**. The background theory utilised for this approach is consistent with the theoretical solution found by Timoshenko and Gere [11], and then the inelastic behaviour is dealt with by the use of the Perry-Robertson approach.

It is also interesting to note that Clause 4.7.1.2 states that the bracing force that bracing systems need to be designed for must not be less than **1.0%** (this is less than SANS 10162 [7] which states a value of **2.0%**) of the axial force in the member, as well as being able to transmit this force to an adjacent point of positional restraint.

No mention is made of pure torsional buckling, as is done in other design codes.

2.4.5. Summary of design code provisions for buckling

Although a limited number of design codes were investigated it seems likely that the general trends can be ascertained. The general procedure when dealing with column buckling can either be handled using the Perry-Robertson approach, or alternatively the approach which uses a single curvature parameter to describe buckling. Specific mention of the case where there is an eccentrically restrained doubly-symmetric column under load was found in explicitly BS 5950 [18] and in an oblique manner in EN 1993 [6].

It is troubling to note that more specific attention is not drawn to this phenomenon in all design codes. There does, however, appear to be a simple manner of introducing the torsional-flexural buckling capacity of eccentrically restrained I- sections into design codes in which it is not mentioned. This will be outlined below.

Since the SANS 10162[7], EN 1993[6] and ANSI[20] codes all propose the same formulation to determine the torsional buckling stress it seems that a designer can simply substitute the torsional buckling stress formulation with the more relevant formulation which includes eccentricity in lateral supports.
For instance, in the SANS notation:

$$f_{ez} = \left(\frac{\pi^2 \cdot E \cdot C_w}{K_z^2 \cdot L_z^2} + G \cdot J \right) \frac{1}{A \cdot \overline{r_o^2}} \tag{2.30}$$

From the code can be substituted by the following expression for torsional-flexural buckling:

$$f_{e,TF} = \left(\frac{\pi^2 \cdot E \cdot \left(C_w + I_y h_y^2 \right)}{K_z^2 \cdot L_z^2} + G \cdot J \right) \frac{1}{A \cdot \left(\overline{r_o^2} + h_y^2 \right)}. \tag{2.49}$$

This would allow designers to use a method which is very similar to that used in BS 5950[18]. It would afford designers a sense of confidence and understanding of the true behaviour of columns as they behave in a given structure when an eccentric restraint is provided in the design, by ensuring that all the possible failure modes have actually been checked.

3. System Definition and Behaviour

To investigate the feasibility of including the sheeting rails in the lateral bracing system it was necessary to perform a number of buckling simulations upon a system of columns, which are connected together by sheeting rails. At this stage it is not essential to deal with exact values, the investigation is aimed more at obtaining an understanding of how this series of interconnected columns will behave under a purely axial load. With that aim in mind, it was decided that a fictitious generic portal frame structural system would be created and then be simplified to allow an analysis in two-dimensional space.

Just prior to making this simplification into two-dimensions, there will be a brief description of the typical load patterns for which a portal frame column is designed. This section serves the purpose of detailing the actual, realistic physical behaviour of a portal frame column, as well as explaining the limitation of the scope of this investigation, which is to be focussed solely on axial loads.

The aims of the investigation into the two-dimensional buckling behaviour of the generic system will be extended to include the extraction of a single column; and the required sheeting rails connected to it. This was performed in such a way that the behaviour of this single column will mirror almost exactly that of a typical column in the full generic system, under axial load only. This then directly allows for the experimental testing of a single column which will still enable conclusions to be drawn for the behaviour of the full generic system.

After investigating the idealised, out-of-plane behaviour, the theoretical three-dimensional behaviour of the column under axial load, as it buckles in both flexural and torsional-flexural modes, will be described in more detail.

3.1. General portal frame layout

To propose a generic system it is necessary to have background information about the typical layout and range of dimensions used for such structures. These general guidelines were obtained from several sources, one of which was Access Steel.

Access Steel is an online electronic steel designer's reference resource, which is aimed at providing resources for structural design engineers and architects who are interested in understanding the proposed methods used in the Eurocode 3-1-1 [6]. One particular reference that provided guidelines, which will be listed below, was entitled "Scheme development: Overview of structural systems for single-storey buildings [21]".

Portal frame structures typically use a relatively small quantity of material to cover a relatively large area, by using a rigid two-dimensional frame which is repeated over the length of the building. This cost-effectiveness of the structure is highly sought after for industrial applications, where aesthetics

are not of major importance. Another advantage of this structural system as stated by Mahachi [22] is the fact that the out-of plane stability of the structure is taken care of by the bracing system, which allows for a relatively simple two-dimensional second-order analysis of the rigid frame.

Due to the versatility of the portal frame structural system and the multiple purposes for which these structures are utilised, there is a wide range of parameters that can be found in practice. Some of these are shown below.

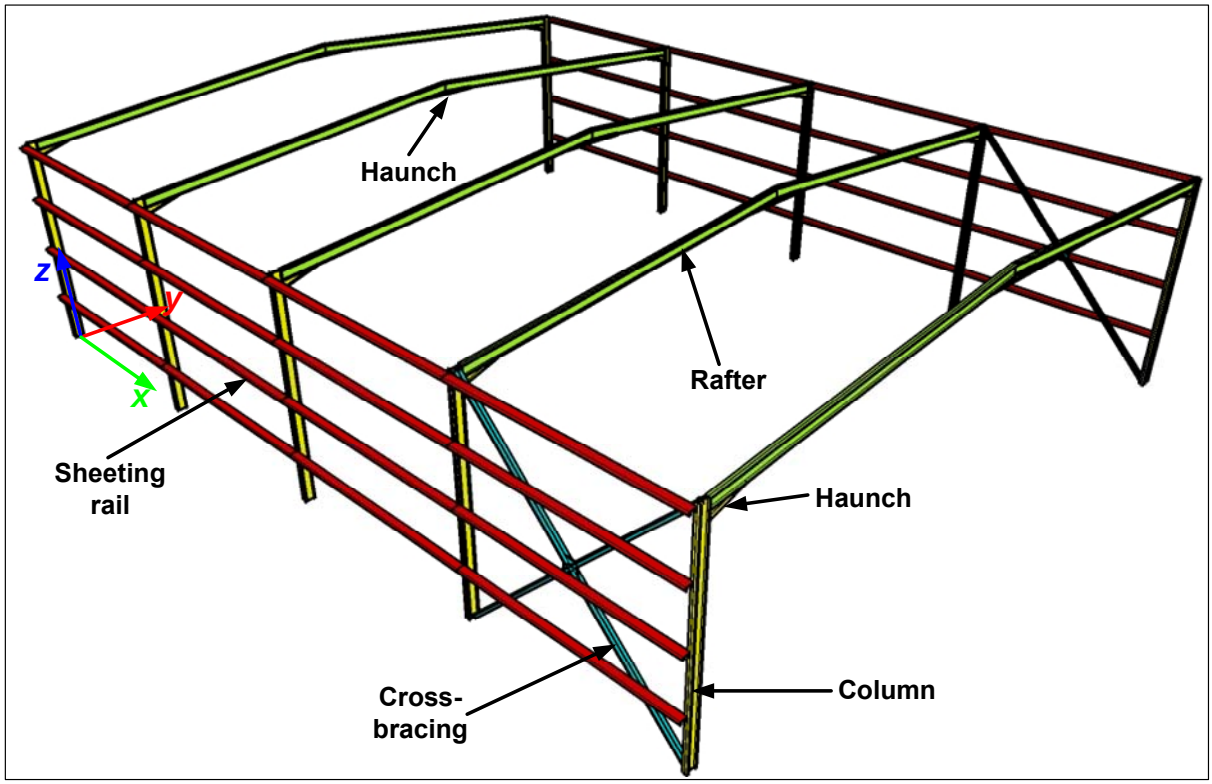

Figure 3.1 - Portal frame structure

Typical members used:

Column:	I- or H- sections
Rafter:	I- sections
Haunches:	Generally cut from the same section used for the rafter
Sheeting rails and purlins:	Cold formed lipped channels (CFLC), Z-sections or hot-rolled angle sections
Bracing members:	Angle sections, Circular Hollow Sections (CHS), etc…
Sheeting:	Profiled steel sheeting (Corrugated, trapezoidal and ribbed profiles)

Typical layout parameters:

Span of portal:	15m to 60m (20m and 30m - found to be most economic.)
Eaves height:	5m to 10m

Roof Slope: Typically 6°.
Frame spacing: Between 5m and 8m.
Sheeting rail/Purlin span: 6m to 8m
Sheeting/cladding span: 1.5m to 2.0m

Figure 3.1 above does not show purlins or roof bracing, so as to have a clearer, uncluttered view of the out of plane elements which are connected to the columns. This was done because the current investigation will be looking only at the out-of plane dimensions and layout of the portal frame structure. Based on the above ranges of values, the following generic system was selected to be used further in this study:

Table 3.1 - Generic system dimensions

Item	Details
Eaves height	5.0m
Frame spacing	5.0m
Number of bays	4 bays
Column	I-section: IPE 200 (5 in total)
Sheeting rails	CFLC: 150 x 65 x 20 x 2.5 (3 in total)
Cross-bracing members	L-section: double 70 x 70 x 8 -back to back (Either 1 or 2 crosses)

The above details are shown below on a sketch of the generic system, which was modelled. It must be emphasised here, that capacity checks and limit state design of the members was not carried out. The members were selected so as to be close to what can commonly be found in practice, not as a proposed structural design.

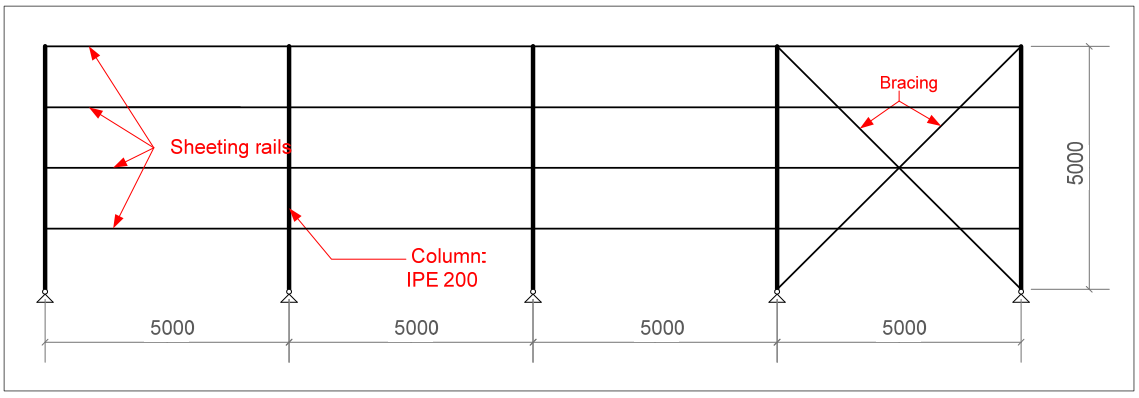

Figure 3.2 - Generic system layout

3.2. Portal frame behaviour

Before limiting the discussion to the case of purely axial load in the columns, it would be wise to expound briefly on the loading and the internal forces that are developed in portal frames. For a portal frame structure without a crane inside, there are relatively few load cases that the structure needs to be designed for. These main load cases are:

Load Case 1: Permanent loads (dead loads);

Load Case 2: Imposed load acting on the whole roof;

Load Case 3: Imposed load acting on half of the roof area;

Load Case 4: Wind along the structure;

Load case 5: Wind across the structure.

Without going into too much detail, we will just briefly look at the structural response to Load Case 2 by considering the idealised structure shown below in Figure 3.3.

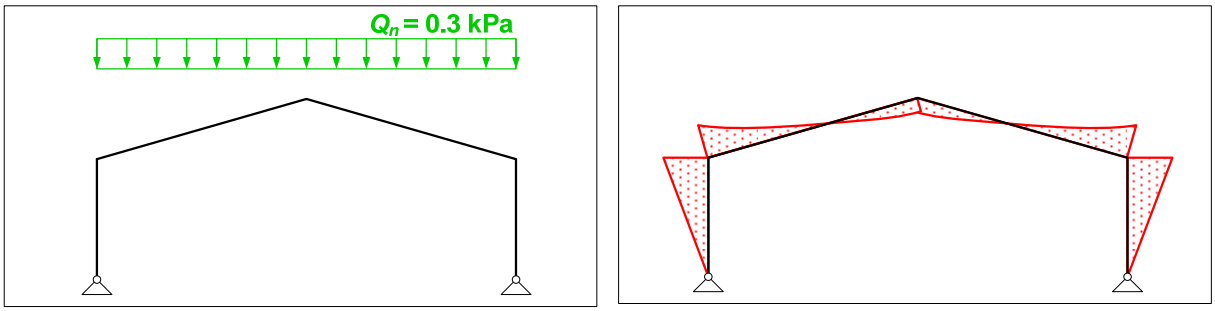

a) Imposed loading pattern b) Bending moment diagram

Figure 3.3 - Loading and Internal forces in a portal frame structure

Each column will support half of the total imposed load as an axial force. In addition to this axial load there will be a relatively large bending moment. The bending moment in the column is distributed as shown in Figure 3.3 b), which is a triangular distribution with the maximum value at the top, whilst there is no bending moment at the column's base. This bending moment is present because of the rigid nature of the portal frame's construction.

The column should thus be designed as a beam-column, as it will always be subjected to axial loads in combination with bending moments. When designing beam-columns the procedure to follow involves first checking that the resistance of the cross-section is sufficient for both the axial compression and the bending moment resistance. If both of these paramters are sufficient then the designer needs to look at the interaction equations for bending moments and axial compression acting together. In SANS 10162 [7] this procedure is defined in Clause 13.8. The specific interaction equation that will be studied here is for lateral torsional buckling strength which is Clause 13.8.2.c) and is as follows:

$$\frac{C_u}{C_r} + \frac{0.85U_{1x}M_{ux}}{M_{rx}} + \frac{\beta U_{1y}M_{uy}}{M_{ry}} \leq 1.0$$

(3.1)

Where:

C_u is the maximum axial load in the column;

C_r is the compression resistance of the cross-section from Clause 13.3;

M_u is the maximum bending moment acting on the column, in either respective direction;

U_1 is a factor to account for moment gradient and for second order effects of axial force acting on the deformed member.

β = $0.6 + 0.4\lambda_y \leq 0.85$

In the present investigation the only term being evaluated from this interaction formula will be the term for the compression resistance of the chosen cross-section, C_r. This limitation can be justified by considering the consequences of inputting an incorrect value of C_r into the above formula.

We have seen that if a column is likely to buckle in a torsional-flexural mode over the length of the column, that the critical load will be lower than the flexural buckling critical load between eccentric lateral restraints. This means that the compression resistance would be over-estimated. If we thus input a lower compression resistance into the interaction formula above [Equation 3.1] then it will increase the value of the term on the left hand side of the inequality. It is feasible that in some cases this can result in the left hand side becoming larger than 1.0; which means that the design is inadequate.

Although a typical portal frame column is not purely subjected to axial loads, it has been shown that the compression resistance of the column plays an important role in the selection of an adequate cross-section. In addition to this, there are other examples of eccentric laterally restrained, doubly symmetric columns from practice which can carry more significant axial loads than a portal frame column. The scope and findings of this investigation will thus be applicable to more than just simple portal frame columns.

3.3. Buckling analyses

The variables in each buckling analysis will be the number of crosses of cross-bracing and the connections between the sheeting rails and the columns. The buckling analyses will be performed in Prokon [24] which will give an indication of the maximum load each column can carry - the critical load - for that situation.

The model in Prokon was set-up as a 2-dimensional model, which is a poor approximation of the system. However, as this section of the investigation is aimed at obtaining an understanding of how the global system will behave, this limitation will be noted and accepted. Thus, in the following models, the sheeting rail centroid is assumed to intersect with the column centroid, at the point of connection between these two members.

A relatively fine mesh of 2-node beam-elements was used to model the generic system. There are 20 beam-elements on each column and 10 beam elements for each of the sheeting rails and bracing members. This fine mesh was chosen to ensure that the models buckled configuration would show an accurate representation of the systems buckled configuration.

The two aspects which are to be varied during the analyses will be explained below in more detail:

Cross-bracing: This will be varied as either **one** or **two** crosses of bracing.

Connection between column and sheeting rail:
Fixed: Simulates a continuous sheeting rail
Pinned: Simulates a single span sheeting rail

It is worth noting that for the single span sheeting rail it is assumed in the design, that the connection is not able to transmit any bending moments onto the column. This is shown below in Figure 3.4. This is different for a continuous sheeting rail, which is able to transmit bending moments onto the column.

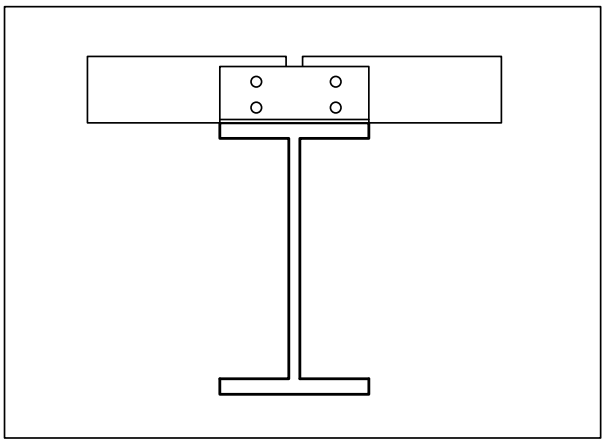

Figure 3.4 - Pinned connection

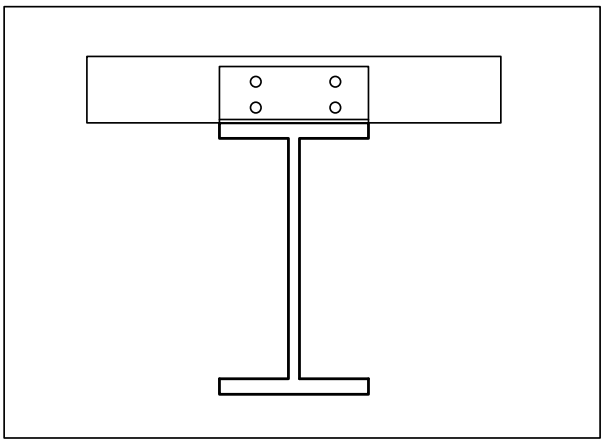

Figure 3.5 - Fixed connection

Five analyses were performed to cover all these variables and these are listed below in Table 3.2:

Table 3.2 - Variables in each analysis

Layout	Column –Sheeting rail connection	Cross bracing
Layout 1	Pinned	1 X
Layout 2	Fixed	1 X
Layout 3	Pinned	2 X
Layout 4	Fixed	2 X
Layout 5	Double span sheeting rails: Alternately Fixed and Pinned	2 X

3.3.1. Results and Buckled configurations

A brief description of each buckled configuration will follow, detailing the specific behaviour of the layout, as well as a justification of why the structural system behaves in that manner.

3.3.1.1. Layout 1

Layout 1 has one cross of bracing and has single-span sheeting rails.

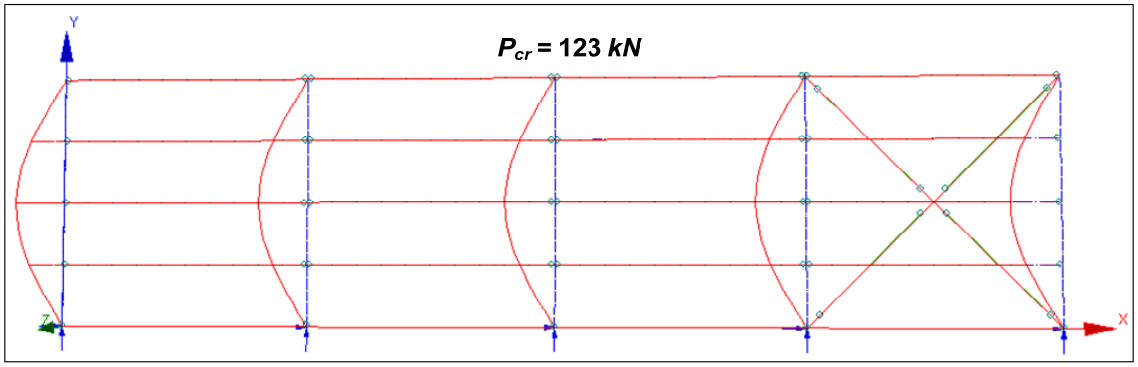

Figure 3.6 - Layout 1

As the load on all the columns approaches the buckling load, the column, which has the worst initial imperfections, will begin to displace laterally. The sheeting rails are forced to move along with the column and thus force the neighbouring columns to displace in the same direction and mode shape. In this case, only the top of the columns are braced laterally and thus the columns buckle in the first mode shape, with the effective length being taken as the full column height.

3.3.1.2. Layout 2

Layout 2 is almost identical as that of Layout 1, except for the connection between the sheeting rail and column. Due to the fixed connection, bending moments are generated in the sheeting rails as the columns begin to displace and curve. These are always restoring bending moments for the reasons stated by de Villiers Hugo [9] in Section 2.3.3.2 above. The sheeting rails will still behave as stated in Layout 1 above and enforce that all the columns buckle in the same mode shape and direction.

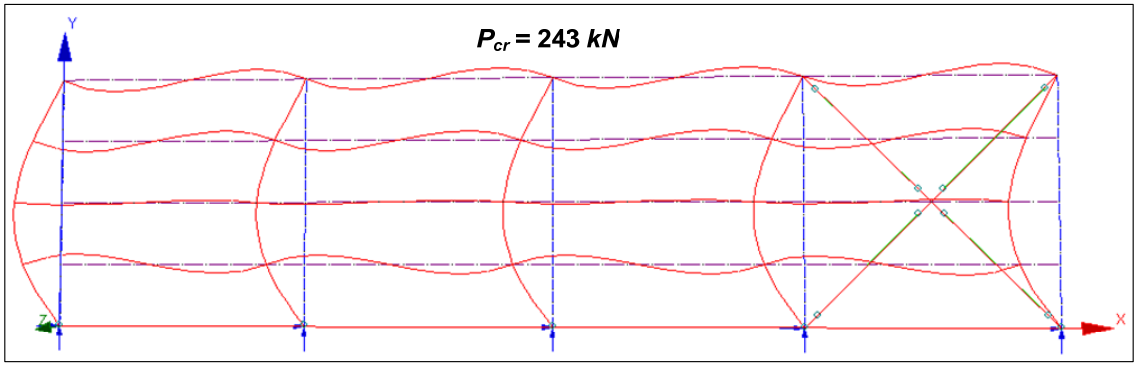

Figure 3.7 - Layout 2

The critical load for this layout is higher than that of Layout 1, due to the positive effect of including the restoring moment developed in the sheeting rails. Three of the sheeting rails are active as restoring springs in this layout. The mid-height sheeting rail does not act as a restoring spring because there is no rotation of the column at that height.

3.3.1.3. Layout 3

Layout 3 now moves on to the case where there are two crosses of bracing. This now means that the columns are braced at two places; the top of the columns and at mid-height.

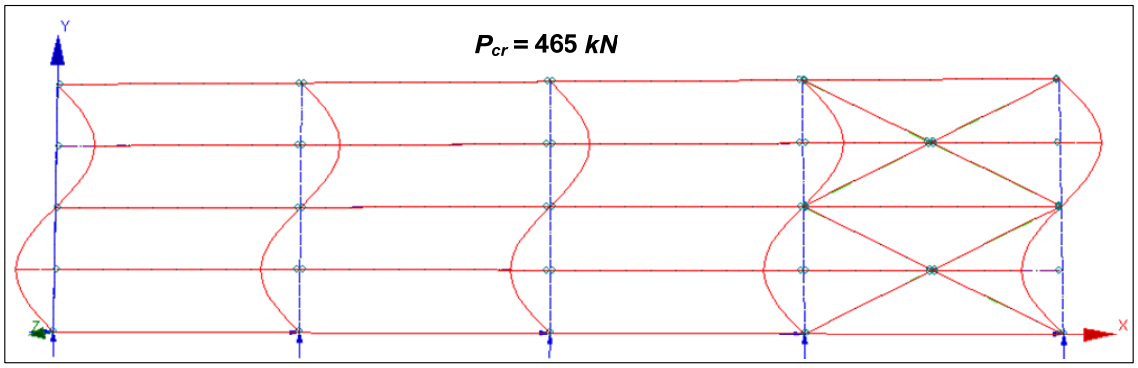

Figure 3.8 - Layout 3

The load carrying capacity of the columns is drastically higher, due to the reduction of the effective length to half the columns height. The columns all buckle in the same mode and in the same direction as seen in the other layouts.

3.3.1.4. Layout 4

Layout 4 too shows a large increase in the load carrying capacity of the columns. The main difference again is the restoring moment from the sheeting rails, which further increases the capacity of the columns. In this case, only two sheeting rails (the sheeting rails that act as lateral restraints) are effective as rotational springs, this is because there is no rotation at 1.25m and 3.75m along the column length.

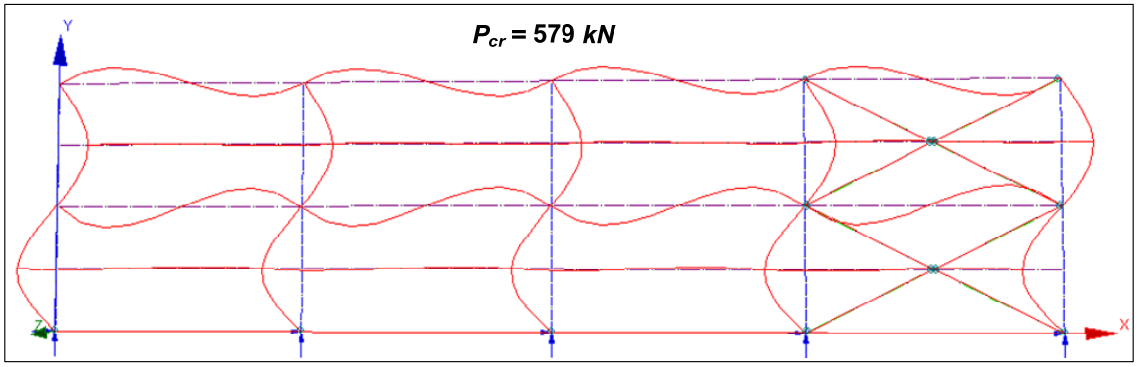

Figure 3.9 - Layout 4

3.3.1.5. Layout 5

Layout 5 is for a case in which a double span sheeting rail is utilised. This means that the restoring moment will only be acting on two of the columns shown below at the points where the connections are fixed, not pinned. This means that the capacity of the system is not as high as that of Layout 4 where the restoring moment acts on each column in the system. The capacity is however still higher than that of Layout 3, where all the connections are pinned. This reinforces the fact that even small restraints can result in a large increase in the capacity of the system restraints.

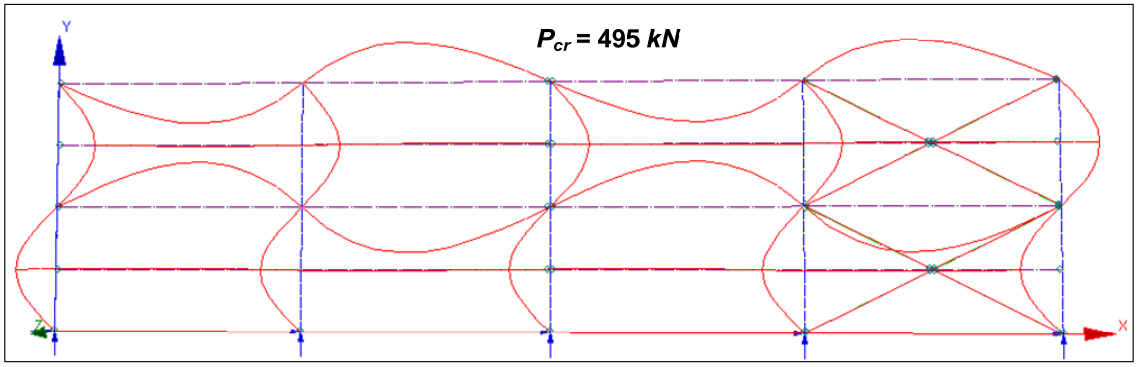

Figure 3.10 - Layout 5

3.3.2. Summary of buckling analyses

It has been shown above, that the critical load of the system can be drastically increased by including the middle sheeting rail in the lateral bracing system. This increase in carrying capacity can be seen in Table 3.3 below in a summarised form. The column labelled **Increase Factor** in Table 3.3 is the increase in the columns critical load due to the addition of a second cross of bracing. This Increase Factor is the result of decreasing the effective length over which buckling occurs, as described in Section 2.1.1.

Table 3.3 - Summary of buckling analyses

Layout	Column – Sheeting rail connection	Crosses of Bracing	Critical load	Increase factor
Layout 1	Pinned	1 X	123*kN*	3.80
Layout 3	Pinned	2 X	468*kN*	
Layout 2	Fixed	1 X	243*kN*	2.38
Layout 4	Fixed	2 X	579*kN*	
Layout 5	Pinned & fixed	2 X	495*kN*	-

It should be noted that the increase in load capacity (due to the effective column length being halved), whilst substantial, does not reach the theoretical value of 4. The theoretical value of the Increase Factor is 4 because the effective length was halved. A possible reason for the lower than expected load capacity increase for the specific case of fixed connections (Layout 2 and 4) is that the number of rotational springs acting on the column decreases from 3 to 2. This results in the restoring moment acting on each column being different in each case and thus they should not be directly compared.

For the case where there are pinned connections between column and sheeting rail (Layout 1 and 3) there are no rotational springs acting on the columns, and thus the increase in load capacity is much closer to the theoretical value of 4. The fact that it is lower than four could be explained by the cross bracing members being less effective in carrying vertical loads, due to the angle of orientation now being less than 45°. What is important is that the capacity of a given column from Layout 4 has a capacity greater than the theoretical value of the second Euler load, which in this case is 451.64*kN* – this is the capacity that should be designed for in such a situation.

3.4. Modelling a representative column

For an experimental test it is not practical to test the whole system of columns because full scale testing of such complexity requires an amount of effort which is disproportional to the results that can be obtained. Thus, it was hoped that a representative column could be modelled which would yield results that could be extended to cover the full systems behaviour. With this aim in mind, further buckling analyses were conducted on such a column, with its relevant length of sheeting rail. Looking at Figure 3.8 and Figure 3.9 it can clearly be seen that the sheeting rails at mid-height and at the top of the column do not displace laterally at all. Also, when the sheeting rails bend as in Figure 3.9 the node midway between columns is an inflection point. To clarify the above statement, it is thus defined that the relevant length of sheeting rail for an individual column is equal to the column spacing, i.e. the length of sheeting rail between inflection points in Figure 3.9.

Buckling analyses were performed for the different connection types shown above, in order to determine what the buckling capacity of a single column will be when the mid-height sheeting rail is a lateral support. Also, the sheeting rails at 1.25m and 3.75m along the columns height have been disregarded from the model. These sheeting rails offer no additional restraint to the buckling of the columns, as there is no rotation in the column at the points of connection. The role of these sheeting rails to ensure that all neighbouring columns will buckle in the same mode and direction is no longer valid, as there is only one column.

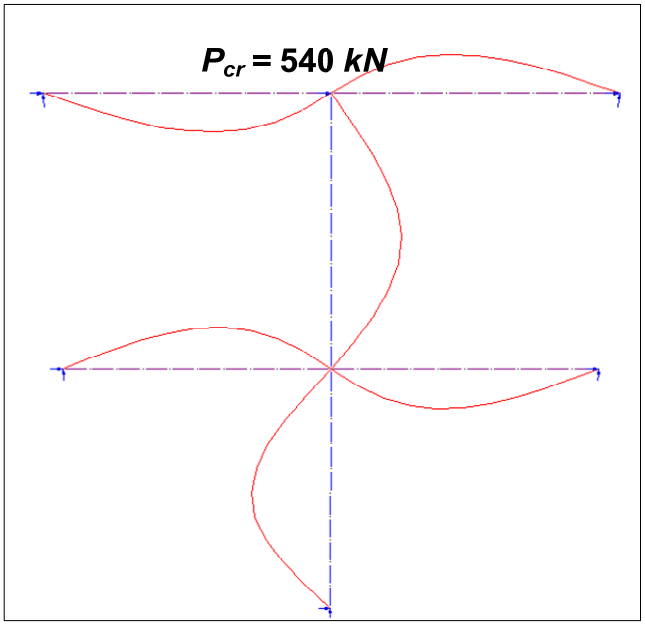

Figure 3.11 - Buckled configuration of a representative column

The buckled configuration shown above in Figure 3.11 is for the case where the top and mid-height sheeting rails are both connected to the column with a fixed (moment transferring) connection. None of the other buckled configurations will be reproduced, as the behaviour can be deduced from the previous section. It should be highlighted here that the above buckled configuration is identical to the buckled configuration of any interior column from Layout 4 above. The small difference in the capacity

of the individual column and the full system of columns is assumed to originate from the behaviour of the cross bracing members, along with the possibility that some small restoring moments were seen to arise due to the neglected sheeting rails. Indeed, upon closer inspection, it was seen that in Layout 4 the sheeting rails did indeed carry bending moments. The magnitude of these bending moments is in the order of 17*Nm*, which is a very small value, but which would have the effect of stiffening the column in the manner witnessed. These bending moments should theoretically not be present in the sheeting rails; however, such small discrepancies can often be attributed to a mesh that is too coarse. In any case, the magnitude of the solutions remains very close, and as such can be said for all practical purposes to be representative.

Table 3.4 - Single columns capacity

Column	Connection to:		Buckling load (*kN*)
	Top sheeting rail	Mid-sheeting rail	
Column 1	Fixed	Fixed	540
Column 2	Pinned	Fixed	505
Column 3	Fixed	Pinned	495
Column 4	Pinned	Pinned	460

The results for the investigations into the single columns behaviour, for the different connections between column and sheeting rail are shown above. From these results it can be deduced that the mid-height sheeting rail increased the columns capacity by 45*kN*; whilst the top sheeting rail increased the columns capacity by 35*kN* because of the restoring moments generated. This gives some indication as to the positive effects of including the sheeting rails into the bracing system.

As a check of the chosen mesh of the model and of the values obtained above, a buckling analysis was performed on the column without any sheeting rails attached. The critical load of the column was found to be 115*kN*. Comparing this value and the critical load of Column 2 from Table 3.4 above is 460*kN*, which is exactly 4 times larger than the first critical load. Thus, it is again speculated that the interaction between bracing members and the columns in the generic system above does not allow the attainment of the maximum increase in load capacity.

Finally, the theoretical Euler buckling load for the full unsupported column length is calculated below, to verify the accuracy of the above results. The value of the Young's modulus used in the Prokon models was 206 *GPa*.

$$P_E = \frac{\pi^2 EI}{L_y^2} = \frac{\pi^2 \cdot 2.06 \times 10^{11} \cdot 1.42 \times 10^{-6}}{5^2} = 115.48kN$$

3.5. Theoretical column behaviour under axial load

The above analyses were performed in two dimensions, looking only at the out-of-plane direction, as well as the sheeting rails being attached in such a manner that the centroid of the column and the centroid of the sheeting rail coincided at the point of connection. In practice, as seen above in Figure 2.9, the sheeting rail centroid is actually offset a substantial distance, (h_y) from the columns centroid.

It was assumed in the preceding sections, that if the mid-height sheeting rail is included as lateral support, that the columns will tend to buckle in a flexural buckling mode with the effective length being half of the columns length. However, the possibility exists that the column can buckle at a torsional-flexural buckling mode over the full column length. Is this buckling load more critical than the second flexural buckling mode?

3.5.1. Pinned column–sheeting rail connection

To answer this question, firstly, the case of a discontinuous sheeting rail, with pinned connections between the column and sheeting rails will be considered. In this scenario there will be no restoring moment developed in the sheeting rails to act on the column. For the same reasons there will be no torsional restraining moment developed to prevent twisting of the cross-section. Now, if one looks at the design equation (2.11), proposed by Timoshenko and Gere [11] from Section 2.3.1 above, there is no torsional restraint, and so the critical torsional-flexural buckling stress can be calculated using the following formula:

$$f_{e,TF} = \frac{\left(C_w + I_y h_y^2\right) \cdot \left(n^2 E\pi^2 / L_z^2\right) + GJ}{A \cdot \left(h_y^2 + \overline{r_o^2}\right)}; \qquad (2.49)$$

Upon investigating the above formula for different column lengths, one can produce the buckling capacity curves shown below. These capacity curves were set up using the column design method according to SANS 10162 [7] to account for initial imperfections and residual stresses. The above critical stress was substituted into the place of f_{ez} (Clause 13.3.2.b)) to calculate the torsional-flexural, rather than torsional buckling. The axial resistance calculated was (in all cases) done without taking into account the resistance factor for structural steel (Φ = 0.9).

The curves shown are the capacity curves for first mode flexural buckling, second mode flexural buckling and first mode torsional-flexural buckling. The first mode of flexural buckling is shown simply as a reference, so as to illustrate the gain of capacity which can be achieved by including a lateral and/or torsional restraint. The horizontal axis of the capacity curves shown is the slenderness ratio considering the full length of the unsupported flange of the column, and is denoted by l_f / r_y. The vertical axis represents the critical load for a given slenderness ratio, which has been normalised by the plastic capacity of the cross-section, C_y.

In Figure 3.12 the value of h_y = 0mm. This means that the above formula reduces to the standard torsional buckling capacity curve; i.e. the twisting occurs around the shear centre of the cross-section. For slenderness ratios greater than approximately 150, the second mode of flexural buckling is critical. For slenderness ratios of less than approximately 150, first mode torsional buckling will be critical. It is common for columns in practice to be chosen such that the slenderness ratio is as close to the upper code limit of 200 as possible. Thus, it can be expected that most practical columns will have slenderness ratios close to the range of 150 to 200. In this range, when h_y = 0mm, the second flexural buckling mode is critical.

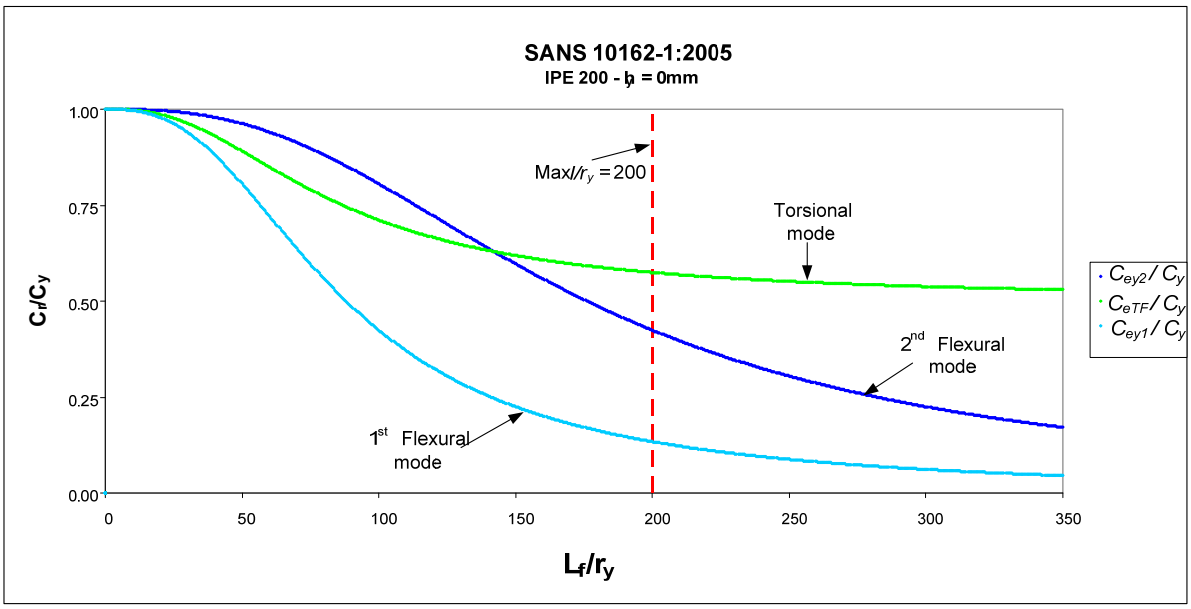

Figure 3.12 - Buckling capacity curve - h_y = 0mm

If the point of lateral restraint is moved from the centroid of the column to the actual point of lateral restraint in portal frame buildings (the centroid of the sheeting rail) then the capacity curve changes to that shown in Figure 3.13 below. For the generic system chosen, the value of h_y = 175*mm*. With this value of h_y the equation shown on the previous page gives the torsional-flexural buckling capacity. First mode torsional-flexural buckling is critical for all slenderness ratios up to approximately 340. At the maximum slenderness ratio allowed by the code, and below this value, the capacity of the column is significantly lower than the second flexural buckling capacity.

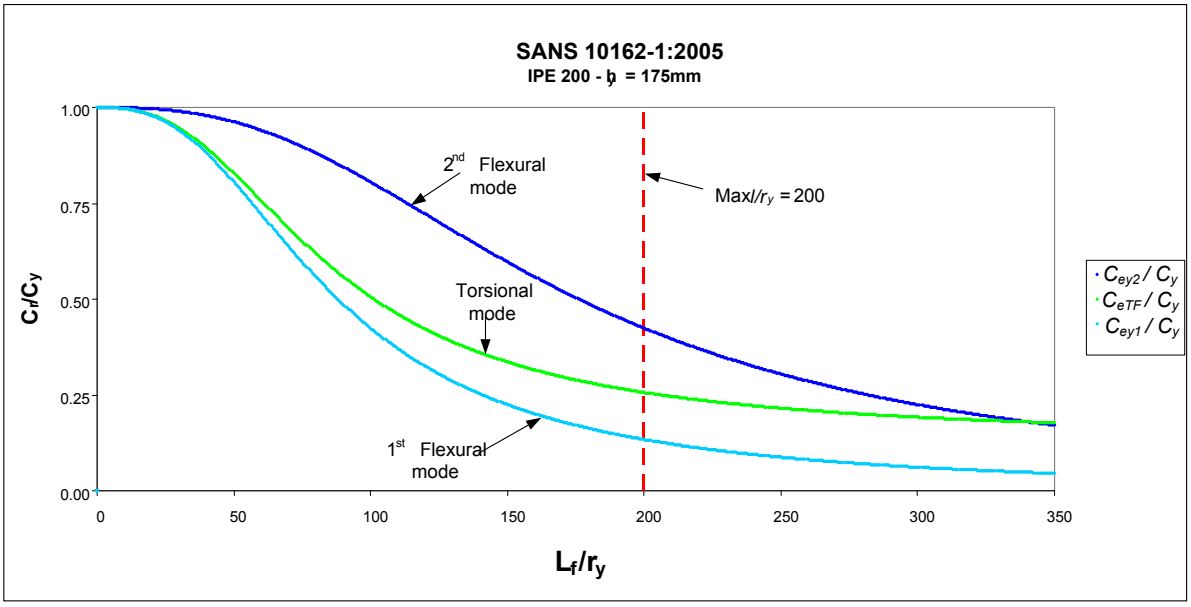

Figure 3.13 - Buckling capacity curve - h_y = 175mm

It is interesting to note, that if the value of h_y is made very large, the torsional-flexural capacity curve is equal to the weak axis flexural buckling capacity curve for the same mode shape. Similarly, if the value of h_y = 0, as in Figure 3.12, then the torsional-flexural buckling capacity is identical to the torsional buckling capacity.

From the above results, it is clear that designers need to be aware that the torsional-flexural buckling capacity needs to be checked, and that it can quite often be critical.

3.5.2. Fixed column–sheeting rail connection

Looking now at case where there is a fixed (moment transferring) connection between the column and the sheeting rail, it can be seen that the sheeting rails will now add torsional restraint onto the column at the point of attachment. Thus, the torsional flexural buckling capacity will now be calculated by the following equation reproduced (selected because it was seen to yield conservative results) again from Helwig and Yura [15]:

$$P_{cr,TF} = \frac{1}{\left(h_y^2 + \overline{r_o^2}\right)}\left[P_{cr,y1}\left(\frac{h^2}{4} + h_y^2\right) + \sqrt{\frac{4n_b K_T E I_y}{L}\left(\frac{h^2}{4} + h_y^2\right)}\right] \qquad (2.20)$$

This connection is of the type shown in Figure 3.5 above. This type of connection detail is not one of the recommended connections proposed by Helwig and Yura [15] which are shown in Figure 2.15. The main difference is that there is no specific measure to prohibit cross-sectional distortion, which was a requirement according to Helwig and Yura [15]. In spite of this difference, the method of calculation used by Helwig and Yura [15] was considered as the most comprehensive in explaining the behaviour that can be expected.

The torsional restraint stiffness which the sheeting rail can provide to the column is determined by:

$$K_T = \frac{2EI_{sr}}{L_{sr}} = \frac{2 \times 2.0 \cdot 10^{11} \times 2.64 \cdot 10^{-6}}{5} = \underline{\underline{211.2 kNm/rad}}$$

This torsional stiffness is large enough to ensure that flexural buckling will always be critical. This can be seen clearly in Figure 3.14 for the 5*m* long IPE 200 section. Also, the ideal torsional stiffness (to prevent torsional-flexural buckling) is approximately 16*kNm/rad* (from Equation 2.20). This ideal stiffness needs to be increased by the magnification factor (Equation 2.21), which yields the required brace stiffness:

$$K_{T,reqd} = K_{T,ideal} \times A = 16 kNm/rad \times \left(4 - \frac{400}{175}\right) - - - - - [A \geq 2]$$

$$K_{T,reqd} = 16 \times 2 = \underline{\underline{32 kNm/rad}}$$

This is much less than the actual stiffness which the sheeting rail can provide.

The torsional-flexural buckling load was calculated as:

$$P_{cr,TF} = \underline{\underline{1028 kN}}$$

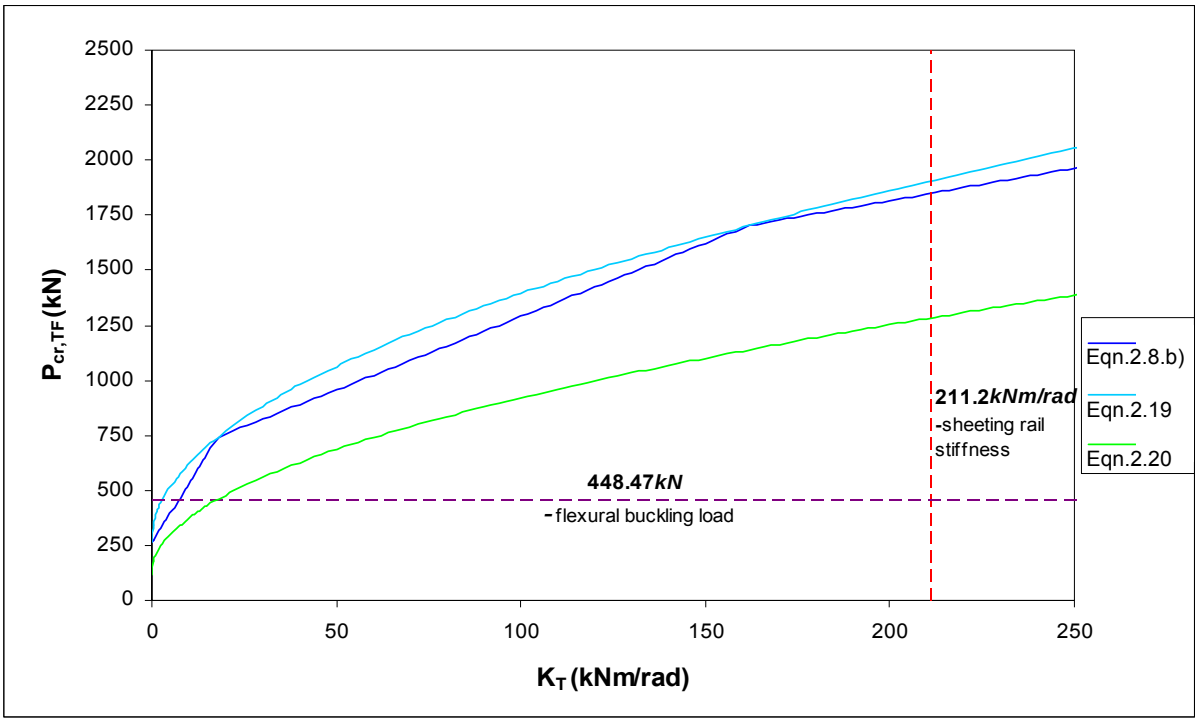

Figure 3.14 – Critical load vs. Torsional restraint

When this information is represented on a capacity curve (Figure 3.15) it can clearly be seen that torsional-flexural buckling is never critical in the practical range of column slenderness from 150 – 200.

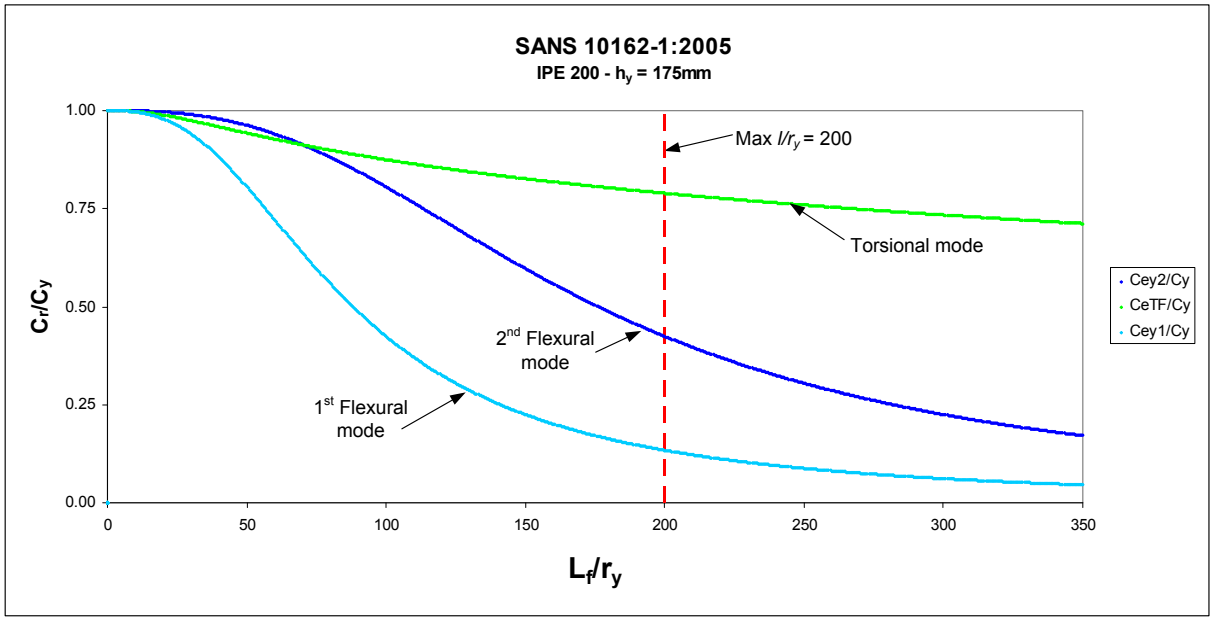

Figure 3.15 –Buckling capacity curve + torsional restraint

It has therefore been shown, that by including the effects of lateral and torsional restraints, a designer can be assured that second mode flexural buckling will be critical for all practical slenderness ratios even when eccentric restraints are present.

3.6. Summary of column behaviour

This section of the investigation was an attempt to predict the behaviour of a column in a portal frame structure under axial load. It was seen that the type of connection between the lateral braces (mid-height sheeting rail) and the column plays a very large role in the mode of failure of the column itself. If the connection is unable to transfer bending moments then the failure of the column is likely to be torsional-flexural buckling. However, if a moment transferring connection is used then the predominant failure mode will be by weak axis flexural buckling. Suitable connections have been proposed by Helwig and Yura [15] which fulfil the roles of transferring bending moments as well as prohibiting cross-sectional deformation at the point of connection.

The method of predicting the buckling capacity and mode of a given column was based on the theoretical equations outlined in the Literature study (Section 2.3 specifically) as well as the method of dealing with inelastic material behaviour as outlined in SANS 10162 [7]. This method was used to produce the buckling capacity curves shown in the preceding sections of this chapter. Some of the variables which do not enter into the standard code method, but which are present in this adapted method, are:

- h_y = the offset point of lateral and/or torsional restraint; and
- K_T = the torsional brace stiffness;
  (determined by the flexural stiffness of the selected sheeting rail)

The adequacy of this chosen method of prediction will be determined once the analytical model of the system has been compiled.

It was also noted in Section 3.5.2 that the torsional stiffness provided by commonly used continuous sheeting rail is far in excess of that which is actually required to prevent a torsional-flexural mode of failure from being critical. This extra stiffness implies that the whole connection is stiffer than required. Does this mean that even simpler connections (less efficient) can still impart the required torsional restraint to the column? For example, would a continuous sheeting rail which is connected onto an angle cleat by two bolts still provide sufficient stiffness to ensure that flexural buckling remains critical without explicitly preventing cross-sectional deformation?

4. Experimental Investigation

It was shown in Chapter 3, by looking at the idealised in-plane behaviour of a system of columns, that each of the columns displays the same buckled configuration. This means that a column can be singled out from the system and tested independently and will (after ensuring the correct boundary conditions) behave in the same manner the columns in the global system.
Close attention thus had to be paid to the boundary conditions of the test column, to ensure that:

- The boundary conditions are close to what one would expect in practice (from the global system).
- The boundary conditions behave as you assume: e.g. a pinned connection will not provide any moment restraint.

The primary goal of this experimental investigation was to determine if a simple column to sheeting rail connection, which is commonly found in practice, can in fact supply sufficient torsional restraint to a column. In order to investigate this behaviour it was decided to test two scenarios. Firstly, the simple case of a continuous sheeting rail connected via two bolts onto a cleat on the column and secondly a connection more in line with what was prescribed by Helwig and Yura [15], simply adding fly braces onto the column in order to support the inside flange as well.

The following chapter will deal with an explanation of the chosen experimental set-up. This explanation will cover all aspects of the experimental set-up, from the selection of relevant test member sizes, to a full description of how the boundary conditions are to be satisfied. Also included will be a description of the testing procedure that was used. This will give insight into the method of collecting data from the tests themselves, specifying where and how these measurements were taken. Finally, the results recorded during the tests are presented.

4.1. Experimental Set-up

Several experimental set-ups, from previously conducted research projects, were reviewed in order to gain insight from the experience of others. Based on the previous work done, it was decided to test the column horizontally, with the web in the vertical plane. The main reason for this is to ensure easy access to all parts of the model during testing which greatly simplifies the collection of data. The horizontal arrangement has been seen to yield positive results in the past (Horne and Ajmani [16] and Gelderblom *et al* [17]). The extra bending moments induced in the column are small (only due to the own weight of the column and sheeting rail) and act about the strong axis of the column, which does not affect the results of weak axis buckling in any meaningful way.

In addition to the two main setups being tested, a control test will be performed on a laterally unsupported column to gauge the effectiveness of the experimental set-up. There are thus three configurations being tested. To reiterate, these are:

- A column, unsupported over the full length,
- A column with a mid-height lateral support on only one flange, and
- A column with a mid-height lateral support to both flanges.

In order to ensure the validity of each result and for statistical purposes, it was decided that three specimens of each configuration would be tested. Thus, there were a total of nine tests performed in the investigation.

Figure 4.1 - Full experimental set-up

4.1.1. Selection of testing members

4.1.1.1. Column

Full scale tests are difficult to accommodate and often require substantial loads to initiate buckling. Therefore, to keep the magnitude of loads, as well as the physical size of the members in the experimental model from becoming exceedingly large, the smallest IPE section, namely the IPE 100, was used. The length was determined by ensuring that the slenderness ratio about the y-axis of the section did not exceed the code stipulated maximum value of 200 (assuming no lateral restraint). Therefore:

$$\frac{K \cdot L_y}{r_y} \leq 200 \; ; \qquad (4.1)$$

with:

K = 1.0;

r_y = 12.4 mm;

Thus:

$$L_y \leq \frac{200 \times r_y}{K} = \frac{200 \times 12.4}{1} = 2480mm \, .$$

For convenience the length of the column was selected as **2400*mm***, which satisfied the slenderness ratio criteria (193.5 ≤ 200) imposed by the code.

It was hoped that some correlation could be maintained (in terms of the relative stiffness's of the column and the sheeting rails) between the model that was tested and the generic system analysed in the previous chapter. There is some leeway, due to the wide range of variables in portal frame structures which was pointed out in Section 3.1. The important stiffness term for the column is the moment of inertia about the y-axis (I_y). Thus, the ratio between these terms for the two cases here mentioned is:

IPE 200 – $\boldsymbol{I_y}$ = 1.42 x 10^6 mm^4.

IPE 100 – $\boldsymbol{I_y}$ = 0.159 x 10^6 mm^4.

$$\therefore \frac{I_{practical}}{I_{model}} = \frac{I_{y-200}}{I_{y-100}} = \frac{1.42}{0.159} = \underline{\underline{8.93}} \, .$$

4.1.1.2. Sheeting rail

When designing a sheeting rail the important stiffness term is the one which deals with the stiffness about the *x*-axis (strong axis) of the profile. This is because the main design criterion for the sheeting rail is to carry the wind load acting on the sheeting, coupled with the fact that the flexural stiffness of the sheeting rail about this axis is linked directly to the torsional restraint supplied to the column. Thus, using the stiffness ratio, found above, for the practical example to that of the model, it follows that:

CFLC – 150 x 65 x 20 x 2.5 (generic) – $\boldsymbol{I_x}$ = 2.64 x 10^6 mm^4.

$$I_{model} = \frac{I_{practical}}{8.93} = \frac{2.64}{8.93} = 0.2956 \approx 0.3$$

Thus, $I_x \geq 0.3 \times 10^6\ mm^4$

The smallest available CFLC (75 x 50 x 20 x 2.0) has an $\boldsymbol{I_x}$ = 0.360 x 10^6 mm^4.
This is then the most appropriate choice to ensure similar stiffness's.

In order to quantify the length of the sheeting rail, it is necessary to look at the spacing of the portal frames in relation to the height of the columns used. A general range of values is proposed below, into which most practical structures will fall.

$$0.75h \leq s \leq 1.5h$$

In the above expression, *h* - is the height of the column and *s* – is the spacing of the portals, as can be seen in Figure 4.2 below:

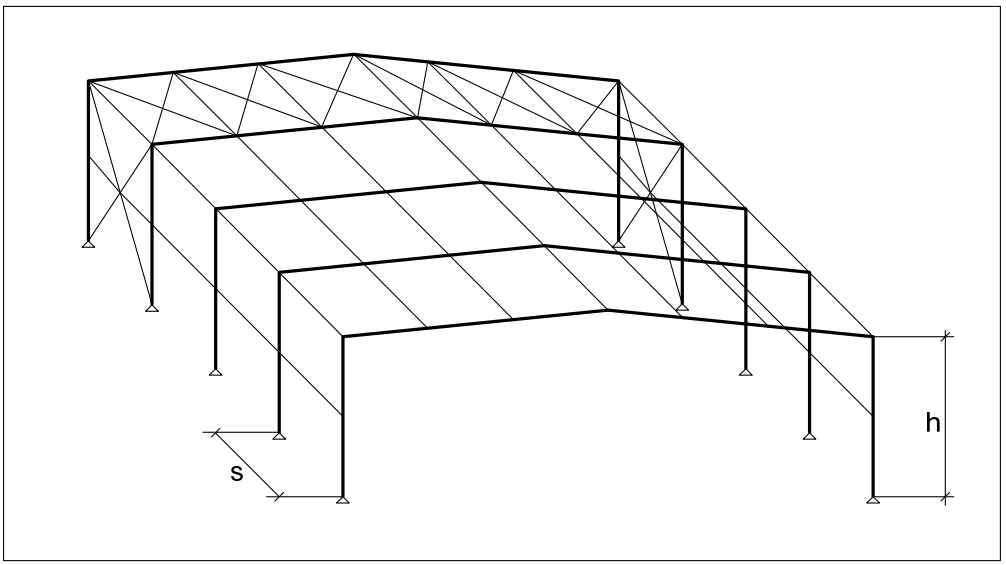

Figure 4.2 – Idealisation of a portal frame

Based on the chosen height of the column (2400 *mm*) the spacing of the columns, and thus the length of the sheeting rail being modelled must fall within the following bounds:

$$1800mm \leq s \leq 3600mm$$

To remain relatively similar to the generic system examined previously, the length was chosen as **3000*mm***.

4.1.1.3. Fly Braces

Clause 9.2.6 of SANS 10162-1:2005 [7] states that a bracing system shall be proportioned to have a strength perpendicular to the longitudinal axis of the braced member in the plane of buckling, at least equal to 0.02 times the factored compressive force in the member or element being braced.

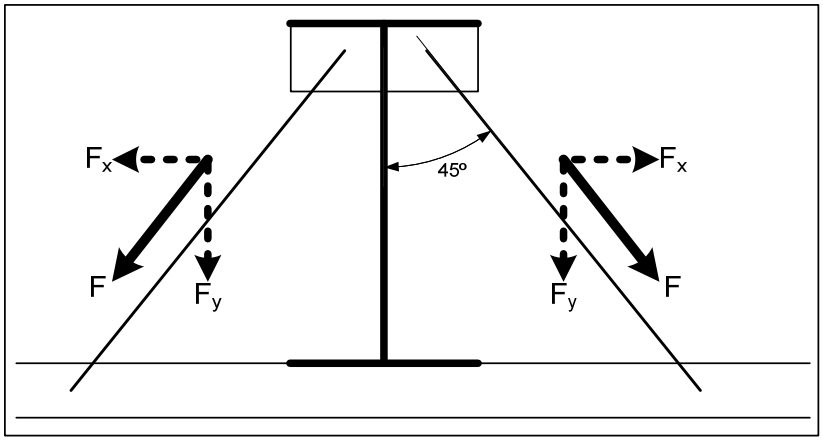

Figure 4.3 - Schematic view of Fly brace

In the tests in which fly braces are present the braces will serve to laterally support the inner (unsupported by a sheeting rail) flange of the column. It is thus necessary to determine the compressive force acting in this flange, as it will determine what size fly brace is necessary. As an upper limit, to ensure that a sufficiently strong brace will be used, the maximum compressive force acting in the column as a whole is taken as the yielding load of 324 *kN* which is calculated in Section 4.1.2.

To determine the force in the flange being braced:

$$\sigma_{\max} = \frac{C_{\max}}{A_g} = \frac{324kN}{1030mm^2} = 314.56MPa \ ; \qquad (4.2)$$

(C_{max} is the maximum expected load on the column.)

Area of the flange: $A_f = b \times t_f = 55 \times 5.7 = 313.5mm^2$

Thus, the force on one flange:

$$C_f = \sigma_{\max} \times A_f = 313.5mm^2 \times 314.56MPa = \underline{98.6kN}$$

From Clause 9.2.6 [7], stated above, the Component of the force in the bracing member perpendicular to the longitudinal axis of the column corresponds to the force $\boldsymbol{F_x}$ in Figure 4.3.

Thus:

$$F_x = 0.02 \times C_f = 0.02 \times 98.6kN = 1.972kN \qquad (4.3)$$

And then:

$$F = {F_x}/{\sin 45^\circ} = {1.972}/{\sin 45^\circ} = \underline{\underline{2.79kN}}$$

From Clause 13.2 [7] of the code the tensile resistance of a member is given by:

$$T_r = \varphi \cdot A_g \cdot f_y$$

thus; (4.4)

$$A_{g,\min} = \frac{T_r}{\varphi \cdot f_y} = \frac{2.79kN}{0.9 \times 200MPa} = 15.5mm^2$$

As can be seen, the required cross-sectional area of the fly brace is very small. Therefore, it was decided to use a **25 x 25 x 3** angle section (as it is the smallest angle section available). This was done because it is typical to use small angle members for bracing in practice, as well as to ensure that at all loads (even at and after failure) the bracing would be sufficient.

Workshop drawings for all members of the different test specimens are attached in Appendix A: and the reader is so referred, if any more technical details are required.

4.1.2. Calculation of expected loads

It was necessary to ensure that all parts of the experimental set-up would have sufficient resistance to cope with the loads applied to cause the columns to buckle. This meant determining the upper bound of these forces before the set-up could be finalised. With this aim in mind, it was reasoned that if the sheeting rail prevents the lower torsional-flexural buckling mode from being critical, then the buckling of the column would be in the second flexural mode. Also to be considered was the matter of the sheeting rail acting as a restoring spring against buckling about the weak axis of the column (de Villiers Hugo [9]) by bending about its weak axis, which serves to increase the columns capacity. It should be noted that the subscript (**y2**) will be used to denote the second flexural mode of buckling about the weak axis from this point forward in this report.

4.1.2.1. Loads according to SANS 10162-1:2005 [7]

Sectional properties (from The Red Book [10])**:**

h = 100 *mm*

b = 55 *mm*

t_w = 4.1 *mm*

t_f = 5.7 *mm*

A = 1.03 x 10^3 mm^2

I_x = 1.71 x 10^6 mm^4

r_x = 40.7 *mm*

I_y = 0.159 x 10^6 mm^4

r_y = 12.4 *mm*

C_w = 0.354 x 10^9 mm^6

J = 12.1 x 10^3 mm^4

Offset of restraint:

h_y = 97.5 *mm*

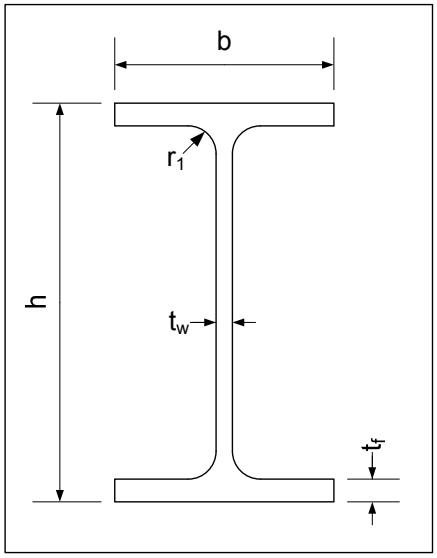

Figure 4.4 – Properties of IPE 100

Classification of the section:

Flange:

$$\frac{b}{2.t_f} = \frac{55}{2 \times 5.7} = \underline{\underline{4.825}} \leq \frac{200}{\sqrt{350}} = 10.690 - - - \underline{Class3}$$

Web:

$$\frac{h_w}{t_w} = \frac{100 - [2 \times 5.7]}{4.1} = \underline{\underline{21.61}} \leq \frac{670}{\sqrt{350}} = 35.813 - - - \underline{Class3}$$

Slenderness ratios:

For all cases K = 1;

$$\frac{L_x}{r_x} = \frac{2400}{40.7} = 58.968$$

$$\frac{L_{y2}}{r_y} = \frac{1200}{12.4} = 96.774 \text{ ……..(for second mode, i.e. } L_{y2} = L_y / 2);$$

It should be noted that the slenderness ratios are below the code stipulated maximum of **200**; and also that, as expected, buckling about the y-axis will be determinant over the buckling about the strong (x-) axis.

Dimensionless slenderness ratio:

$$\lambda = \frac{K.L_{y2}}{r}\sqrt{\frac{f_y}{\pi^2 E}} = 96.774\sqrt{\frac{350}{\pi^2 \times 2. \times 10^5}} = 1.2886 \qquad (2.25)$$

Axial Capacity:

$$n = 1.34;$$

$$C_r = \varphi.A.f_y\left(1+\lambda^{2n}\right)^{\frac{-1}{n}} \qquad (2.24)$$

$$C_{r,y2} = \underline{\underline{144.61\,kN}}$$

Yield Capacity of the column:

$$C_y = \varphi.A_g.f_y \qquad (4.5)$$

$$C_y = 0.9 \times 1.03 \times 10^3 \times 350 = \underline{\underline{324\ kN}}$$

4.1.2.2. Second Flexural Euler buckling load

Using the general Euler formula, as given in Section 2.1.1 above:

$$P_{E2} = \frac{\pi^2.E.I}{(K.L^2)} \qquad (2.4)$$

$$P_{E2} = \frac{\pi^2 \times 2 \times 10^{11} \times 0.159 \times 10^{-6}}{1.2^2}$$

$$P_{E2} = \underline{\underline{217.954\ kN}}$$

4.1.2.3. Prokon model's load

An out-of-plane (2-dimensional) buckling analysis was done in Prokon [24] for the chosen experimental model, which found that the critical load for the set-up was 300 *kN*. This load is for failure by weak-axis flexural buckling, and includes the restraining moment produced due to the bending of the mid-height sheeting rail, assuming a full moment transferring joint.

4.1.2.4. Summary

The above loads have been summarised in Table 4.1. The critical load, at which the model can be expected to buckle, will almost certainly be larger than the code calculated value, due to safety factors that are necessary in codes to obtain a certain reliability level. By the same token, the Euler load and especially the Prokon load calculated here neglect imperfections (such as the residual stresses and initial imperfections that are unavoidable) and will thus be overestimates of the actual loads that can be expected. However, the Euler load does not take the restoring action of the sheeting rail into account either, so we should rather rely on the Prokon load to give us the upper bound of the buckling load.

Table 4.1 - Summary of the expected loads

Method	Elastic Buckling load
SANS 10162-1:2005 (2^{nd} mode)	144.61 *kN*
Euler (2^{nd} Mode)	217.954 *kN*
Prokon model	300 *kN*
Yielding load	324 *kN*

The actual load that will cause buckling under experimental conditions is thus expected to be lower than this upper bound of **300 *kN***. A suitable safety factor was used to increase the value of the upper bound design load to ensure that adequate stiffness and strength was provided. The design load was therefore taken as **400*kN*** and all the test set-up members were designed accordingly.

4.2. Boundary Conditions

As stated in Section 4.1 the assumed boundary conditions are as follows:

- Base BC's: pinned.
- Top BC's: roller support (fixed for x and frees to move in y direction).

These boundary conditions were derived only for a 2-dimensional case. For the more general (realistic) 3-dimensional case the boundary conditions that exist in such a structure need some discussion. The physical boundary conditions that can be found for columns in standard portal frame construction are discussed in detail. Assumptions were made in order to reduce the often complex boundary conditions to physical boundary conditions that can be implemented in a laboratory setting whilst still ensuring that the laboratory boundary conditions agree very favourably to those found in the practical case.

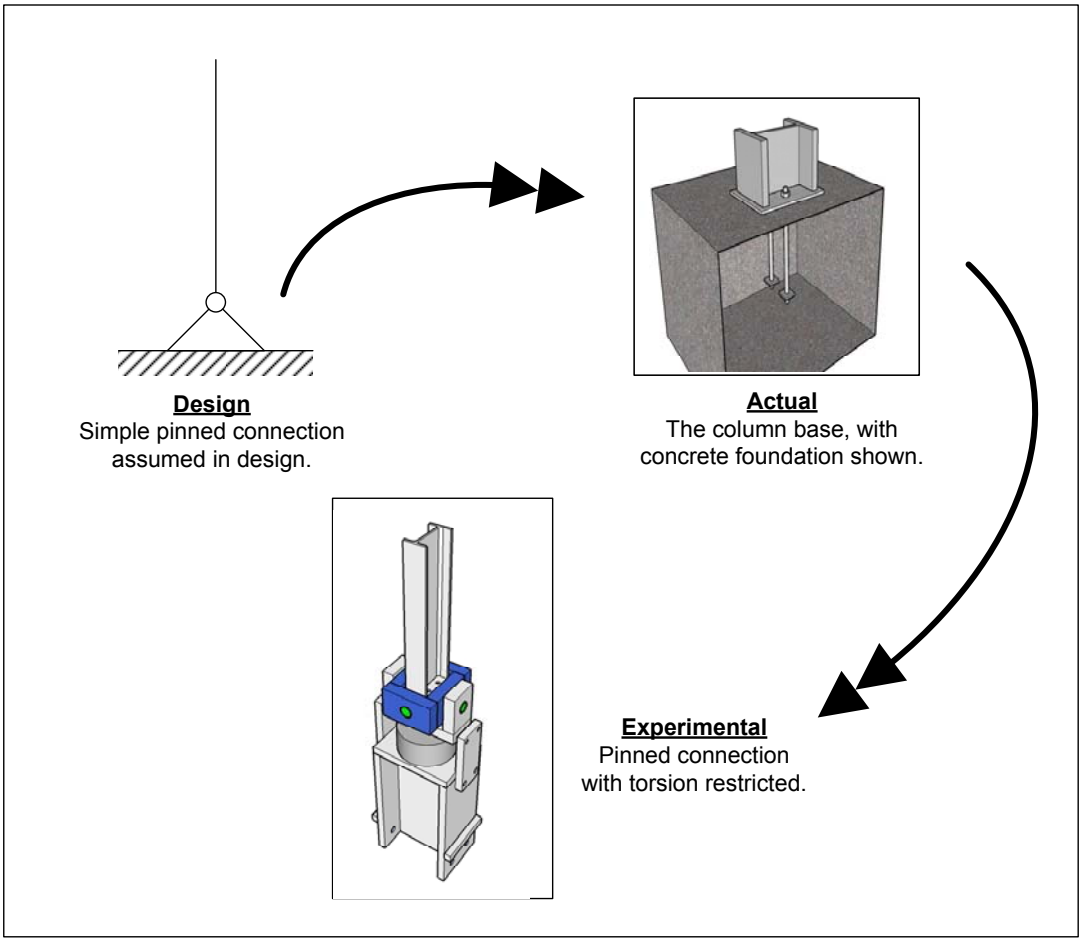

Figure 4.5 - Boundary condition - increasing complexity

4.2.1. Column boundary conditions

4.2.1.1. Base boundary conditions

In the general design of portal frames it is assumed that the base connection is a pinned connection. This means that there is no rotational restraint about the two horizontal axes (x- and y- axes). This is a design simplification.

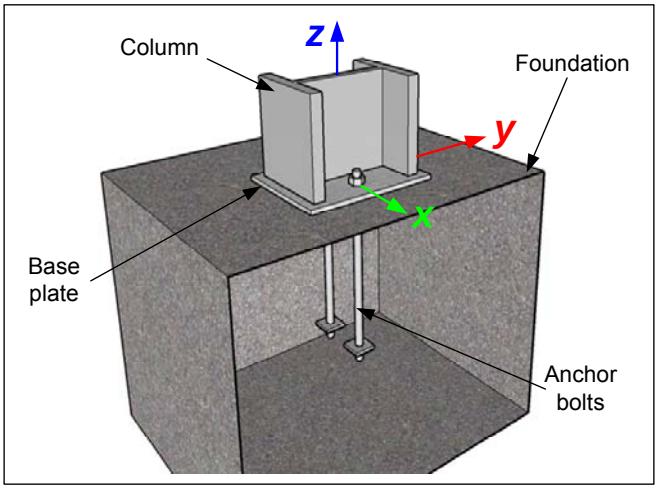

Figure 4.6 - Column base and foundation block

As can be seen in Figure 4.6 the actual connection which is used will provide a degree of fixity against rotation. This is especially true for rotation about the weak (*y*-) axis. However, the resistance that would be calculated for such a member is still based on the pinned end condition. Thus, it was deemed appropriate for the experimental set-up to stay true to the design assumptions, and a true pinned base connection was designed for the column base.

It can also be seen that there is a welded connection between the column end and the base plate. The holding down bolts are cast into the foundation, this will provide torsional fixity at this point. Some cases are seen where 4 holding down bolts are used, which increases the torsional fixity at the base. The column was thus modelled so that rotation about the longitudinal (*z*-) axis was restrained at the base.

4.2.1.2. Top boundary condition

The top boundary conditions are more difficult to quantify than the base boundary conditions. The idealised condition is a pinned roller support. This means that all deflections in the horizontal plane are supported whilst the vertical deflections are left free. The rotational degrees of freedom, except that about the longitudinal axis of the column, are also left free.

In practice the connection is often very similar to that seen in Figure 4.7. The particular connection shown has a haunch attached to the beam-column connection (to improve the moment transfer capacity of that connection). The eaves beam shown is a channel section, although various other configurations exist for eaves beams.

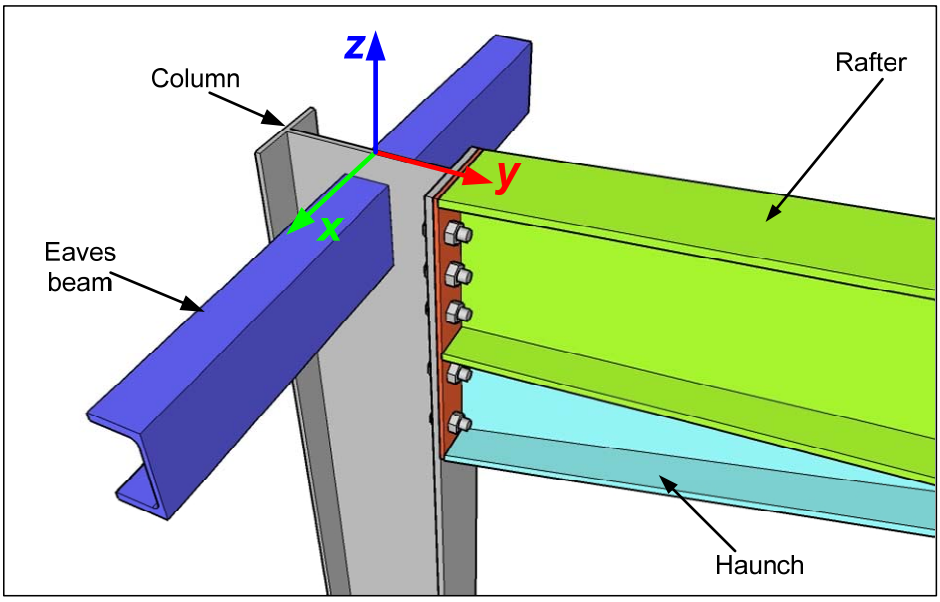

Figure 4.7 - Top connection of portal frame column

In Figure 4.7, the in-plane deflections are limited by the portal frame itself (although the frame itself can still sway), whilst out of plane deflections are prohibited by the eaves beam because it is connected to the cross bracing system. There is no measure in place to prevent movement in the vertical deflection, i.e. vertical displacement is left free. Thus, the deflection degrees of freedom coincide with the design assumptions. The fixity of the rotational degrees of freedom is more difficult to explain and justify.

Rotation about the *x*-axis of the column (the out-of plane direction, in-plane rotations) will be resisted by the haunch and rafter. This connection allows rotation to some degree and cannot be classified as fixed. Rotation about the *y*-axis of the column (the in-plane direction, out-of-plane rotations) will be resisted by the bending stiffness of the eaves beam and/or the sheeting rail at the top of the column. It would require special attention in design and a very stiff eaves beam to ensure that a fixed connection is provided. This is not practical, so, as for the previous rotation direction, this scenario will fall in the "grey area" in between a fully fixed and free boundary condition. It was decided that, because the design methodology does not aim to prevent either of these rotations from occurring, that it would be adequate to assume that there will be no fixity and thus allow for rotation about the *x*- and *y*-axes to occur freely.

Eaves beams are often used in portal frame structures, not only to transfer gable wind loads to the longitudinal bracing system, but also to prevent torsional deformations at the top of the column. Therefore, it was decided to fix the torsional (rotation about the longitudinal axis) degree of freedom at the top. This leads to a scenario with identical boundary conditions at the top and bottom of the column.

4.2.1.3. Universal Joint

To enforce the above boundary conditions in a practical way was a difficult thing to manage. It was eventually decided that designing a so-called universal joint would be the most effective way of ensuring that the boundary conditions were present. The universal joint concept is extensively used in machinery where there is a driveshaft and it is necessary to transmit rotary torque. By making a few modifications a suitable joint can be envisaged (see Figure 4.8 below) which will be able to transmit the axial load, whilst not resisting any rotation about both the *x*- and *y*-axes.

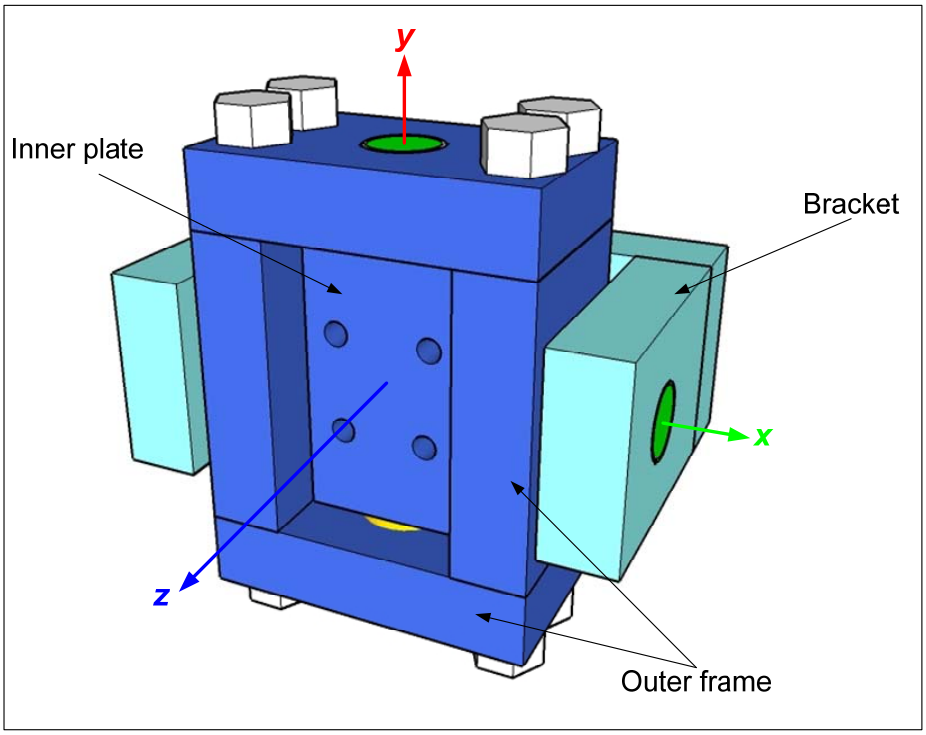

Figure 4.8 - Universal joint (modified)

The functioning of the universal joint is explained as follows. The column base is bolted onto the inner plate. This inner plate is mounted on an axle through its centre line, and can thus rotate around the *y*-axis of the column. The inner plate's axis then rests into the outer frame. This outer frame has an axis in the columns *x*-direction (through its centre line) and thus the whole set-up can rotate around both *x*- and *y*-axes, which is the desired behaviour. The whole universal joint rests into a bracket which is then attached either to the load actuator or the load measuring cell. Special torsion resisting restraints were made, which restricted the universal joint from moving about its centre axis.

As stated in Section 4.1.2 the design load was taken as 400 *kN*. The detail designs of the various parts of the universal joint have been attached in Appendix A (these include the calculations and details for the connecting brackets and the details of the torsional restraints).

4.2.2. Sheeting rail boundary conditions

It is expected that the sheeting rail will behave in the following way when the column is loaded under axial compression:

- As the column is loaded and nears the buckling load, rotation will occur at the height of the sheeting rail (about the *y*-axis of the column) as we have seen from the preliminary 2-dimensional investigations performed in Prokon in Section 3.
- This rotation will exert a moment in the sheeting rail (double curvature) that will cause bending about the weak axis of the sheeting rail.
- In addition to this moment, we have seen in Section 2.3 (refer to Helwig and Yura [15] for torsional restraint) that there will also be some rotation of the column about the centre line of the sheeting rail. This twisting of the column will exert a bending moment about the strong axis of the sheeting rail (the torsional restraint provided by the sheeting rail to the column is a factor of the sheeting rails bending stiffness about its strong axis).
- Thus we can expect bi-axial bending in the sheeting rail.
- We have previously seen (Section 3) that an inflection point is present mid-way between columns (due to the rotation caused when the column buckles in flexure). No mention has thus far been given to whether or not a similar inflection point is present for strong axis sheeting rail bending (which is caused when the column buckles in torsion).

To determine if such an inflection point exists (for strong axis sheeting rail bending), one can look at the behaviour of the columns, viewed in plan as shown in Figure 4.9. Similar to the flexural buckling of the columns themselves, there are many possible (and mathematically valid) outcomes for the behaviour of these members. It therefore comes down to the question of which outcome is the most likely.

As with column buckling described in Section 2.1.1 the most probable buckled configuration is the one which uses the least amount of energy to reach. De Villiers Hugo [9] states that if the sheeting rails were to bend as in Figure 4.9 b) the sheeting rails would then need to be extended to ensure equilibrium. This has a higher energy “cost” for the system. So it becomes more likely that all columns will twist in the same direction. This is shown in Figure 4.9 a), and has the added advantage of an inflection point at the same position as for the case of weak axis bending in the sheeting rail.

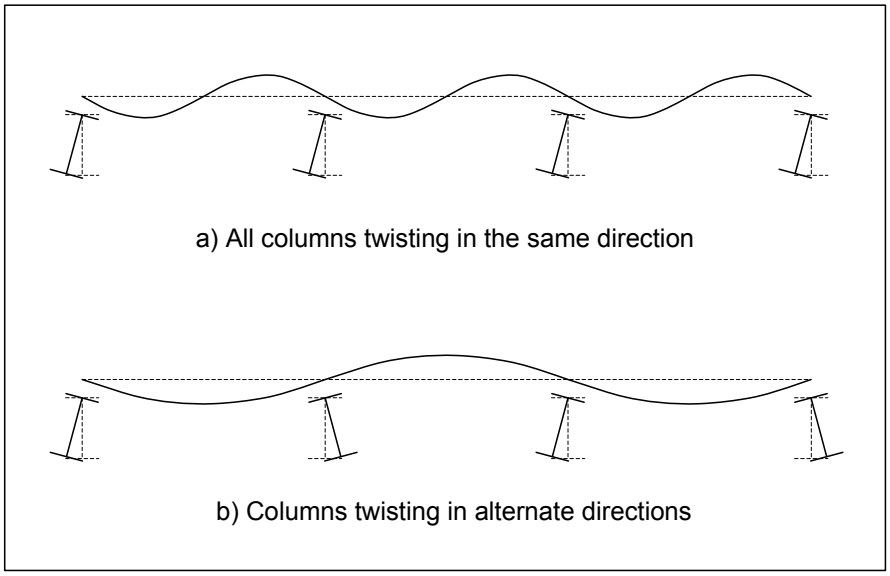

Figure 4.9 - Twisting behaviour of columns.

These inflection points were approximated by the relatively simple system shown below. The shaft prevents the movement in the x- and z-directions whilst lock nuts, on either side of the sheeting rail wall, prevent the sheeting rail from translating in the y-direction.

Figure 4.10 - Sheeting rail boundary condition

A limitation to the chosen experimental model is that, as the axial load is applied the column will shorten axially. In the full generic system all of the columns will shorten by an equivalent amount under the same load. This means that the inflection points between columns on the sheeting rails will actually move vertically down accordingly. In the experimental set-up these inflection points will be fixed in space, and will not move vertically down as the column is squashed. This causes the sheeting rail to resist the applied loading in a way that it would not in a practical, full scale system. This type of limitation was unavoidable when selecting a sub-model from the whole system. However, since the

bending moments are the same on either side of the column they will not induce any additional twisting in the column and this limitation is thus considered acceptable.

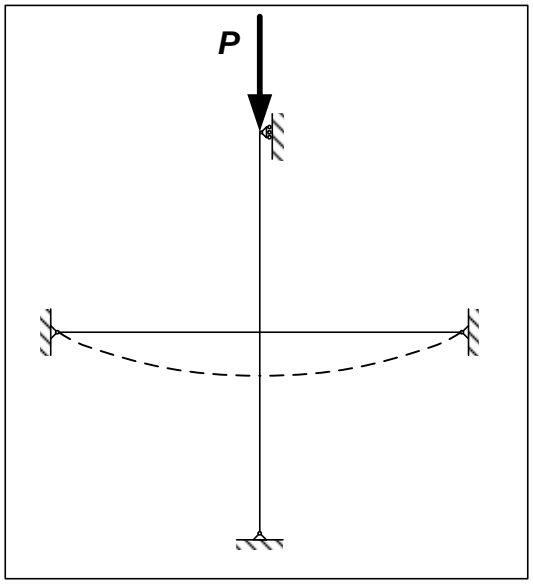

Figure 4.11 - Limitation of the experimental model

4.3. Experimental tests

More information about the experimental set-up seen in Figure 4.1 at the start of this chapter is provided in this section. Also, the location and techniques used for measuring the required data from each test is explained.

4.3.1. Testing frame

The testing frame was assembled from a number of existing stiff structural members, part of a set in the Stellenbosch structural laboratory. This set-up was made up of the following members:

Table 4.2 – Test frame members

Member	Cross-section	Length (mm)	Number used
Universal Column	254 x 254 x 89	5000	4
Channel Beam	BS Taper channel: 381 x 102 x 55	4860	6

In addition to these members there are shoes, which connect the universal columns to the strong floor of the laboratory. These shoes allow for a fixed connection between the columns and the strong floor. The shoes can be attached to the strong floor via the bolt holes in the floor, which are spaced on a grid of 3 feet by 3 feet (or approximately 914.4mm). The final arrangement of the layout in plan view is shown in Figure 4.12 below.

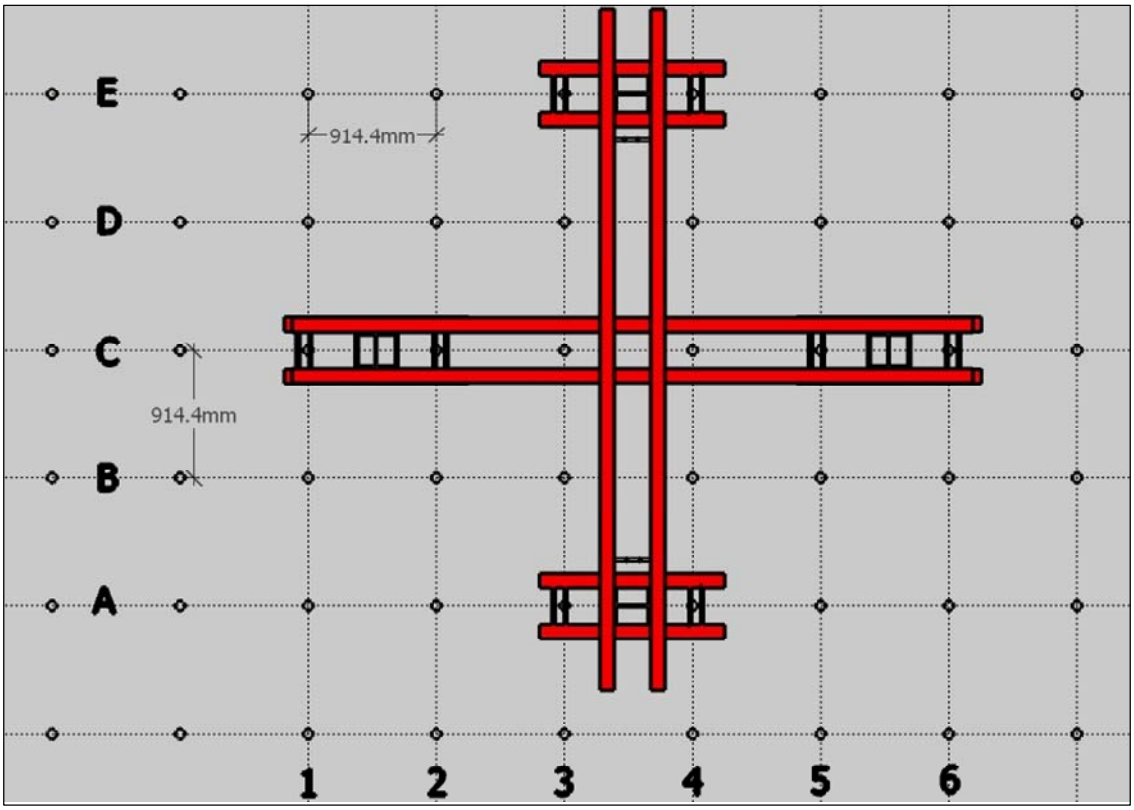

Figure 4.12 – Test frame layout (Plan view)

The test column (IPE100) coincides with gridline C, whilst the sheeting rail was positioned along the midline between gridline 3 and 4. Four channel beams were used to frame the test column, two below and two above, at a distance of approximately 1.3*m* between the centre-lines of the two beam groups. This was a measure of reducing the bending moments generated in the universal columns as a result of the high design applied load of 400kN, which was applied to the universal column about its weak axis.

The remainder of the experimental set-up was designed to ensure that the completed assembly would fit directly into this testing frame layout. The workshop drawings of all the items that had to be manufactured are attached in Appendix A.

4.3.2. Load application and measurement

The devices chosen to apply and measure the load form an important component of the test set-up, in terms of geometric size and placement as well as the capacity of the devices. The devices that were utilised are listed below in Table 4.3:

Table 4.3 - Load application and measurement

Function:	Device	Capacity
Application	Enerpac: RCH-603	60 tonnes
	Electric Enerpac pump	700 bar - pressure
Measurement	HBM: C2 Load Cell	50 tonnes

The electric pump used on the Enerpac load actuator was very helpful, and allowed for an almost constant rate of load application, which would not have been possible if a hand pump had been used.

A universal joint was placed on either end of the test column, to enforce the desired boundary conditions. The load cell was connected to the base universal joint whilst the Enerpac load actuator was connected to the top universal joint. Each universal joint has a different method of connection which is designed to fit onto the relevant device at the respective end of the column (see detail drawing in Appendix A).

The universal joint at the column base was designed to slot onto the knob of the load cell. It was originally planned that the torsional restraint of the column base could be provided by three grub screws which would create sufficient friction between the load cell and the universal joint. However, it was observed during the first test set-up that this method of torsional restraint was ineffective, and thus it was decided that twist-resisting plates, bolted onto the end-connection columns, should rather be used to ensure the torsional fixity of this end connection. Detailed drawings are provided in Appendix A:.

The universal joint at the top of the column was made to connect to the Enerpac load actuator by threading directly into the hollow cylinder of the actuator. It was originally planned that the torsional degree of stiffness would be fixed by means of a locknut, which would prevent any rotation between the universal joint and the piston of the load actuator. However, it was observed that the piston of the load actuator was able to rotate about its centroid. This rotation was not fully free, as there are frictional forces that need to be overcome to cause the rotation. It was initially assumed that this semi-free torsional boundary condition would be a closer approximation to the boundary condition found in practice, as described in Section 4.2.1.2, rather than enforcing zero rotation on the end of the column. For the first 4 tests this was left as it was, with the rotation of the piston of the hydraulic actuator being measured during the tests. After analysing the results, it was noticed that the rotations were larger than originally anticipated. Thus, twist-resisting devices were made, similar to those at the other end of the column, to reduce the twisting of the top of the test column.

A further connection needed to be devised to connect the load application and measurement devices onto the testing frame universal columns. These connections, called the end connection columns hereinafter, were manufactured from flame cut plates and had to provide sufficient stiffness to cope with the design load of 400kN. The detailed drawings are attached in Appendix A:.

4.3.3. Displacement and rotation measurements

4.3.3.1. Lateral deflections and twist along the column

In order to reduce the complexity of the test, the number of measuring points along the column was limited to two positions. These were near mid-height of the column, and at a quarter-point along the length of the column, nearer to the top of the column. The positioning of these measuring points is shown in Figure 4.13. The measuring position near mid-height of the column could not be positioned any closer to the actual mid-point position due to the presence of the sheeting rails and the cleat. Furthermore, the theoretical symmetrical nature of the lateral displacements of the buckled configuration led to the decision to only measure the displacements of one half of the column.

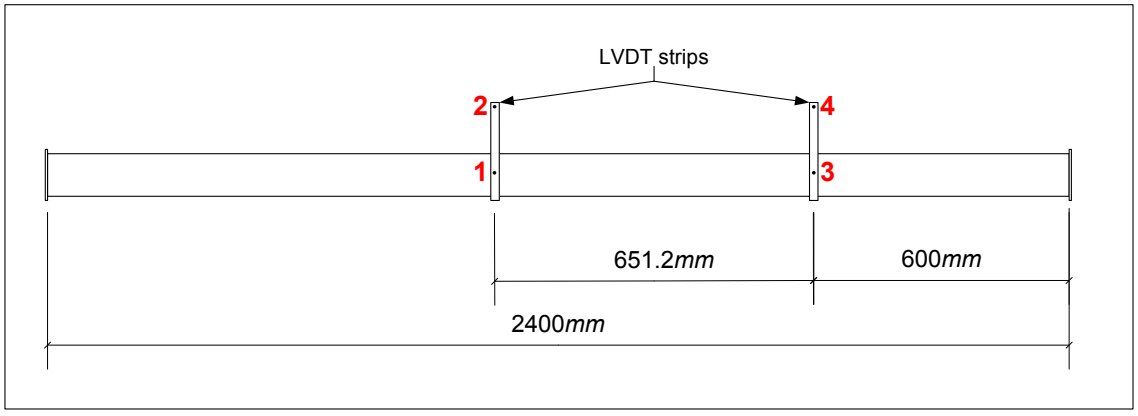

Figure 4.13 - Placement of LVDT's

Measurements **1** and **2** from above were placed to the left of the mid-span point of the column. This was ideal as it allowed the direction of the twist of the column to be measured on either side of the

sheeting rail. This provided a more complete understanding of the distribution of the twist over the columns length.

At each of the measuring points on the column, two plunger Linear Variable Displacement Transducers (LVDT's) were put into position. It was necessary to use two at each position, so that the twist in the column could be determined as well as the lateral displacement. A 260*mm* length of 16 x 16 x 1.5 *mm* angle cross-section was used and can be seen in Figure 4.13 labelled as the LVDT strips. The large length of these LVDT strips was used to increase the difference between the two displacement measurements at each point to facilitate calculating the angle of twist.

According to the literature, when an eccentric lateral restraint is used, it is expected that the column will twist around the centroid of the sheeting rail. It was thus decided that the holes on the LVDT strip would be spaced 100*mm* either side of the centroid of the sheeting rail. This means that the lateral displacement of the column at a point will be given as the average of the top and bottom readings and the twist angle will be given by the arctangent of the difference between the two readings divided by the distance between measuring points, which in this case was set as 200*mm*. This can be represented mathematically as shown below in Figure 4.14, which shows the translated and rotated position of the LVDT strip. In the formula's presented below, Δ is the lateral displacement of the member and Φ is the rotation of the member.

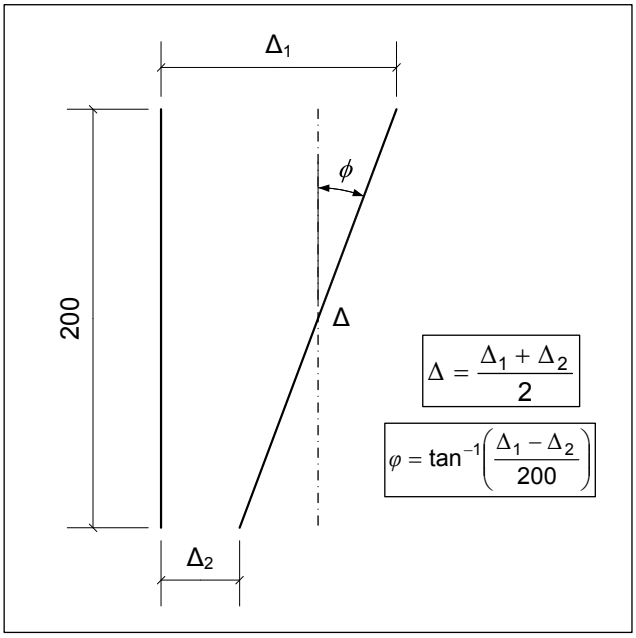

Figure 4.14 - Calculation of lateral deflection and twist angle

4.3.3.2. Axial deflections and twist at the top universal joint

Axial deformations were measured by simultaneously measuring the deflection of the load actuator piston and the flexural deflection of the testing frame universal column at the opposite side of the test column. For this purpose two Wi10 spring LVDT's were used. The difference between these two results yields the axial shortening of the test column as the load is applied.

Twist of the top universal joint was measured for all the experiments by logging the lateral movement of a point 10*mm* from the top of the universal joint. This was measured using another Wi10 spring LVDT. The twist was then calculated by using the following formula:

$$\varphi_{end} = \tan^{-1}\left(\frac{LVDT_{reading}(mm)}{80mm}\right); \qquad (4.6)$$

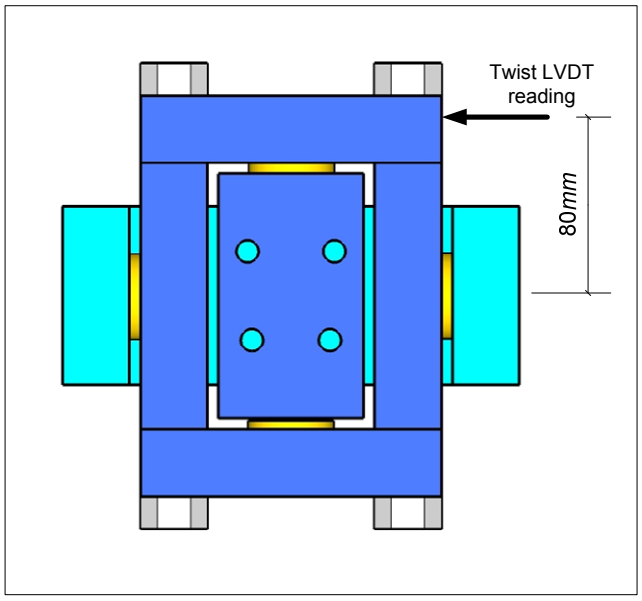

Figure 4.15 - Twist of top universal joint

4.3.4. Test procedure

The procedure that was followed for each test was as follows:

1. The top universal joint was threaded into the Enerpac hydraulic actuator,
2. The column is bolted onto both universal joints,
3. The hydraulic actuator was extended until the base universal joint made contact with the knob on the load cell,
4. The twist resisting members and (if appropriate) the lateral bracing members were positioned
5. All LVDT's were aligned and zeroed,
6. Each of the columns was given a preload of approximately $\boldsymbol{P_{cr} / 1.6}$. The preload was then removed.
7. Then the LVDT's were re-zeroed and the actual test was performed until failure was observed.

Whilst all possible care was taken in the set-up of each experiment, there was still the possibility that the column was not completely unloaded. This could be seen to slightly reduce the critical load.

4.4. Experimental results

The experimental tests were performed at the slowest possible rate of extension of the electric load pump. During the tests, data was recorded at a rate of 25 *Hz*. This rapid measurement rate ensured that the behaviour of the column at failure could be mapped correctly for all points along the load-deflection curves. The important results obtained from the experimental set-up, were the lateral deflections and twist of the column as the load is applied, as this illustrates what the mode of failure for the column was. Also important was the critical load itself. The critical load from the tests was taken as the maximum load carried by the column. After this maximum load is reached there was always some unloading due to the sudden unstable nature of failure and the displacement based testing method.

A method that has been successfully used to determine the critical buckling load of a column, without actually testing the column until failure, is the Southwell plot. In this method, the lateral deflection (y_e) of the column is measured as the increasing load is applied. Then the following graph can be plotted:

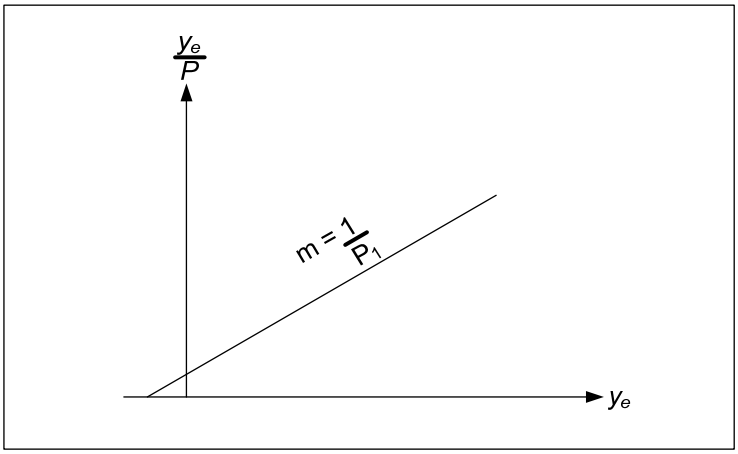

Figure 4.16 - Southwell plot [9]

The critical load of the column is found to be the inverse of the slope of the above graph. This is a useful non-destructive testing technique to find the critical load of columns. It was decided that the Southwell plot would be constructed on the recorded experimental data in order to determine, using a separate approach, what the buckling capacity of the column is and then compare it to the actual observed maximum load carried by the column. The data points that were plotted were selected from before the column buckled, so as to ensure that a linear trend was present. The Southwell plots for each test have been attached in Appendix B: Southwell plots.

The placement of LVDT's was outlined in the previous section but will briefly be repeated here. For all tests, the lateral deflections, and thus twisting of the cross section, were measured at two points on the column. These were at a quarter-point along the columns length and also close to mid-height on the column. These deflections and twists formed were the main method of determining the mode of column failure, and as such will be presented herein.

The universal joints were seen to perform relatively successfully. The one major drawback was that the bolted method of connection, employed to joint all the members together, allowed a slight amount of settling to occur under the loaded condition. This had the effect of causing misalignment between the shafts and the bearings. Thus, although it was ensured that the universal joint was able to freely rotate at the start of each test, it was observed that when the set-up was disassembled the universal joints were stiff. Realignment was performed between each test in an effort to mitigate any effects this behaviour might have caused.

4.4.1. Initial Imperfections

It is useful to know what the initial imperfections of a test piece are before the test begins because the magnitude of initial imperfections can influence the observed capacity of a test to a large degree. Data was measured for seven of the nine tests. The maximum limit on the magnitude of initial imperfections in structural steel is set at a value of *L/1000*, which in context means a maximum out of straightness of 2.4*mm*.

The procedure used to determine the initial imperfections was relatively simple, which resulted in a few measurements which gave an indication of the trend of deformation over the columns length. Fishing line was drawn tight between the base and the top of the column. The value of the imperfection (the distance of the flange away from the fishing line) was then measured at three points along the column, as indicated in Figure 4.17, by using Feeler gauges. This was performed for both horizontal and vertical imperfections. No measurements were taken of the initial twist of the column although it was seen to vary significantly over the length of the column.

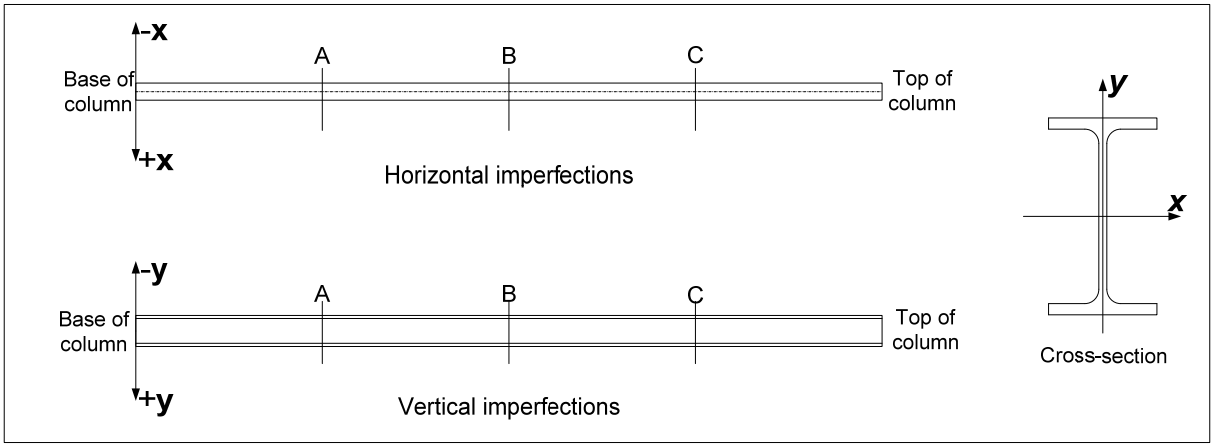

Figure 4.17 - Measuring points for initial imperfections

These measurements have been compiled below in Table 4.4. It can clearly be seen that the initial imperfections do not form the assumed sinusoidal pattern which is always assumed in design. Most of the imperfections are smaller than the maximum acceptable value of 2.4*mm*, except for the column used in Test 7 which had a maximum measured value of 2.74*mm* which is equivalent to *L/876*. The critical loads of the columns with the worst imperfections were seen to be somewhat lower than

expected (as will be outlined in more detail shortly). It thus seems likely that the initial imperfections can be attributed as the reason for this reduction in capacity.

Table 4.4 - Measured initial imperfections

Test number	Initial imperfections (mm)					
	Horizontal			Vertical		
	A	B	C	A	B	C
3	1.48	1.03	0.96	-0.65	-0.95	-0.2
4	-1.01	-1.2	-0.35	0.4	-0.5	-0.05
5	0.4	0.65	0.7	-0.55	-0.7	0.25
6	0.25	0.6	1.15	-0.12	-0.47	0.18
7	1.64	2.74	2.04	0.85	0.65	-0.05
8	0.4	0.95	0.55	0.2	-0.35	-0.35
9	-0.65	-0.3	0.2	0.35	-0.35	-0.2

4.4.2. Determination of the yield stress

It is desirable to have specific information about the actual material used during the experimental tests. To obtain this information tensile tests were performed on a sample of coupons cut from the columns. The information obtained from this was the yield stress of the material (f_y) and the ultimate tensile strength (f_u). A sample of 15 coupons was tested in order to determine the values for f_y and f_u by using some statistical basis. The results are included below in Table 4.5. It is important to note that all of the steel tested had a yield strength greater than the value of 350 MPa.

The average failure stress for this steel was found to be **416 MPa**. The graphical results are attached in Appendix C.

Table 4.5 - Tensile test results

Sample No.	f_y (MPa)	f_u (MPa)
1.1	393.35	535.149
1.2	437.7	565.248
1.3	411.74	535.111
1.4	455.09	582.65
1.5	414.01	541.924
2.1	406.28	531.995
2.2	418.29	548.804
2.3	406.1	537.439
2.4	409.79	544.257
2.5	406.84	537.792
3.1	418.63	533.945
3.2	420.84	544.282
3.3	406.78	524.002
3.4	419.45	551.697
3.5	417.41	548.48

Mean	416.15	544.19
Std. Dev	14.60	14.48

4.4.3. Unsupported column – Test 1, 2 and 3

The first three tests were mainly performed in order to determine the effectiveness of the test set-up and the boundary conditions. There were no lateral supports and the buckling mode of failure was predicted as being the first mode of flexural buckling. The critical loads measured for the experiments are tabulated below alongside the expected upper bound (Euler capacity) and lower bound (code capacity) of the critical loads. Also tabulated are the results obtained from making a Southwell plot of the results from each test. There was seen to be a strong correlation between the maximum load carried by the column and the critical load predicted from the Southwell plot.

Table 4.6 - Test 1 – 3 critical loads

Test number	Code capacity (kN)	Euler capacity (kN)	Southwell – P_{cr} (kN)	Experimental - P_{max} (kN)
1	46.15	54.27	51.81	55.98
2			47.17	48.71
3			44.05	44.2
		Mean	**48.62**	**49.63**

The above figures represent the lateral displacement and twist recorded as the axial load was applied. The solid lines above represent the calculated twist of the column in **x10^3** ***radians***. The dashed lines represent the lateral deflection of the column in ***mm***.

The results observed from these first three experiments clearly indicated that the failure mode was first mode flexural buckling (Figure 4.19). However, based on data shown above, there are two concerns.

4.4.3.1. Lateral deflections

The first concern is the shape of the load-deflection curve for Test 1 (Figure 4.18 a)). Typical load-deflection curves for unsupported columns have a shape similar to that seen for Tests 2 and 3 where the deflection remains small for a stable part of the load-deflection curve, and then is seen to increase at a rapid rate, for little increase in the applied load. The asymptote of this load-deflection path is the critical load for the column. Test 1 was witnessed to have very small deflections right up to the very sudden buckling of the column. Also, the maximum load supported by the column was recorded as being larger than the Euler load for such a column; this should not be possible for a pin-ended connection.

During the pre-load cycle of the Test 1 the electric pump was set at a slightly higher rate than expected. This resulted in a pre-load that was in fact larger than the code capacity, a value of slightly over 48*kN*. It is thought that the initial loading of the universal joints due to the high pre-load could potentially have caused the joint to tighten up, as explained earlier. This might have caused a somewhat less than ideal pinned connection for the actual experiment, which might also explain the high capacity.

Figure 4.18 - Lateral deflections and rotations for unsupported column

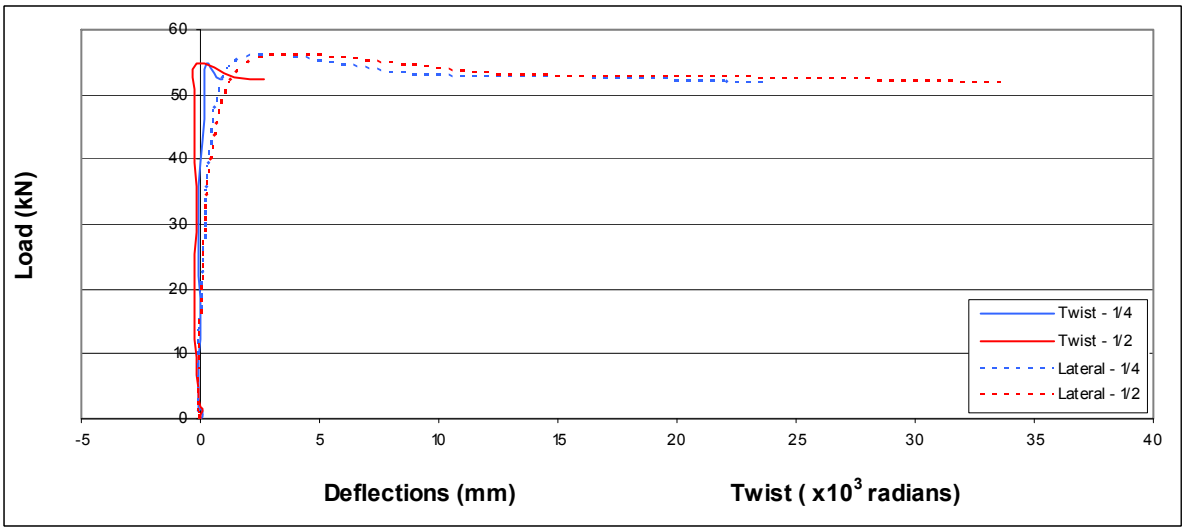

a) Test 1

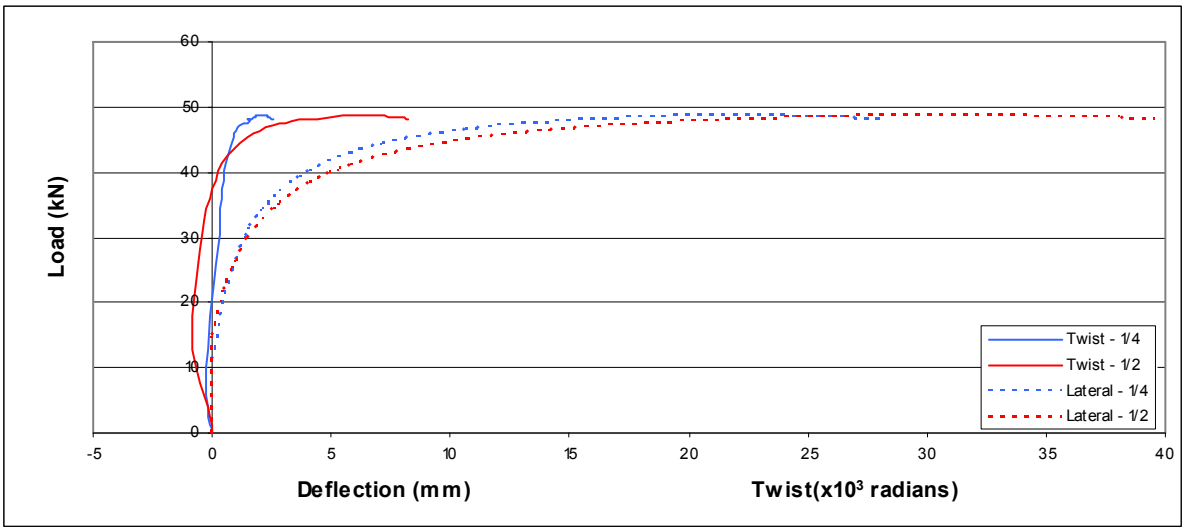

b) Test 2

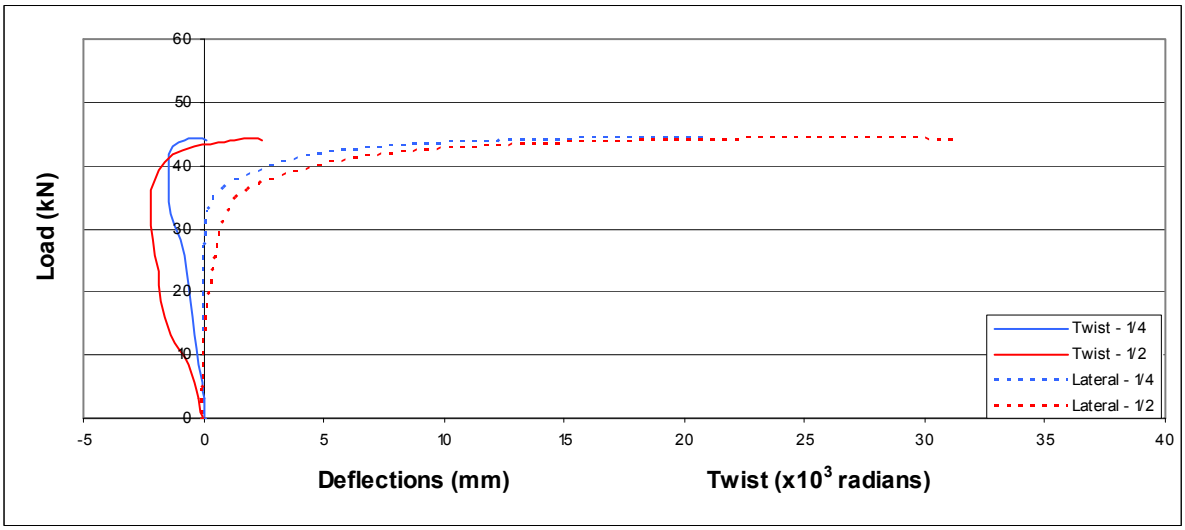

c) Test 3

Figure 4.19 - Buckled shape of Test 1

Secondly, and more troubling, was the very low critical load of the column in Test 3. The critical load is in fact less that the code calculated capacity. The only explanation for this is thought to be the initial imperfections in the column. Table 4.4 above shows that this column had the second largest horizontal imperfections and the largest vertical imperfections. This fact seems to give credibility to this argument. It is unfortunate that no initial imperfections were measured for the first two tests, as this could have validated this argument.

4.4.3.2. Twisting of the column

The twist measurements in all three of the tests were seen to follow a similar path to that of the corresponding lateral deflections. It is interesting to observe that for all cases the initial stages of the loading were accompanied by twisting in the negative direction. However, as the column began to buckle in a flexural mode this twist was observed to change direction as well as increase in magnitude. The twist does not increase in magnitude nearly as drastically as the lateral deflections were observed to. For example from Test 2:

Table 4.7 - Mid-height deflection and twist - Test 2

	Load (kN)	Lateral deflection (mm)	Twist ($x10^3$ radians)
	24	0.717	-0.606
	48	25.82	4.9737
Increase by:	**2.0**	**36.0**	**9.14**

The above data illustrates that the failure mode is a flexural mode. For an increase in load by a factor of **2** (so the upper limit is close to the critical load) the lateral deflections increase by a factor of **36**. For the same increase in load the twist increases only by a factor of **9.14**.

In conclusion, the experimental set-up exhibited good behaviour and, in spite of some stiffening of the universal joint under load, the set-up facilitated the predicted failure by first mode flexural buckling. It is always to be expected that there will be variations in any set of experimental readings. The mean value of the critical loads measured is also shown at the end of Table 4.6 and falls squarely between the upper and lower predicted bounds.

4.4.4. Eccentrically supported column – Tests 4, 5 and 6

The second series of tests dealt with the behaviour and failure modes that form part of the actual interest of this investigation. The column is supported at mid-height by a continuous sheeting rail. The sheeting rail is connected to the column simply by a two bolt connection onto a cleat. There are no specific measures used to limit distortion of the columns cross-section. The predicted critical loads are based on the buckling being by second mode flexure. No torsional and/or rotational restraint was assumed effective in the calculation of these envelopes.

Table 4.8 - Test 4 – 6 critical loads

Test number	Code capacity (kN)	Euler capacity (kN)	Southwell – P_{cr} (kN)	Experimental - P_{max} (kN)
4	143.9	217.95	227.27	220.5
5			204.1	203.4
6			200	200.3
		Mean	**210.46**	**208.07**

The position of the measuring points for the LVDT's lie on different sides of the sheeting rail. The quarter-point reading is taken on the top half of the column; whilst the mid-height reading is actually 51*mm* below the sheeting rail on the bottom half of the column. This explains why the direction of the lateral deflections was seen to be opposite when the column buckled, as it deformed into the s-shape of double flexure.

4.4.4.1. Lateral deflections

The columns were all observed to buckle in the second flexural mode. Figure 4.22 shows that the mid-height lateral support provided by the sheeting rail, was very effective as was witnessed by the very small magnitude of the lateral deflections until loads well over the code capacity of 143.9*kN*. Beyond this load, the lateral deflections increase rapidly.

After buckling there was a rapid drop-off of the load in the column. This must have been the case due to the yielding caused by the high bending stresses at the failure point.

Figure 4.20 - Buckled configuration of Test 4

4.4.4.2. Twisting of the column

Figure 2.1 a) and c) show that the twist in the columns of Test 4 and 6 are initially in the same direction, with the mid-height twist reading actually seen to be larger than the reading at a quarter-point. After buckling the quarter-point twist increased in the same direction, in which it was originally twisting, as the load decreases. The mid-height twist of the column changed direction after buckling occurred. This behaviour infers that, prior to buckling, there was one half sine wave of torsional-flexural behaviour, with the magnitudes of all displacements being relatively small. The sheeting rail only provides elastic restraint against twisting of the column, so this allows for this manner of deformations to occur, as witnessed during the experiments. In spite of the initial single half sine wave in torsional-flexural deformations, these two columns still failed in a flexural buckling mode as was expected. Thus, after buckling, the columns displayed two half sine waves over the columns length which shows that they were deforming in the second torsional-flexural mode. The twist in the columns did not increase rapidly in magnitude, which means that failure was by flexure.

Figure 4.21 - Large mid-height twist - Test 5

The column in Test 5 behaved in a different manner. Figure 4.22 b) is only the initial part of the load-deformation curve. The full load-displacement curve is shown in Figure 4.23. The initial, stable region of the load-deformation curve displays very similar behaviour to the other two tests in this series. However, the postbuckling behaviour differs greatly. Both the quarter-point and mid-height readings increased in the same direction after buckling, which is already different from the previous two tests. At the final point on the load-deformation curve shown in Figure 4.22 b) the lateral deflections and the twist in the column both become larger. After this point, the twist increases rapidly, the maximum twist was recorded at mid-height and this twist was clearly visible to the eye, as shown in Figure 4.21. This shows that the column underwent a failure mode which included maximum twist at the connection to the sheeting rail, whilst maximum displacement was recorded at the quart-point position. This is a combined second flexural mode and first torsional-flexural mode of buckling. This buckled configuration is illustrated by Figure 2.14 [12] which shows that the deformation of the cross-section is mapped by both a twist (φ) and a lateral deflection (u). In this case the twist was distributed as one half sine wave over the length of the column, whilst the lateral deflection was two half sine waves over the columns length. Thus, Test 5 buckled in a torsional-flexural mode.

Figure 4.22 - Lateral deflections and rotations for column with sheeting rail

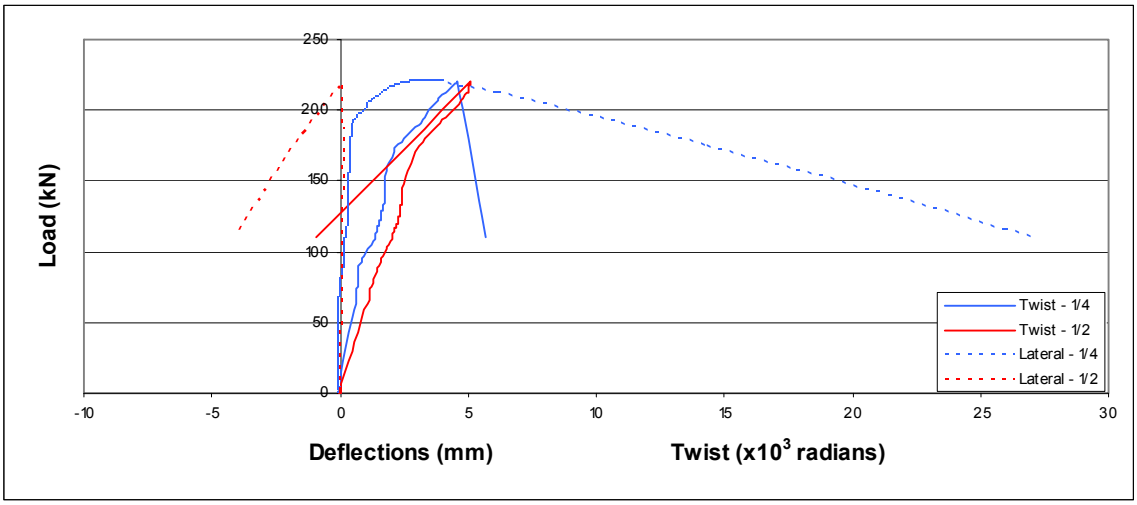

a) Test 4

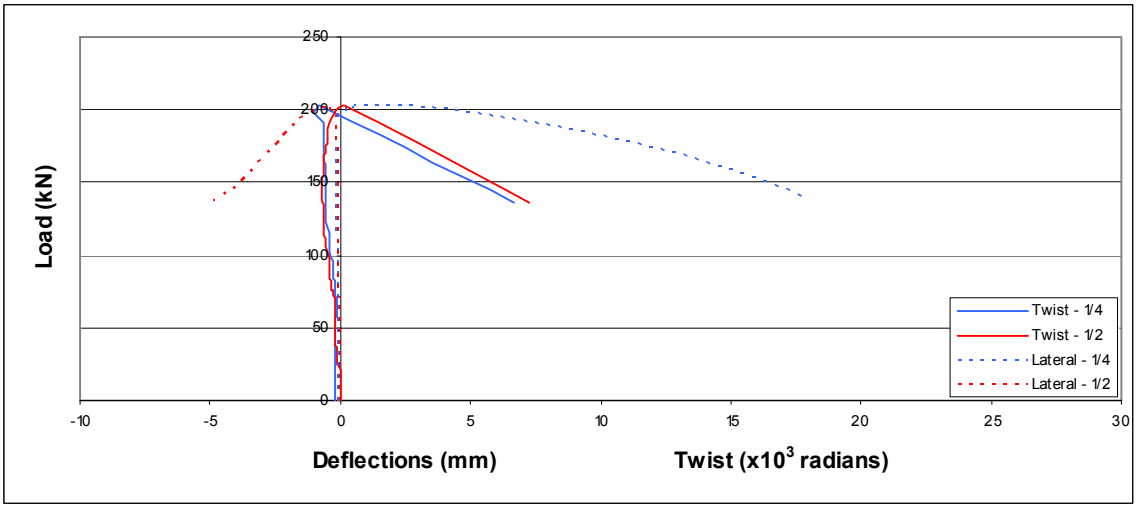

b) Test 5

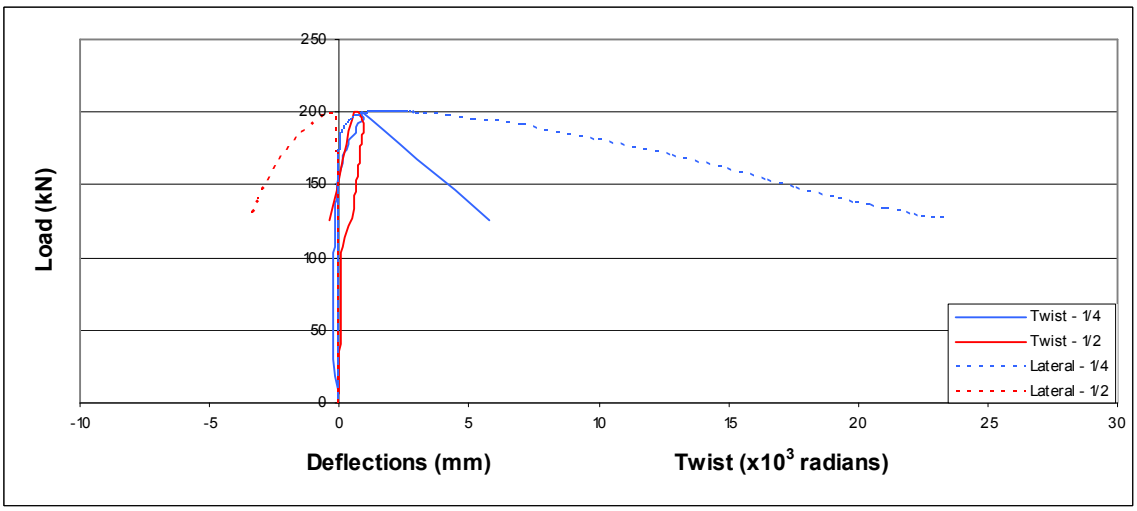

c) Test 6

In spite of the differences in post-buckling behaviour the observed critical loads (Table 4.8) of all three columns was in the same order of magnitude, i.e. no lower failure mode was seen to occur

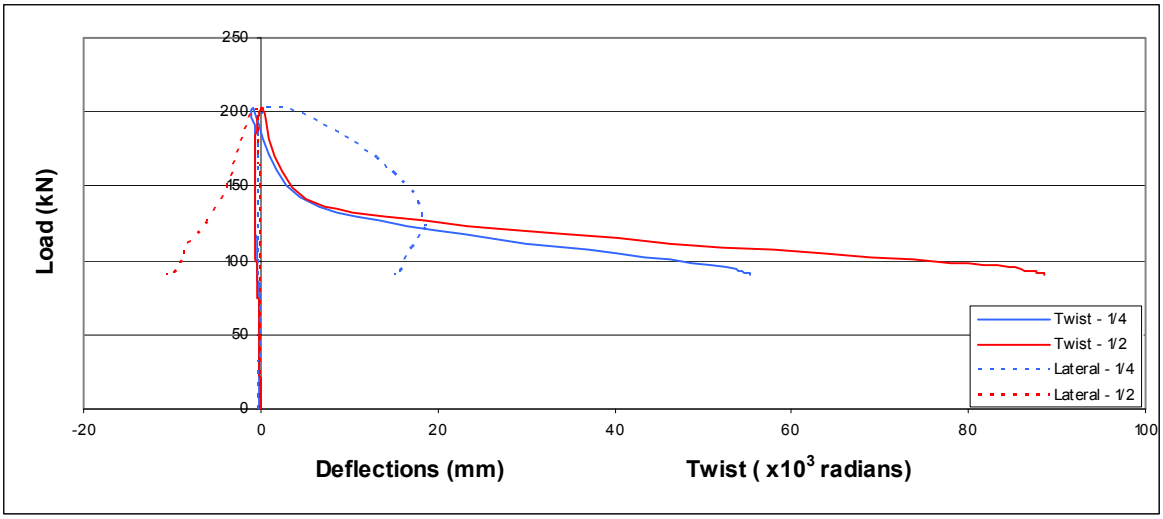

Figure 4.23 - Lateral deflections and twist - Test 5

.

4.4.5. Laterally supported column – Test 7, 8 and 9

The connection between the sheeting rail and the column was reinforced by the addition of fly braces. The specific aim of this type of connection is to ensure that the whole cross-section is supported against rotation, as well as local deformations. The predicted mode of failure remained the same as that of the previous series of tests, which was expected to be second mode flexural buckling.

Table 4.9 - Test 7 – 9 critical loads

Test number	Code capacity (kN)	Euler capacity (kN)	Southwell – P_{cr} (kN)	Experimental - P_{max} (kN)
4	143.9	217.95	196.1	187.8
5			208.3	209.54
6			227.3	221.3
		Mean	**210.57**	**206.21**

The failure of columns was very sudden and, unfortunately, this meant that the epoxy used to keep the LVDT measuring angles in place failed just after the buckling of the column occurred. The measuring angles located at the quarter-point position on the columns from Test 8 and Test 9 became separated from the column in this manner. Fortunately the measuring angles were still in position when the maximum load was reached. The data collected after the angles came loose from the column were neglected.

The critical load from Test 7 was recorded to be 187.8*kN*, which is almost 40*kN* lower than the critical load recorded for Test 9. This low capacity is still above the lower bound of the code capacity. The most likely explanation for this low critical load is the initial imperfections. The imperfections measured for Test column 7 were excessively large as shown in Table 4.4. The column failed in the predicted buckling mode; however, the magnitude of the load was significantly lower than expected.

4.4.5.1. Lateral deflections

Similarly to the previous series of tests, the direction of the deflection measurements (on either side of the sheeting rail) was in opposite directions. The maximum mid-height deflection measured for Test 9 seems disproportionately small; this is only the case because the data represented on Figure 4.25 c) is cut short due to the measuring angle (at the quarter-point position) coming loose from the column. However, the data was measured at mid-height through to the conclusion of the test, and so was available, but was neglected from the curve below to be consistent. This data showed that there was indeed negative deflection, similar to all the other tests in this series.

4.4.5.2. Twisting of the column

Figure 4.25 a) and b) show that the twist in the columns of Test 8 and 9 twisted in opposite directions on either side of the sheeting rail connection, during the stable portion of the load-deflection curve. This indicates that the columns are twisting in two half sine waves over the length of the column.

The behaviour observed from Test 9 was slightly different. The measured twist was in the same direction on each side of the sheeting rail. Right before buckling, the twist measurements were beginning to diverge. It is speculated that the behaviour would have been very similar to that observed during Test 4 and Test 6 from the previous series of tests. The magnitude of twist measured when the fly-brace was attached, seems to be much smaller than for the previous series of tests.

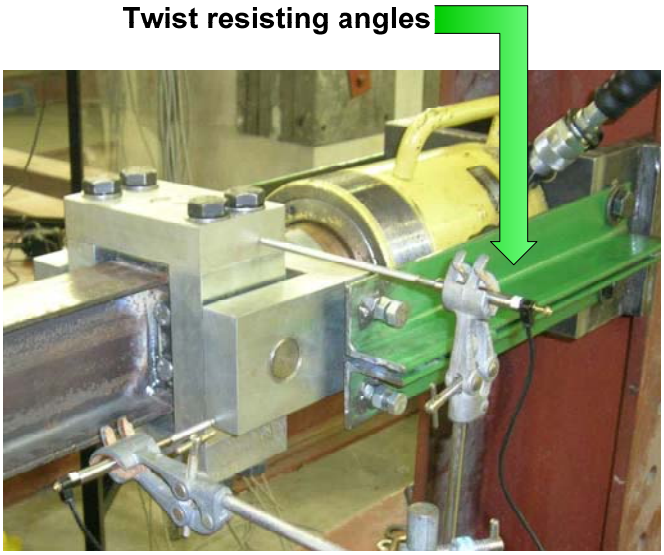

Figure 4.24 - Twist resisting angles at column top

Figure 4.25 Lateral deflections and rotations for column with sheeting rail and fly brace

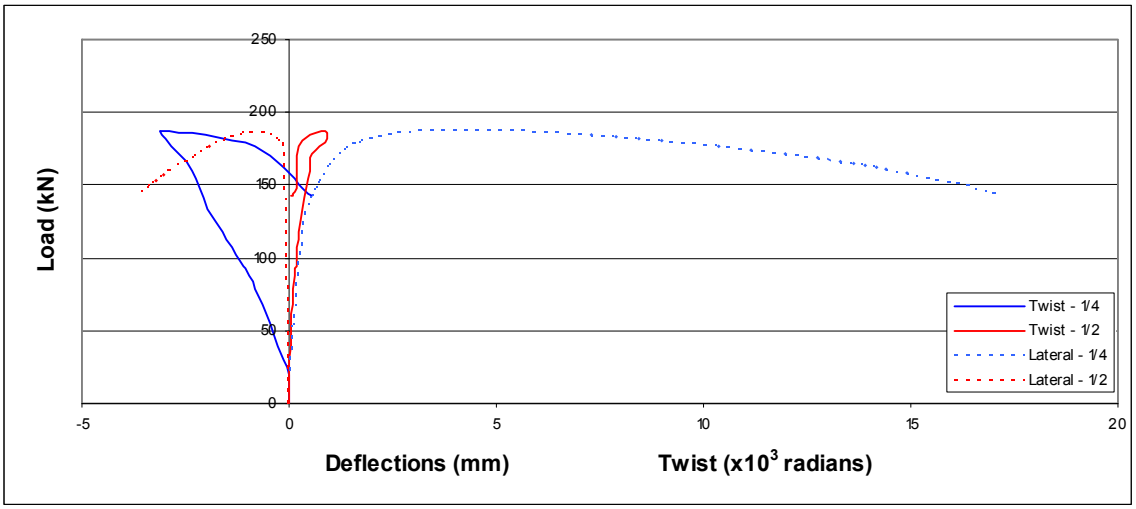

a) Test 7

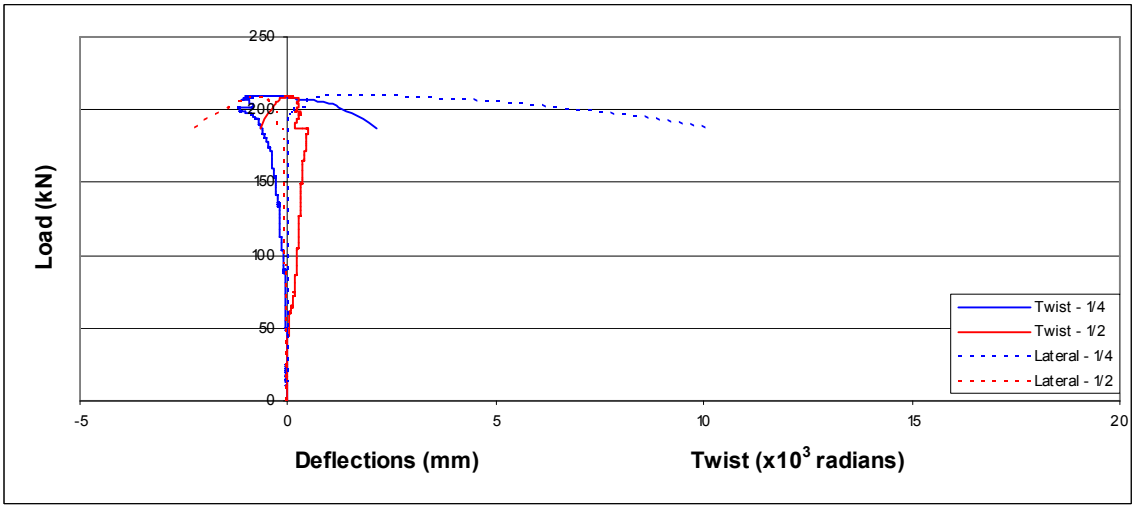

b) Test 8

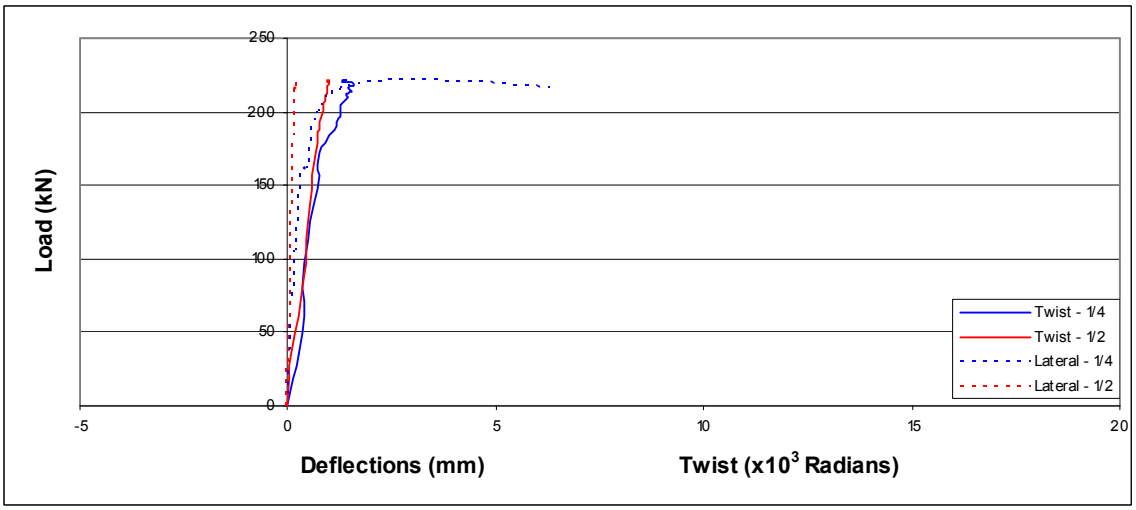

c) Test 9

4.4.6. Twisting of the top universal joint

The first four tests were performed with only the base of the column prevented from twisting. The recorded results of this twist during these first four experiments was much larger than expected, therefore this prompted the provision of twist resisting measures, similar to those found at the base of the column. This was realised by using two lengths of double angle sections to span the distance from the top end connection column to the top universal joint. These twist resistors did not eliminate the twist of the end of the column, but they were seen to reduce the twist. For detail drawings please refer to Appendix A:.

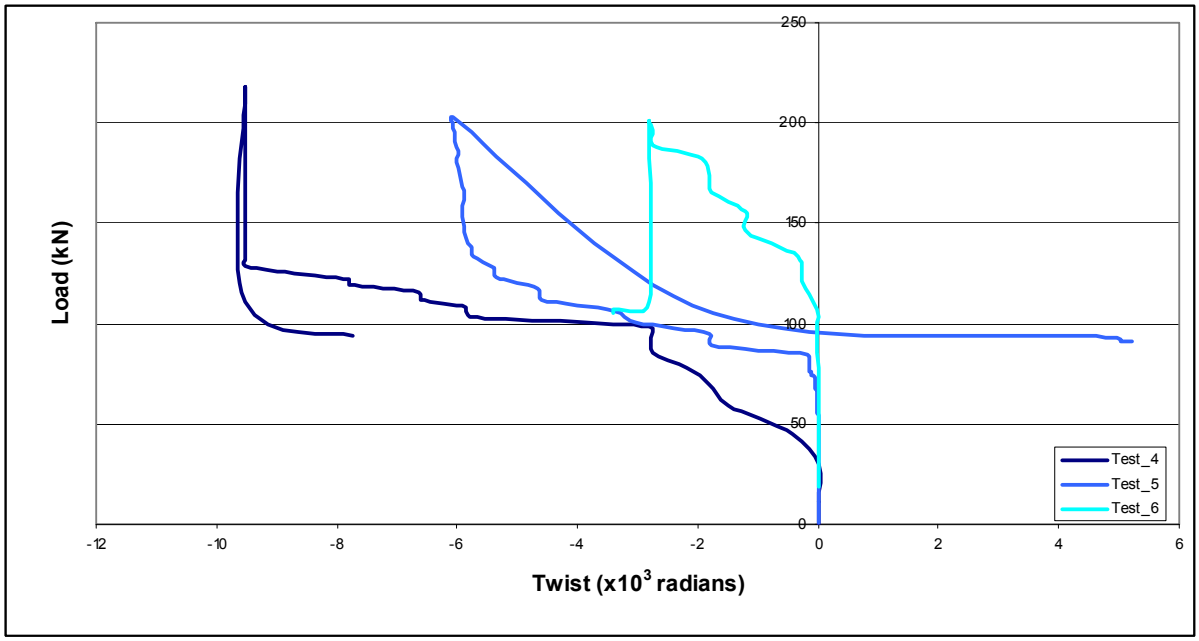

Figure 4.26 - Measured twist of the top universal joint

The magnitude of twist at the top universal joint during Test 4 was larger than the twist that was measured over the length of the column. However, for all remaining tests (with the twist resisting angles in place) the twist at the top was smaller than that measured over the length of the column.

4.4.7. Summary of test results

All possible care was taken to design a testing set-up that would exactly provide the idealised boundary conditions, in order to monitor the failure of the eccentrically restrained column. However, the following difficulties were encountered:

- The magnitude of the initial imperfections was larger than the acceptable tolerances in some cases. Although not specifically measured, the flanges of the columns were noticed to not be parallel - this varied over the column length as well.
- The piston of the hydraulic load actuator was free to pivot around its centroid. This had to be monitored during the tests, and measures to reduce this were put into place part way through the testing programme.
- Settling occurred in the universal joints under the high loads exerted on them, due to the tolerances left in using bolted fasteners. The joint was realigned between all tests in an effort to provide the desired boundary conditions.

It is thought that these difficulties listed above had the effect of increasing the variation of the recorded data from each series of tests. In spite of these difficulties, the outcomes of the test remain positive because the predicted behaviour of the members was actually observed to occur (even if at slightly varying load capacities).

4.4.7.1. Tests 1 – 3

The columns all failed in first mode flexural buckling at the average critical buckling load measured to be 49.63*kN*, which is a value that lies slightly above the code capacity of 46.15*kN*. It is postulated that the twist that was measured during these experiments was larger than would have been the case if there had been a fixed torsional restraint at the top of the column.

4.4.7.2. Tests 4 – 6

Test columns 4 and 6 failed in second mode flexural buckling. However, Test column 5 failed in a torsional-flexural buckling mode, with the twist distributed as one half sine wave and the lateral deflections distributed as two half sine waves over the columns length.. The average critical buckling load was measured to be 208.07*kN*.

4.4.7.3. Tests 7 – 9

The value of the twist measured at all points along the column was reduced with the addition of the fly braces, especially at mid-height on the column. The failure mode was observed to be second mode flexural buckling for all three of the tests. The measured average critical load of 206.21*kN* was very similar to that found above, even with the extremely low value measured for Test 7.

5. Analytical investigation

In a perfect world it would be possible to experimentally model every possible combination of column and sheeting rail combinations to determine explicitly what the behaviour is. Sadly, this is not possible on account of the very mundane factors of cost and time. The amazing and rapid progress in information technology has fortunately offered an alternative solution. Practically every engineer now has access to powerful Finite Element Software which has been seen to support and indeed drive the profession into areas that were previously unattainable.

The mundane factors of cost and time are unfortunately unavoidable, especially for research projects. As a result of this it has become common practice to perform a few select experimental tests and use the observed results to calibrate or validate a finite element model. Once a reliable model has been produced on the computer, it now becomes a relatively simple matter to obtain results for all of the multiple combinations from which results are desired. This is commonly referred to as a parameter study.

This section of the report aims to explain all the steps taken to produce a reliable and yet relatively simple model. All the modelling was performed in ABAQUS [25] which is a general, yet powerful finite element software package. In the initial stages of designing the analytical model, valuable guidance was gathered from previous research (Helwig and Yura [15], Taras and Greiner [1], and Bastiaanse [5]) which was performed on torsional-flexural buckling and other stability issues. This helped make decisions such as element type, mesh density, boundary conditions and analysis type. In the conclusion of this chapter it will be shown how the results derived from the analytical model compare with the observed experimental results.

5.1. Design of the model

In order to model the column and sheeting rail system, a number of assumptions had to be made. The assumptions made throughout the modelling process will briefly be explained and motivated. To a large degree most of the assumptions dealt with the method of connecting all of the members together in an applicable and reasonably accurate manner, even though the connections are not being investigated.

5.1.1. Element type and mesh density

In order to model the columns as well as the offset sheeting rail, it was decided that using shell elements would allow the most accurate three dimensional layout, whilst not causing the model to become excessively large (in terms of storage space). Due to the nature of shell elements, all fillets were neglected in the cross-sectional designation of the members in the analytical models.

The shape of each shell element was made a quadrilateral, in order to ensure that the same element could be used repetitively to mesh the whole part. There were two shell-elements that suited the purpose of the model, these were:

- **S4R:**
  4-node, (24 Degree's of Freedom [DOF's]) doubly curved general-purpose shell, reduced integration with hourglass control, finite membrane strains.
  Linear shape functions along each shell edge.
- **S8R:**
  8-node, (48 DOF's) doubly curved thick shell, reduced integration.
  Quadratic shape functions along each shell edge.

In order to determine which shell element and what mesh density to use, a short mesh sensitivity analysis was performed. The model used to test the mesh was chosen as the column being used in the experimental set-up with a length of 2400*mm*. For this column the theoretical Euler load (the solution) was known. The three meshes (Figure 5.1) were set-up in ABAQUS [23] and then each of the meshes was modelled using both S4R and S8R shell elements. An Eigenvalue analysis was performed on each mesh in order to obtain the buckling load of the modelled column.

The buckling load for each mesh and element was collected, and is summarised below in Table 5.1. The buckling load for each case was then compared to the Euler load for the column to obtain an idea about how accurate the modelling technique is. The smaller this error was, the more accurately the mesh models the column. Any further refinement in the mesh created a cumbersome model which took too long to analyse.

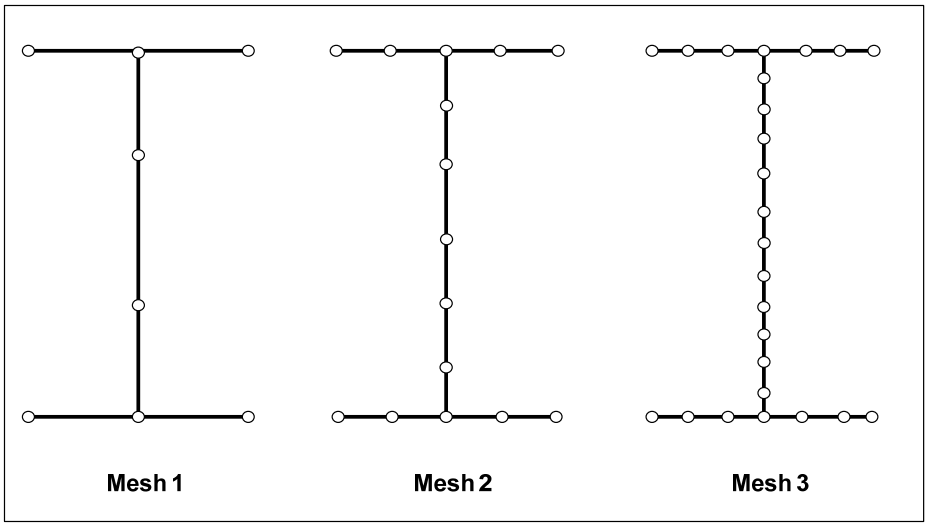

Figure 5.1 - Mesh sensitivity analysis

It can clearly be seen from the results, that using the S8R quadratic shell elements will always provide superior results when compared to those of the linear S4R elements. The other main conclusion that can be drawn from this exercise is that when using the quadratic S8R shell-elements the mesh refinement plays a small role in the accuracy of the results.

Table 5.1 - Mesh sensitivity results

Mesh	Number of elements	Element	Load (kN)	Error (%)
Euler			54.488	0%
1	609	S4R	40.842	25.0%
1	609	**S8R**	54.312	0.323%
2	2625	S4R	51.081	6.25%
2	2625	**S8R**	54.292	0.360%
3	10470	S4R	53.520	1.78%
3	10470	**S8R**	54.287	0.369%

It was decided that for the remainder of the proceedings the quadratic S8R shell element was to be used, and the mesh density chosen to correspond with that of Mesh 1 shown in Figure 5.1 which has relatively few elements but maintains a high accuracy. All of the members in the set-up, (column, cleat, sheeting rail, fly braces and gusset plates) were modelled using these elements and the element size was kept as regular as possible.

A bilinear, elastic-perfectly plastic material definition was given to the steel. The grade 350W steel used in the columns was given a yield strength of 350*MPa*, whilst the cold formed sheeting rails were furnished with a yield strength of *200MPa*.

5.1.2. Modelling of joints

The connection of the column to the sheeting rail by means of the cleat is a very difficult connection to realise when using shell elements. To accurately model the weld between the cleat onto the column and the bolt holes and bolts, would mean that a very fine mesh of continuum elements would need to be used. This would considerably increase the effort involved in modelling the column and sheeting rail.

Furthermore, the local behaviour of the sheeting and stress flow in the cleat and the area surrounding is not under investigation in this study. Keeping this outcome in mind it was decided to make a modelling assumption and continue the model with the S8R shell-elements. To connect the cleat to the column and the sheeting rail it was necessary to create constraints. The specific constraints chosen were node to node Coupling constraints. These constraints utilise the master and slave principle which can simply be described as constraints that enforce the selected DOF's motion of the master node to be followed exactly by the slave node. The modeller has the choice of which DOF's to activate for a given constraint.

These Coupling constraints were used to model both the column to cleat connection and the cleat-sheeting rail connection. In the physical experiment the cleat was welded onto the column along the heel and toe of the 50*mm* leg. These welds were simulated by coupling all six DOF's of each node along these edges to master nodes on the column. Thus, the twist or displacement of the column is transferred directly to the cleat along these edges. The same technique was used to model the welds of the gusset plate onto the column.

All of the active constraints that were eventually used in the model are shown in Figure 5.2. The nodes highlighted in red are the master nodes and the purple nodes are thus the slave nodes.

The bolted connection (with two bolts) had to be oversimplified to incorporate it in this model. Two nodes on the cleat (roughly at the centre of the bolts on the actual cleat) were selected as the master nodes, and the corresponding nodes on the sheeting rail were selected as the slave nodes. All three translational DOF's were activated, whilst the rotational DOF's were left free. This is a very rough manner of accommodating the bolted connection. The bolts on either end of the fly braces were handled in the same way.

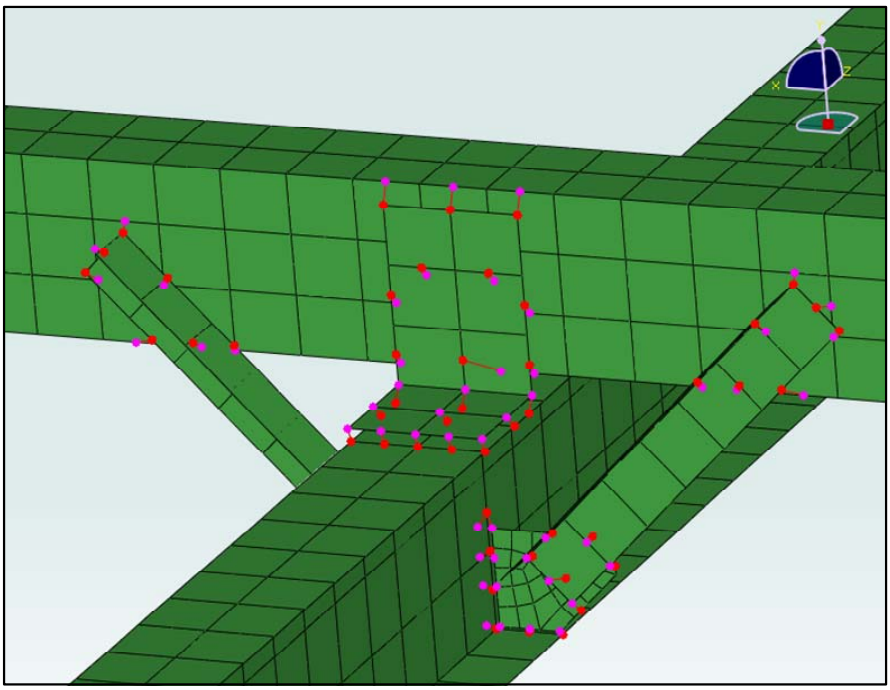

Figure 5.2 - Coupling constraints

More coupling constraints were needed to simulate the fact that the members will press upon each other when the load is applied. An example, is the cleat pressing onto the sheeting rail. If improper constraints were used, then parts of the cleat would move through the sheeting rail - which is physically impossible. These constraints were labelled as pressure constraints and were used between any surfaces that were touching in the physical model. Only the translational DOF perpendicular to the surfaces was activated. Although this prevented material from crossing through other members these pressure constraints still have limitations. For instance, the sheeting rail and cleat are in reality only held together at two “points” on their surfaces. This means that if a bending moment develops in the sheeting rail, as shown in Figure 5.3 below, one of the edges of the sheeting rail will be pressing against the cleat whilst the other edge will be pulling away from the cleat.

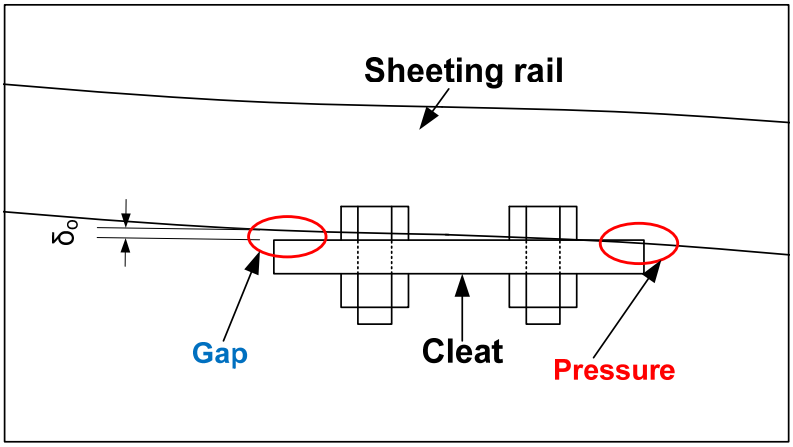

Figure 5.3 – Physical cleat to sheeting rail connection

This type of behaviour could not be modelled with the method of constraint selected. In the analytical model with the pressure constraints activated, no gap would be able to open up as in Figure 5.3. This means that the analytical model is potentially more effective in transferring bending moments than the physical set-up would be. These limitations were accepted as inherent to the model, and are deemed necessary to avoid unnecessary complexities from creeping in. A number of these master-slave connections were eccentric, the co-ordinates of the linked nodes did not line up, which is another potential problem, and should be investigated.

5.1.3. Boundary conditions and loads

The idealised boundary conditions have been thoroughly explained in Section 4.2. These same boundary conditions were applied in the analytical model. The pinned and roller boundary conditions at either end of the column, were applied to each node along the web. This had the added advantage of providing torsional restraint to each end of the column. The bolted ends of the sheeting rail are pinned for all translations at the same position as this was done in the experimental model - the inflection point between columns. Warping restraints were provided on the ends of the sheeting rails to reduce distortion of the open cross-section. These boundary conditions are shown on Figure 5.4, represented by the orange arrows.

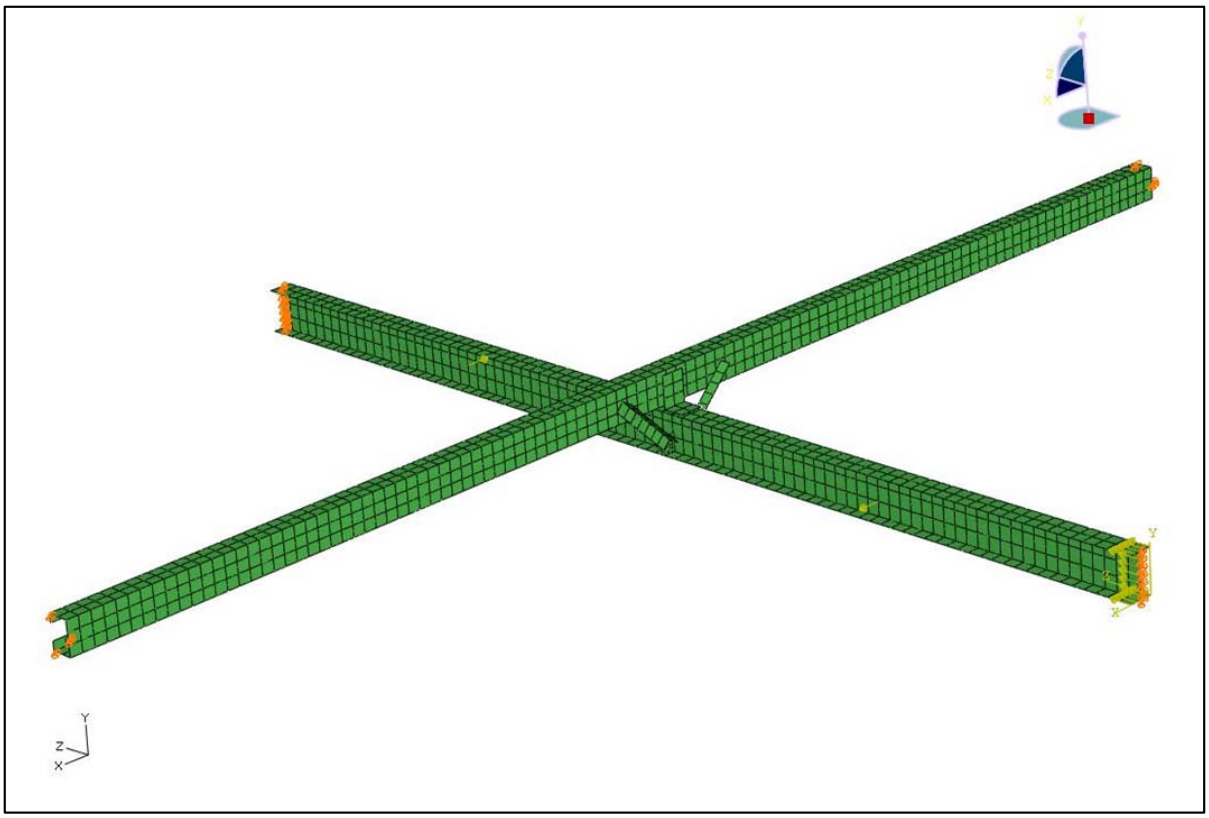

Figure 5.4 - Assembled analytical model showing boundary conditions and loads

The method of load application in the experimental set-up was a uniform pressure load on the whole cross section of the column and this type of load was approximated by applying a constant load at each node on the cross-section at the top of the column. This load can also be seen Figure 5.4,

represented by the yellow arrows. In some of the analyses performed it was necessary to include perturbation loads to ensure that buckling will occur in the column. The perturbation load applied was always taken as the value of **0.5% x *P***.

5.1.4. Analysis method

Two analysis types were used in the investigations that were performed in ABAQUS. These two analysis types can be roughly equated to calculating the theoretical buckling load and then calculating the code resistance load.

The first method of analysis used was an Eigenvalue buckling prediction. This analysis type is a linear perturbation procedure. In this method the programme determines what the theoretical buckling capacity of the column is - the accuracy of which depends on many factors such as element type and mesh density. The mode shape of the buckled configuration is also output. This analysis type follows only the linear material behaviour; this is why it is equivalent to the theoretical behaviour of the column. By requesting that a number of mode shapes be calculated during the analysis, the higher modes shapes can also be reproduced.

Using the knowledge gained from this Eigenvalue buckling prediction, a perturbation load is positioned on the column which initiates the lateral displacement of the column into the specified first mode of failure, i.e. the initial imperfection. The application of the perturbation load was be performed in a different analysis type. A Geometrically and Materially Non-Linear Analysis (GMNLA) was then performed on the column. During this method all loads that are applied to the model are ramped up linearly from zero, until the columns behaviour became unstable, at which point the analysis was terminated. In order to determine the buckling capacity of the column, the applied axial load was given a magnitude which is known to be higher than the critical load of the column.

During this GMNLA modelling it would have been more correct to include the effects of residual stresses in addition to those of the initial imperfections. This was not done on the basis that this applied perturbation load is conservatively large, and was thus already slightly over-exaggerating the size of the imperfection.

5.2. Benchmark problem

In order to further determine whether the selected method of modelling the problem was sufficient a benchmark problem was performed. This benchmark problem was set up to determine the critical load for IPE 100 cross-section column of varying lengths with a mid-height lateral restraint. The location of this restraint was initially positioned at the centroid of the column and then moved to the intersection of the bottom flange and the web. The initial placement of the lateral support at mid-height causes the column to buckle into the second flexural mode. Once this lateral support is placed eccentrically onto the intersection of the flange and the web, the column will buckle into the torsional-flexural mode - as discussed extensively in Section 2.3.

The ability of the model to accurately calculate the response to varying the position (on the cross section) of the lateral restraint was investigated and then compared to the known theoretical values. The element mesh and boundary configuration outlines in the preceding section were used in this model, although there is no sheeting rail in this sub-investigation. The element size was kept constant for all lengths of column being investigated. This has the consequence that a longer column will have more elements along its length. Both types of analysis outlined above, were used to further understand the behaviour of the model.

The Eigenvalues obtained for the initial placement of the lateral support, represented by the red squares in Figure 5.5, again show the accuracy which was highlighted by the results shown for the mesh refinement exercise in Table 5.1. For slender columns (L/r > 150) the results were almost exact. The results of the GMNLA analysis were not as accurate as the Eigenvalue results. However, for slender columns the GMNLA results are seen to be slightly higher than the code value, which is acceptable, as the code method of calculation should always result in conservative solutions. For columns with a slenderness ratio of 100 and less, the error in the both the Eigenvalue and GMNLA methods of analysis are seen to increase, and the GMNLA results became lower than the code values, which is then unacceptable. The higher number of elements over the length of the longer columns could be the reason for the more accurate results.

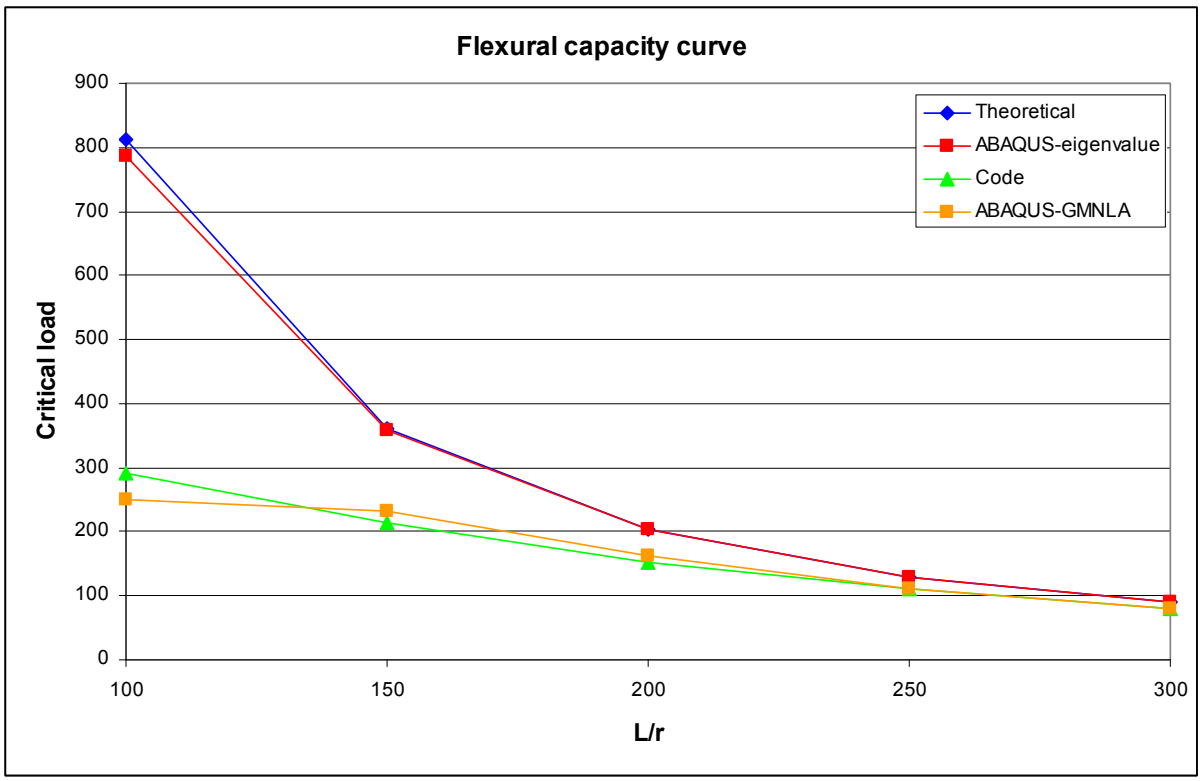

Figure 5.5 - Theoretical and analytical capacity curve, h_y = 0*mm*

The behaviour of the model with the eccentric lateral support (Figure 5.6) was not as neat and easily explainable as the flexural buckling case shown above. The discrepancy seen between the Eigenvalues that were calculated and the theoretical solution show that the longer, more slender elements have a higher error margin. This appears to be counter-intuitive because for most finite element problems a refined mesh will yield better results. The error in results went from being 7% for columns with a slenderness ratio of 100, to a value of 36% with a corresponding slenderness ratio of 300. This outcome is a little troubling. It can be seen from Figure 3.12 that the torsional-flexural buckling is critical for more squat columns, whilst the flexural buckling capacity dominates for more slender columns. This means that the smaller error margin in the squat column range is desirable; however the size of this error is still troubling.

The results from the GMNLA analysis were seen to show a much closer correlation to the code calculated capacity of the columns. For slenderness ratios in the range of **150 < *L*/*r* <250**, the GMNLA results are seen to be slightly above the code capacity which is the desired outcome for such a model. Excessively slender (***L*/*r* = 300**) and squat (***L*/*r* = 100**) columns had results which lay below the code limit, which was not acceptable. As previously stated, most columns found in practice will have slenderness ratios of **150 < *L*/*r* <200** and as seen in Figure 5.6, the values of the GMNLA model provides sufficiently safe answers.

A very slight improvement in accuracy was seen for the GMNLA results when the mesh was refined. However, the error increased for the Eigenvalue analysis which does not warrant making a mesh refinement. Also, the computing time more than doubled, which made the model very impractical.

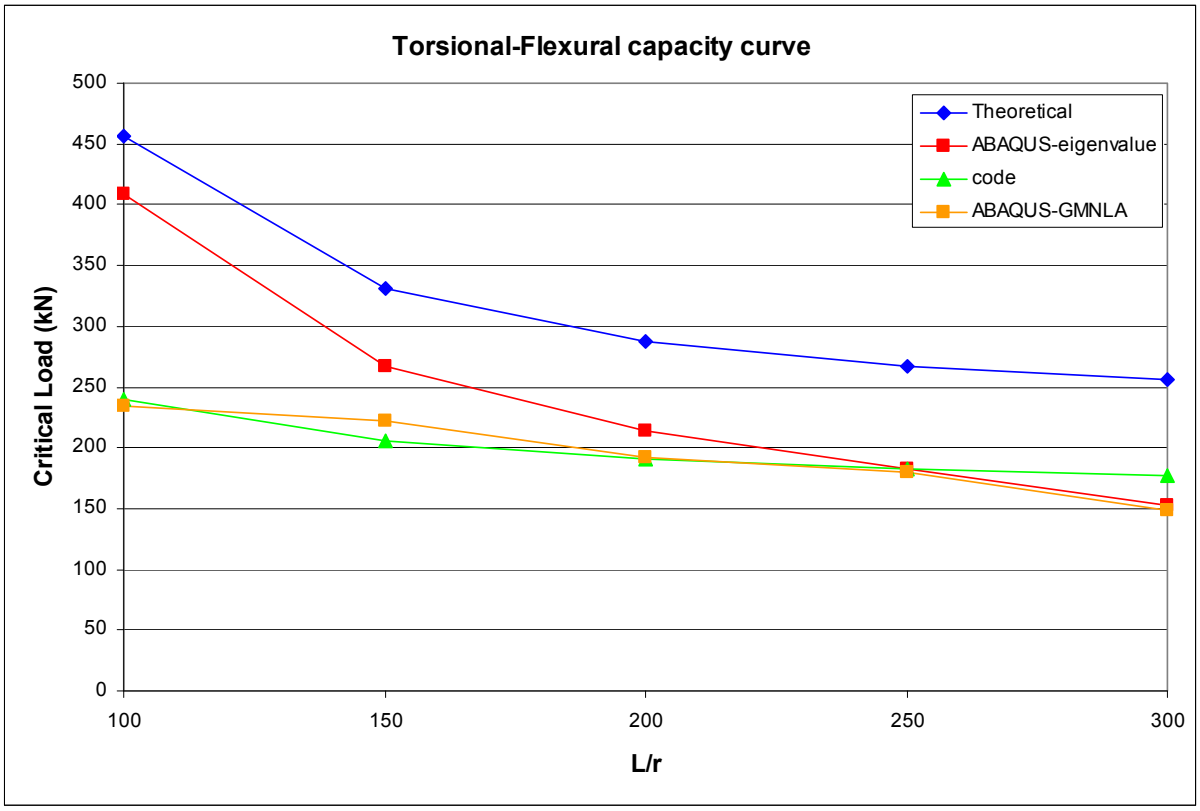

Figure 5.6 - Theoretical and analytical capacity curve, h_y = 47.15*mm*

This large inaccuracy in the torsional-flexural buckling mode could be attributable to the following:

- The cross-sectional definition lacks the fillet, which influences the GJ term in the torsional-flexural equations;
- The method of providing lateral support, at one node on the member, might create local behaviour patterns that are not correct, which could influence the global behaviour.
- The equation used to calculate the theoretical values was that originally proposed by Timoshenko and Gere [11], and was derived for the case of a continuous axis of restraint along the columns length, whilst the model has only the one discrete point as a restraint.

The justification for the continued use of this model is that, in spite of the few errors that arose in the modelling process, both analysis methods correctly determined which buckling mode of the column would be critical. This result provides confidence that when the properties of the lateral restraint are varied, as will be performed in the next section, one can still confidently determine which mode of failure is most likely.

5.3. Comparison between experimental and analytical results

The analytical model was assembled in order to simulate the three different configurations that were experimentally tested. Both Eigenvalue predictions and GMNLA analyses were performed on each configuration. The results of lateral deflections obtained from the GMNLA analysis will be compared directly with those observed from the experimental results in a graphical manner.

5.3.1. Unsupported column

The mode of failure witnessed for this configuration during the experimental tests was undoubtedly first mode flexural buckling. This too was the first mode of failure predicted by the Eigenvalue analysis. The load-deflection path of all three experiments and the load-deflection path obtained during the GMNLA analysis, have all been compiled onto one graph. This graph also shows the upper bound determined from the Eigenvalue analysis, and the lower bound of the code capacity (including the material factor, φ =0.9).

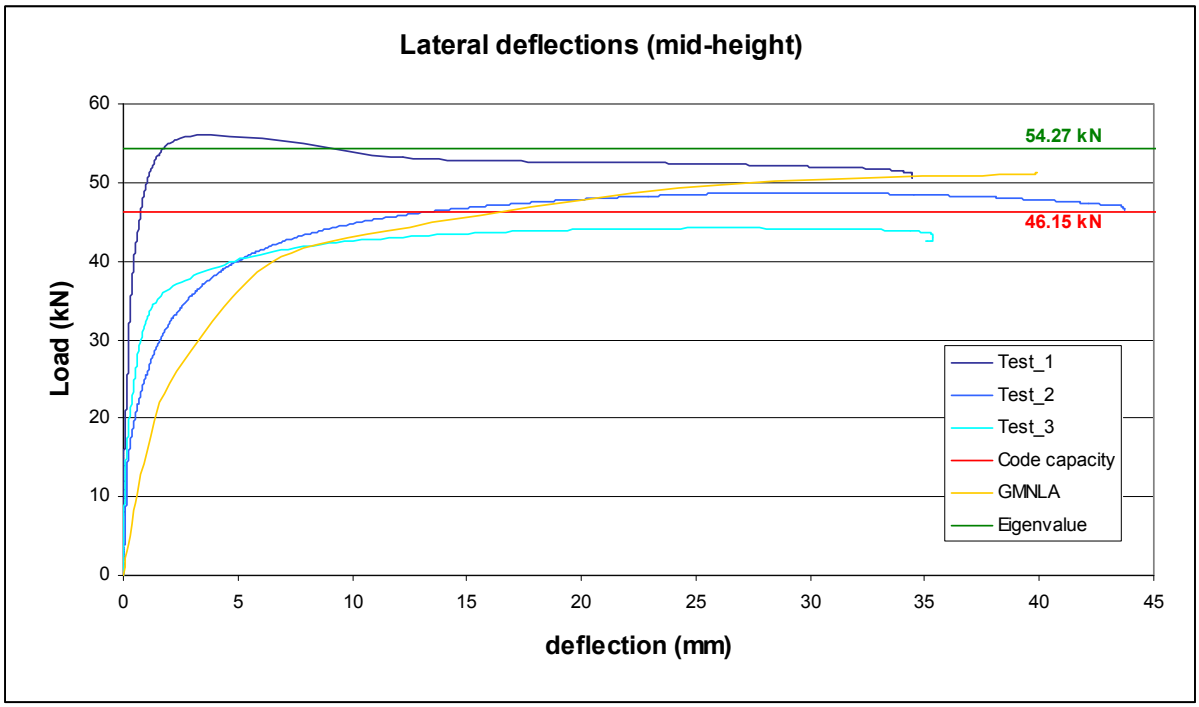

Figure 5.7 - Lateral deflections - unsupported column

The shape of the load-deflection curve of the analytical model shows a similar trend to those measured during the experimental tests. Furthermore, the critical load from the analytical model is very similar to the average maximum load reached during the experiments.

5.3.2. Eccentrically supported column

Two of the columns tested in this series of tests exhibited definite second mode flexural buckling as the failure mode. The remaining column was observed to display a torsional-flexural buckling with both large lateral deflections and large twisting of the cross-section.

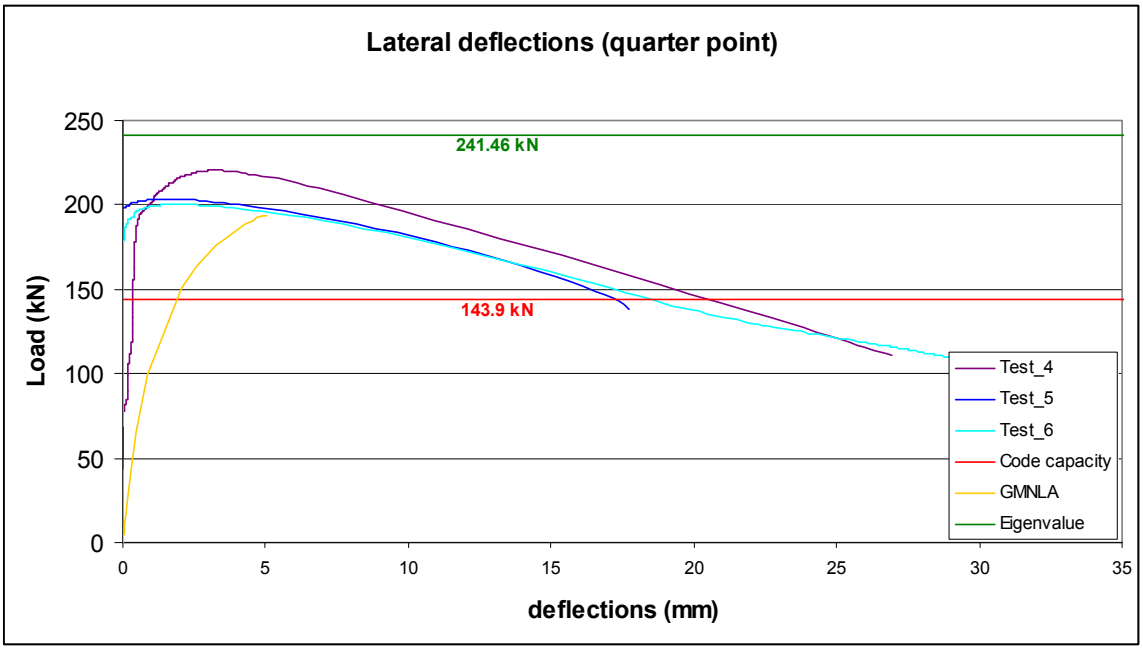

Figure 5.8 – Lateral deflections – column + sheeting rail

The magnitude of the lateral deflections observed from the GMNLA analysis was much larger during the initial elastic range of behaviour. It is thought that the method of applying the perturbation load could have caused these over-large deflections. Two point loads were applied in opposite directions as perturbation loads, the magnitude of each of these was made equal to **0.005 x $P_{applied}$**. If the sum of the two perturbation loads used had been equal to **0.005 x $P_{applied}$** it can be expected that a higher buckling load would have been obtained and also that the lateral deflections would have been closer to those actually measured during the experiments. Nonetheless, the buckling load from the GMNLA analysis was of the same order of magnitude than the average maximum load carried by the columns.

5.3.3. Laterally supported column

The final series of tests saw the addition of fly-braces at the sheeting rail to column connection. The aim of these fly braces was to limit the potential for any twisting of the cross-section at this connection point. This means that the column had full lateral restraint in this configuration.

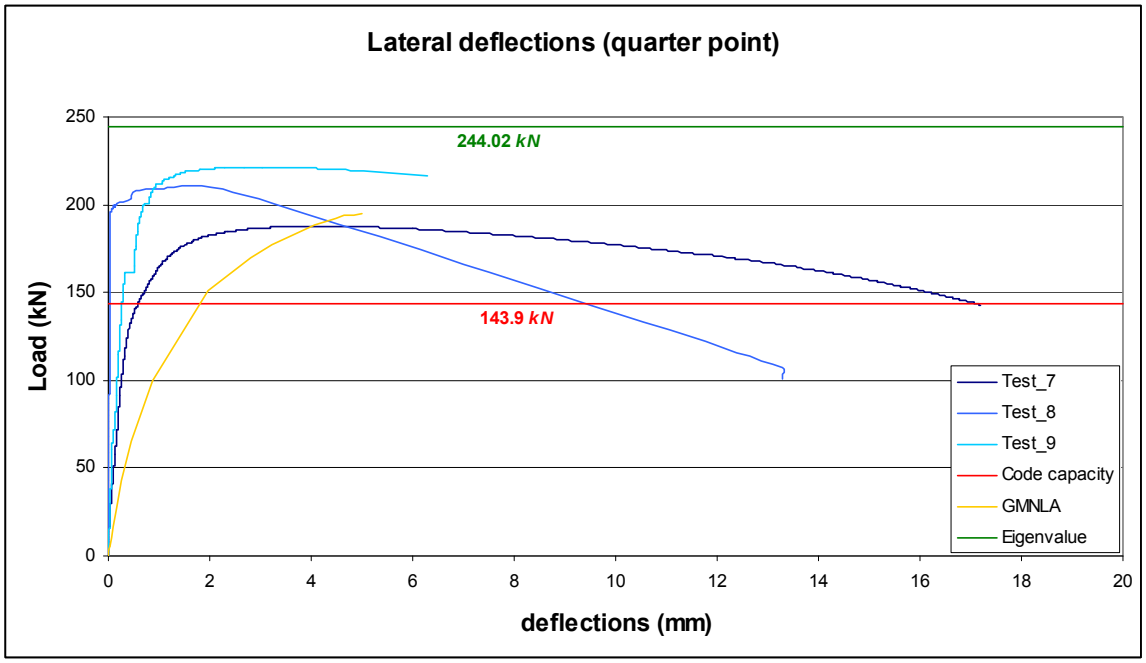

Figure 5.9 - Lateral deflections - column + sheeting rail + fly-braces

The model was once again observed to have lateral deflections which were larger than the observed measurements. The conclusion made in Section 5.3.2, that these large deflections were caused by overly large perturbation loads, is backed up when comparing the load-deflection path for Test 7 with that from the GMNLA analysis. The shape of the curves is very similar, only the magnitude of the deformations is different. The buckling capacity determined from the model is again slightly lower than the average maximum load carried by the columns.

5.3.4. Summary

The success of the analytical model is evident due to both the behaviour witnessed as the load increases (the load-deflection path) and the fact that the calculated critical loads were all of the same order of magnitude and for the same failure patterns as observed in the experimental tests. A tabulated summary some of the important results that were found is included below.

Table 5.2 - Comparison between code limits, analytical loads and experimental loads

Configuration	Code capacity (*kN*)	Eigenvalue (*kN*)	GMNLA (*kN*)	Experimental average (*kN*)
Column	46.15	54.31	51.17	49.63
Column + sheeting rail	143.88	241.46	193.85	208.07
Column + sheeting rail + braces	143.88	244.02	194.70	206.21

The buckling capacity for the configuration, which includes fly-braces in addition to the sheeting rail, as determined from the analytical model was slightly higher than that observed for the configuration with only the sheeting rail. This was not what was observed during the experimental tests. However, it is believed that the low buckling load obtained from Test 7 pulled the average value down lower than it should be. The Eigen modes, as calculated by the Eigenvalue prediction method, for each of these two configurations are shown below. Both columns show a similar buckled shape, which again shows that the fly-braces are not necessary for this system. From these two Figures it is also interesting to note that, as predicted, the sheeting rail is in biaxial bending.

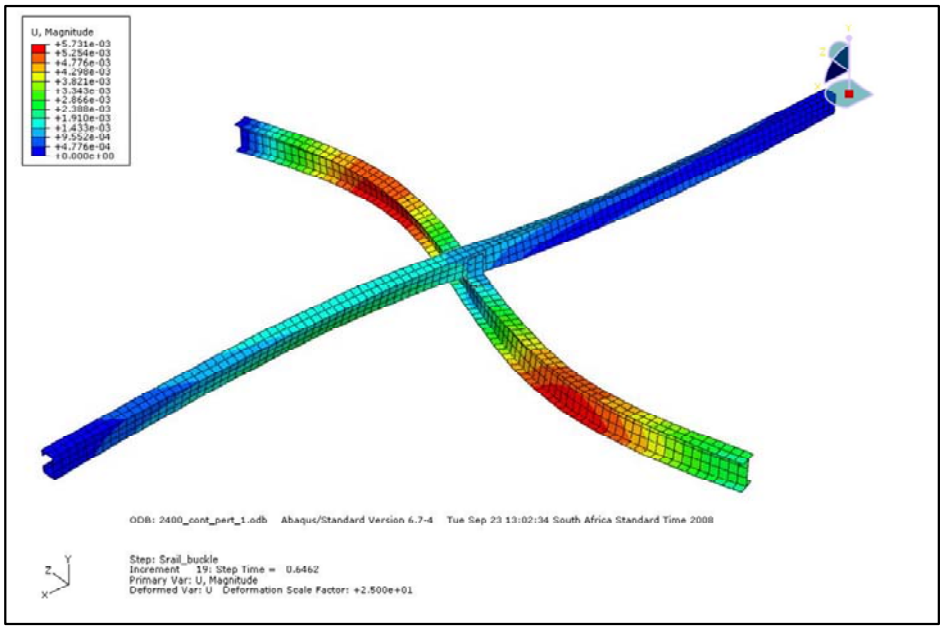

Figure 5.10 - Critical buckling mode - column + sheeting rail

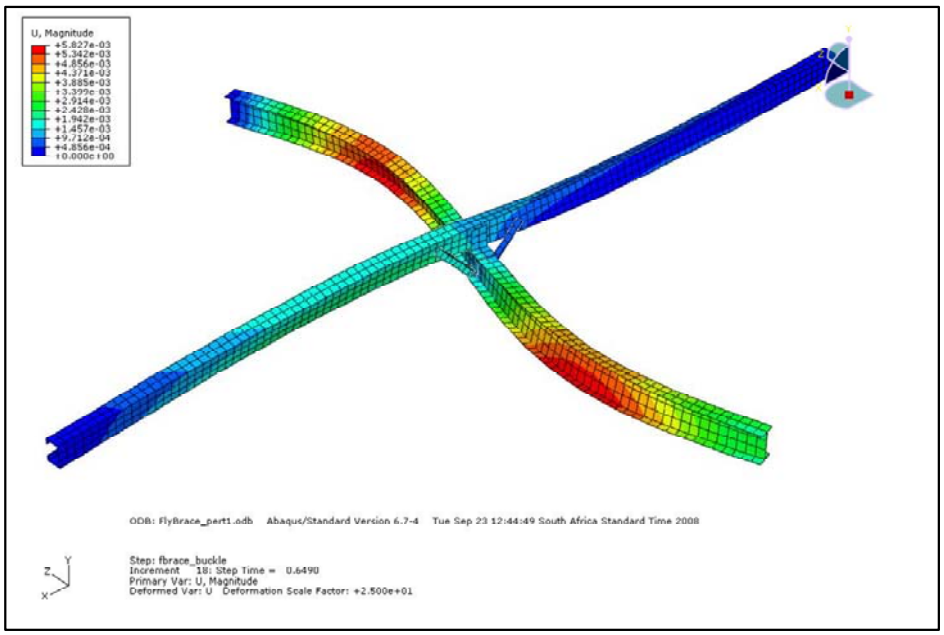

Figure 5.11 - First buckling mode - column + sheeting rail + fly- braces

6. Parameter study

It has been shown that a system of columns, connected together by sheeting rails, will all buckle in the same mode when acted upon by a very simple loading pattern. This system of interconnected columns can be simplified in such a way that the behaviour of the whole system can be understood by looking at a single column and its relevant length of sheeting rail. A limited number of experimental tests were conducted on such columns. Two different configurations for the connection between the column and sheeting rail were investigated. The aim of these tests was to determine if a connection comprising of a sheeting rail connected to the column (at mid-height) by means of a simple two bolt connection, could provide sufficient restraint to eliminate a lower torsional-flexural mode of buckling from being critical. The other configuration tested employed specific measures (fly-braces) which were implemented to eliminate the possibility of this lower buckling mode from occurring.

An analytical model was made of both these configurations in the general finite element package, ABAQUS. This model provided relatively accurate values for the critical loads and was seen to accurately predict which buckling mode would be critical for a given configuration.

This analytical model of the experimental tests can be modified in several manners which will allow for the testing of other column to sheeting rail connections. The resultant failure mode and buckling load for each of the columns with these connection types, can thus be determined without the need for performing a whole long series of experimental tests.

Unfortunately, this type of parameter study is very difficult to conduct on a finite element model which is composed primarily of shell elements. This is because, for each variation in the analytical model, all boundary conditions, loads and constraints need to be re-input. As a result of this difficulty, a few limited models were selected in order to gain a broader understanding of the phenomena under examination. The column cross-sections that were selected for closer examination were the IPE 100 section (which had already been investigated) and the IPE 200 cross-section. It was attempted to analyse the model for two slenderness ratios, for each type of connection, with each of the two cross-sections.

The method of analysis that was used was to first perform an Eigenvalue analysis and determine what the critical load of the system was. The location of the perturbation load was chosen to deform the column into this critical mode shape and then a GMNLA analysis was performed. In this way results could be compared directly with the theoretical values, and the behaviour of the joint was monitored.

The methodology recommended at the close of the Study of code of practice (Section 2.4) of substituting the torsional-flexural formulation into the codes formulas to replace the pure torsional buckling formula, was used to generate what was referred to as the “code capacity” of torsional-flexural buckling. The torsional brace stiffness - the flexural stiffness of the sheeting rail - was determined by the method proposed by Helwig and Yura [15].

6.1. Continuous sheeting rail

We have seen that a relatively light and slender column can be effectively supported at mid-height with the provision of one torsional brace. However, we do not know whether the results obtained up until now can be extended to cover all general cases. The sheeting rail was given the following properties for these analyses:

- IPE 100: CFLC – 75 x 50 x 20 x 2, with a 3*m* column spacing;
  Stiffness = 48*kNm/rad*;
- IPE 200: CFLC – 75 x 50 x 20 x 2, with a 5*m* column spacing;
  Stiffness = 28.8*kNm/rad*.

Therefore, the goals of these analyses were to verify that the proposed method of determining the above stiffness' is correct or at least reasonably accurate. That the assembled model, even with a much heavier cross-section in combination with a more flexible sheeting rail, is still able to generate sufficient torsional bracing restraint to ensure that the second mode of flexural buckling is still critical. The results of all the theoretical calculations and analytical models are presented below.

The table shown below (as well as the other tables in this chapter) needs a brief explanation, to avoid any confusion. For each column investigated the critical load, calculated from both the Eigenvalue analysis and the Theoretical calculations is highlighted in bold. For these terms, the sub-headings **y_2** and **TF** indicate second mode flexural buckling and torsional-flexural buckling respectively. Based on this critical value the GMNLA analysis was determined, as well as the code capacity to obtain a more realistic physical value for the critical load.

Table 6.1 - Theoretical and analytical results for continuous sheeting rails

		Analytical - P_{cr} *(kN)*			Theoretical - P_{cr} *(kN)*		
Section	**Slenderness ratio**	**GMNLA**	**Eigenvalue**		**Code Capacity**	**Theoretical value**	
			y_2	**TF**		**y_2**	**TF**
IPE 100	150	**233.6**	**389.97**	602.73	**215.19**	**361.45**	651.00
IPE 100	193.5	**193.84**	**241.46**	420.36	**159.87**	**217.09**	546.18
IPE 200	150	**682.92**	1003.43	**986.085**	**555.62**	1000.12	**875.80**
IPE 200	200	**473.6**	**570.85**	920.30	**423.25**	**562.57**	676.17

From the above results it can be inferred that the failure loads predicted using the method described in SANS 10162 [7] to predict column buckling, will yield conservative results - this is ideal.

The torsional-flexural buckling capacity calculated using the torsional brace stiffness was seen to over estimate the torsional flexural buckling capacity found from the Eigenvalue analysis. This could be attributed to either one of two possible reasons:

- The connection does not limit the cross-sectional deformation as recommended by Helwig and Yura [15], and this results in the connection being less efficient than anticipated; or
- The method proposed by Helwig and Yura [15] to calculate the torsional brace stiffness (which was determined for angle sheeting rails) is not sufficient when cold formed lipped channels are used as sheeting rails.

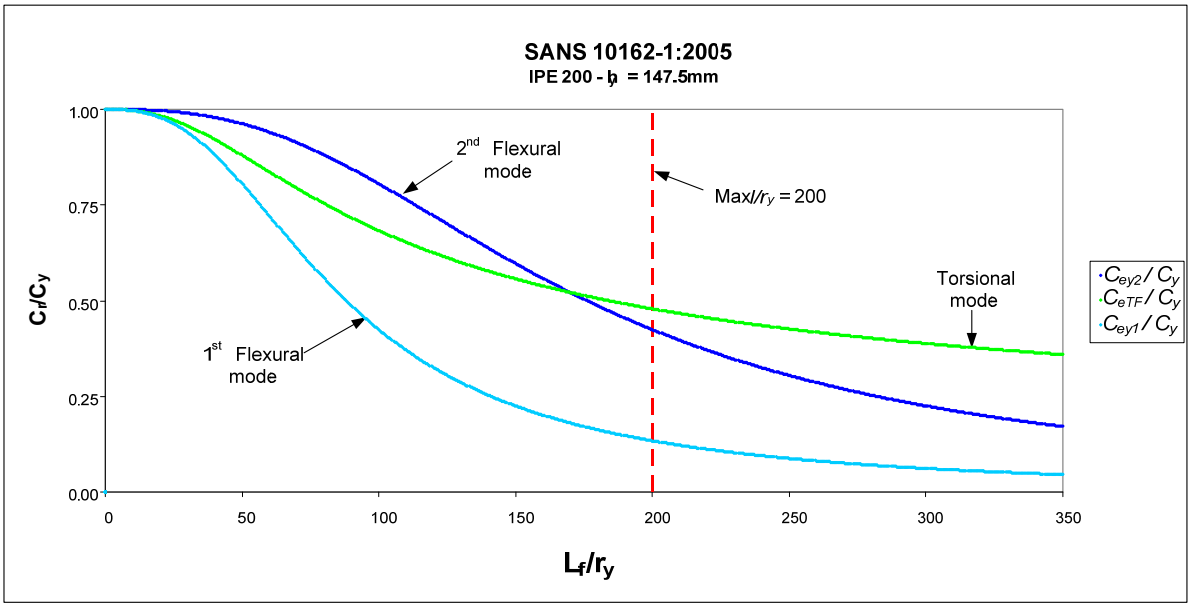

Figure 6.1 - Buckling capacity curve + torsional restraint (K_T = 28.8*kNm/rad*)

There is strong correlation between the results found in the above analyses and the theoretical values in all cases except for those of the IPE 200 column with a slenderness ratio of 150. When the buckling capacity curve for this combination of column and sheeting rail is examined, it is seen that this column lies in a region where the torsional-flexural buckling is still critical, although the magnitude of both of these buckling loads is seen to lie very close together. The results from the Eigenvalue analysis show that the critical buckling mode will be the torsional-flexural mode. However, when the mode shape was examined, it was observed that the failure was not by first mode torsional-flexural buckling. Similarly, the second mode of failure was seen to be a torsional-flexural mode as well with large lateral displacements and twisting of the column. This seems to be similar to what was witnessed during the experimental Test 5.

This torsional-flexural buckling mode can be visualised from the buckled configuration shown below. The lateral deflections show the second mode flexural buckling, but the twist exhibited is in one half sine-wave over the length of the column.

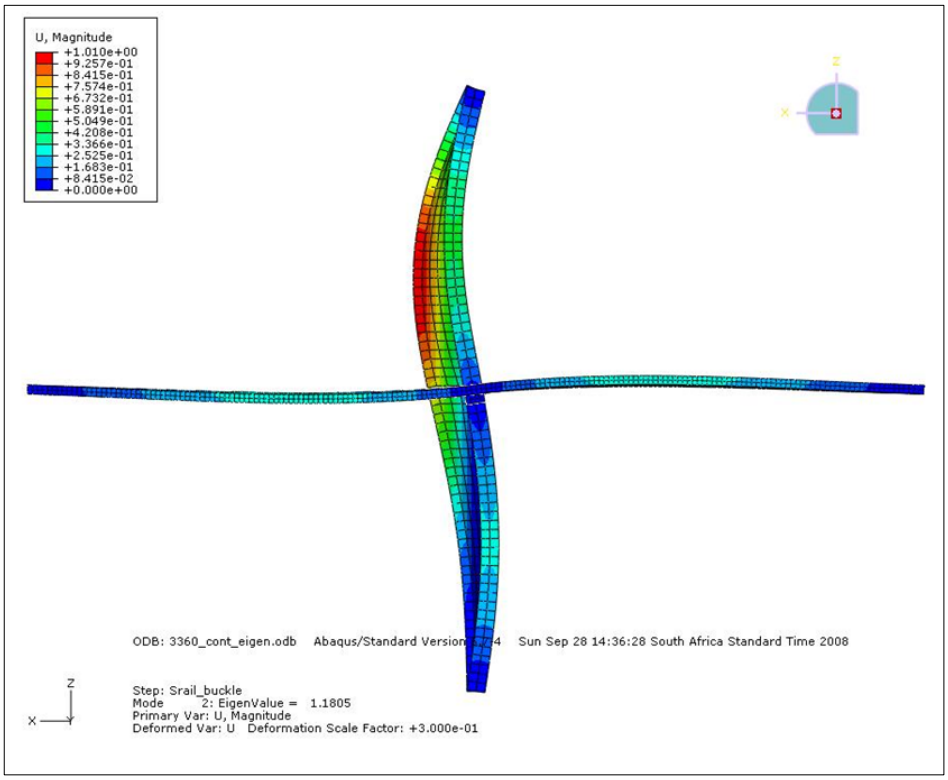

Figure 6.2 - Combined torsional-flexural and flexural buckling mode

This is a torsional-flexural buckling mode similar to what was used by Dooley [12] in the derivations whe using the energy methods. The buckled shape can be described by Figure 2.14.. It seems that the proximity of each buckling capacity curve (for 2nd mode flexural and torsional-flexural buckling) to each other (Figure 6.1) has the effect of causing the column to buckle in a combination of the two independent buckling modes. It is pleasing to see that although the observed buckling mode shows different than expected behaviour, the buckling capacity of the column is in the same order of magnitude as the theoretical values calculated. This places some confidence in the Analytical model.

6.2. Discontinuous sheeting rail

It was stated in Section 2.2.3, that the decision about which sheeting rail spanning system to use, can often be an economic decision rather than a purely structural decision. Thus, it can be expected that there will be scenarios when there will be a discontinuity in the sheeting rail at the connection onto the column. This could be either with a single span sheeting rail or with a double span sheeting rail. What would happen if a designer had planned on incorporating the mid-height sheeting rail into the lateral bracing system and had inadvertently specified neither a continuous sheeting rail nor any twist prohibiting measures such as sheeting rails? Could the column potentially not fail in the second flexural mode that the designer assumed when he made it a lateral restraint - could it in fact fail a lower torsional-flexural mode?

Table 6.2 - Theoretical and analytical results for discontinuous sheeting rails

		Analytical - P_{cr} *(kN)*			Theoretical - P_{cr} *(kN)*		
Section	**Slenderness ratio**	**GMNLA**	**Eigenvalue**		**Code Capacity**	**Theoretical value**	
			y_2	**TF**		y_2	**TF**
IPE 100	150	**150.72**	361.41	**146.18**	**124.43**	361.45	**176.09**
IPE 100	193.5	**128.14**	218.91	**109.02**	**103.91**	217.09	**138.64**
IPE 200	150	**443.35**	982.86	**393.26**	**325.69**	1000.12	**451.69**
IPE 200	200	**360.93**	559.34	**278.45**	**258.32**	562.57	**335.40**

The results of a similar series of investigations to that seen in Section 6.1 are presented above. The same combinations of columns and sheeting rails as used above were also used in these models. The one difference made, was that the sheeting rail was cut in half and then a 10*mm* gap placed between each separate length of sheeting rail. The buckled configuration of this type of connection is shown in Figure 6.3. The Theoretical values and the Code capacity of these tests was determined by assuming that there will now be zero torsional bracing stiffness (i.e $K_T = 0$); the values can be said to be for pure torsional-flexural buckling, with no added restraint.

It should be brought to the attention of the reader here that by simply providing a continuous sheeting rail, the load carrying capacity of a column can be drastically increased. For example, it can be seen that for the IPE 100 column cross-section with slenderness ratio of 193.5 (a length of 2400*mm*) that, with a discontinuous sheeting rail, the buckling load is in fact 128.14*kN*. If a continuous sheeting rail is used instead, the carrying capacity is increased to a value of 193.84*kN*. This is equivalent to a 51.3% increase in carrying capacity for very little effort on behalf of the designer.

The tabulated results shown above are very positive, with the GMNLA results higher than the code calculated resistance of the member. The only surprising observation that can be made is that all of the results from the GMNLA analyses are larger than the corresponding Eigenvalue analysis results for torsional-flexural buckling.

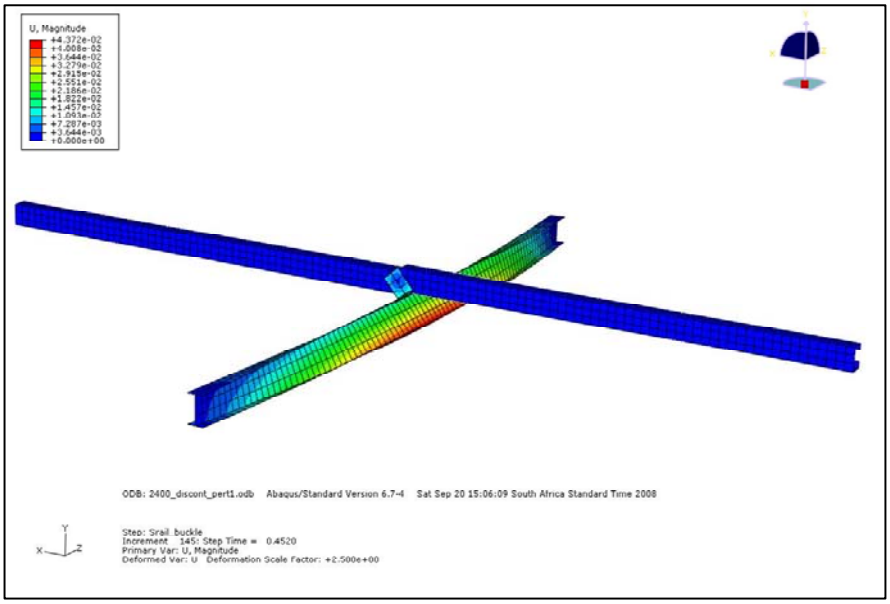

Figure 6.3 - Torsional-flexural buckling due to discontinuous sheeting rail

One possible explanation for the larger critical load values obtained from the GMNLA analyses could be that as the column begins to twist around the centroid axis of the sheeting rail the cleat is forced to rotate by the same amount. In order for this to happen, it means that the bolt holes will have to move horizontally. This is shown schematically in Figure 6.4, with the rotated position of the cleat shown in red. This horizontal motion means that both lengths of sheeting rail will be pulled into tension. This will have the effect of stiffening the analytical model as the load increases - which can impact on the critical load in a manner such as this. The GMNLA model took approximately 10 times as long to determine a solution, when the failure mode was torsional-flexural buckling, compared to the when the failure was by flexural buckling. This could very well be the result of both the stiffness and load terms increasing during the analysis.

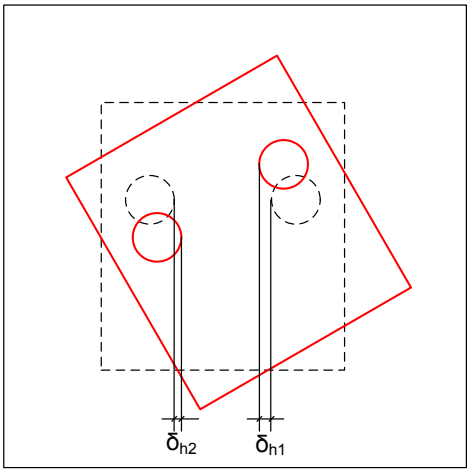

Figure 6.4 - Horizontal movement of bolt holes

6.3. Discontinuous sheeting rail with fly-braces

The following model was set-up as a response to the small critical loads witnessed from the low torsional-flexural buckling capacity when a discontinuous sheeting rail is present. This connection is one of those recommended by Helwig and Yura, shown in Figure 2.15. The braces act to ensure that each flange of the column is supported and they are used to eliminate cross-sectional deformations at the point of connection.

Table 6.3 - Theoretical and analytical results for discontinuous sheeting rail + fly-brace

		Analytical - P_{cr} *(kN)*			Theoretical - P_{cr} *(kN)*		
Section	**Slenderness ratio**	**GMNLA**	**Eigenvalue**		**Code Value**	**Theoretical value**	
			y_2	**TF**		**y_2**	**TF**
IPE 100	193.5	**180.99**	**221.00**	637.65	**159.87**	**217.09**	307.58

The results from analysing this should be compared directly with the values seen for the IPE 100 column (with a slenderness ratio of 193.5*kN*) with a discontinuous sheeting rail from Table 6.2. When the results of the GMNLA analysis are compared for these slightly different connections the increase is seen to be significant.

The capacity of the column is increased from a value of 128.14*kN* to a value of 180.99*kN.* This is an increase in capacity of 41.2%, which is comparable to (but slightly smaller than) the increase in capacity which resulted from using a continuous sheeting rail which increased the buckling capacity of the column to a value of 193.84*kN*.

The buckled configuration of this model has been included below, and should be compared with Figure 5.10, Figure 5.11 and Figure 6.3 to understand the benefits of using each type of connection. Note that the buckled configuration below shows that there is no twisting in the column, which is an added advantage of this connection type. The previous three connection types all allow twist to occur over the column length.

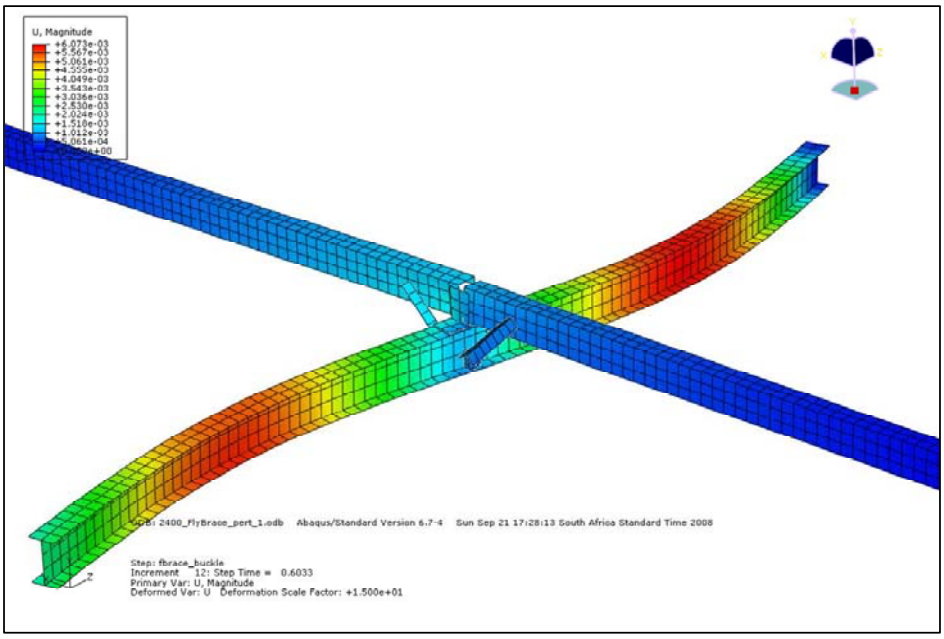

Figure 6.5 - Flexural buckling due to the addition of fly-braces

6.4. Three continuous sheeting rails

This final model that was analysed simulates the more realistic case which has three continuous sheeting rails distributed over the height of the column. This is more realistic when compared to the generic system (from Section 3), upon which all of the research is based. These three sheeting rails all act as torsional restraints distributed over the height of the column. However, only the middle sheeting rail acts as a lateral support. This is exactly what was described in Section 3.5.

The analytical model of this scenario consisted of an IPE 200 column section of length 3360*mm* and continuous 75 x 50 x 20 x 2 CFLC sheeting rails with a length between inflection points of 5*m*. This corresponds well to the generic system with the only differences being that the column height was not taken as 5*m*, and that the cross-section of the sheeting rail has been reduced to the smallest possible CFLC section. The first change was made for two reasons. Firstly, because the length of 5*m* was actually over the maximum slenderness ratio allowed by the code, and secondly because the results (when including the effects of only one torsional brace at mid-height) were seen to be slightly confusing because of the closeness in the Eigenvalue buckling loads. Thus, by including the additional two torsional braces, which are in any case present on the structure, the designer can be sure that the flexural buckling capacity of the column will be critical. The second change was made to show that large increases in the carrying capacity of the columns can be achieved, even for a relatively low value of the torsional brace stiffness.

Table 6.4 - Theoretical and analytical results for 3 continuous sheeting rails

Section	Slenderness ratio	Analytical - P_{cr} (*kN*)			Theoretical - P_{cr} (*kN*)		
		GMNLA	Eigenvalue		Code Capacity	Theoretical value	
			y_2	TF		y_2	TF
IPE 200	150	682.78	**1005.89**	1386.44	595.43	**1000.12**	1706.02

The results of the analyses are tabulated in Table 6.4 and they should be directly compared with the corresponding results from Table 6.1. It was seen that for the scenario with three sheeting rails, that the torsional-flexural buckling capacity was increased to a value of 1386.44*kN*, as compared to the case with only one torsional brace which had a torsional-flexural buckling capacity of 1018.13*kN*. This is an increase in capacity of 36% which is achieved by simply including the restraining effects of some of the members which were previously ignored.

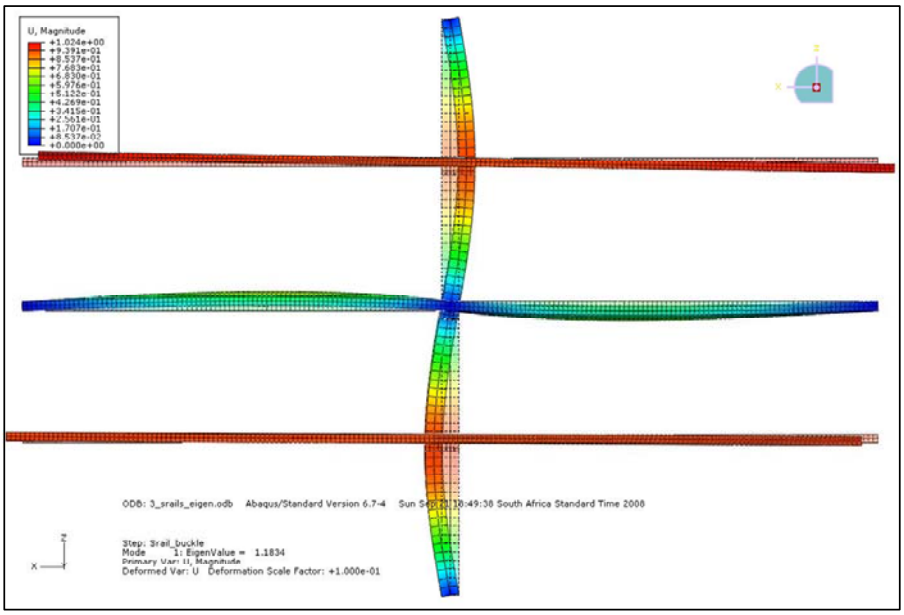

Figure 6.6 - Critical flexural buckling mode with 3 continuous sheeting rails

The buckled configurations of both the critical (flexural) and second mode (torsional-flexural) of buckling have been presented here to show that the model can realistically be trusted to provide results, which display the behaviour patterns which are expected to occur. Some slight adjustments could potentially have been applied to the boundary conditions of the sheeting rails that have now been added to the model, to ensure that the exact behaviour of these members will be modelled.

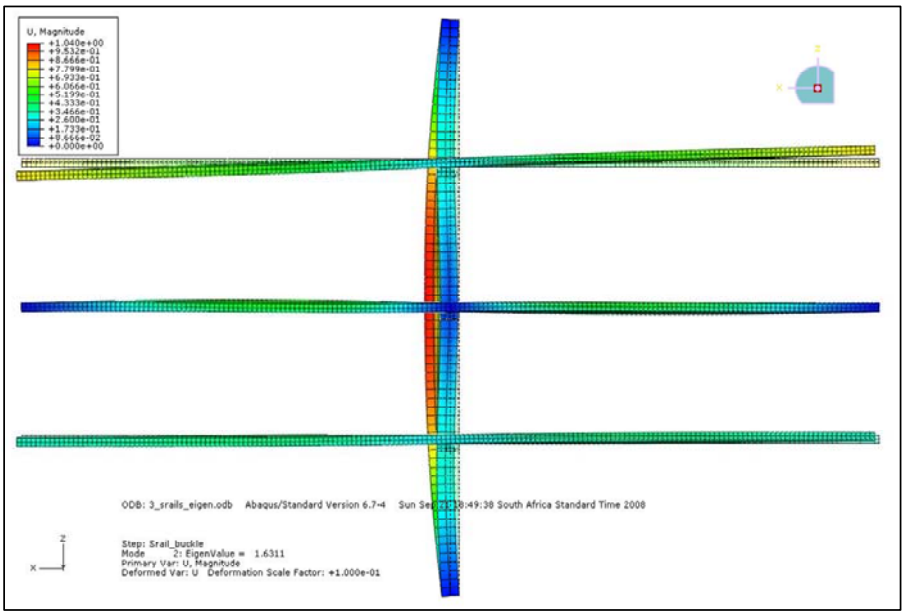

Figure 6.7 - Non-critical torsional-flexural buckling mode

7. Conclusions

The following conclusions may be drawn, based on the findings of this investigation:

7.1. Experimental set-up

- The boundary conditions - which were needed so that the test column could imitate a column from the global system - were reasonably provided in the experimental set-up. Except for the following:
    - The initial method of preventing twist was inadequate, as the piston of the hydraulic load actuator was free to rotate about its axis, and was indeed seen to do so;
    - The modified twist resisting techniques that were put in place did reduce the twist, although it was not eliminated;
    - The universal joint (made to provide a pinned end connection for the column) stiffened up during each analysis.

  In spite of these deficiencies, it can be concluded that the boundary conditions did not inhibit the behaviour of the column, and the modes of failure were as expected.

- Data was recorded from each test - with sufficient accuracy and from the correct positions - such that the behaviour of the column could be clearly seen and understood.

7.2. Analytical model

- The finite element model of the system under investigation was relatively simple to define due to the use of shell elements.

- The use of quadratic shell elements allowed for high accuracy with fewer nodes in the system, which resulted in the analysis being performed over a reasonable time interval.

- When flexural buckling was the critical failure mode, the model predicted solutions which were very accurate when compared with the theoretical solutions.

- When torsional-flexural buckling was the critical failure mode, the results displayed a much reduced accuracy relative to what was seen with the flexural buckling results. The results for squat columns, for which the torsional-flexural buckling capacity often dominates, displayed a smaller error than longer, more slender columns.

- It can, however, still be concluded that the magnitude of the load determined by the analytical model will be slightly higher than the predicted code capacity for the column, which will still result in a safe column design.

- In spite of the large margin of error between the theoretical and analytical solutions for the torsional-flexural buckling capacity, the analytical model was seen to fail by the same buckling mode as that predicted by the method used earlier in the report.

- The failure of the columns from the GMNLA method of analysis is very comparable to the results from the experimental tests. This is true for both the load capacity reached, and the load deflection path followed by the model as the load is increased.

7.3. Eccentrically restrained column behaviour

- The type of connection present between the sheeting rail and column has a considerable effect on the load carrying capacity of the column. This is deemed to be true if the sheeting rail under consideration is included in the lateral bracing system of the columns.

- A continuous sheeting rail, only connected to one flange of the column by a simple cleat, was seen to provide sufficient torsional restraint to ensure that the column buckled in a torsional flexural mode. The addition of a fly-brace to this connection type reduces the twist in the column. However, if this is done, there is no appreciable increase in the capacity of the column.

- A discontinuous sheeting rail cannot be relied upon as an eccentric lateral restraint, because the column will buckle at a much lower torsional-flexural capacity. However, fly-braces are added to this configuration, the column will buckle by the second flexural mode.

- A column, for which the Eigenvalues of both of the expected buckling modes were close together, was seen to show different behaviour patterns than the theoretical failure mode predicted. The analytical model shows a failure mode which is a torsional-flexural buckling mode, but with a combination of 2^{nd} mode flexural buckling and first mode torsional-flexural buckling. This, slightly different buckling mode still shows a magnitude for the critical loads determined from the analytical model which correlate very well with those from the theoretical formulations.

7.4. Prediction method

- The method of predicting the flexural buckling loads is well known, and very accurate. The only discrepancies were due to the sheeting rail acting as a restoring spring which increased the analytical results slightly. This was an anticipated occurrence.

- The methods of calculating the torsional-flexural buckling load as proposed by several previous researchers was implemented in the SANS 10162-1:2005 [7] code approach to dealing with torsional bucking. The results obtained by this prediction method seem to correlate very well

with the analytical results obtained from the GMNLA method of analysis. However, the theoretical values were actually found to be an overestimate when compared to the Eigenvalue prediction. It is thought that this difference could be due to an erroneous determination of the stiffness of the sheeting rail.

- The predicted code capacity value was seen to be conservative for all cases investigated. This is without including the material factor (φ =0.9), which would make the code capacity even more conservative.

- BS 59590-1:2005 [18] does provide a method to determine the torsional-flexural capacity. This method does not include the effects of a torsional brace. The method used is derived from the early work by Timoshenko and Gere [11], and uses the Perry-Robertson approach to include imperfections and inelastic behaviour.

8. Recommendations

The following recommendations can be made, based on the findings and conclusions of this investigation:

- The universal joint designed to provide the pinned end condition for the column, needs to be aligned in a manner that will not allow any settling to occur when high loads are applied. Expert advice should be sought to ensure that the whole concept design is still sufficient.

- A more efficient method of eliminating the twist of the piston of the hydraulic actuator should be put into place.

- A more accurate and comprehensive method of measuring the initial imperfections is needed. This is because the ultimate behaviour of the column is greatly impacted by these imperfections.

- During this study, only two connection types were investigated experimentally. More connection types should be investigated. Potential connections which could be tested (in the test set-up developed) are:
    - Discontinuous sheeting rail;
    - Discontinuous sheeting rail with the addition of a fly-brace;
    - A spliced continuous sheeting rail, which is spliced at the location of the connection to the column;
    - A continuous sheeting rail with transverse web stiffener extending at least half the depth of the columns cross-section.

  These experimental tests should be modelled analytically in the manner presented herein. This would give more credibility and reliance on this model.

- The further experimental work should also focus on any local effects that occur at the connection between the column and the sheeting rail. This should include monitoring local buckling, cross-sectional distortions and excessive twisting. These factors all should be checked for several combinations of cross-sections of both column and sheeting rail.

- If sheeting rails are to be used as torsional braces, as suggested in this report, then some research needs to be performed on determining what the torsional bracing stiffness that these members can provide to the column. The bracing against torsional deformation of the column is provided for by the bending stiffness of the sheeting rail. This needs to be extended so that the design of these sheeting rails can be applied in a safe way, i.e. the behaviour of the sheeting rail needs to be analysed under a combination of the restraining (biaxial bending moments and lateral forces) forces, the wind loads and the weight of the sheeting.

- The analytical model should be critically examined and potentially re-defined with a mesh refinement in the area of the connection. This mesh refinement could be realised by using triangular shell elements. In addition to the mesh refinement the possibility of using thin shell elements should also be investigated.

9. References

1. Taras, A. and Greiner, R.; ***Torsional and flexural torsional buckling – A study on laterally restrained I-sections***; Journal of Constructional Steel Research; Volume 64; 2008; pp. 725 - 731
2. Bresler, B., Lin, T.Y., Scalzi, J.B.; ***Design of Steel Structures***; 2nd edition; John Wiley and Sons, INC; 1968
3. Dowling, P.J., Harding, J.E., Bjorhovde, R.; ***Constructional Steel Design – An International Guide***; Elsevier Science Publishers, LTD; 1992
4. Galambos, T.V.; ***Structural Members and Frames***; Prentice-Hall Series in Theoretical and Applied Mechanics - Structural Analysis and Design Series; Prentice-Hall, Inc., Englwood Cliffs, N. J.; 1968
5. Bastiaanse, G.; ***Flexural-Torsional buckling of single, eccentrically loaded, unequal-legged angle struts***; Thesis presented for the Degree of Master of Engineering at the University of Stellenbosch; 1994
6. BS EN 1993-1-1:2005; ***Eurocode 3: Design of steel structures - Part 1-1: General rules and rules for buildings***; British Standards Institution (BSI); London; 2006
7. SANS 10162-1:2005; ***The structural use of steel; Part 1: Limit-state design of hot-rolled steelwork***; Standards South Africa; 2005
8. Galambos, T.V.; ***Guide to Stability Design Criteria for Metal Structures***; 4th Edition; John Wiley and Sons, INC; 1988
9. de Villiers Hugo, F; ***Restrained columns in single storey buildings***; Thesis presented for the Degree of Doctor of Philosophy in Engineering at the University of Stellenbosch; 1973
10. South African Institute of Steel Construction; ***Southern African Steel Construction Handbook – "The Red Book"***; 5th edition; SAISC; 2005
11. Timoshenko, S.P., Gere, J.M.; ***Theory of Elastic Stability***; 2nd Edition; McGraw-Hill Book Company, Inc.; 1961
12. Dooley, J.F.; ***On the torsional buckling of columns of I-section restrained at finite intervals***; International Journal of Mechanical Sciences; Volume 9; 1967; pp. 1 - 9
13. Horne, M.R. and Ajmani, J.L.; ***Stability of columns supported laterally by side-rails***; International Journal of Mechanical Sciences; Volume 11; 1969; pp. 159 – 174
14. Horne, M.R. and Ajmani, J.L.; ***Design of columns restrained by side-rails***; The Structural Engineer; No. 8, Volume 49; August 1971; pp. 339 – 345
15. Helwig, T.A. and Yura, J.A.; ***Torsional bracing of columns***; Journal of Structural Engineering; Volume 125; 1999; pp. 547 – 555

16. Horne, M. R. and Ajmani, J. L.; ***Failure of columns laterally supported on one flange***; The Structural Engineer; No. 9, Volume 50; September 1972; pp. 355 – 366

17. Gelderblom, J.H., van Rensburg, B.W.J. and Dekker, N.W.; ***The behaviour of eccentrically restrained I-sections subjected to axial loads***; Journal of Constructional Steel Research; Volume 34; 1995; pp. 145 – 160

18. BS 5950-1:2005; ***Structural use of steelwork in building – Part 1: Code of practice for design – Rolled and welded sections***; British Standards Institution (BSI); London; 2000

19. Bureau, A.; ***NCCI: Critical axial load for torsional and flexural torsional buckling modes***; Access Steel online resource; SN001a-EN-EU
URL: http://www.access-steel.com Date of download: 11 June 2008

20. ANSI/AISC 360-05; ***Specification for Structural Steel Buildings***; American Institute of Steel Construction, Inc.; 9 March 2005

21. Raven, G.; ***Scheme development: Overview of structural systems for single-storey buildings***; Access Steel Scheme Development; SS048a-EN-EU; 2006
URL: http://www.access-steel.com Date of download: 11 June 2008

22. Mahachi, J.; ***Design of Structural Steelwork to SANS 10162***; CSIR Building and Construction Technology; 2004

23. Malik, A.S.; ***Scheme development: Details for portal frames using rolled sections***; Access Steel Scheme Development; SS051a-EN-EU; 2007
URL: http://www.access-steel.com Date of download: 11 June 2008

24. Prokon Sructural Analysis and Design; Version 2.4; Prokon Software Consultants

25. ABAQUS; Version 6.7.4; Simulia; 2007

26. Dassault Systèmes; ***ABAQUS Analysis Users Manual***; Version 6.7; 2007

A. Appendix A: Design calculations and drawings

A1. Universal Joint

The universal joint is made up of 5 discrete parts, which are shown opposite:

- Inner plate
- Shafts
- Outer frame
- Spacers
- Bearings

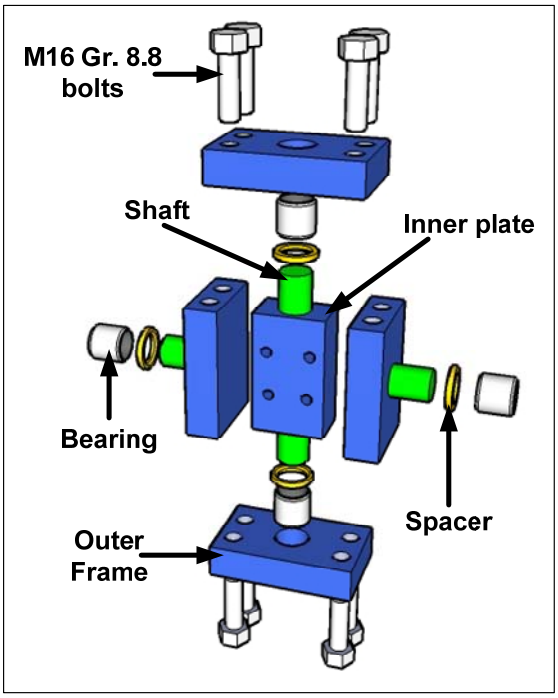

Figure A.1 - Exploded view of universal joint

A1.1. Bearings

The layout of the universal joint calls for two pairs of bearings to allow for rotation about the two major axes. The total design load will thus be carried by a pair of bearings. Thus the radial load per bearing will be 200 *kN*. For a standard roller or cylindrical needle roller bearing to carry such large radial loads really large bearings need to be chosen. These large bearings are expensive. To approach the problem from a different way it was decided to use a composite dry sliding bushing. This is a very thin layer of composite material, called Glycodur® F, which combines the attractive properties of different substances and results in an effective and strong bearing material. This allowed for a smaller bearing (both the shaft diameter and external diameter of the bearing were dramatically reduced) which was in turn a lot cheaper to purchase.

The selected bearing had the following dimensions:
Internal diameter – 28mm
Outer diameter – 32mm
Length – 30mm

A1.2. Inner Plate

The major factor determining the dimensions of the plate are the following:

- The dimensions of the base plate of the column – 110mm x 65mm.
- The shaft – 28mm diameter.

To ensure enough material remains to insert the shaft a plate thickness of 40 mm is selected.

Thus the Inner Plate will be 110mm x 65mm x 40mm.

A1.3. Outer Frame

The major determining factor in the design of the outer frame was the length of the bearing needed to transmit the load of 200 *kN*. This length is 30mm, which was thus selected as the width of the plate. To verify the capacity of the remainder of the outer frame, a rough model was set-up in Prokon [23], and the magnitude of the forces was calculated.

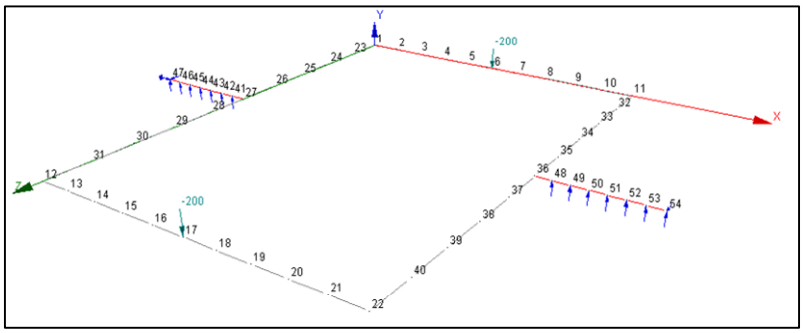

Figure A.2 - Prokon model of outer frame

The forces calculated from the Prokon model and those from a rough hand check are indicated below:

Table A.1 - Loads in outer frame of universal joint

Member	M_{max} (kNm)	
	Prokon	Hand-calculations
Short arm	7.498	7.5
Long arm	5.302	5.25

The maximum bending moment in the Universal joint outer frame occur where there is the least material. This is because at mid-span of each "beam" there is the hole drilled through for the shaft.
The section that was chosen is 80mm x 30mm in cross section, and is to cut from 300WA steel plate. A cross-section of the piece from the universal joint outer frame at mid-span is shown to the right.

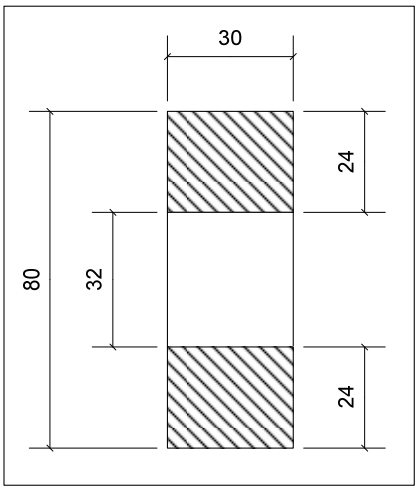

Figure A.3 - Cross-section of outer frame

Based on this cross section the resistive moment can be worked out as shown below:

$$I_x = \frac{b}{12}(h^3 - 32^3)$$
$$I_x = \frac{30}{12}\left(80^3 - 32^3\right) = \underline{1.19808 \times 10^6 mm^4} \qquad \text{(A.1)}$$

$$\text{Then } z = \frac{I_x}{(y/2)} = \frac{1.19808 \times 10^6}{40} = 29952 mm^3 \qquad \text{(A.2)}$$

And thus:

$$M_r = \varphi.z.f_y = 0.9 \times 29952 \times 300 MPa$$
$$M_r = 8.087 kNm \qquad \text{(A.3)}$$

Using plate sections of these dimensions and steel of grade 300WA will ensure that the resistive moment is greater than the applied moment of 7.5*kNm*.

The shear transfer in the joints of the outer frame will be carried by two bolts. The size of the outer frame would not permit more than two bolts. The bolts are chosen as M16, and the shear resistance of the bolts needs to be checked. The resistances are calculated as from The Red Book [10] – Table 7.1. for shear on bolts with threads in the shear plane:

$$V_r = 0.42.\varphi_b.A_b.f_u$$
$$V_r = 0.42 \times 0.8 \times \left(\frac{\pi \times 16^2}{4}\right) \times 800 \qquad \text{(A.4)}$$
$$V_r = \underline{54.05 kN} > 50 kN ----OK!!!$$

Thus, with 2 M16 Gr. 8.8 bolts per edge, a suitably strong shear connection has been achieved.

A1.4. Shaft

There are four shafts per universal joint and each shaft needs to withstand a shear force of 200kN. The internal diameter of the selected bearing is 28mm. Thus, I need to ensure that a shaft of that diameter can withstand the applied shear force. To ensure that this high shear strength criteria is met, it was decided to use a specialist steel made for use of machine shafts, rotors and connecting rods in the heavy duty uses. This steel is called V155 and is manufactured by Bohler Uddeholm Africa.

The resistance check is as follows, again from Table 7.1 of The Red Book [10] for Shear on bolts with the threads excluded from the shear plane:

$$V_r = 0.6.\varphi_b.A_b.f_u$$
$$V_r = 0.6 \times 0.8 \times \left(\frac{\pi \times 28^2}{4} \right) \times 1100 \qquad \text{(A.5)}$$
$$V_r = \underline{325.12kN} > V_u = 200kN - - - OK!$$

Two of the shafts will be press fit into the inner plate, and then rest on the bearings into the outer frame. The other two shafts will be press fit into the outer frame, and will then rest in two bearings which are in the brackets, the layout of which will be discussed in the next section.

A1.5. Spacers

To prevent any relative motion between the individual parts of the universal joint it was necessary to place spacers, which will prevent any translational movement and still allow rotation. The spacers were machined from brass due to its desirable characteristics in bearing applications. The spacers are to fit between the inner plate and the outer frame, as well as between the outer frame and bracket.

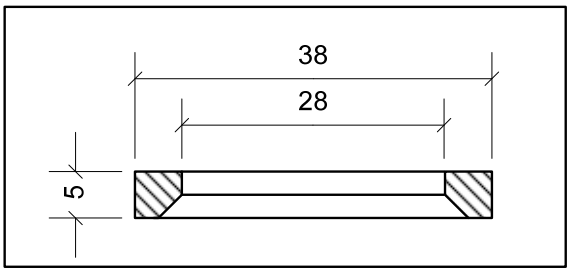

Figure A.4 – Spacer dimensions

A1.6. Bracket

The bracket is the connection between the universal joint and the load application and measurement devices. The universal joint sits into the bracket on two shafts, which lie in two bearings as mentioned previously.

The connector varies for each of the brackets at either end. At the load cell side, it is a hollow sleeve into which the load cell's knob rests. The whole joint is prevented from twisting by three grub screws which are set 120° from each other.

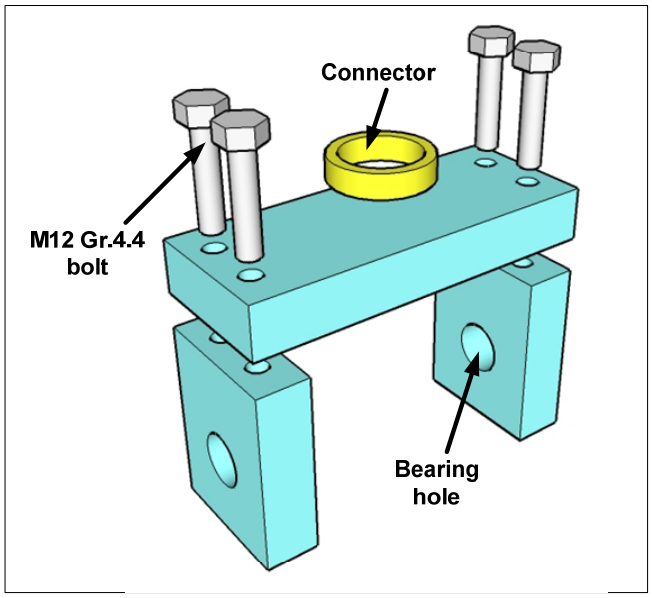

Figure A.5 - Exploded view of bracket

At the other end, the joint between the Enerpac load actuator and the bracket is in the form of a threaded bar, which threads directly into the actuator. The joint is prevented from twisting by the lock nut, which will be tightened once the bracket is threaded into place.

A2. Workshop drawings

The workshop drawings are attached and are ordered in the following way:

A2.1. Universal joints

1. Assembly
2. Detailed assembly – Actuator end of set-up
3. Detailed assembly – Load cell end of set-up
4. Outer frame
5. Inner plate
6. Outer frame assembly
7. Bracket frame
8. Bracket assembly – Actuator end of set-up
9. Bracket assembly – Load cell end of set-up
10. Shaft ad spacer details
11. Sleeve detail – from Load cell end bracket

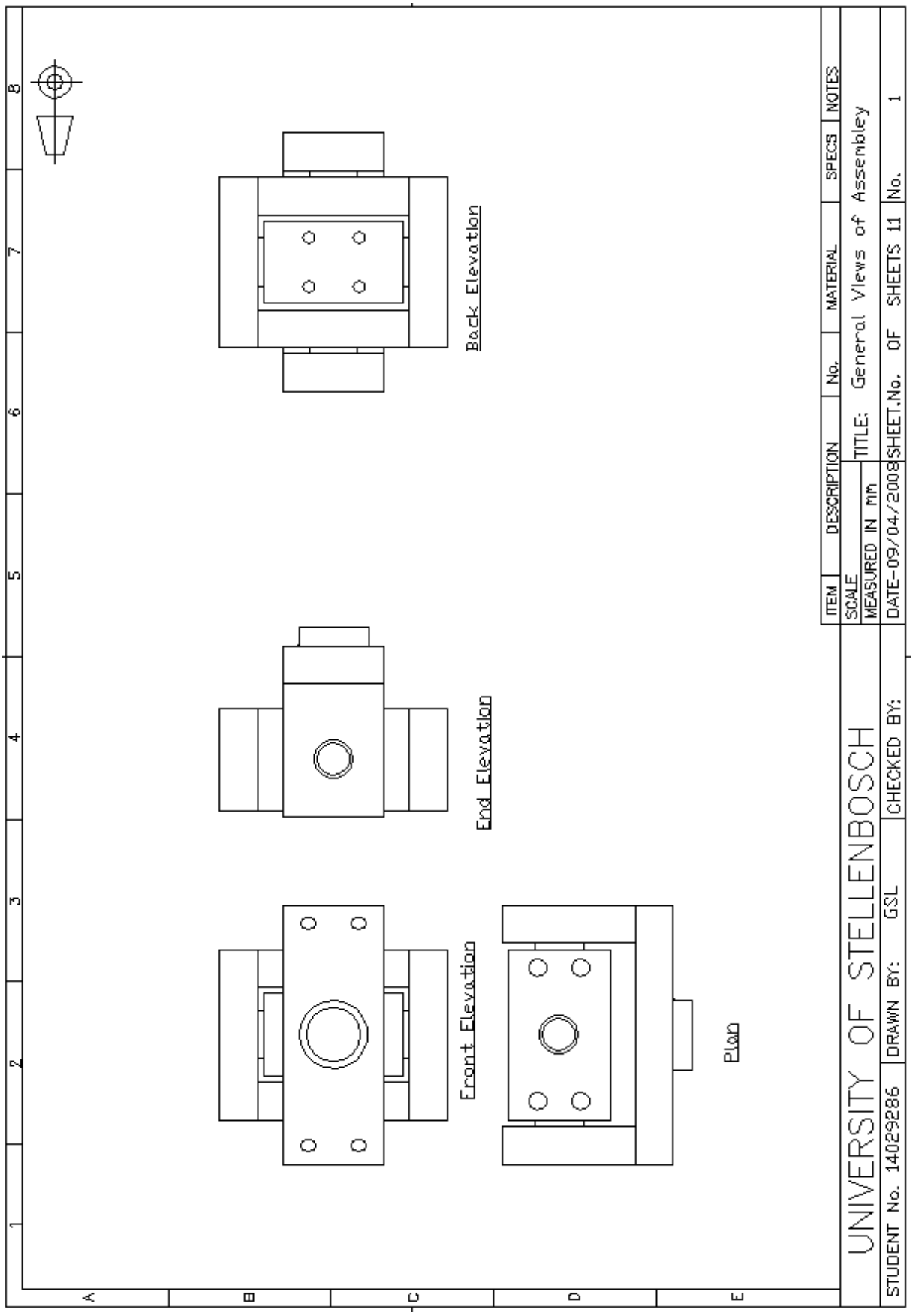
Back Elevation
End Elevation
Front Elevation
Plan
UNIVERSITY OF STELLENBOSCH
ITEM | DESCRIPTION | No. | MATERIAL | SPECS | NOTES
SCALE
MEASURED IN mm
TITLE: General Views of Assembley
DATE-09/04/2008
SHEET No. OF SHEETS 11 No. 1
STUDENT No. 14029286
DRAWN BY: GSL
CHECKED BY:

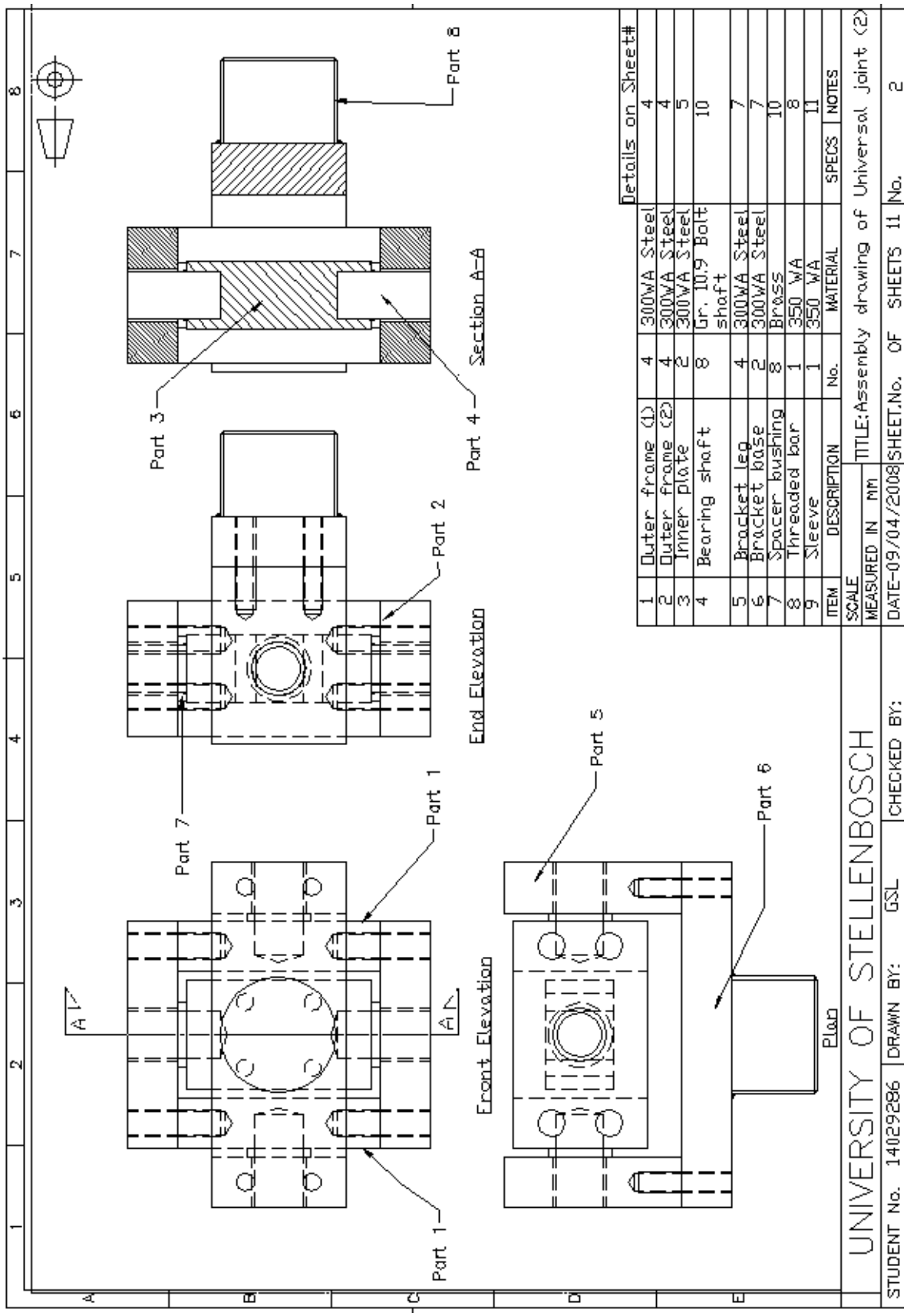
Part 8
Part 3
Part 4
Section A-A
Part 2
End Elevation
Part 7
Part 1
Part 5
Part 6
Front Elevation
Plan
Part 1
A
A
UNIVERSITY OF STELLENBOSCH
STUDENT No. 14029286 DRAWN BY: GSL CHECKED BY:
SCALE
MEASURED IN mm
TITLE:Assembly drawing of Universal joint (2)
DATE-09/04/2008 SHEET.No. OF SHEETS 11 No. 2
Details on Sheet#
ITEM DESCRIPTION No. MATERIAL SPECS NOTES
1 Outer frame (1) 4 300WA Steel 4
2 Outer frame (2) 4 300WA Steel 4
3 Inner plate 2 300WA Steel 5
4 Bearing shaft 8 Gr. 10.9 Bolt shaft 10
5 Bracket leg 4 300WA Steel 7
6 Bracket base 2 300WA Steel 7
7 Spacer bushing 8 Brass 10
8 Threaded bar 1 350 WA 8
9 Sleeve 1 350 WA 11

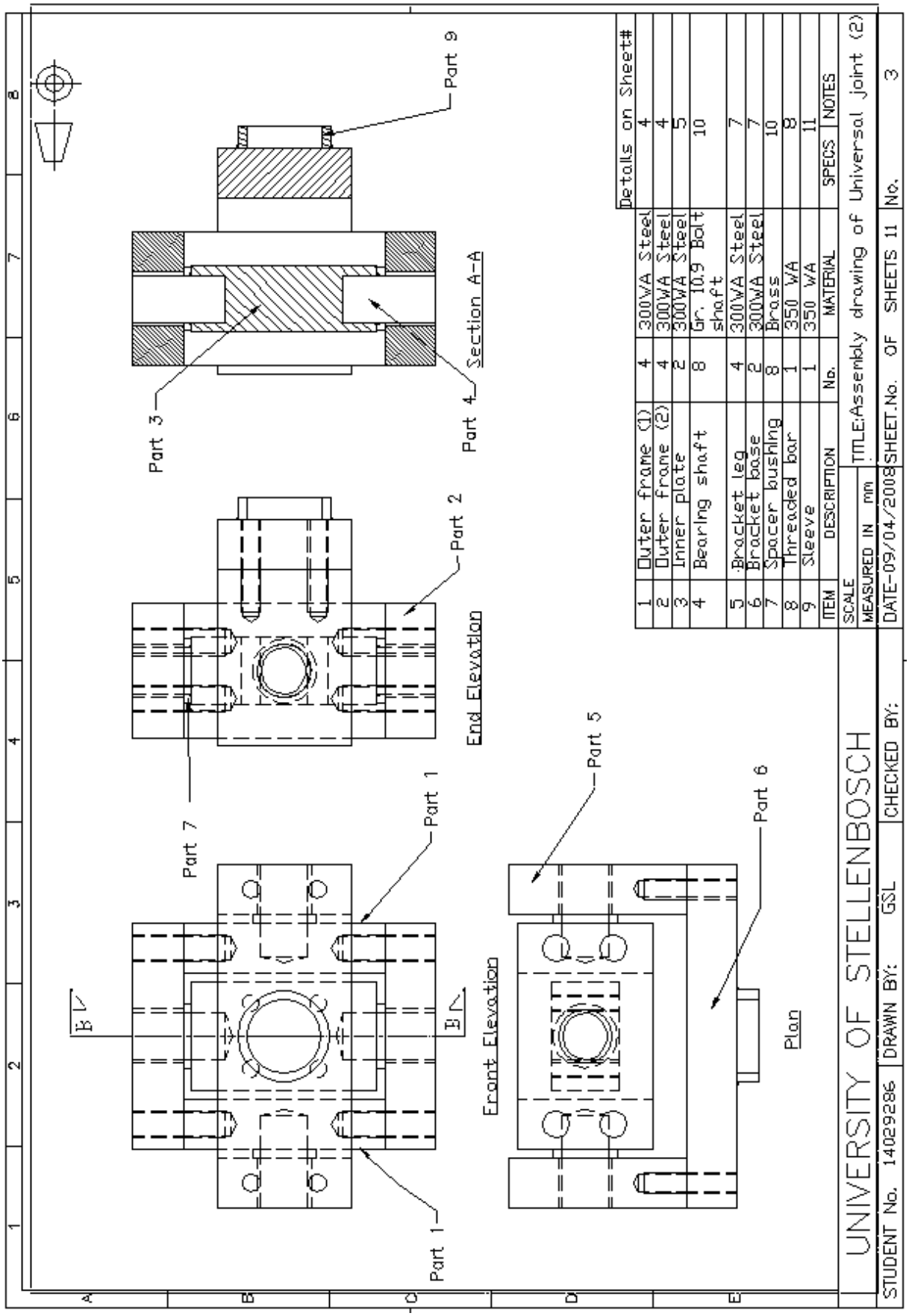
Part 9
Part 3
Part 4
Section A-A
Part 2
End Elevation
Part 7
Part 1
Part 5
Part 6
Front Elevation
Plan
Part 1
B
B
Details on Sheet# 4 4 5 10 7 7 10 8 11 3
1 Outer frame (1) 4 300WA Steel
2 Outer frame (2) 4 300WA Steel
3 Inner plate 2 300WA Steel
4 Bearing shaft 8 Gr. 10.9 Bolt shaft
5 Bracket leg 4 300WA Steel
6 Bracket base 2 300WA Steel
7 Spacer bushing 8 Brass
8 Threaded bar 1 350 WA
9 Sleeve 1 350 WA
ITEM DESCRIPTION No. MATERIAL SPECS NOTES
SCALE
MEASURED IN mm
TITLE:Assembly drawing of Universal joint (2)
UNIVERSITY OF STELLENBOSCH
STUDENT No. 14029286 DRAWN BY: GSL CHECKED BY:
DATE-09/04/2008 SHEET.No. OF SHEETS 11 No. 3

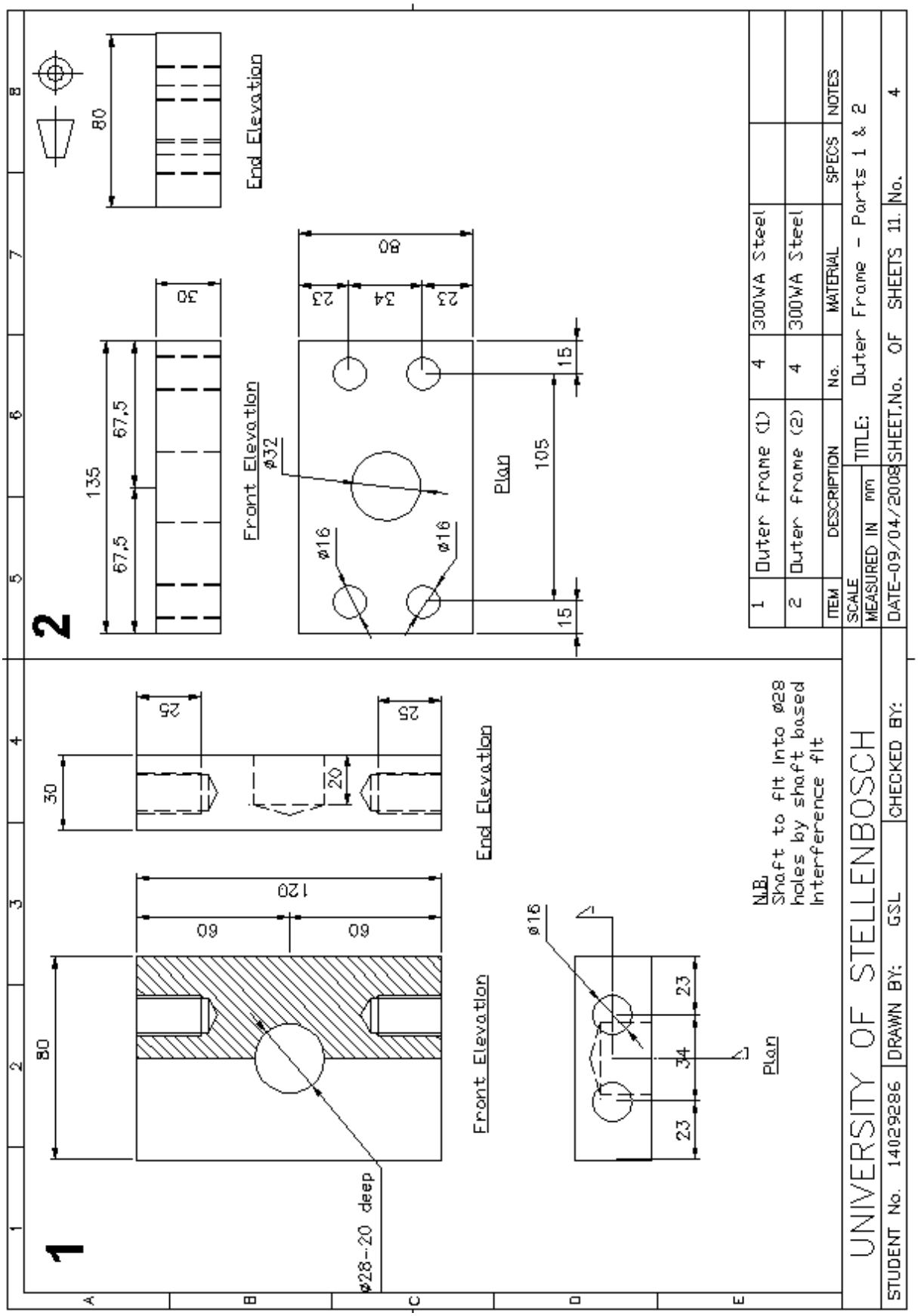
2
End Elevation
80
Front Elevation
ø32
135
67,5
67,5
30
Plan
80
23
34
23
105
15
15
ø16
ø16
1
Outer frame (1) 4 300WA Steel
2 Outer frame (2) 4 300WA Steel
ITEM DESCRIPTION No. MATERIAL SPECS NOTES
SCALE
MEASURED IN mm
TITLE: Outer Frame - Parts 1 & 2
DATE-09/04/2008
SHEET No. OF SHEETS 11. No. 4
STUDENT No. 14029286
DRAWN BY: GSL
CHECKED BY:
UNIVERSITY OF STELLENBOSCH
N.B.
Shaft to fit into ø28 holes by shaft based interference fit
End Elevation
25
25
30
20
Front Elevation
120
60
60
80
ø28-20 deep
ø16
Plan
23
34
23

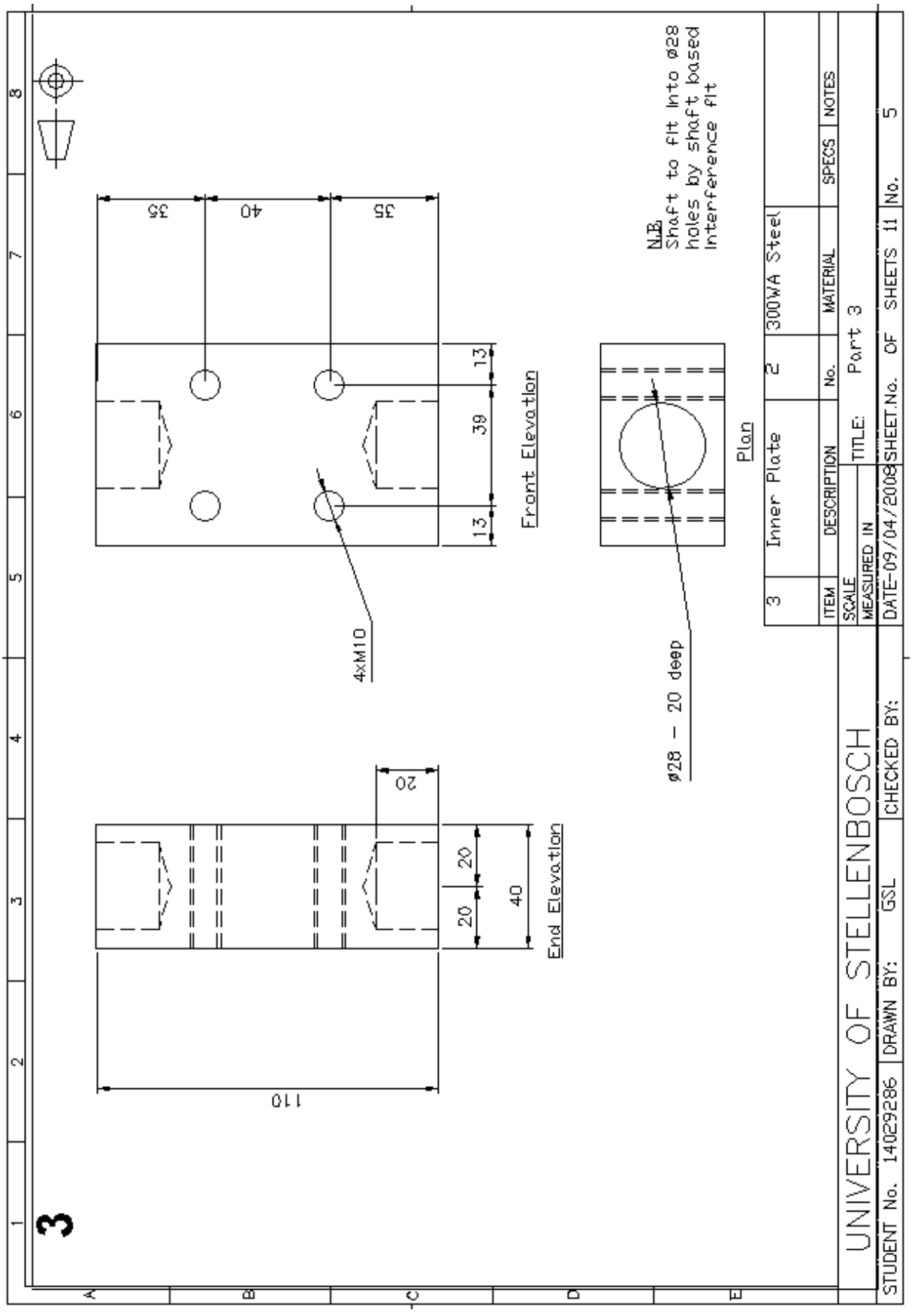
UNIVERSITY OF STELLENBOSCH
STUDENT No. 14029286
DRAWN BY: GSL
CHECKED BY:
DATE-09/04/2008
SHEET No. 5 OF SHEETS 11
TITLE: Part 3
SCALE
MEASURED IN
ITEM DESCRIPTION No. MATERIAL SPECS NOTES
3 Inner Plate 2 300WA Steel
N.B. Shaft to fit into ø28 holes by shaft based interference fit
Front Elevation
End Elevation
Plan
4xM10
ø28 - 20 deep
35
40
35
13
39
13
20
20
20
40
110

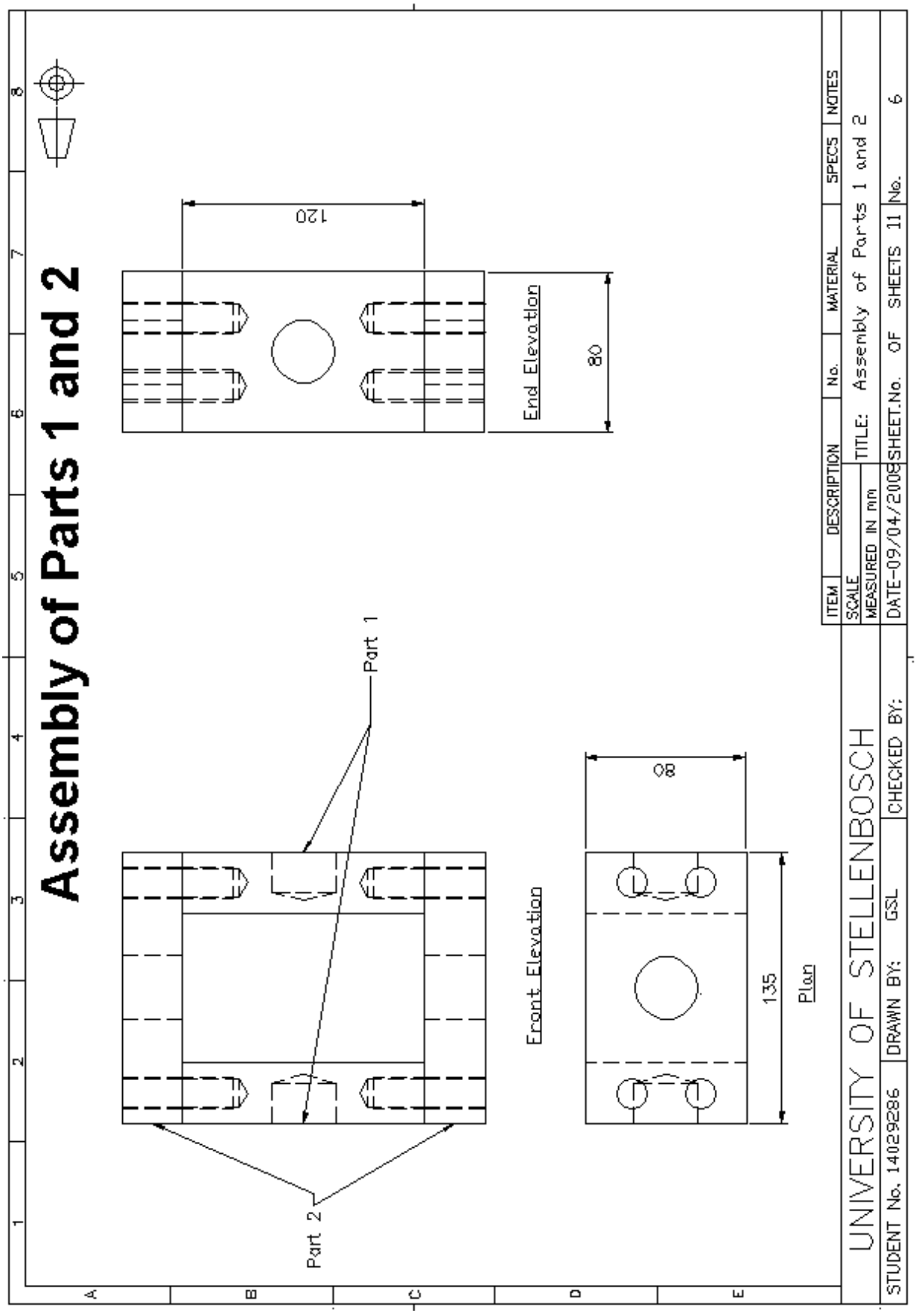
Assembly of Parts 1 and 2
120
End Elevation
80
Part 1
Part 2
Front Elevation
80
135
Plan
UNIVERSITY OF STELLENBOSCH
ITEM
DESCRIPTION
No.
MATERIAL
SPECS
NOTES
SCALE
MEASURED IN mm
TITLE: Assembly of Parts 1 and 2
DATE-09/04/2008
SHEET.No. OF SHEETS 11
No. 6
STUDENT No. 14029286
DRAWN BY: GSL
CHECKED BY:

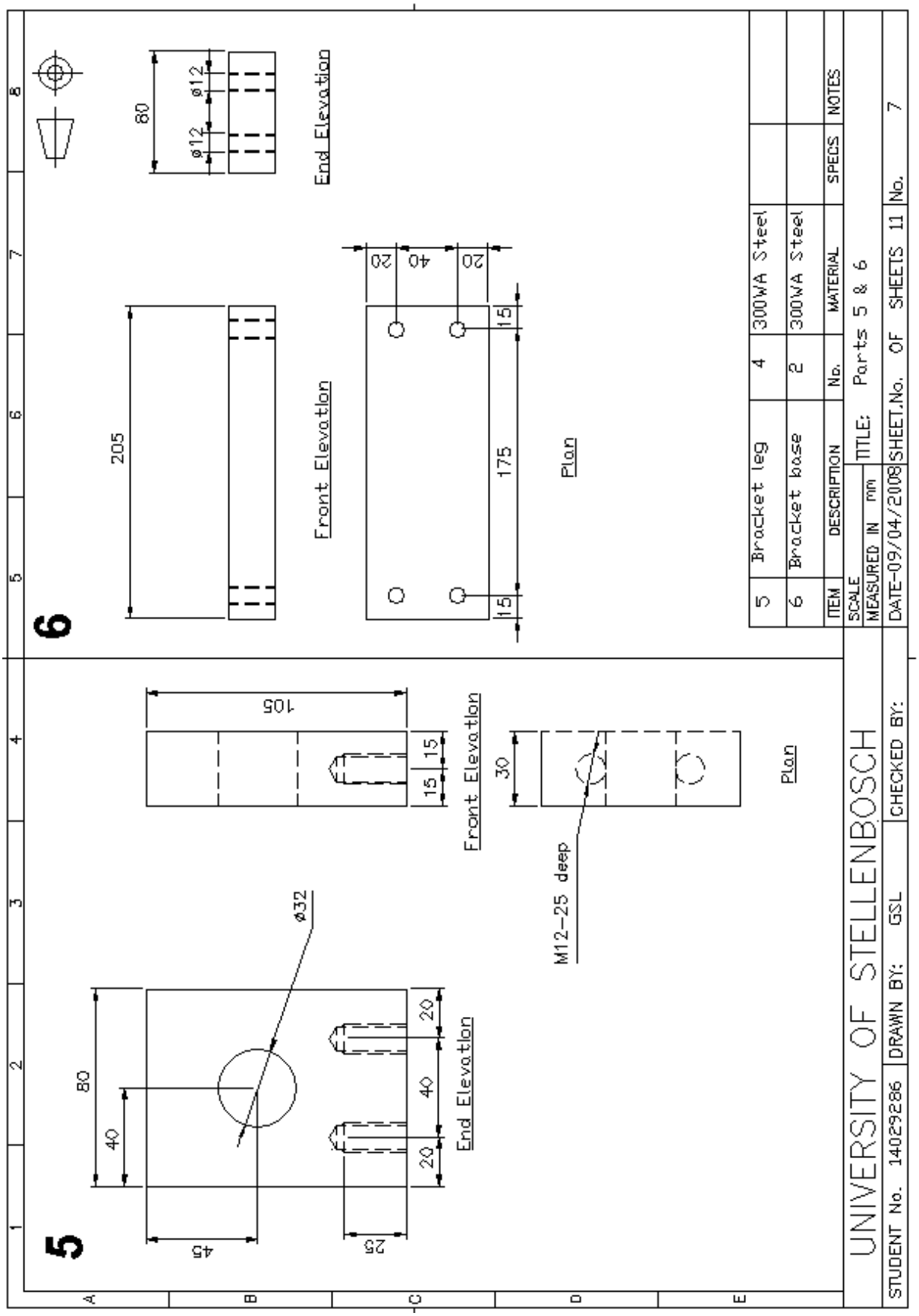
6
205
Front Elevation
End Elevation
80
ø12
ø12
20
40
20
15
175
15
Plan
5
105
15
15
Front Elevation
30
M12-25 deep
Plan
ø32
80
40
20
40
20
End Elevation
45
25
ITEM DESCRIPTION No. MATERIAL SPECS NOTES
5 Bracket leg 4 300WA Steel
6 Bracket base 2 300WA Steel
SCALE
MEASURED IN mm
TITLE: Parts 5 & 6
DATE-09/04/2008
SHEET No. OF SHEETS 11 No. 7
STUDENT No. 14029286
DRAWN BY: GSL
CHECKED BY:
UNIVERSITY OF STELLENBOSCH

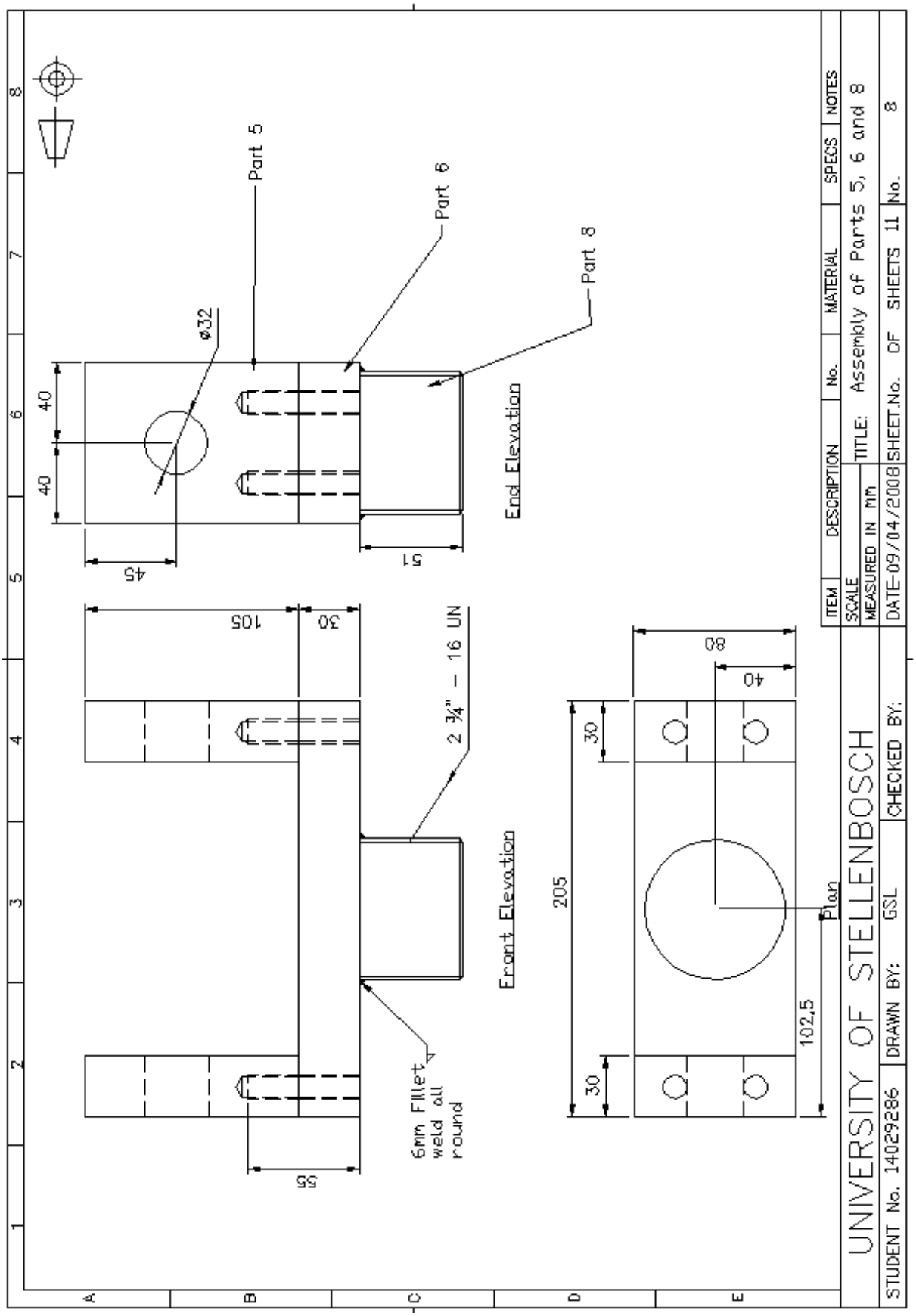
Part 5
Part 6
Part 8
ø32
40
40
45
51
End Elevation
105
30
2 ¾" - 16 UN
55
6mm Fillet weld all round
Front Elevation
80
40
30
205
30
102,5
Plan
ITEM
DESCRIPTION
No.
MATERIAL
SPECS
NOTES
SCALE
MEASURED IN mm
TITLE: Assembly of Parts 5, 6 and 8
DATE 09/04/2008
SHEET No. OF SHEETS 11
No. 8
UNIVERSITY OF STELLENBOSCH
STUDENT No. 14029286
DRAWN BY: GSL
CHECKED BY:

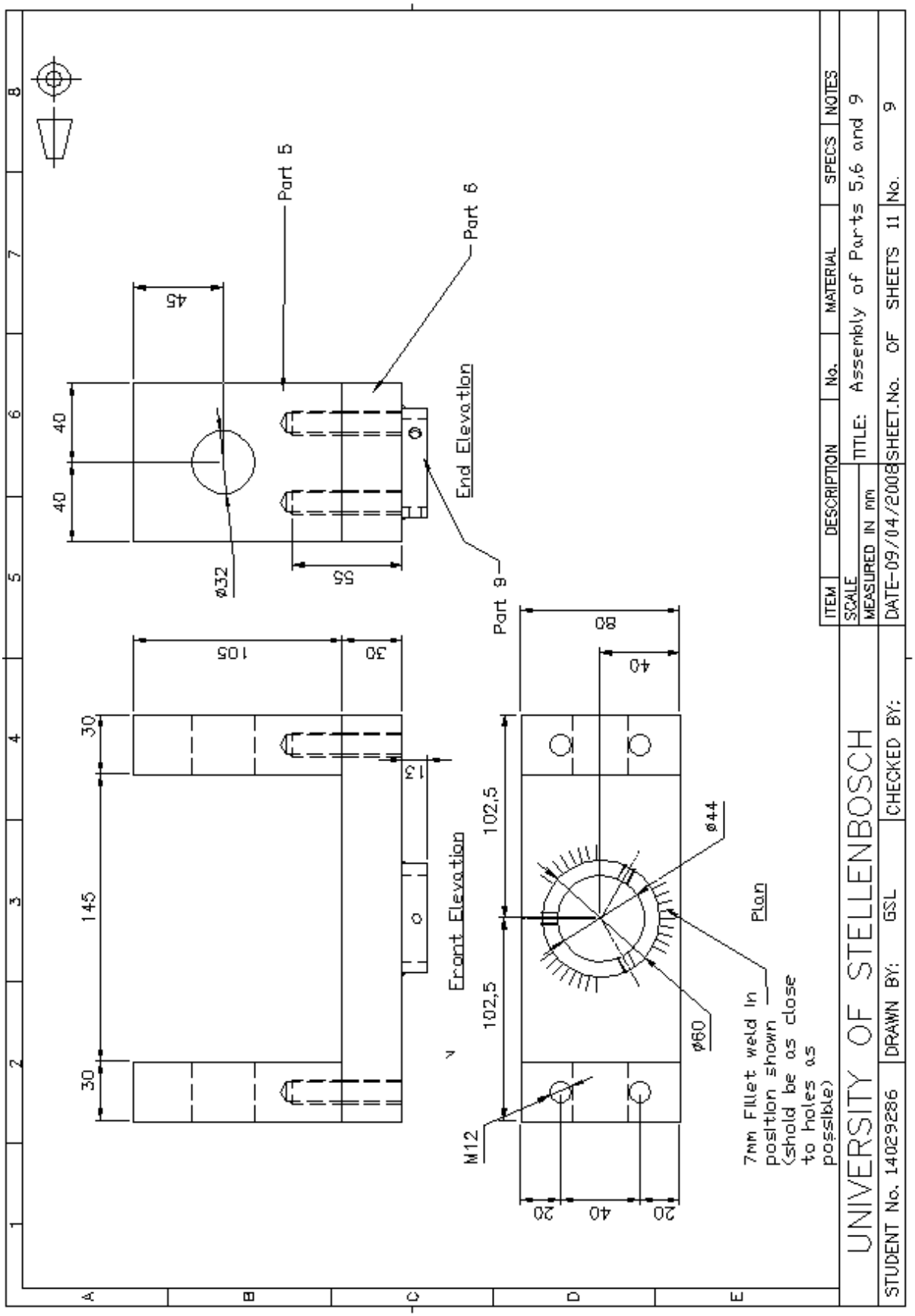
Part 5
Part 6
Part 9
End Elevation
Front Elevation
Plan
45
40
40
Ø32
55
105
30
30
145
30
3
8
102,5
102,5
80
40
Ø44
Ø60
M12
20
40
20
7mm Fillet weld in position shown (shold be as close to holes as possible)
ITEM
DESCRIPTION
No.
MATERIAL
SPECS
NOTES
SCALE
MEASURED IN mm
TITLE: Assembly of Parts 5,6 and 9
DATE-09/04/2008
SHEET No. OF SHEETS 11
No. 9
UNIVERSITY OF STELLENBOSCH
STUDENT No. 14029286
DRAWN BY: GSL
CHECKED BY:

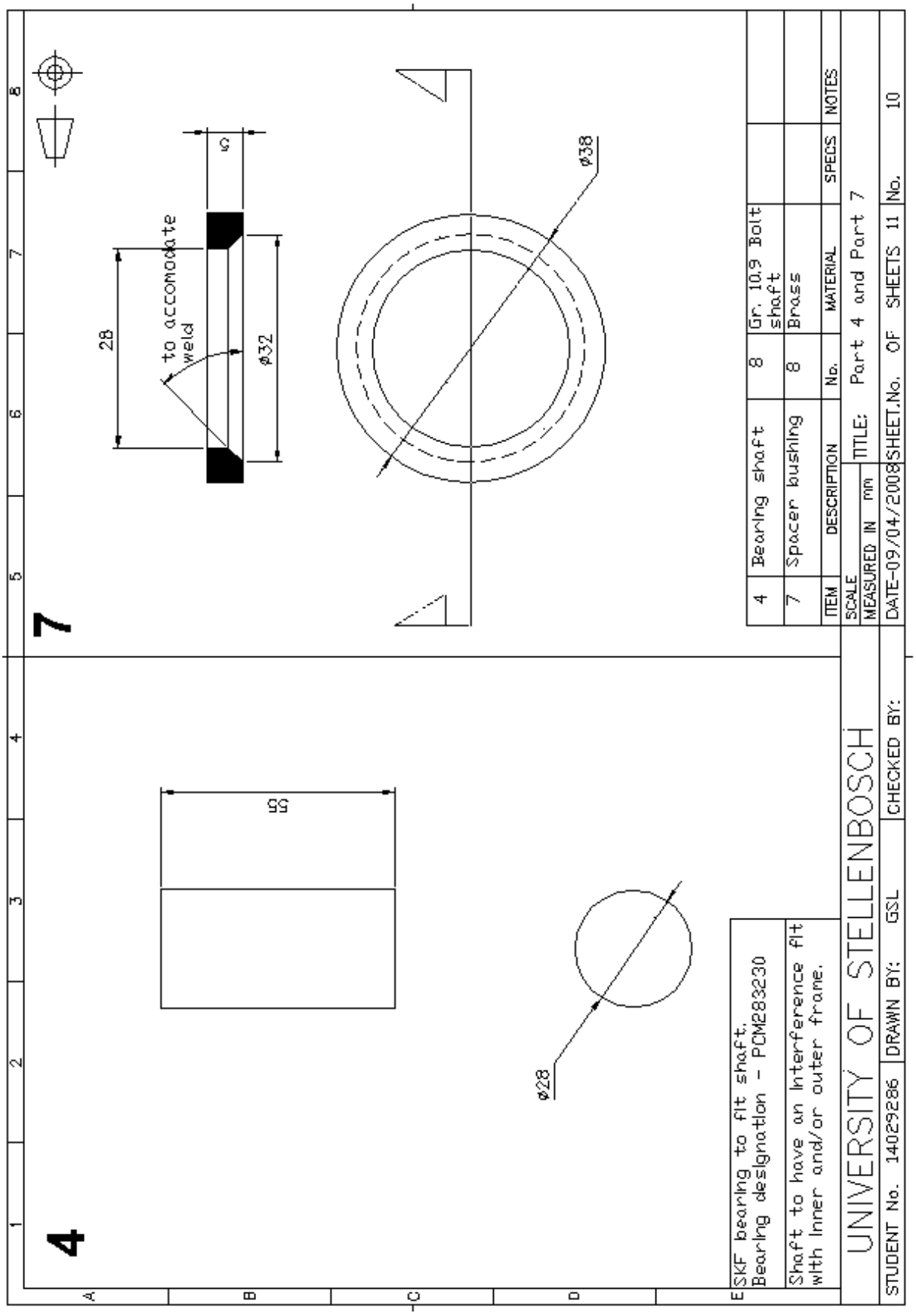
7
28
to accomodate weld
5
ø32
ø38
4 Bearing shaft 8 Gr. 10.9 Bolt shaft
7 Spacer bushing 8 Brass
ITEM DESCRIPTION No. MATERIAL SPECS NOTES
SCALE
MEASURED IN mm
TITLE: Part 4 and Part 7
DATE-09/04/2008 SHEET No. OF SHEETS 11 No. 10
STUDENT No. 14029286 DRAWN BY: GSL CHECKED BY:
UNIVERSITY OF STELLENBOSCH
4
55
ø28
SKF bearing to fit shaft.
Bearing designation - PCM283230
Shaft to have an interference fit with inner and/or outer frame.

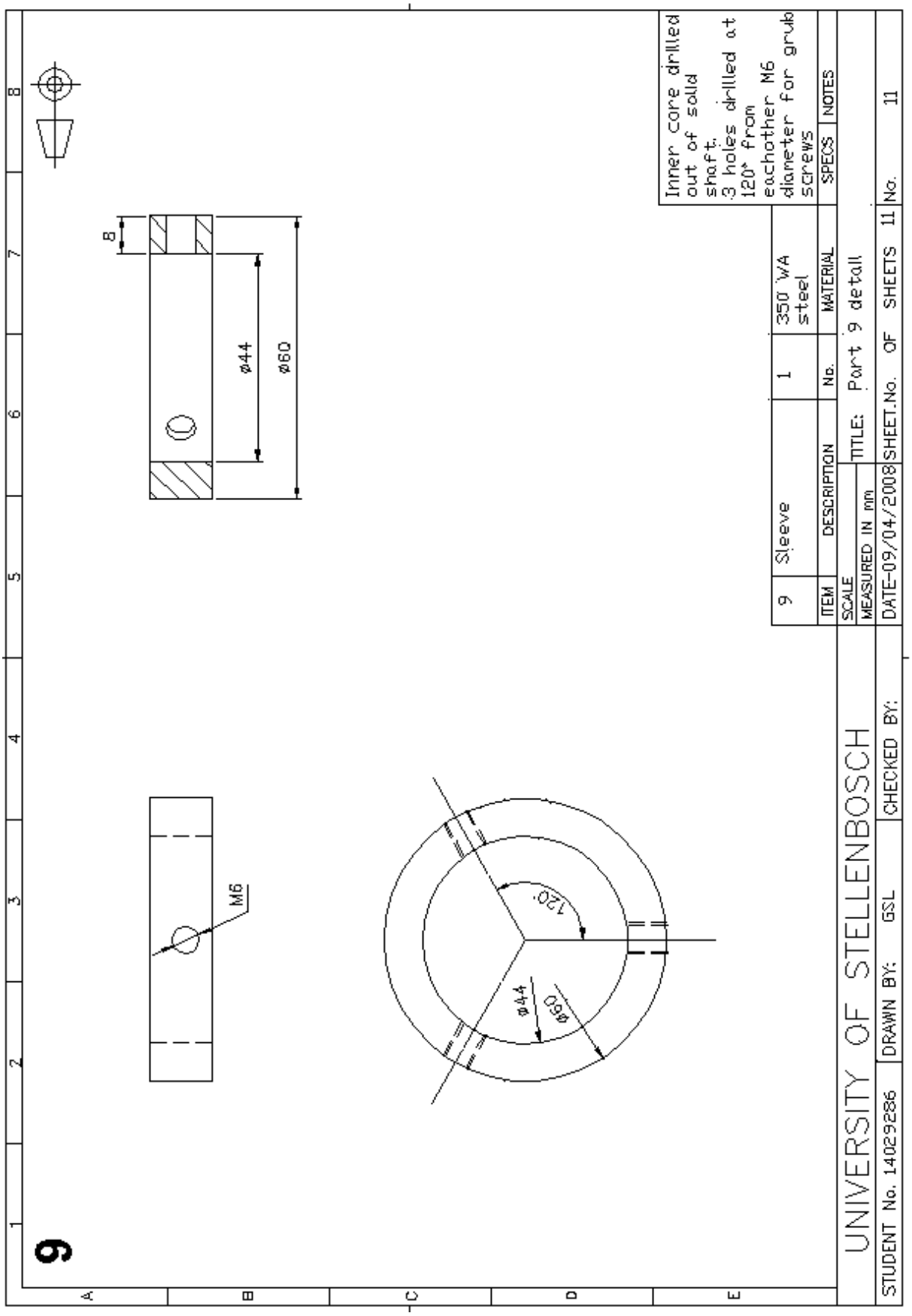
9
8
7
6
5
4
3
2
1
A
B
C
D
E
8
ø44
ø60
M6
120°
ø44
ø60
Inner core drilled out of solid shaft.
3 holes drilled at 120° from eachother M6 diameter for grub screws
9 Sleeve 1 350 WA steel
ITEM DESCRIPTION No. MATERIAL SPECS NOTES
SCALE
MEASURED IN mm
TITLE: Part 9 detail
UNIVERSITY OF STELLENBOSCH
STUDENT No. 14029286 DRAWN BY: GSL CHECKED BY:
DATE-09/04/2008 SHEET.No. OF SHEETS 11 No. 11

A2.2. Test Columns

1. Column
2. Column + cleat
3. Column + cleat + gusset plates
4. Sheeting rail
5. Sheeting rail for fly braces
6. Cleat
7. Base plate
8. Fly-brace
9. Gusset plate

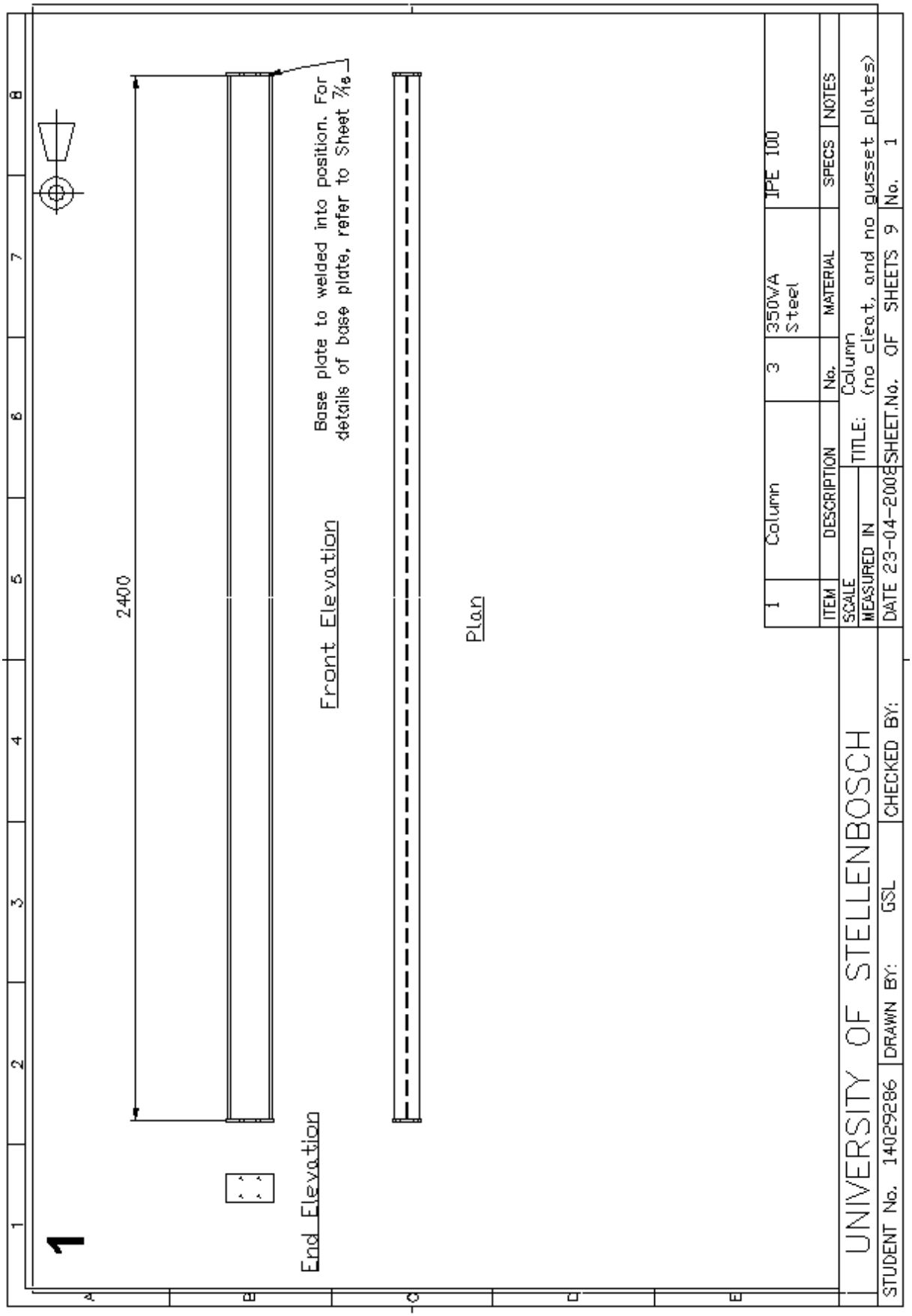
1
2400
Front Elevation
Base plate to welded into position. For details of base plate, refer to Sheet 7/6
End Elevation
Plan
1 Column 3 350WA Steel IPE 100
ITEM DESCRIPTION No. MATERIAL SPECS NOTES
SCALE
MEASURED IN
TITLE: Column (no cleat, and no gusset plates)
DATE 23-04-2008 SHEET No. OF SHEETS 9 No. 1
UNIVERSITY OF STELLENBOSCH
STUDENT No. 14029286 DRAWN BY: GSL CHECKED BY:

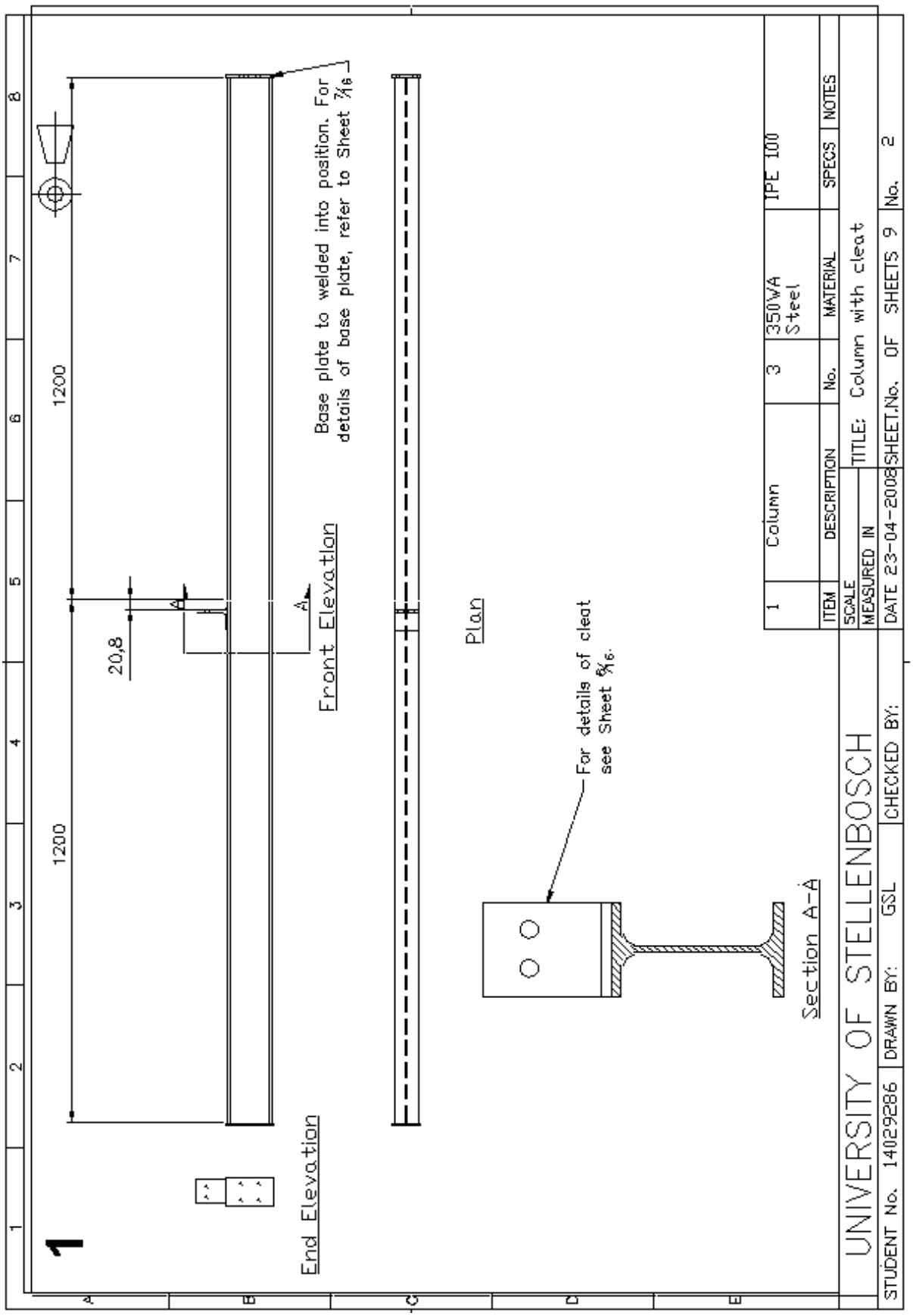
1200
1200
20,8
A
A
Base plate to welded into position. For details of base plate, refer to Sheet 2/6
Front Elevation
End Elevation
Plan
For details of cleat see Sheet 6/6.
Section A-A
1
Column
3
350WA Steel
IPE 100
ITEM
DESCRIPTION
No.
MATERIAL
SPECS
NOTES
SCALE
MEASURED IN
TITLE: Column with cleat
DATE 23-04-2008
SHEET No. OF SHEETS 9
No. 2
UNIVERSITY OF STELLENBOSCH
STUDENT No. 14029286
DRAWN BY: GSL
CHECKED BY:

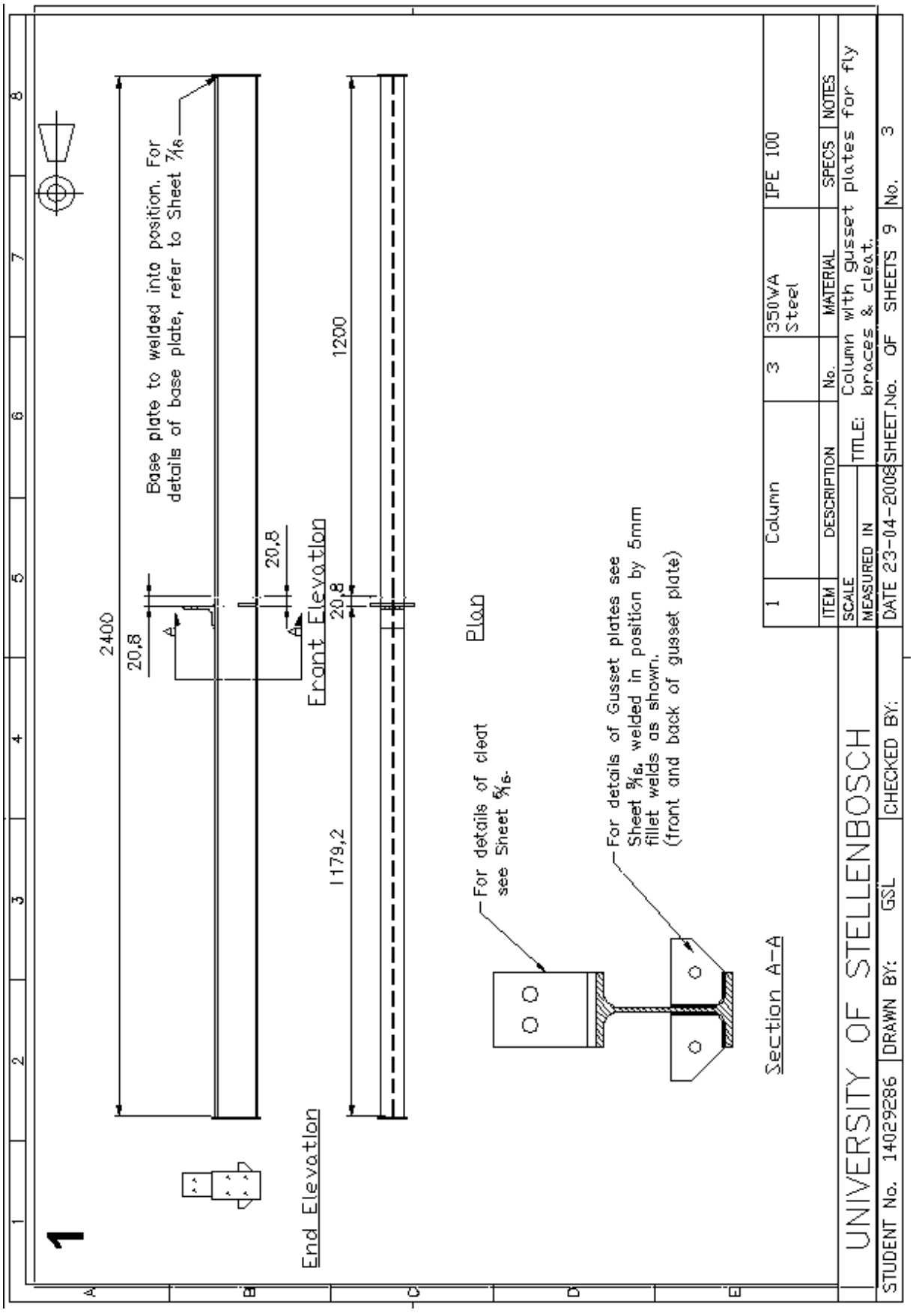
Base plate to welded into position. For details of base plate, refer to Sheet 7/6
2400
20,8
20,8
20,8
1200
1179,2
Front Elevation
End Elevation
Plan
Section A-A
For details of cleat see Sheet 5/6.
For details of Gusset plates see Sheet 5/6, welded in position by 5mm fillet welds as shown. (front and back of gusset plate)
1 Column 3 350WA Steel IPE 100
ITEM DESCRIPTION No. MATERIAL SPECS NOTES
SCALE
MEASURED IN
TITLE: Column with gusset plates for fly braces & cleat.
DATE 23-04-2008
SHEET No. OF SHEETS 9 No. 3
UNIVERSITY OF STELLENBOSCH
STUDENT No. 14029286 DRAWN BY: GSL CHECKED BY:

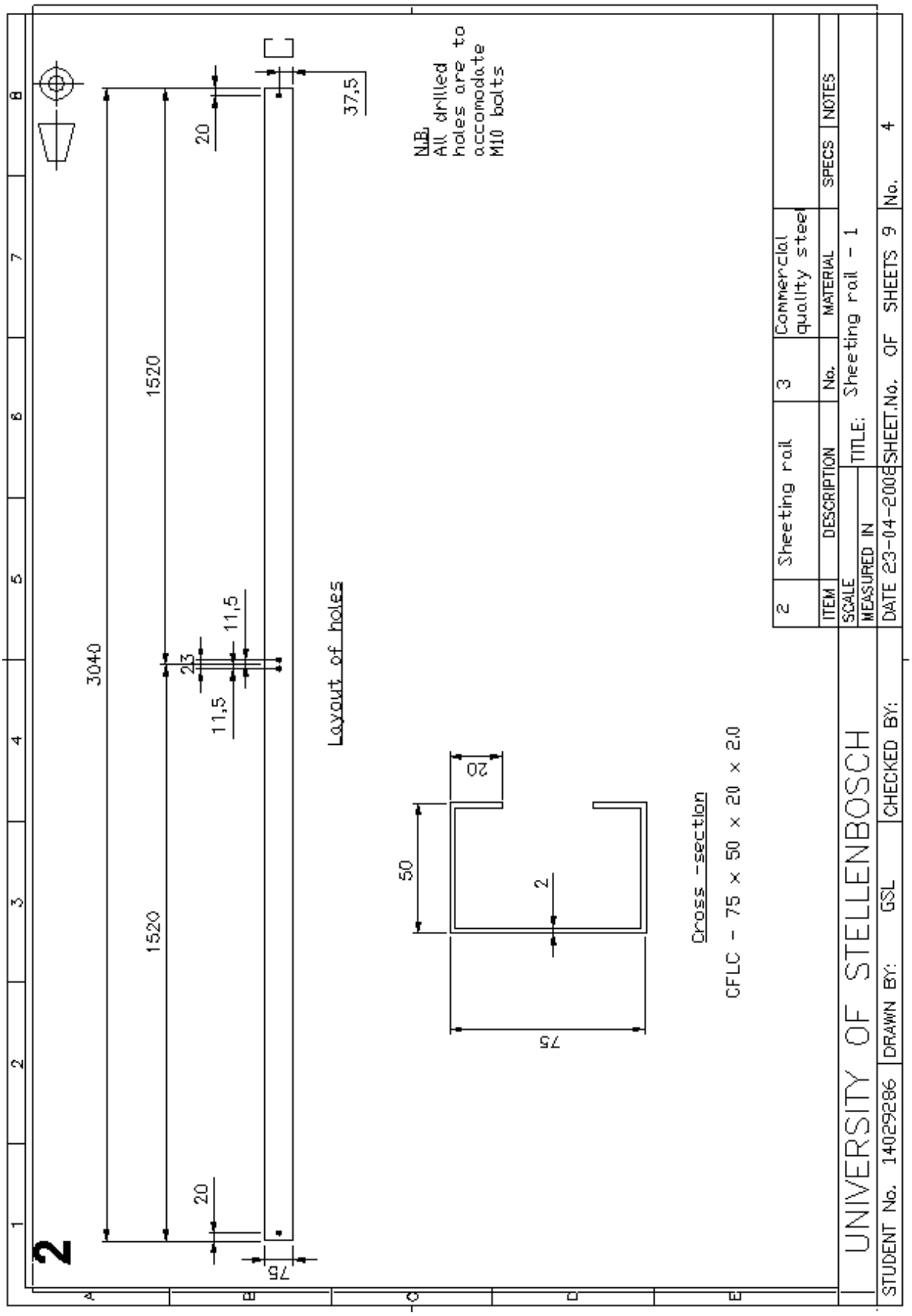
2
3040
1520
1520
20
20
75
37,5
11,5
11,5
23
Layout of holes
N.B.
All drilled
holes are to
accomodate
M10 bolts
20
50
2
75
Cross -section
CFLC - 75 x 50 x 20 x 2.0
2 Sheeting rail 3 Commercial quality steel
ITEM DESCRIPTION No. MATERIAL SPECS NOTES
SCALE
MEASURED IN
TITLE: Sheeting rail - 1
DATE 23-04-2008
SHEET No. OF SHEETS 9 No. 4
UNIVERSITY OF STELLENBOSCH
STUDENT No. 14029286 DRAWN BY: GSL CHECKED BY:

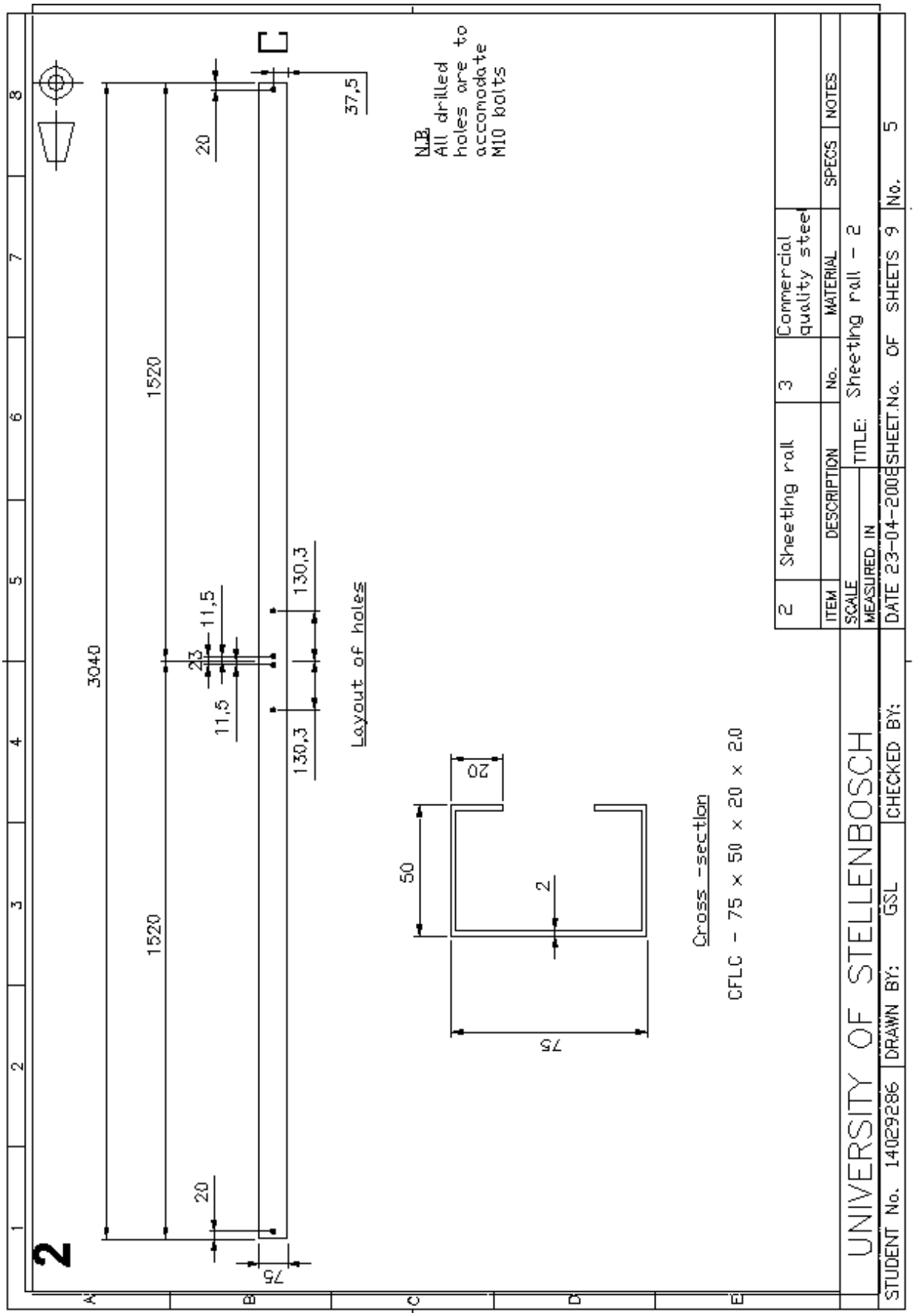
2
3040
1520
1520
20
20
75
37,5
11,5
23
11,5
130,3
130,3
Layout of holes
N.B
All drilled holes are to accomodate M10 bolts
20
50
2
75
Cross -section
CFLC - 75 x 50 x 20 x 2.0
2 Sheeting rail 3 Commercial quality steel
ITEM DESCRIPTION No. MATERIAL SPECS NOTES
SCALE
MEASURED IN
TITLE: Sheeting rail - 2
UNIVERSITY OF STELLENBOSCH
STUDENT No. 14029286 DRAWN BY: GSL CHECKED BY:
DATE 23-04-2008 SHEET No. OF SHEETS 9 No. 5

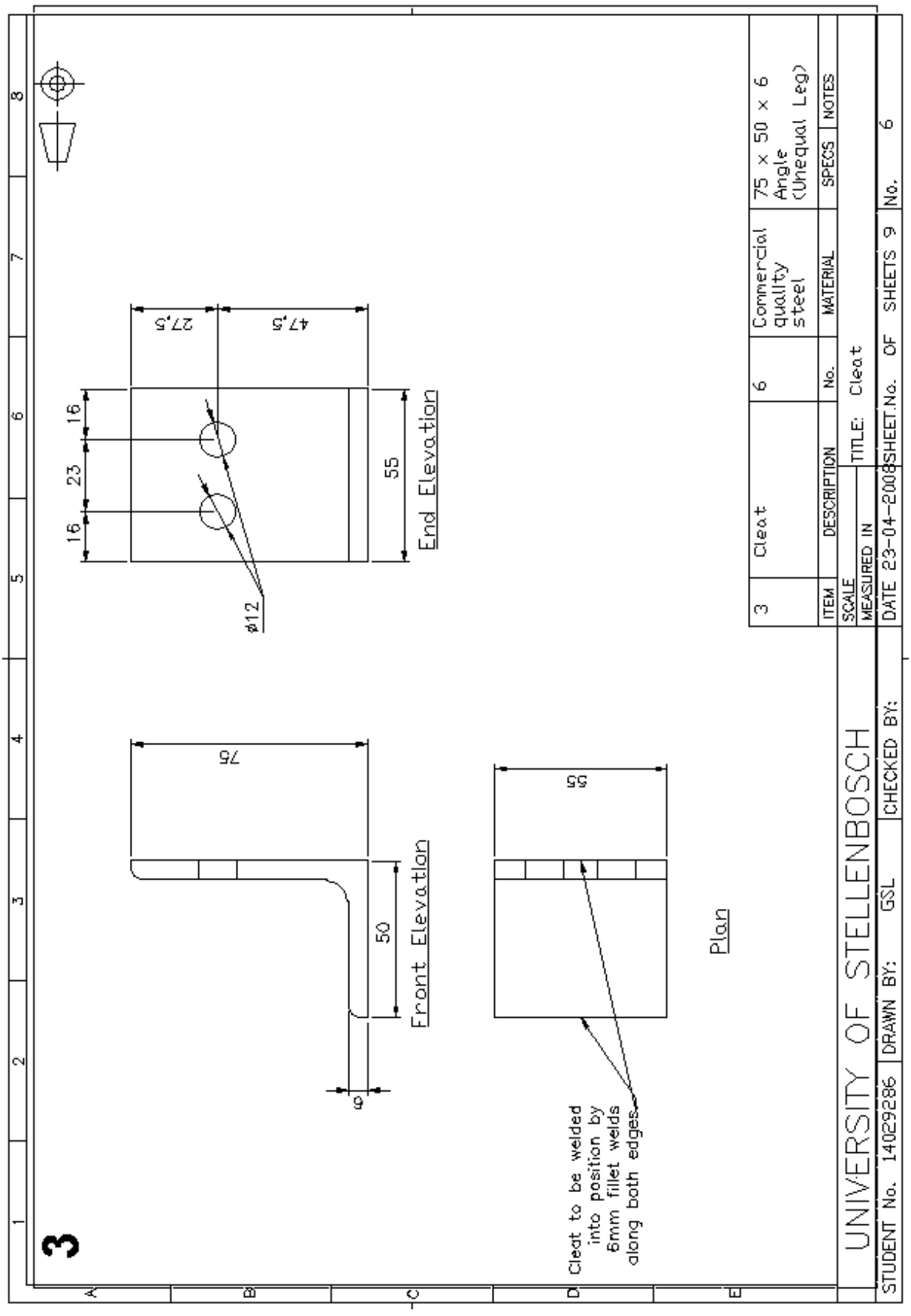
3
Cleat to be welded into position by 6mm fillet welds along both edges
Plan
75
50
6
Front Elevation
55
55
16
23
16
ø12
27,5
47,5
End Elevation
UNIVERSITY OF STELLENBOSCH
TITLE: Cleat
SCALE
MEASURED IN
DATE 23-04-2008
SHEET No. OF SHEETS 9
No. 6
STUDENT No. 14029286
DRAWN BY: GSL
CHECKED BY:
ITEM DESCRIPTION No. MATERIAL SPECS NOTES
3 Cleat 6 Commercial quality steel 75 x 50 x 6 Angle (Unequal Leg)

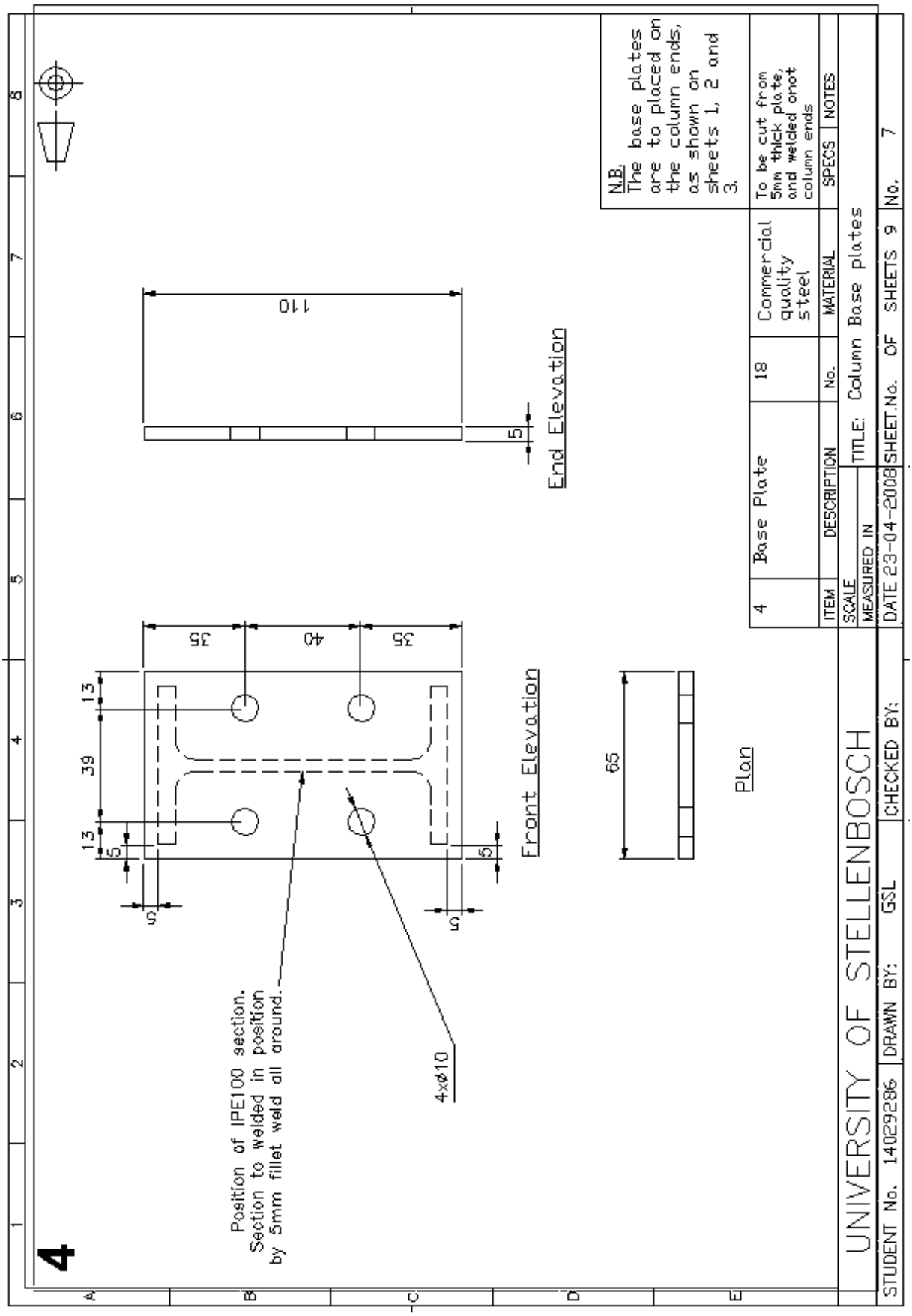
4
Position of IPE100 section.
Section to welded in position
by 5mm fillet weld all around.
4xø10
35
40
35
13
39
13
5
5
5
5
Front Elevation
65
Plan
110
5
End Elevation
N.B.
The base plates
are to placed on
the column ends,
as shown on
sheets 1, 2 and
3.
4 Base Plate 18 Commercial quality steel To be cut from 5mm thick plate, and welded onot column ends
ITEM DESCRIPTION No. MATERIAL SPECS NOTES
SCALE
MEASURED IN
TITLE: Column Base plates
DATE 23-04-2008
SHEET No. OF SHEETS 9
No. 7
UNIVERSITY OF STELLENBOSCH
STUDENT No. 14029286
DRAWN BY: GSL
CHECKED BY:

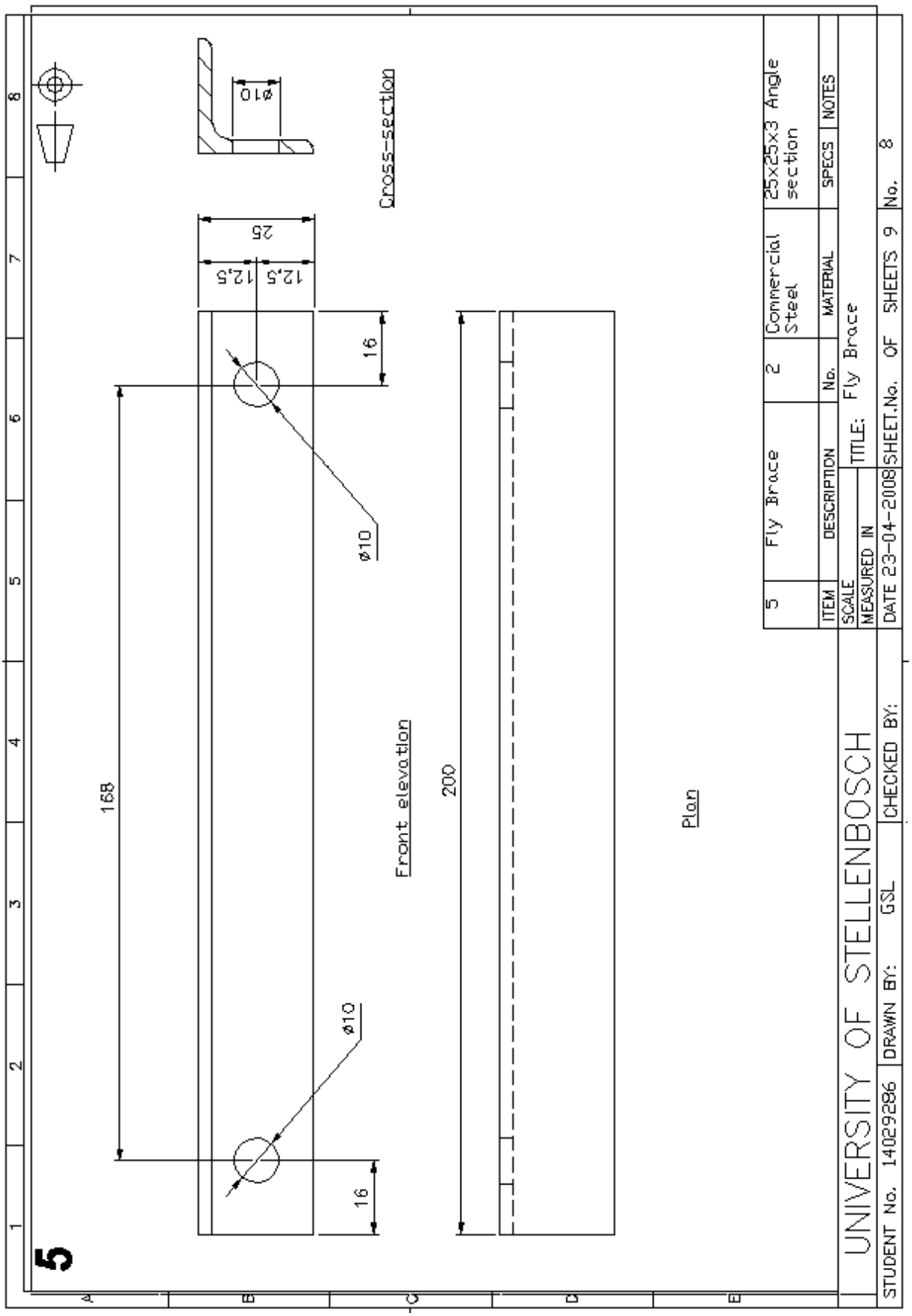
Cross-section
ø10
25
12,5
12,5
16
ø10
168
Front elevation
200
Plan
ø10
16
5
Fly Brace
2
Commercial Steel
25x25x3 Angle section
ITEM
DESCRIPTION
No.
MATERIAL
SPECS
NOTES
SCALE
MEASURED IN
TITLE: Fly Brace
UNIVERSITY OF STELLENBOSCH
STUDENT No. 14029286
DRAWN BY: GSL
CHECKED BY:
DATE 23-04-2008
SHEET No. OF SHEETS 9
No. 8

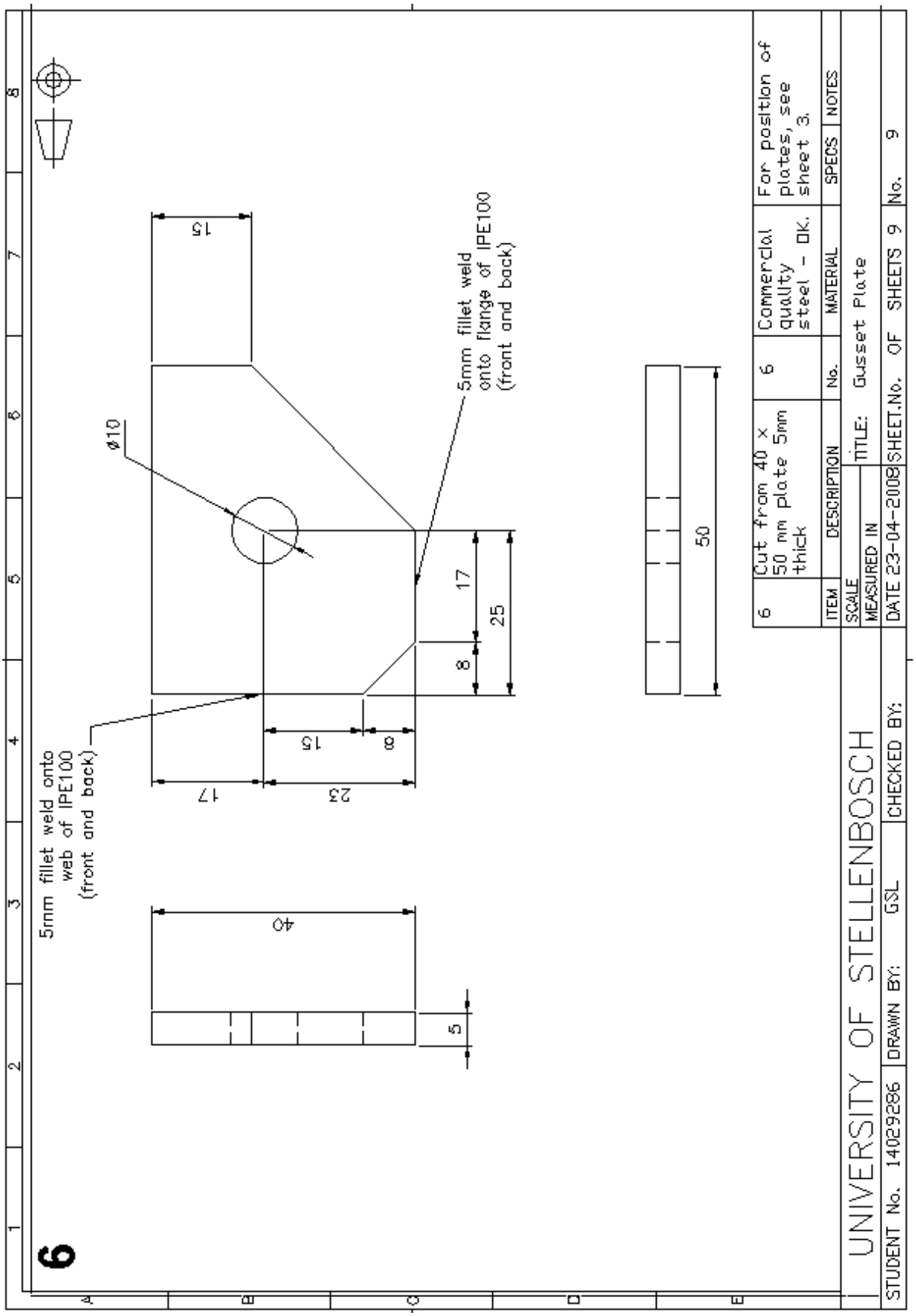
6
5mm fillet weld onto web of IPE100 (front and back)
5mm fillet weld onto flange of IPE100 (front and back)
ø10
15
17
23
15
8
8
25
40
5
50
UNIVERSITY OF STELLENBOSCH
STUDENT No. 14029286
DRAWN BY: GSL
CHECKED BY:
DATE 23-04-2008
SHEET No. OF SHEETS 9
No. 9
TITLE: Gusset Plate
SCALE
MEASURED IN
ITEM DESCRIPTION No. MATERIAL SPECS NOTES
6 Cut from 40 x 50 mm plate 5mm thick 6 Commercial quality steel - OK. For position of plates, see sheet 3.

A2.3. End connections

1. Top connection strut – flange
2. Top connection strut – web
3. Base connection strut – flange
4. Base connection strut – web
5. Seat detail
6. End plates for connection struts
7. End connection details
8. Sheeting rail connector
9. Twist resisting plates
10. Twist resisting angles

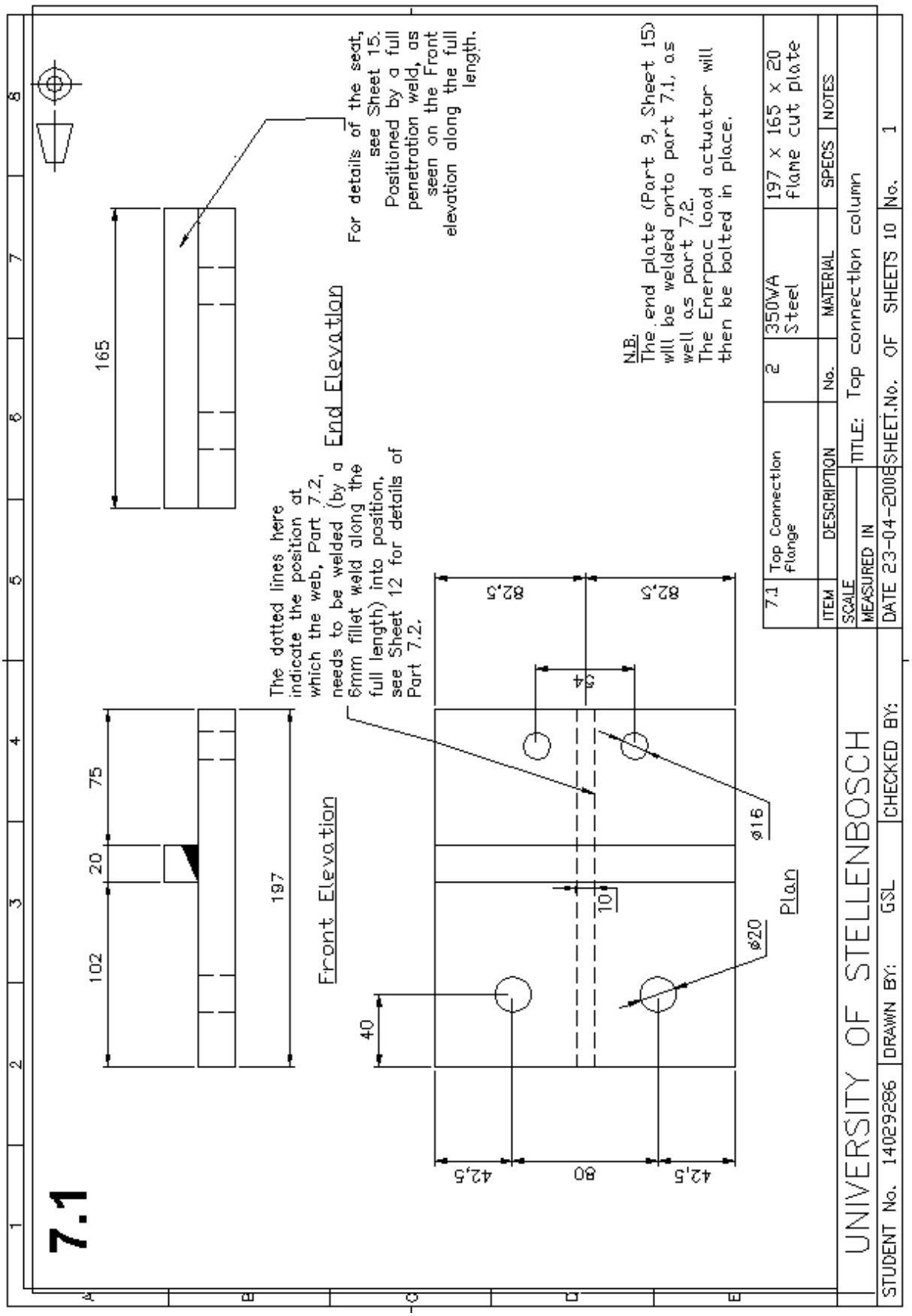
7.1
UNIVERSITY OF STELLENBOSCH
STUDENT No. 14029296
DRAWN BY: GSL
CHECKED BY:
DATE 23-04-2008
SHEET No. OF SHEETS 10
No. 1
TITLE: Top connection column
SCALE
MEASURED IN
ITEM DESCRIPTION No. MATERIAL SPECS NOTES
7.1 Top Connection Flange 2 350WA Steel 197 x 165 x 20 flame cut plate
Front Elevation
End Elevation
Plan
165
75
20
102
197
40
80
42,5
82,5
74
10
ø16
ø20
The dotted lines here indicate the position at which the web, Part 7.2, needs to be welded (by a 6mm fillet weld along the full length) into position, see Sheet 12 for details of Part 7.2.
For details of the seat, see Sheet 15. Positioned by a full penetration weld, as seen on the Front elevation along the full length.
N.B.
The end plate (Part 9, Sheet 15) will be welded onto part 7.1, as well as part 7.2.
The Enerpac load actuator will then be bolted in place.

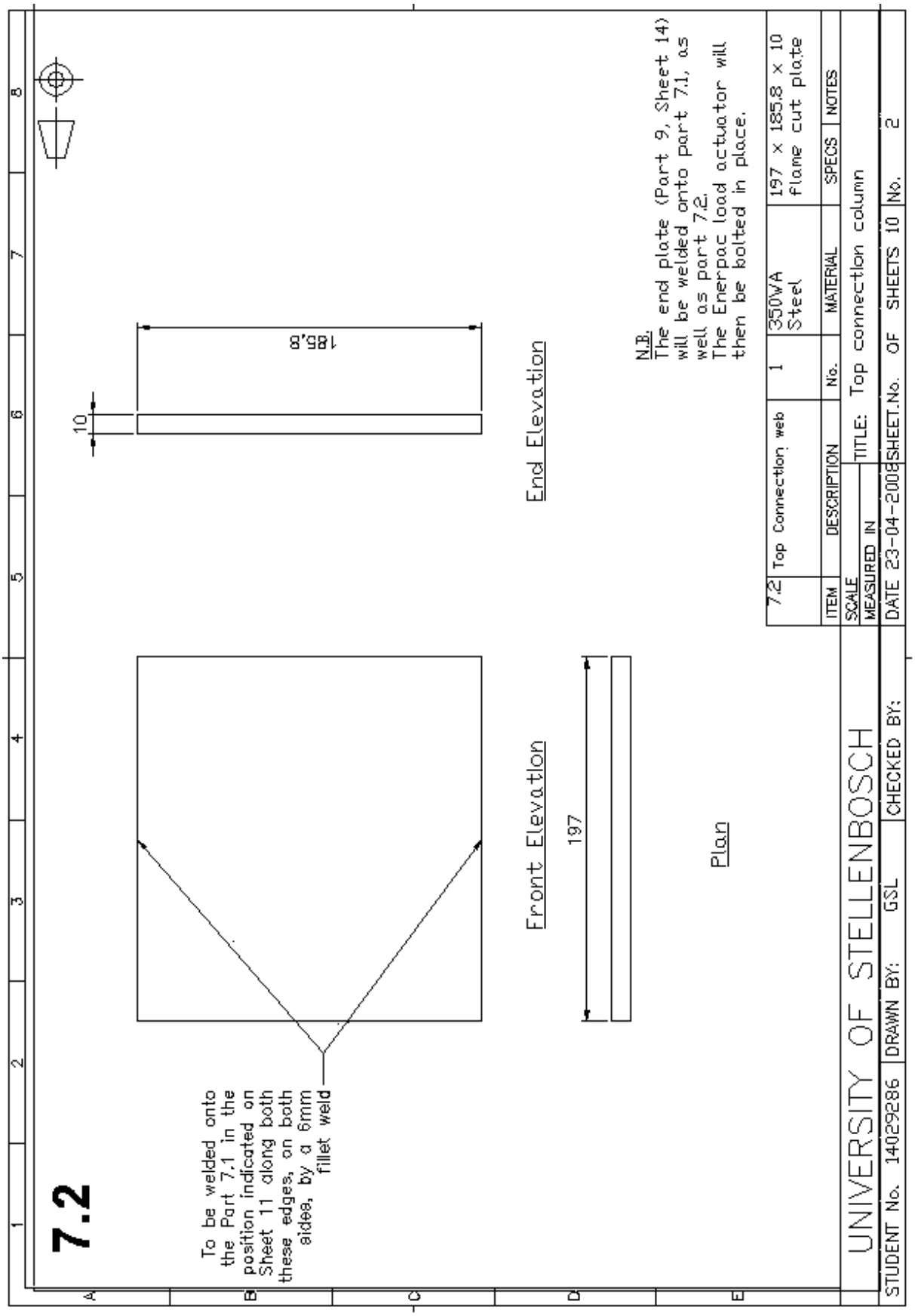
7.2
To be welded onto the Part 7.1 in the position indicated on Sheet 11 along both these edges, on both sides, by a 6mm fillet weld
End Elevation
185,8
10
Front Elevation
197
Plan
N.B.
The end plate (Part 9, Sheet 14) will be welded onto part 7.1, as well as part 7.2.
The Enerpac load actuator will then be bolted in place.
7.2 Top Connection web 1 350WA Steel 197 x 185.8 x 10 flame cut plate
ITEM DESCRIPTION No. MATERIAL SPECS NOTES
SCALE
MEASURED IN
TITLE: Top connection column
UNIVERSITY OF STELLENBOSCH
STUDENT No. 14029286 DRAWN BY: GSL CHECKED BY:
DATE 23-04-2008 SHEET No. OF SHEETS 10 No. 2

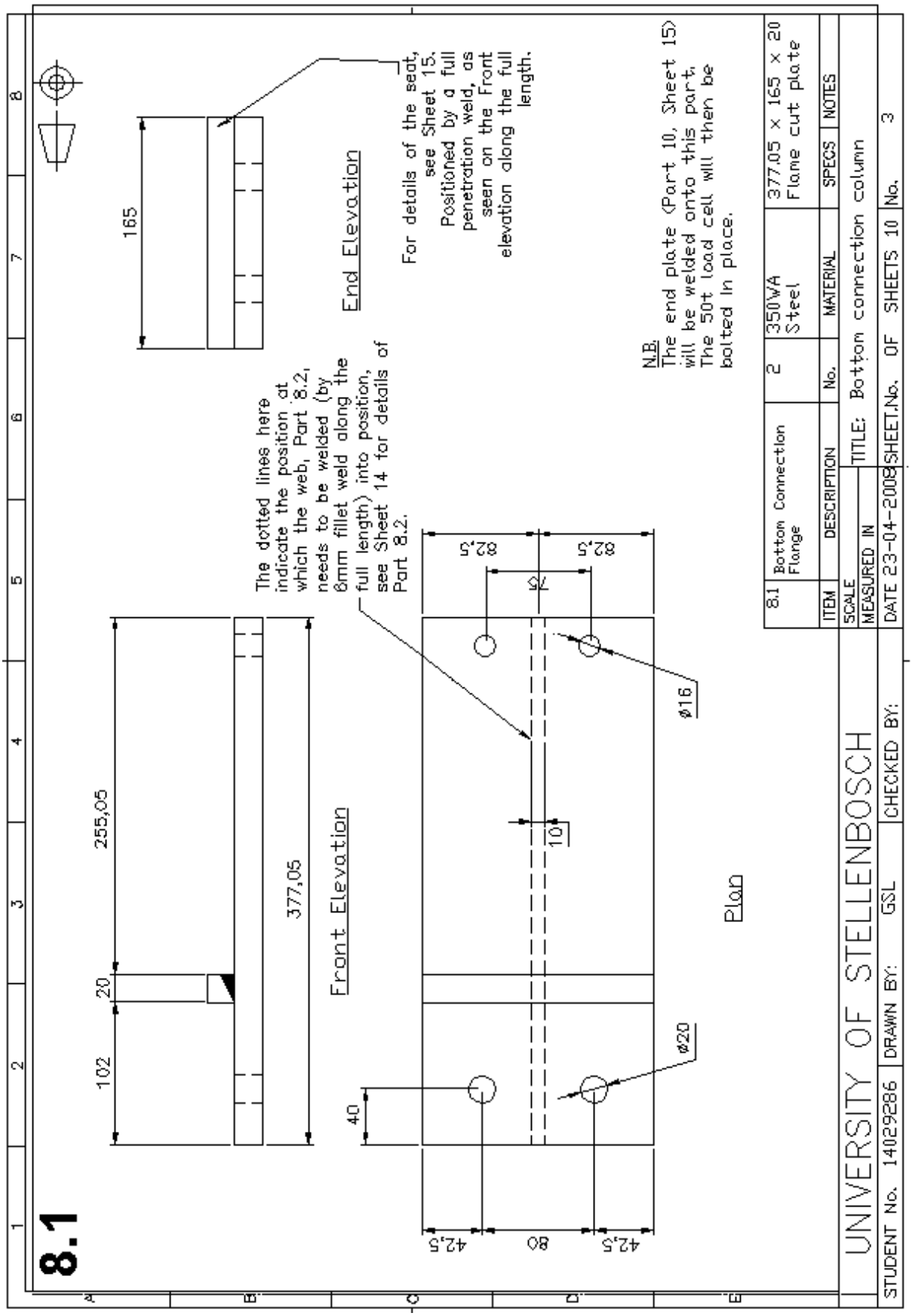
8.1
End Elevation
165
For details of the seat, see Sheet 15. Positioned by a full penetration weld, as seen on the Front elevation along the full length.
The dotted lines here indicate the position at which the web, Part 8.2, needs to be welded (by 6mm fillet weld along the full length) into position, see Sheet 14 for details of Part 8.2.
N.B.
The end plate (Part 10, Sheet 15) will be welded onto this part. The 50t load cell will then be bolted in place.
Front Elevation
255,05
377,05
20
102
40
Plan
82,5
82,5
42,5
80
42,5
10
ø16
ø20
8.1 Bottom Connection Flange 2 350WA Steel 377.05 x 165 x 20 Flame cut plate
ITEM DESCRIPTION No. MATERIAL SPECS NOTES
SCALE
MEASURED IN
TITLE: Bottom connection column
UNIVERSITY OF STELLENBOSCH
STUDENT No. 14029286 DRAWN BY: GSL CHECKED BY:
DATE 23-04-2008 SHEET No. OF SHEETS 10 No. 3

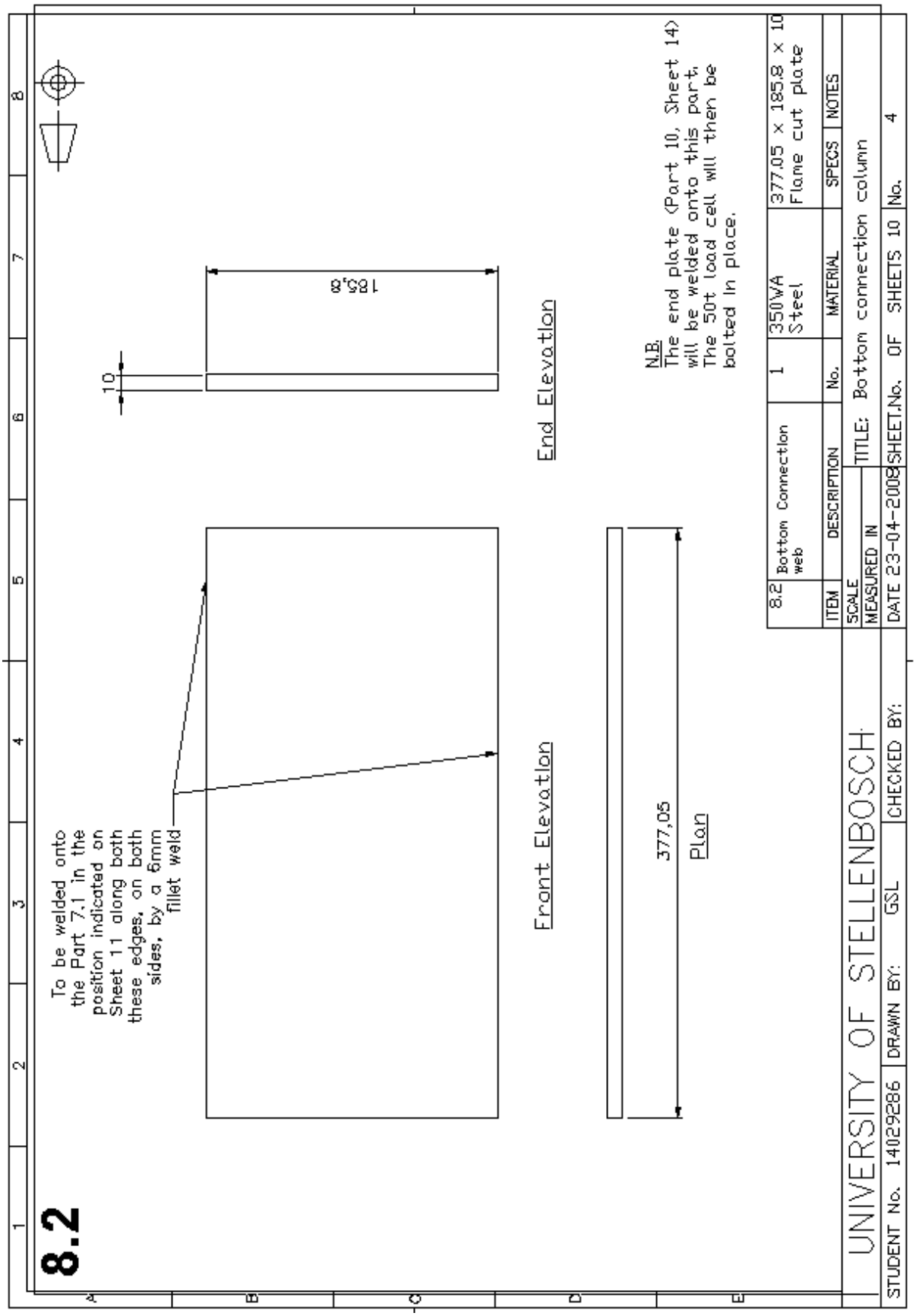
8.2
To be welded onto the Part 7.1 in the position indicated on Sheet 11 along both these edges, on both sides, by a 6mm fillet weld
10
185,8
End Elevation
Front Elevation
377,05
Plan
N.B.
The end plate (Part 10, Sheet 14) will be welded onto this part. The 50t load cell will then be bolted in place.
8.2 Bottom Connection web 1 350WA Steel 377,05 x 185,8 x 10 Flame cut plate
ITEM DESCRIPTION No. MATERIAL SPECS NOTES
SCALE
MEASURED IN
TITLE: Bottom connection column
DATE 23-04-2008
SHEET No. OF SHEETS 10 No. 4
STUDENT No. 14029286 DRAWN BY: GSL CHECKED BY:
UNIVERSITY OF STELLENBOSCH

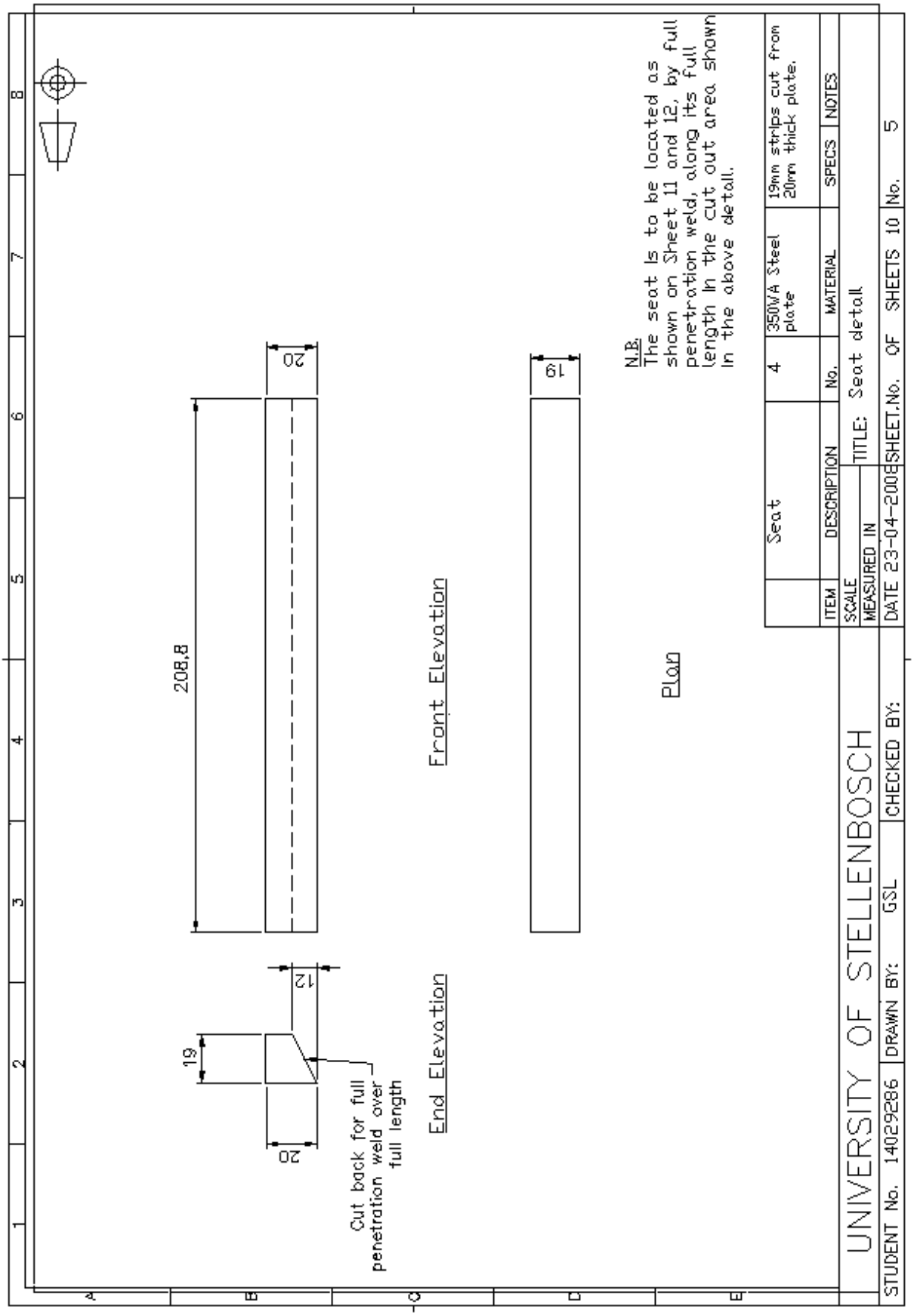
208.8
20
19
12
20
Front Elevation
End Elevation
Cut back for full penetration weld over full length
19
Plan
N.B.
The seat is to be located as shown on Sheet 11 and 12, by full penetration weld, along its full length in the cut out area shown in the above detail.
Seat
4
350WA Steel plate
19mm strips cut from 20mm thick plate.
ITEM
DESCRIPTION
No.
MATERIAL
SPECS
NOTES
SCALE
MEASURED IN
TITLE: Seat detail
UNIVERSITY OF STELLENBOSCH
STUDENT No. 14029286
DRAWN BY: GSL
CHECKED BY:
DATE 23-04-2009
SHEET No. OF SHEETS 10
No. 5

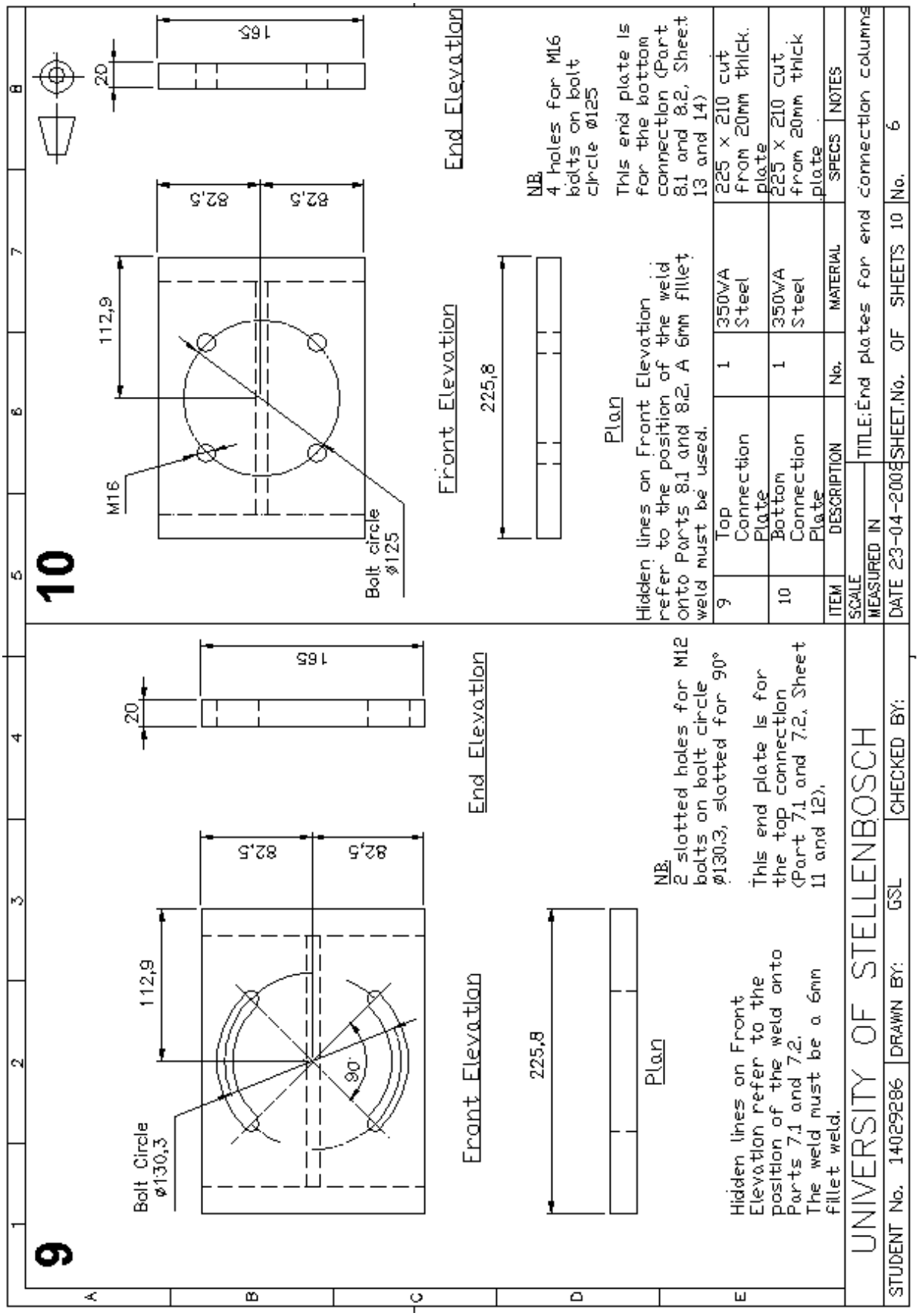
10
112,9
82,5
82,5
M16
Bolt circle
ø125
20
165
End Elevation
Front Elevation
225,8
Plan
NB.
4 holes for M16
bolts on bolt
circle ø125
This end plate is
for the bottom
connection (Part
8.1 and 8.2, Sheet
13 and 14)
Hidden lines on Front Elevation
refer to the position of the weld
onto Parts 8.1 and 8.2 A 6mm fillet
weld must be used.
9 Top Connection Plate 1 350WA Steel 225 x 210 cut from 20mm thick. plate
10 Bottom Connection Plate 1 350WA Steel 225 x 210 cut from 20mm thick plate
ITEM DESCRIPTION No. MATERIAL SPECS NOTES
9
112,9
82,5
82,5
Bolt Circle
ø130,3
90°
20
165
End Elevation
Front Elevation
225,8
Plan
NB.
2 slotted holes for M12
bolts on bolt circle
ø130,3, slotted for 90°
This end plate is for
the top connection
(Part 7.1 and 7.2, Sheet
11 and 12).
Hidden lines on Front
Elevation refer to the
position of the weld onto
Parts 7.1 and 7.2.
The weld must be a 6mm
fillet weld.
UNIVERSITY OF STELLENBOSCH
SCALE
MEASURED IN
TITLE:End plates for end connection columns
STUDENT No. 14029286 DRAWN BY: GSL CHECKED BY:
DATE 23-04-2008 SHEET.No. OF SHEETS 10 No. 6

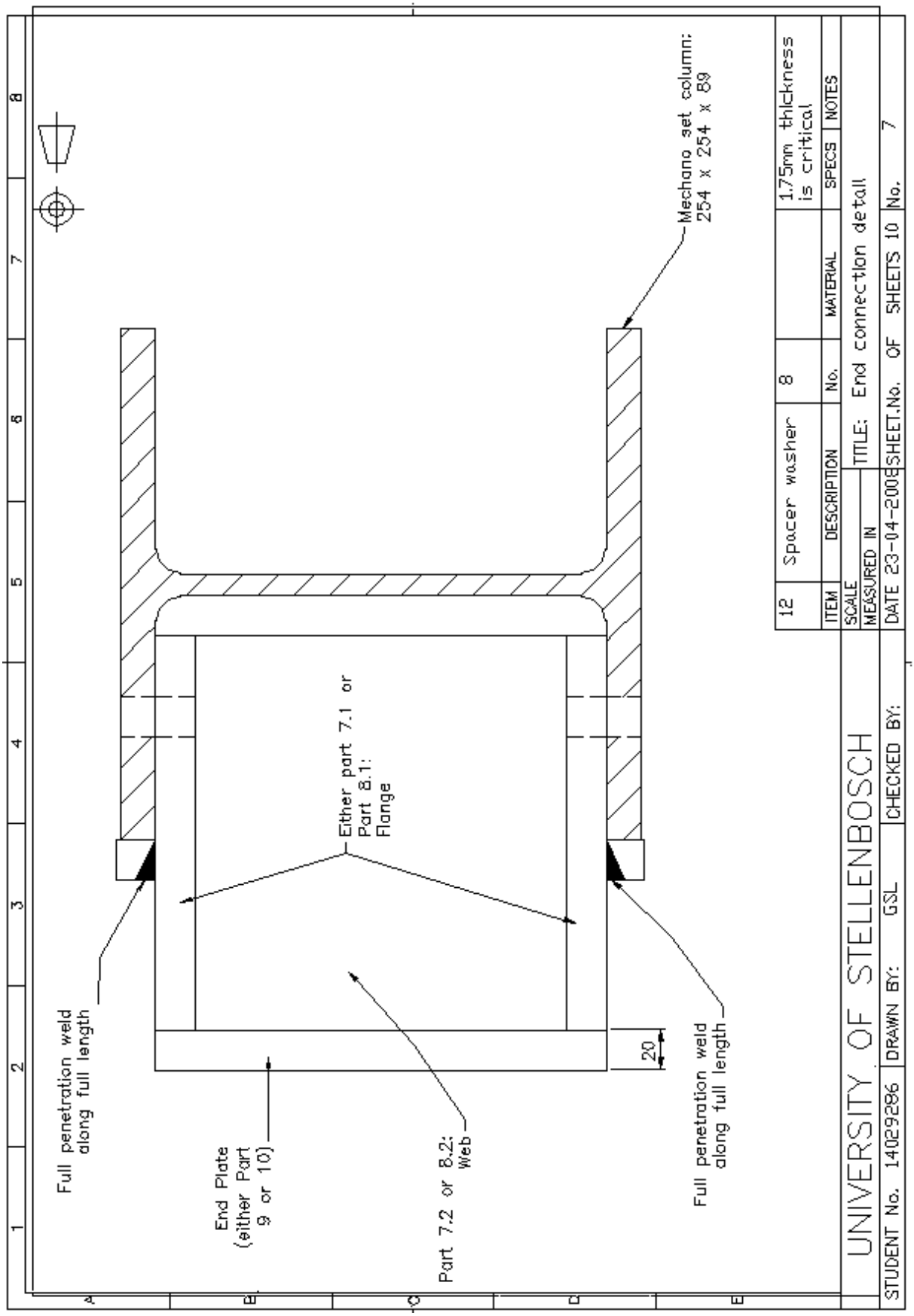
Mechano set column:
254 x 254 x 89
Either part 7.1 or
Part 8.1:
Flange
Full penetration weld
along full length
End Plate
(either Part
9 or 10)
Part 7.2 or 8.2:
Web
Full penetration weld
along full length
20
12 Spacer washer 8
ITEM DESCRIPTION No. MATERIAL SPECS NOTES
1.75mm thickness
is critical
SCALE
MEASURED IN
TITLE: End connection detail
UNIVERSITY OF STELLENBOSCH
STUDENT No. 14029286 DRAWN BY: GSL CHECKED BY:
DATE 23-04-2008 SHEET No. OF SHEETS 10 No. 7

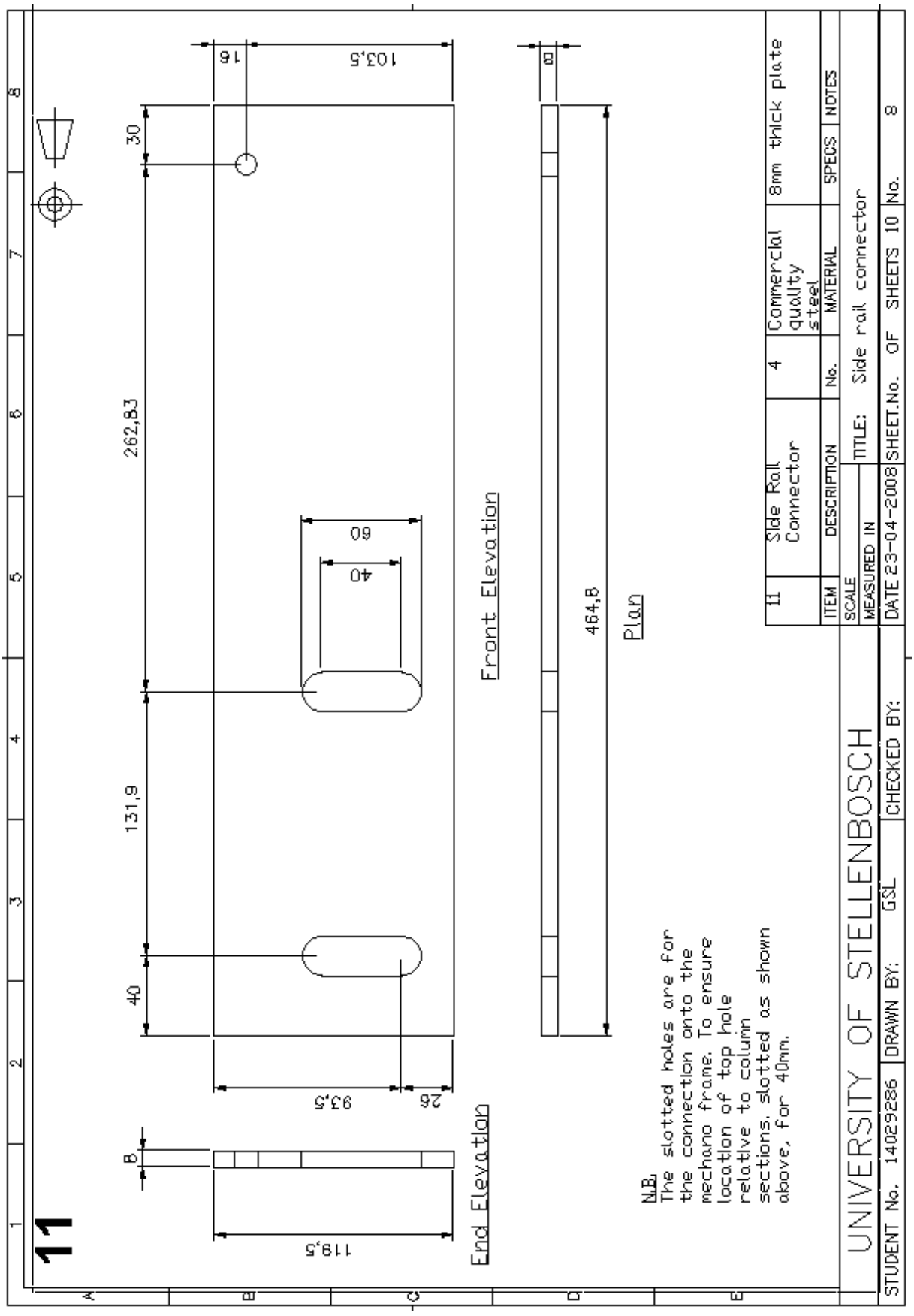
11
103,5
16
30
262,83
131,9
40
60
40
Front Elevation
464,8
8
Plan
119,5
93,5
26
8
End Elevation
N.B.
The slotted holes are for the connection onto the mechano frame. To ensure location of top hole relative to column sections, slotted as shown above, for 40mm.
11 Side Rail Connector 4 Commercial quality steel 8mm thick plate
ITEM DESCRIPTION No. MATERIAL SPECS NOTES
SCALE
MEASURED IN
TITLE: Side rail connector
UNIVERSITY OF STELLENBOSCH
STUDENT No. 14029286 DRAWN BY: GSL CHECKED BY:
DATE 23-04-2008 SHEET.No. OF SHEETS 10 No. 8

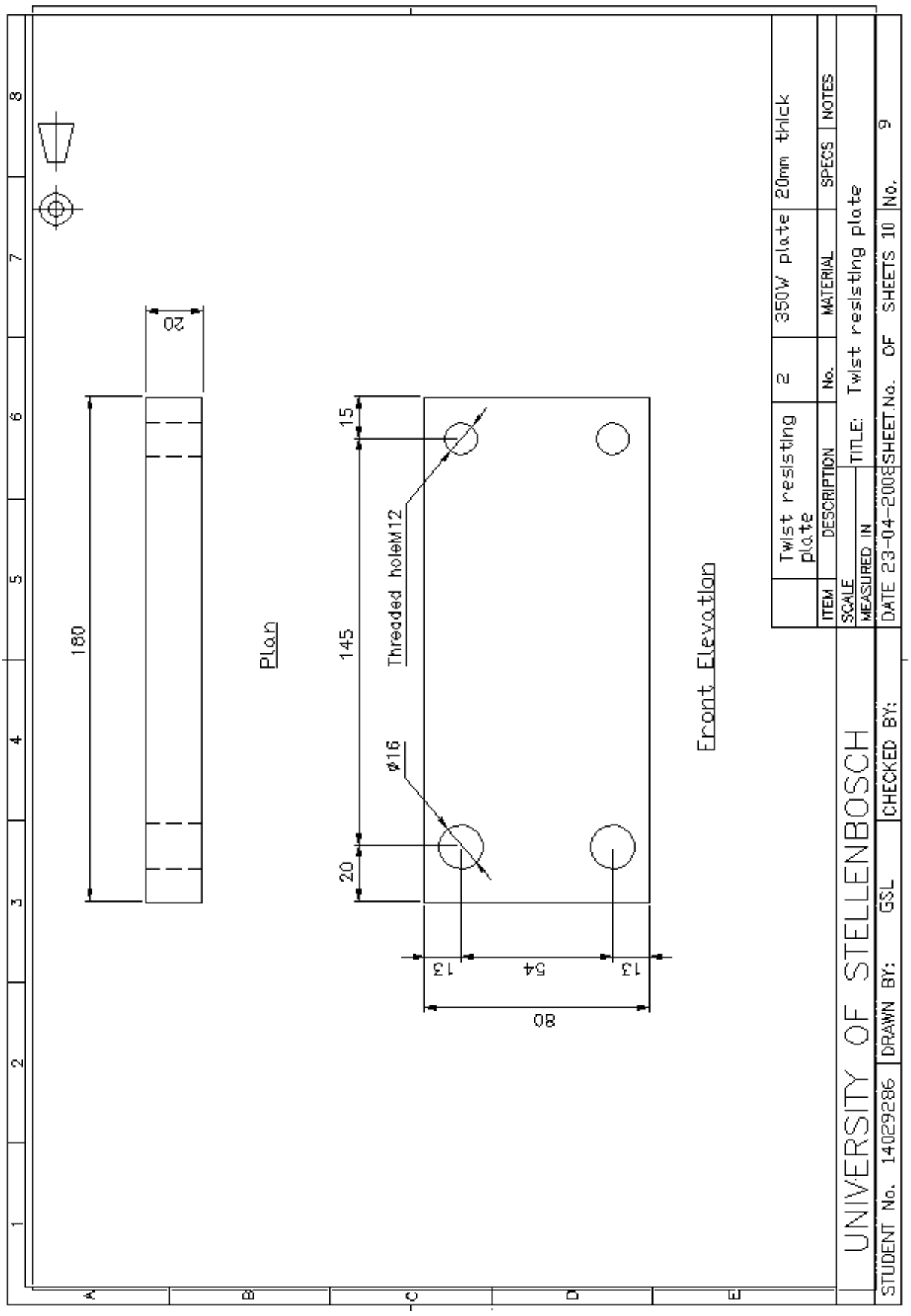
UNIVERSITY OF STELLENBOSCH
Twist resisting plate
Front Elevation
Plan
Threaded holeM12
ø16
180
145
20
15
80
54
13
13
20
350W plate
20mm thick
DESCRIPTION
MATERIAL
SPECS
NOTES
ITEM
No.
SCALE
MEASURED IN
TITLE: Twist resisting plate
DATE 23-04-2009
SHEET No. OF SHEETS 10
No. 9
STUDENT No. 14029286
DRAWN BY: GSL
CHECKED BY:

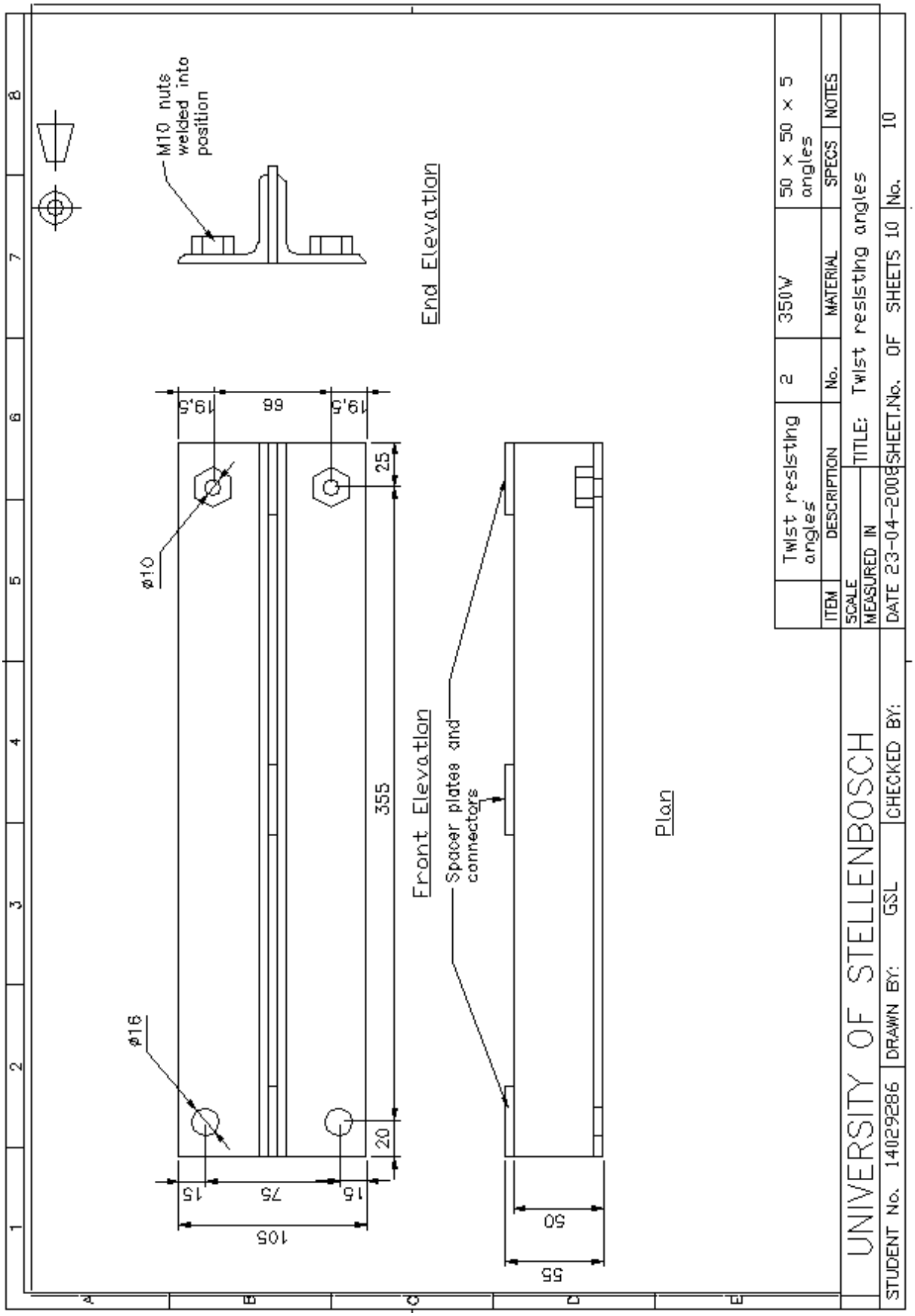
M10 nuts welded into position
End Elevation
19,5
66
19,5
25
ø10
355
ø16
20
15
75
15
105
Front Elevation
Spacer plates and connectors
Plan
50
55
Twist resisting angles
2
350W
50 x 50 x 5 angles
ITEM
DESCRIPTION
No.
MATERIAL
SPECS
NOTES
SCALE
MEASURED IN
TITLE: Twist resisting angles
UNIVERSITY OF STELLENBOSCH
STUDENT No. 14029286
DRAWN BY: GSL
CHECKED BY:
DATE 23-04-2008
SHEET No. OF SHEETS 10
No. 10

B. Appendix B: Southwell plots

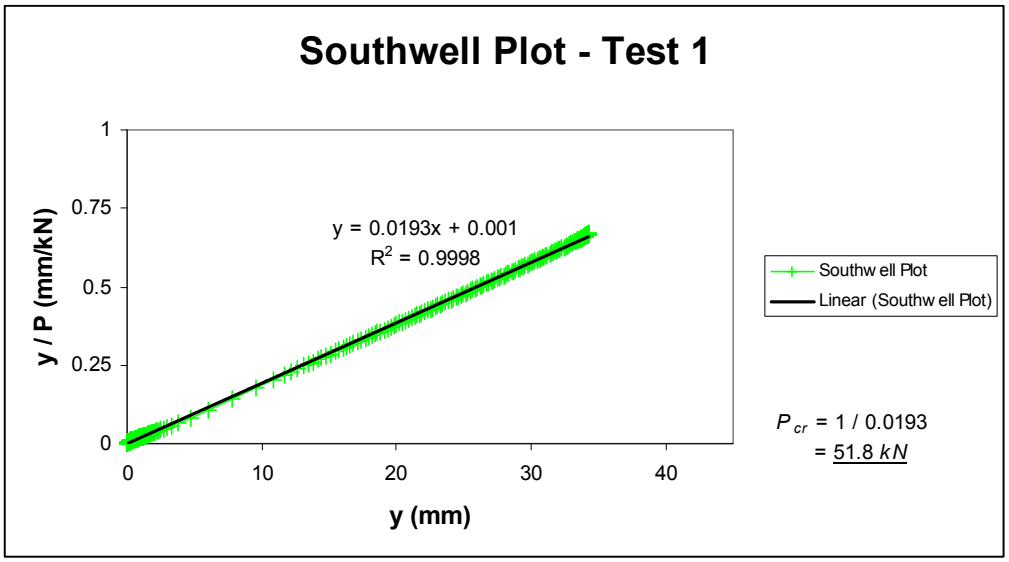

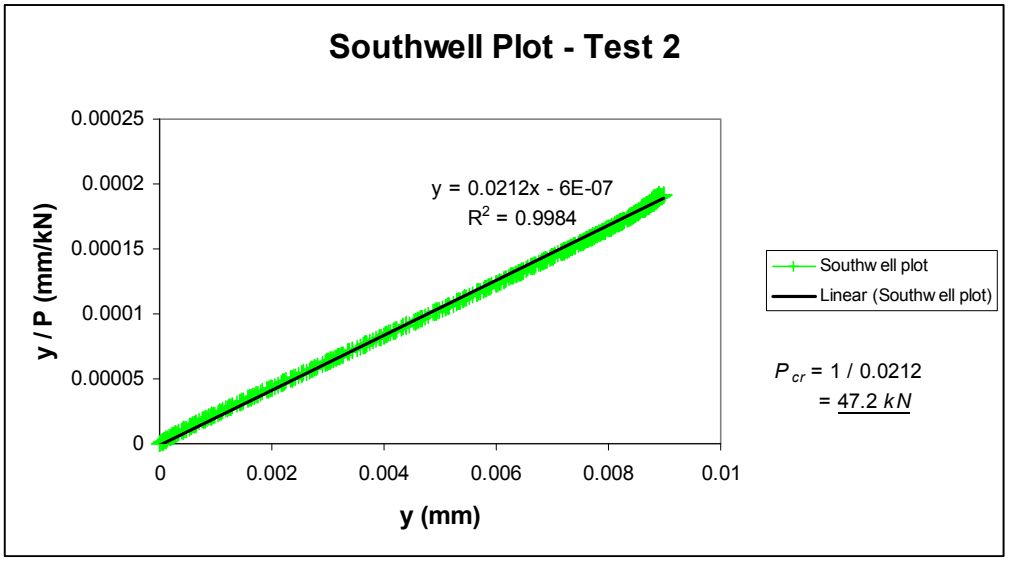

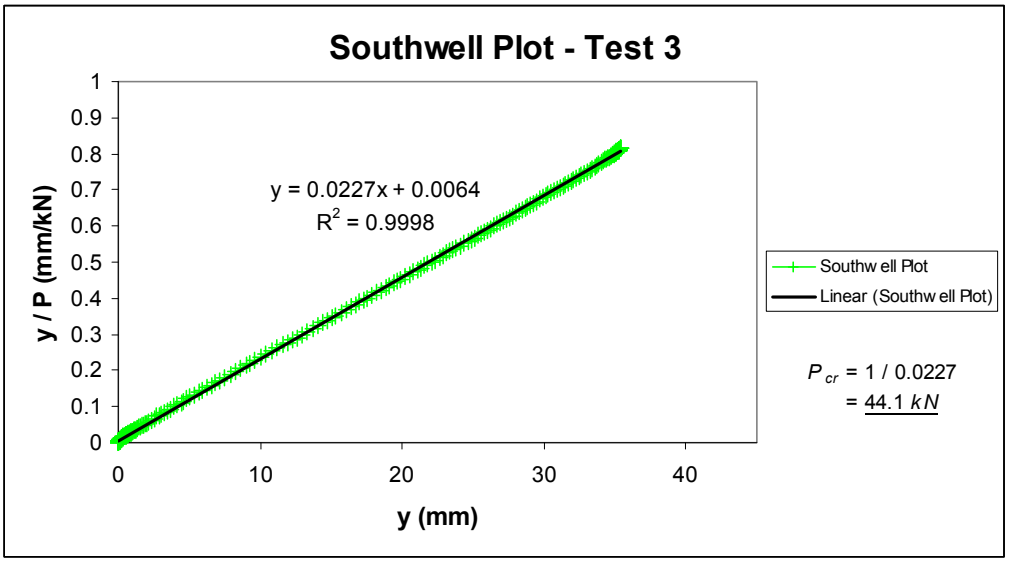

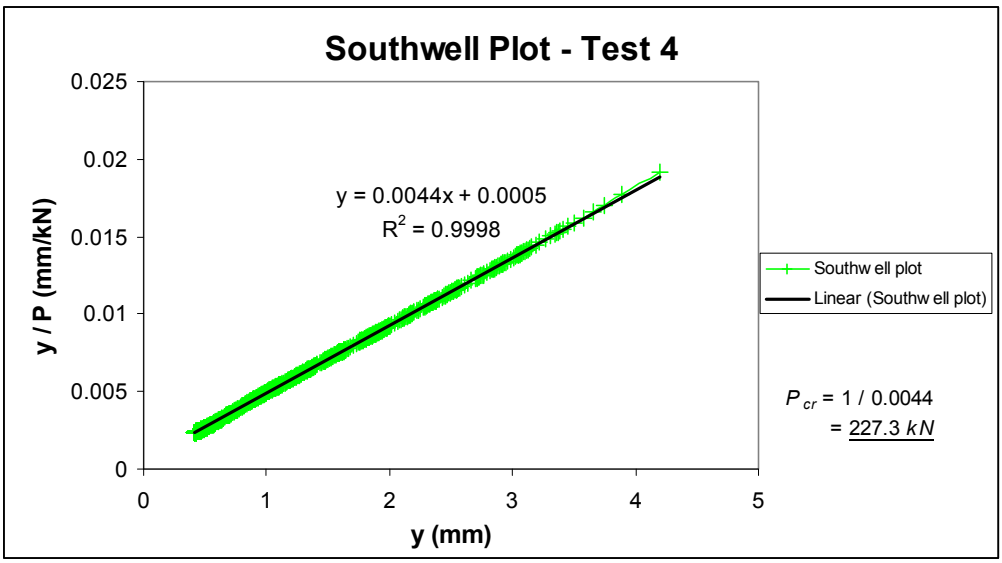
Southwell Plot - Test 4
y = 0.0044x + 0.0005
R2 = 0.9998
y / P (mm/kN)
y (mm)
Southw ell plot
Linear (Southw ell plot)
P cr = 1 / 0.0044
= 227.3 kN

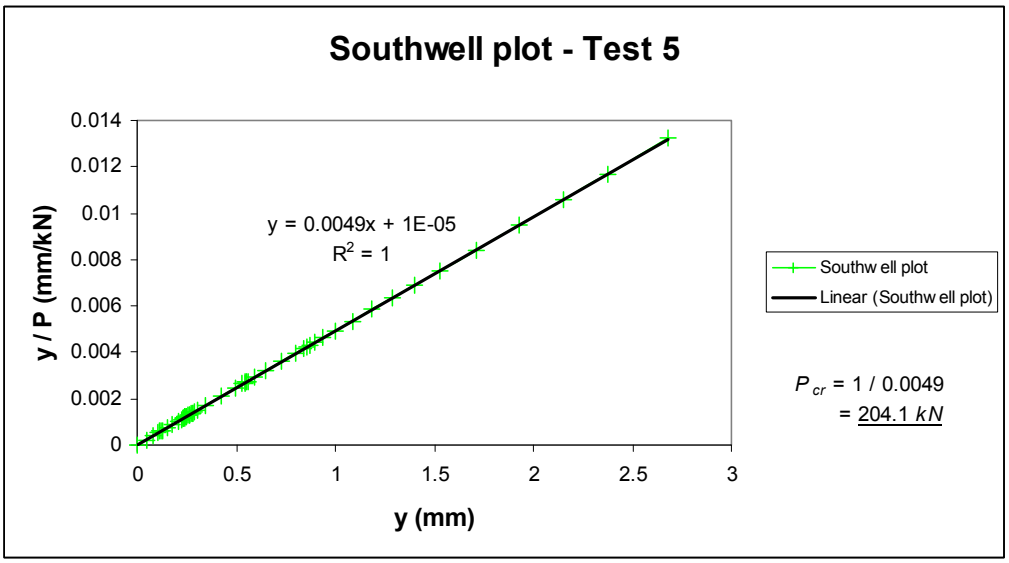
Southwell plot - Test 5
y = 0.0049x + 1E-05
R2 = 1
y / P (mm/kN)
y (mm)
Southw ell plot
Linear (Southw ell plot)
P cr = 1 / 0.0049
= 204.1 kN

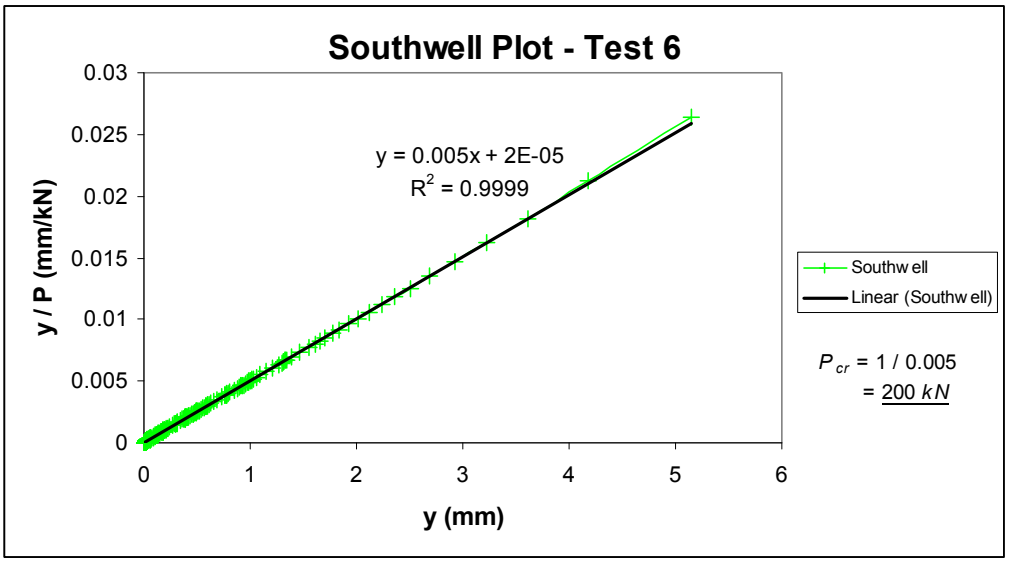
Southwell Plot - Test 6
y = 0.005x + 2E-05
R2 = 0.9999
y / P (mm/kN)
y (mm)
Southw ell
Linear (Southw ell)
P cr = 1 / 0.005
= 200 kN

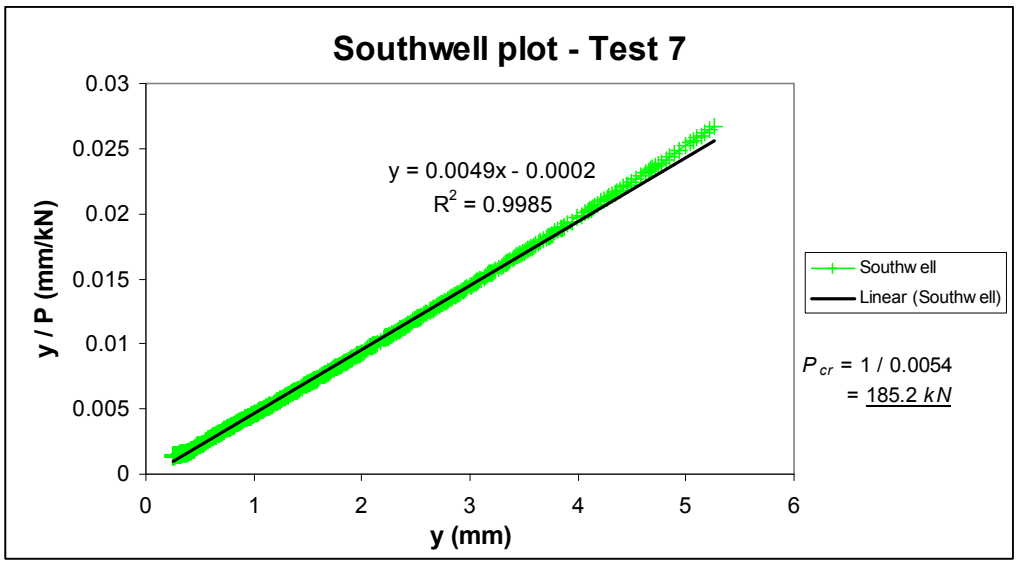
Southwell plot - Test 7
y = 0.0049x - 0.0002
R2 = 0.9985
y / P (mm/kN)
y (mm)
Southw ell
Linear (Southw ell)
Pcr = 1 / 0.0054
= 185.2 kN

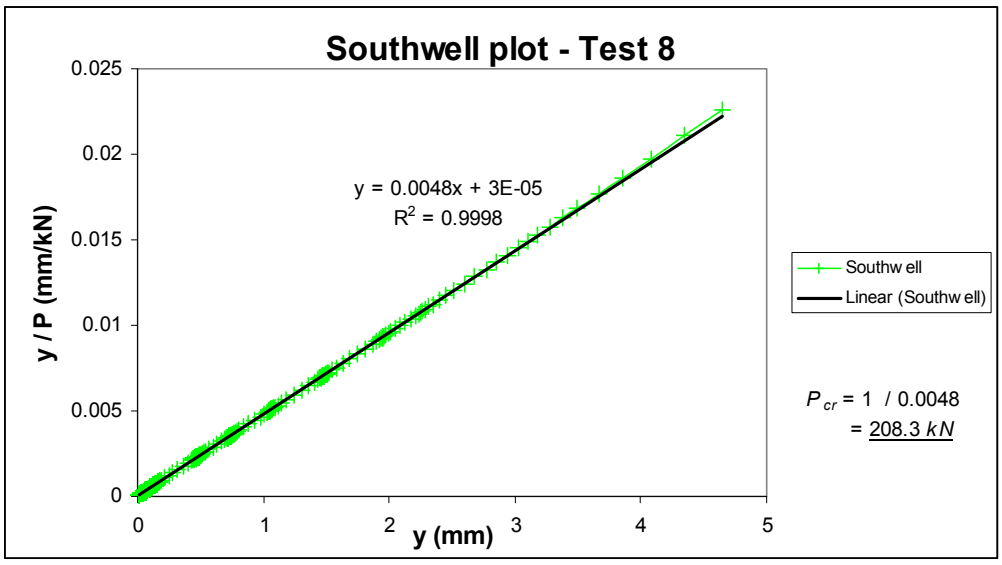
Southwell plot - Test 8
y = 0.0048x + 3E-05
R2 = 0.9998
y / P (mm/kN)
y (mm)
Southw ell
Linear (Southw ell)
Pcr = 1 / 0.0048
= 208.3 kN

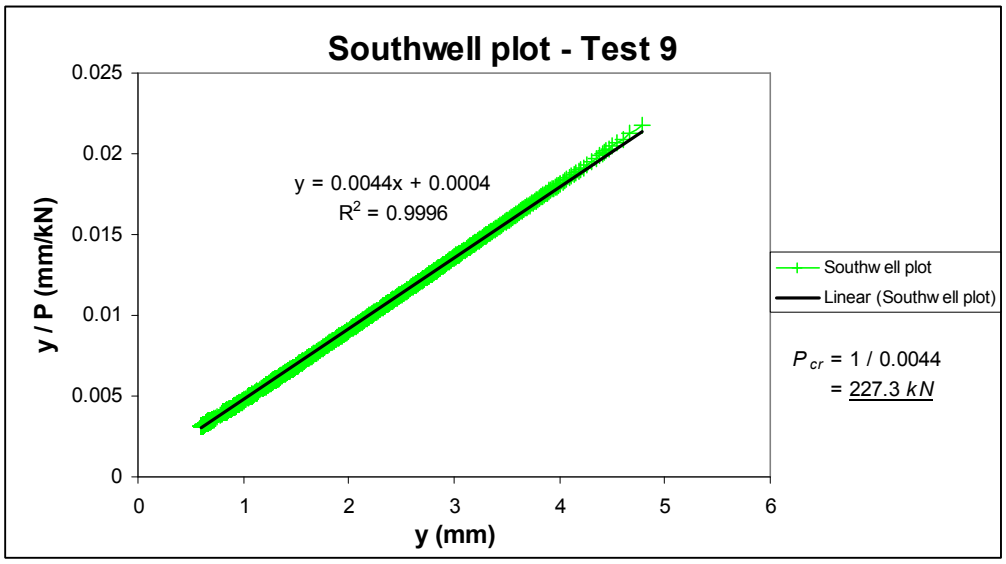
Southwell plot - Test 9
y = 0.0044x + 0.0004
R2 = 0.9996
y / P (mm/kN)
y (mm)
Southw ell plot
Linear (Southw ell plot)
Pcr = 1 / 0.0044
= 227.3 kN

C. Appendix C: Tensile test results

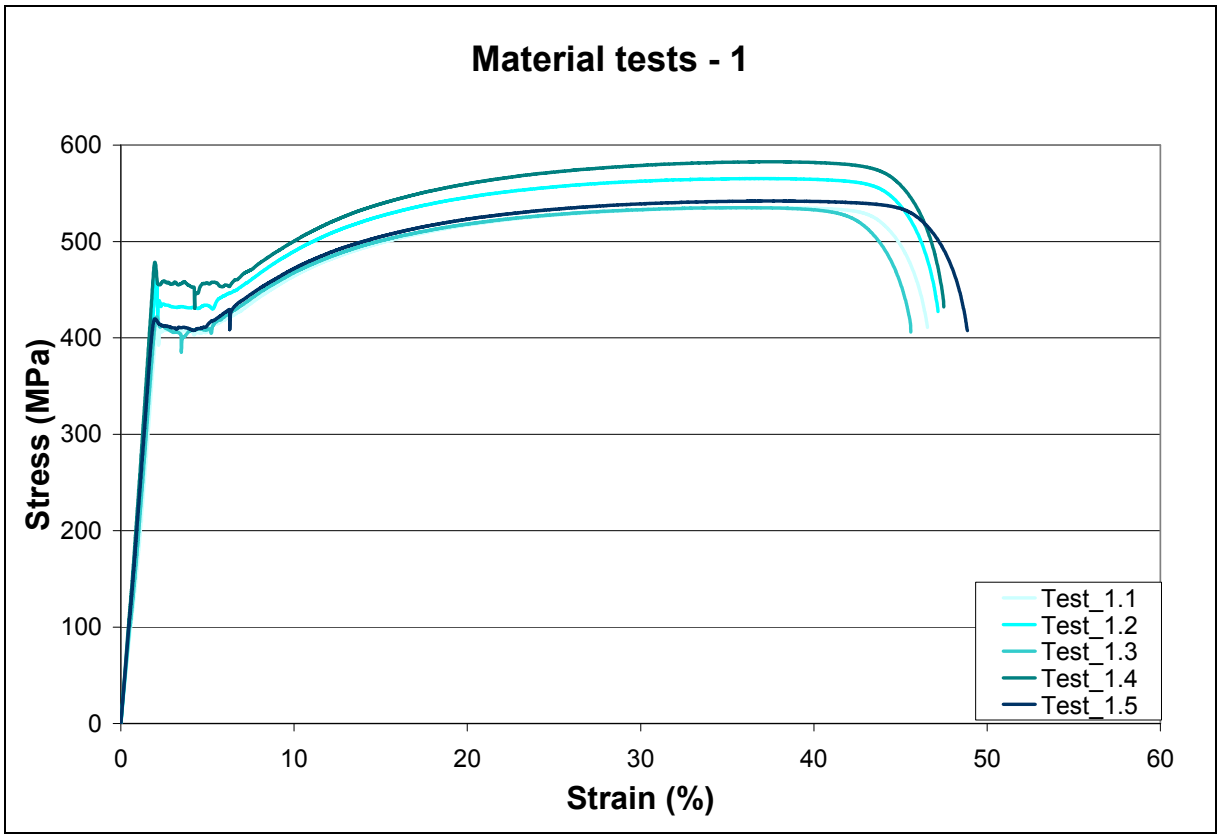

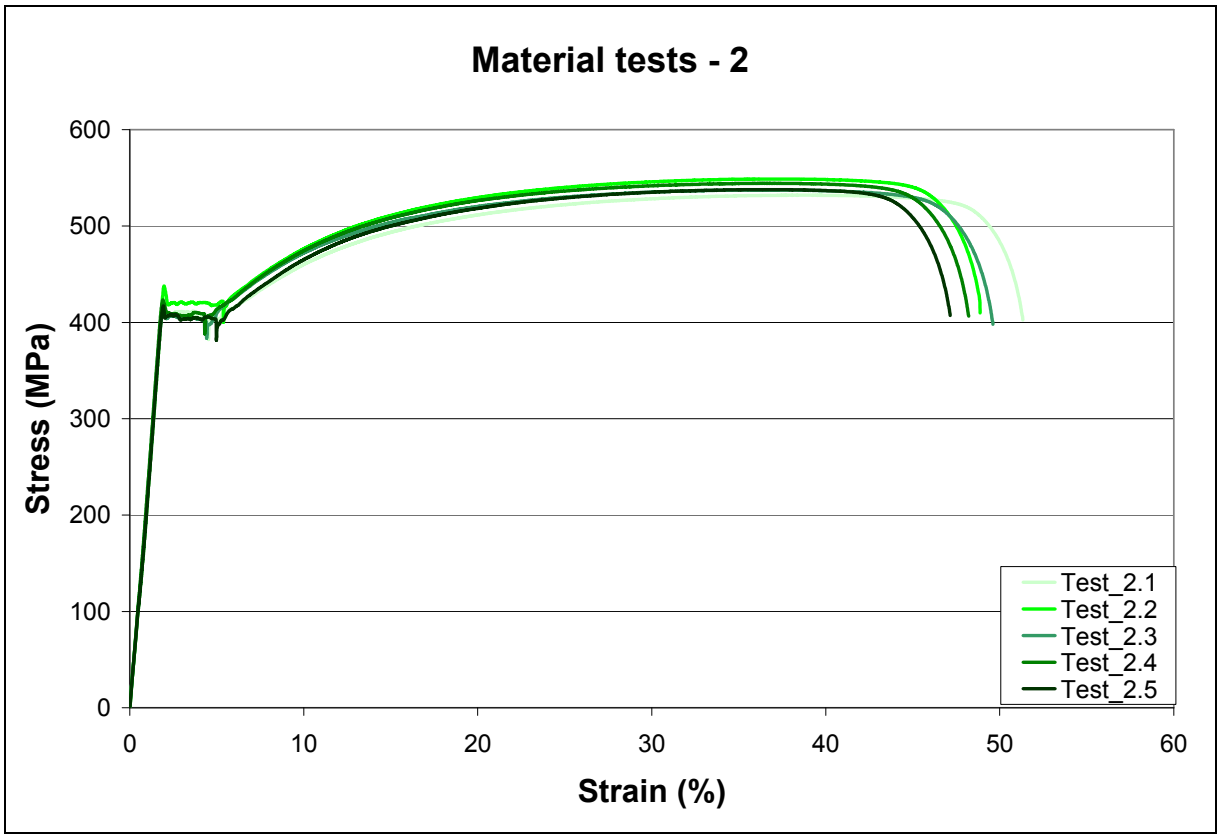

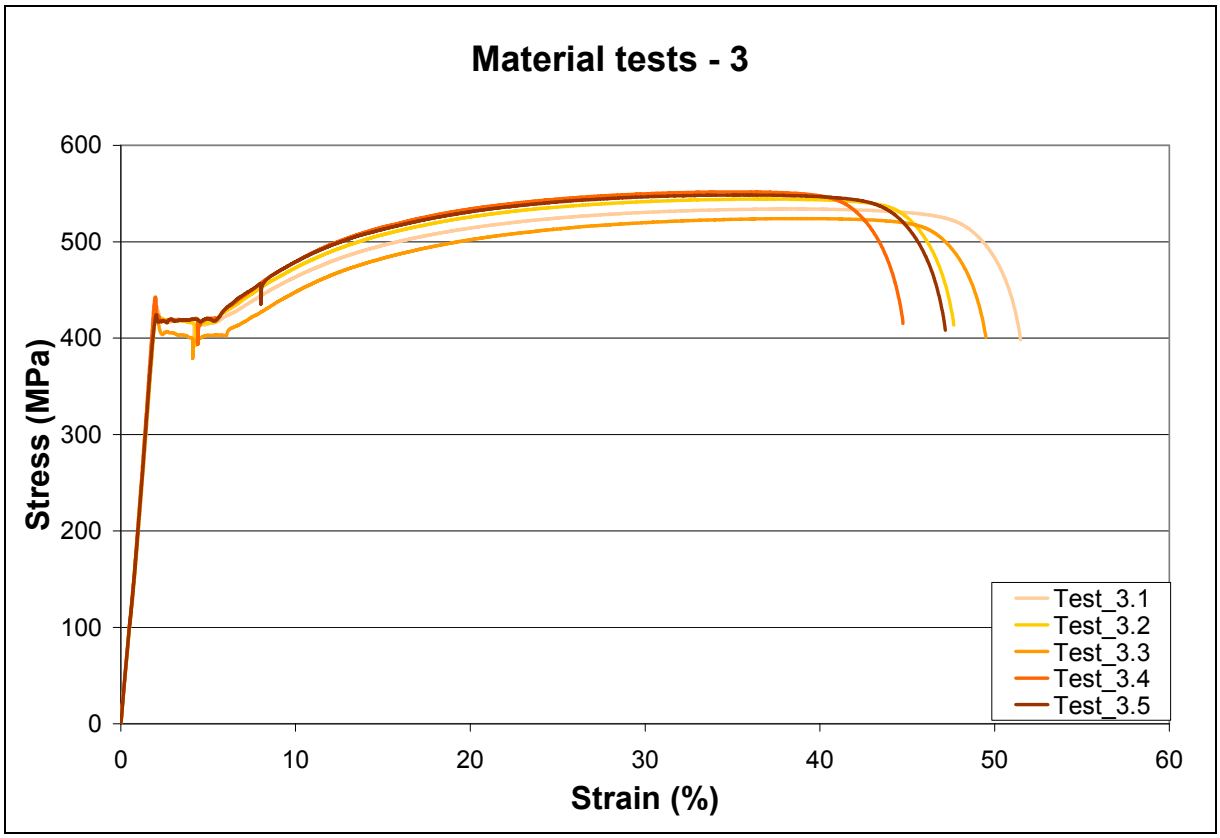
Material tests - 3
Stress (MPa)
600
500
400
300
200
100
0
0
10
20
30
40
50
60
Strain (%)
Test_3.1
Test_3.2
Test_3.3
Test_3.4
Test_3.5